Obesity enhances breast cancer risk, metastasis, and response to immunotherapy

By

Abbey E. Williams

A dissertation submitted in partial fulfilment of the requirements for the degree of

Doctor of Philosophy

(Comparative Biomedical Sciences)

at the

UNIVERSITY OF WISCONSIN-MADISON

2024

Date of final oral examination: 7/12/2024

The dissertation is approved by the following members of the Final Oral Committee:

Lisa M. Arendt, Associate Professor, Comparative Biosciences
Suzanne Ponik, Assistant Professor, Cell and Regenerative Biology
Xuan Pan, Associate Professor, Medical Sciences
Matthew Reynolds, Associate Professor, Pathobiological Sciences
Linda Schuler, Emeritus Professor, Comparative Biosciences

Dissertation Abstract

Obesity increases breast cancer risk, progression to metastasis, and potentially patient immunotherapy responses. However, there are still gaps in knowledge on the mechanisms on how obesity promotes these changes. Women can also have multiple risk factors for breast cancer development, and obesity may interact with other risk factors like breast density. It is unknown how these risk factors may cooperatively enhance breast cancer risk. To model breast density, we used heterozygous Col1a1^{tmjae} (Het) mice, which have a mutation that limits collagen degradation, leading to increased mammary collagen deposition. Het and wild type (WT) littermates were fed either a low-fat diet (LFD) or a high-fat diet (HFD) to induce obesity. In non-tumor bearing mice, obesity and excess collagen deposition enhanced macrophages, while obesity led to diminished CD8+ T cells. When crossed with MMTV-PyMT mice to examine tumor growth, we saw increased pulmonary metastasis in HFD-fed Het mice. Overall, we demonstrated that breast density and obesity may cooperatively increase breast cancer progression to metastasis in the lungs. Obesity is known to increase the risk for metastasis following diagnosis. We hypothesized CD8+ T cells could play a role in elevating metastasis to the lungs. Prior to tumor formation, CD8+ T cells had characteristics of exhaustion, which limits T cell responses. We transplanted estrogen receptor positive (ER+) TC2 cells into the mammary fat pads of obese and lean mice, then surgically resected the tumors. While obesity reduced expression of genes associated with T cell response in immune cells from metastatic lungs, CD8+ T cells isolated from metastatic lungs of obese mice had increased responses to stimulation in culture. These results suggest that obesity increased T cell dysfunction in lung metastasis from ER+ breast cancer, but stimulation of CD8+ T cells uncovered elevated functional responses. Our data suggests that CD8+ T cells from obese mice may respond to immune checkpoint blockade (ICB) therapies targeting PD-1, however, immunosuppressive macrophages may limit their ability to kill tumor cells. We hypothesized that obese mice may benefit more than lean mice from a combination therapy of anti-CSF-1R and anti-PD-1 antibodies. Anti-PD-1 antibodies alone reduced lung metastasis in LFD-fed mice and enhanced expression of genes associated with cytotoxicity. In contrast, anti-CSF-1R antibodies treatment reduced PD-L1+ myeloid

cells and metastasis only in HFD-fed mice. When these therapies were combined, HFD-fed mice responded better to anti-CSF-1R and anti-PD1 antibodies to reduce metastasis in the lungs. These studies highlight how the metastatic environment in the lungs under conditions of obesity alter therapy responses. Further analysis of obesity-associated breast cancer is needed to fully understand these differences in risk, progression to metastasis and immunotherapy responses for the benefit of future patients with breast cancer.

TABLE OF CONTENTS

LIST OF FIGURES AND TABLES

Figures:

CHAPTER 2

CHAPTER 3

CHAPTER 4

CHAPTER 6

Tables:

CHAPTER 3

CHAPTER 4

ACKNOWLEDGEMENTS

There are many people that have supported, mentored, and encouraged me to pursue my dreams of pursuing a Ph.D. and a career in science. First, I would like to thank my Ph.D. advisor, friend, and now colleague Dr. Lisa M. Arendt for her unwavering support, guidance, and valuable critiques. Lisa has always encouraged me to pursue my passions and interests in and outside of the lab. Thank you for taking a chance on me as a direct admit student and shaping me into a confident and proficient scientist. Thank you for always being patient and kind during this journey and helping me see potential in myself.

Secondly, I would like to thank former and present lab members for their guidance and contributions to this body of work. Thank you to former lab members, Victoria Thompson, Dr. Lauren Hillers-Zeimer, and Dr. Genevra Kuziel for their expertise, advise, and teaching. Without your help I would not have been able to finish this dissertation. Thank you to Yue (Tim) Xiong for helping me with very challenging overnight flow cytometry experiments and troubleshooting many roadblocks I have had in my research. Furthermore, thank you to Brenna Walton for your input on these projects and presentations throughout graduate school.

I would also like to thank many undergraduates, veterinary students, interns, and rotating students that have contributed to my dissertation. Special thanks to Mason McGuire for helping me with various mouse experiments that have been foundational to my Ph.D. research and Dr. Brittney Moore, Megan Halembeck, and Taeho Lee for contributions to work featured in upcoming chapters.

Thank you to my thesis committee, former members Dr. Jyoti Watters, and Dr. Mark Burkard for your contributions and input throughout my Ph.D. training. Thank you to Dr. Suzanne Ponik and Dr. Xuan Pan for your contributions to this work and for writing recommendation letters that have led me to receive awards, scholarships, and gain admittance into veterinary school. I would like to further extend my thanks to Dr. Suzanne Ponik, Erica Hoffmann, and other members of Dr. Ponik's lab for collaborating on work in the obesity and breast density project featured in Chapter 2. Thank you to Dr. Matt Reynolds and Dr. Linda Schuler for stepping in to evaluate my thesis and for

joining my committee. Also, thank you to Dr. Linda Schuler for her recommendation letter to veterinary school, contributions to this work by providing our lab with TC2 mammary tumor cells, and comments on presentations and data throughout the years.

Thank you to members of the Developmental Endocrinology research group for their input on my thesis projects and presentations. Special thanks to Kathy O'Leary and Fern Murdoch from the Schuler Lab for their expertise and helping me troubleshoot issues that have arisen during my projects. Also, thank you to Mike Huelsmeyer for your scientific advice and guidance throughout this process.

I wouldn't have been able to be successful in graduate school without the support of my friends. Thank you to Dr. Brittney Moore, RevaLu Ronnefeldt, Megan Bunne, and Kara Wegner for always supporting me, lifting my spirits, and reminding me that I am more than just my work. Thank you to Jorge Gonzolez for his friendship and Spanish lessons during late night experiments in the lab.

Lastly, I would like to thank my family for their support. Above all, my parents, David and Tina Williams for encouraging me to follow my dreams no matter how big or small. Thank you to my extended family for always being supportive. Of course, lastly, a big thank you to my cat Max for your valued companionship.

In memory of:

Joy Donaldson, Bruce Donaldson, Kenneth Williams, and Linda Carlston

LIST OF ABBREVIATIONS

ANOVA	analysis of variance analysis
APC	antigen presenting cell
BCR	B cell receptor
BCS	bovine calf serum
BDNA	Breast Density Notification Act
BMI	body mass index
BRCA	breast cancer gene
BTLA	B- and T-lymphocyte attenuator
CCL2	chemokine ligand-2
CD	cluster of differentiation
CLS	crown-like structures
Col1a1	collagen 1a1
CSF-1	colony stimulating factor-1
CSF-1R	colony stimulating factor-1 receptor
CTLA-4	cytotoxic T lymphocyte-associated antigen-4
DAPI	4’6-diamidine-2’-phenylidole dihyrochloride
DC	dendritic cell
DCIS	ductal carcinoma in situ
DIO	diet-induced obesity
DMEM	dulbecco's modified eagle medium
ECM	extra cellular matrix
EGRF	epidermal growth factor receptor
EMT	epithelial-to-mesenchymal transition
ERα	estrogen receptor alpha
ERβ	estrogen receptor beta
FACS	fluorescence-activated cell sorting
FBS	fetal bovine serum

FDA	Food and Drug Administration
FFA	free fatty acid
FMO	fluorescence minus one
FOV	field of view
G-CSF	granulocyte colony-stimulating factor
GFP	green fluorescent protein
GITR	glucocorticoid-induced tumor necrosis factor receptor-related protein
GM-CSF	granulocyte macrophage-colony stimulating factor
H&E	hematoxylin and eosin
HD	high density
HER2	human epidermal growth factor receptor 2
HET	heterozygous
HFD	high fat diet
HIF1α	hypoxia-inducible factor 1 alpha
HR	hormone receptor
ICB	immune checkpoint blockade
IF	immunofluorescence
IFN-γ	interferon-gamma
IGF-1	insulin-like growth factor-1
IgG	immunoglobulin G
IHC	immunohistochemistry
IL	interleukin
IME	immune microenvironment
IP	interperitoneally
iNOS	intermediate nitrogen and oxygen species
IrAE	immune-related adverse event
JNK	c-Jun N-terminalkinase
LAG-3	lymphocyte-activation gene-3

LD	live dead
MAM	metastasis associated macrophage
MDM	metastasis derived macrophage
MCP-1	monocyte chemoattractant protein-1
M-CSF	macrophage-colony stimulating factor
MHCI	major histocompatibility complex class I
MHCII	major histocompatibility complex II
MIN	mammary intraepithelial neoplasia
MME	metastatic microenvironment
MMP	metalloproteinase
MMTV-PyMT	mouse mammary tumor virus-polyoma middle T antigen
NCI	National Cancer Institute
NET	neutrophil extracellular trap
NF-κB	nuclear factor-kappaB
NIH	National Institutes of Health
NK	natural killer
NS	not significant
NSCLC	non-small cell lung cancer
Ob-R	obesity receptors
ORR	objective response rate
OS	overall survival
PBS	phosphate buffered saline
PD-1	programmed cell death-1
PD-L1	programmed death-ligand 1
PD-L2	programmed death-ligand 2
PFS	progression free survival
PI3K	phosphoinositide 3-kinase
PLX3397	Pexidartinib
PMAI	phorbol myristate acetate and Ionomycin

PR	progesterone receptor
QC	quality control
RT	room temperature
Stim	stimulated
SARS-CoV2	severe acute respiratory syndrome coronavirus 2
SD	standard deviation
SEM	standard error of the mean
TAM	tumor associated macrophage
TBST	Tris-buffered saline with 0.1% Tween® 20 detergent
TCF1	T cell factor 1
TCR	T-cell receptor
TGF-b1	transforming growth factor- beta 1
Th	T helper cell
TIGIT	T cell immunoreceptor with immunoglobulin and ITIM domain
TIL	Tumor infiltrating lymphocytes
TIM-3	T-cell immunoglobulin and mucin domain-3
TLR	toll-like receptor
TME	tumor microenvironment
TNBC	triple negative breast cancer
TNF-a	tumor necrosis factor-alpha
Treg	regulatory T cell
Un	unstimulated
VAT	visceral adipose tissue
VCAM-1	vascular cell adhesion molecule-1
VEGF	vascular endothelial growth factor
VISTA	V-domain immunoglobulin suppressor of T-cell activation
WAT	white adipose tissue
WT	wild type
ZNF217	zinc finger protein 217

CHAPTER 1:

Introduction

Obesity and Breast Cancer Risk

Obesity is defined as having a body mass index (BMI) of ≥30 kg/m^2 (1) and is associated with higher risk for many cancers, including breast cancer (2). Obesity is a risk factor for breast cancer in postmenopausal women, particularly, estrogen receptor alpha (ERα) and progesterone receptor (PR) positive breast cancer, while the risk for triple negative breast cancer (TNBC), which lack receptors for ERα, PR, and human epidermal growth factor receptor 2 (HER2), are minimally associated with obesity in this group of aging women (3) (4). For premenopausal women, the association between obesity and risk for different breast cancer subtypes is less clear. Multiple studies suggest that premenopausal women who are obese have a lower risk for breast cancer (5-7). However, other studies show an increased risk for breast cancer in premenopausal women of Asian-Pacific populations (8, 9). While other studies show that premenopausal women with obesity have an increased risk for TNBC (9, 10). Increased BMI may also be associated with higher risk of TNBC and a lower risk of ERα+ cancer particularly in nulliparous women (11). The risk for HER2+ breast cancer appears to be unaffected by obesity, however women diagnosed with HER2+ breast cancer may have worsened outcomes following diagnosis (12). Overall, the influence of obesity as a risk factor for breast cancer is dependent on stage of life, ethnicity, and expression of hormone receptors.

Once breast cancer develops, women with obesity have higher mortality rates (13). At the time of diagnosis, patients who have breast cancer and obesity have higher grade and more progressed tumors (14). Patients who are obese also develop metastasis more frequently than their lean counterparts and have a higher risk of dying from their disease

(15, 16). One analysis found a 36.1% increase in overall mortality risk due to obesity was potentially related to tumor characteristics (stage at diagnosis, grade, tumor size, and nodal status at the time of diagnosis) while 38–41% of patients with luminal subtypes (ERα +, PR+/-, HER2 +/-) had an increased mortality risk. However, breast cancer specific mortality was not different for TNBC and HER2+ tumors, compared to ERα+ tumors (17). These results suggest that mortality due to obesity was due partially to higher grade tumors and progression but also due to cardiovascular pathology, other systemic disorders, and treatment mortality related to obesity. Other studies confirm that breast cancer patients with ERα+ tumors have worse overall and disease-free survival with increased risk for metastasis (18, 19). Breast cancer recurrence has also been associated with weight gain in both postmenopausal and premenopausal women (20). Interestingly, one study found a higher association of ERα- tumors in patients with obesity and worse chance of having pathological complete response and reduced overall survival regardless of cancer subtype following chemotherapy (21) Overall, obesity is associated with poor outcomes, faster progression to metastatic disease, higher risk for recurrence and higher mortality whether it relates to breast cancer or other factors.

Breast Density

Breast density is defined as having higher proportions of glandular and fibrous tissue in the breast as opposed to fatty tissue according to the National Cancer Institute (22). Women with highly dense breasts of >75% have a 4 to 5-fold increase in the risk for developing breast cancer compared to women with low breast density (23). Breast density is heterogeneous and can make up a majority of the space of the breast, or breasts can have scattered areas of density. Breast tissue density widely varies based on a woman’s

age, menopausal status, BMI, parity, and genetic predisposition. Density generally reduces with age and after the transition to menopause (24). However, the prevalence of breast density effects a significant number of women. Of women 25-29 years of age, 39% had very dense breasts, with density making up ≥90% of the total breast area. Of this same age group, 39% had mostly fatty breast and by the age of 75-79, this increased to 76% of women having predominantly fatty breasts (≥50%) and only 6% having very dense breasts. Although breast density decreases after menopause, in this same study, it was shown that nearly half of women ages 40-44 and 50-79 that were undergoing hormone replacement therapy had dense breasts (25). This study highlights the predominance of breast density among young women but also the effects of hormone replacement after menopause in increasing density (26). In the U.S., it has been shown that 43.3% of women 40-74 had heterogeneous to extremely dense breast, and this was again shown to be inversely associated with age and BMI (27). Recent studies have shown a higher level of density compared to more scattered density can increase breast cancer risk 2-fold (28). Other studies have defined an increase of 10% risk for a 3-6% increase in density (29). Studies are mixed in whether breast density affects the risk for specific subtypes of breast cancer. (30). Breast density is a risk factor for breast cancer because it lowers sensitivity and specificity of mammograms compared to women with higher levels of fat in breasts (31). Digital mammography is now more effective for detecting cancer in women with extremely dense breasts compared to screen-film mammography (32). Despite improved imaging, breast density is still such a prominent risk factor it's a law for physicians to inform women of their breast density status through the Breast Density Notification Act (BDNA) in states like Pennsylvania (33). However, most recently,

the Food and Drug Administration (FDA) has enforced breast density to be included on mammogram reports as a national standard in March of 2023 (34). As screening methods improve, recent work has uncovered that the microenvironment of dense breast tissue may affect risk, rather than simply causing an obstruction to accurate diagnostic imaging.

Breast Density and Risk Mechanisms

Recent work has shown that dense breast tissue is more inflammatory, with increased levels of extracellular IL-6, IL-8, and CCL5, CD45+ immune cells, and CD206+ M2 alternatively activated macrophages (35, 36). Further characterization of immune cells also revealed increased B lymphocytes and dendritic cells with elevated expression of IL-6, IL-8, and interferon-gamma (IFN-γ) in dense tissue (37). These findings may suggest that one way that breast density may contribute to breast cancer risk is through tumor promoting chronic inflammation, which is a hallmark for cancer risk (38, 39). Further, after tumor formation, in a mouse model with excess collagen I, neutrophils have been shown to promote tumor formation and metastasis (40). Overall, these data suggest that the immune mediated progression of breast cancer in dense extracellular matrix (ECM) environments may be different than those that originate in less dense environments.

Although immune cell infiltration has shown to be different for dense breasts, the expression of proliferation markers and hormone receptor expression has shown to be similar. Ki67, ERα, and PR have all been shown to be similar in expression between dense and non-dense breasts in humans (36, 41, 42). However, dense breast tissue has a higher level of stroma in addition to glandular tissue in dense breast patients (41, 42).

Although epithelial ERα expression is not associated with breast density, Gabrielson et. al. showed stromal cell ERα expression was enhanced in dense breast tissue. This study suggests that there may be differences in hormonal regulation within the stromal compartment of breasts with higher density. Given that the stromal compartment of dense breasts has higher expression of ERα, inhibition of estrogen signaling could be particularly beneficial for women with high breast density. Supporting this idea, tamoxifen use led to reduced breast density and subsequently breast cancer risk in some women (43).

Although stroma may not affect ERα expression in the epithelium, stiffness of stroma can induce oncogenes such as zinc finger protein 217 (ZNF217) in breast epithelium (44). Stiffened ECM has also been shown to induce phosphoinositide 3-kinase (PI3K) signaling and increase transformed pre-malignant epithelial invasiveness (45). In addition to oncogenic changes and altered cell signaling, breast density has been associated with increased numbers of epithelial columnar cells, which may be an indicator for increased risk of cancer development but are not cancerous cells (46). In mouse models, increased stromal collagen enhances tumor formation and metastasis (47). Indicating breast density's ability to increase risk but promote tumorigenesis and metastasis.

Obesity and Breast Density

While increased BMI and elevated breast density both raise the risk for breast cancer in postmenopausal women, obesity is generally associated with reduced

radiographic breast density. However, there are populations of women who have both risk factors. In a population of Korean women, obesity and breast density were shown to increase risk for breast cancer compared to women who were underweight with a BI-RADS category-1 score (low density). This risk was more than three times higher in postmenopausal women than premenopausal women (48). Although this study was limited to Korean women, other populations of women may also have an interaction between these two risk factors. In particular, black women show a 37% rate of breast density (4th highest) and the highest rate of obesity at 58.4% (49). Shieh et. al. also showed an increased risk associated with combined breast density and obesity. However, the interactions identified were specific to premenopausal women and ERα- breast cancer not ERα+ breast cancer (50). Recent data shows that after menopause, density declines in the breast, and with a larger BMI, this decline in density is faster than in women with a BMI in the normal range (51). However, obesity may impact the percent of the tissue defined as dense rather than reducing areas defined as dense. While, weight loss over time was associated with increased percent breast density (52, 53), the total dense area of the breast was not altered with a change in weight, rather weight loss decreased the total non-dense breast area (53). Little is known about changes in the breast microenvironment that occur in dense breast tissue with obesity.

Potential Interactions between Obesity and Breast Density

Macrophages within the mammary gland in obesity include both resident macrophages and those that are recruited from the bone marrow. Monocyte chemoattractant protein-1 (MCP-1/CCL2) levels are increased in response to obesity and

facilitate macrophage infiltration (54). Increased macrophage infiltration and the development of crown-like structures (CLS), which are formed by macrophages surrounding necrotic adipocytes, are hallmarks of obesity (55). Free fatty acid release by dying adipocytes and the dysregulation of lipid metabolism upregulates inflammatory factors by adipocytes and macrophages (56). Free fatty acids activate nuclear factor-kappa B (NF-κB) and c-Jun N-terminal kinase (JNK) pathways to further promote inflammation by binding to toll-like receptors (TLR) (57). This then upregulates CCL2 furthering macrophage infiltration (58). CLS have been shown to strongly correlate with BMI in healthy breast tissue, with breast tissue from individuals with BMI ≥30 kg/m^2 having the most CLS (59). Macrophages have also been shown to upregulate IL-1β, IL-6, and tumor necrosis factor-alpha (TNF-α) in response to leptin (60), which is elevated in adipose tissue in obesity. While some of these cytokines are also elevated in dense breast tissue, differences in immune cells in the mammary glands in the context of obesity and breast density have not been explored. While macrophages are greatly enhanced in the context of obesity, it is not clear how the complement of immune cells or their function change when both obesity and breast density are present.

In addition to inflammation, obesity also enhances fibrosis in mammary tissue (61-63). Obesity-associated fibrosis and extracellular matrix deposition have been linked to insulin resistance in several studies (64, 65). Mechanisms underlying the increases in collagen and extracellular matrix observed in obesity have recently been reviewed (62). In addition to increasing collagen around adipocytes, obesity has been shown to increase collagen and fibronectin around mammary ducts (66, 67). While obesity promotes some fibrotic changes within mammary tissue, it is not clear if obesity could enhance further

collagen deposition in areas of breast tissue that are already dense. Further studies are necessary to determine how obesity impacts collagen deposition with the risk factor of breast density.

Immune Checkpoint Blockade Therapy

Immunotherapy has become a routine approach to personalized cancer treatment. Immunotherapy is a category of cancer treatment which acts to reprogram or assist the immune system in clearing tumorigenic cells and facilitating anti-tumor immunity (68). The ideal immunotherapy is potent against tumor cells, protects normal cells, and is sustained over a long period of time, preventing relapse (69). A major class of immunotherapies target immune checkpoints. Immune checkpoints function as immunosuppressors by mitigating immune responses and preventing self-antigen autoimmunity. The checkpoint ligands are present on cancer cells, immune cells, or somatic cells and bind to receptors on other immune cells to affect their function (70, 71). The binding of the ligands to the receptors results in downstream signaling that decreases immune cell reactivity. Immune checkpoints can be utilized by tumor cells to evade cytotoxic T lymphocytes by shutting down their proliferation and secretion of cytotoxic proteins. Antibodies designed to block the binding of checkpoint proteins with their partner proteins are utilized for immune checkpoint blockade (ICB) therapy. Two targets for ICB that shown therapeutic efficacy are cytotoxic t-lymphocyte protein-4 (CTLA-4) and programmed cell death protein 1/ programmed death ligand-1 (PD-1/PD-L1). Their function is to control T lymphocyte activation and maintain immune homeostasis. Anti-CTLA-4 (ipilimumab), anti-PD-1 (nivolumab, pembrolizumab, cemiplimab), and anti-PD-L1 (atezolizumab, avelumab,

durvalumab) therapies are all FDA approved for various cancers, mostly for advanced or metastatic disease (72).

Currently, pembrolizumab is FDA approved for treatment of advanced TNBC in conjunction with chemotherapy (73). In a clinical trial that selected for patients with pretreated metastatic PD-L1+ TNBC, patients that received pembrolizumab as a single agent only had an 18.5% response rate (74). The mechanisms behind why targeting immune checkpoints with antibody-based therapies are more effective in some patients with breast cancer is not widely understood. Data from clinical trials suggests that cancer patients with obesity that have solid tumors have an increased response to checkpoint therapy (75) (76). Recent data has shown these trends in breast cancer models in obese mice (77). Further studies are necessary to examine how obesity may impact immune cell function to enhance immunotherapy responses.

T Cell Dysfunction

T cells can demonstrate dysfunction through exhaustion, anergy, and senescence. T cell exhaustion has been identified in T cells that have distinct epigenetic and transcriptional phenotypes, loss of effector functions, and prolonged and increased expression of inhibitory markers, such as PD-1 (78, 79). CD8+ T cells as well as CD4+ T cells can express PD-1 (80). Beyond PD-1, other markers for immune exhaustion have been identified, including CTLA-4, T-cell immunoglobulin and mucin domain-3 (TIM-3), lymphocyte activation gene-3 (LAG-3), T cell immunoreceptor with immunoglobulin and ITIM domain (TIGIT), B- and T-lymphocyte attenuator (BTLA), V-domain immunoglobulin suppressor of T-cell activation (VISTA), and glucocorticoid-induced tumor necrosis factor

receptor-related protein (GITR) (81-83). In contrast to chronically stimulated, exhausted T cells, anergic T cells that lacked co-stimulation are thought to be induced to prevent autoimmunity and induce self-tolerance (84). Anergy occurs due to a lack of co-stimulation by CD28 or high inhibitory signals by CTLA-4 (85, 86) and is characterized by low IL-2 production, inhibited TCR signaling, and cell cycle arrest. Anergic T cells can also express PD-1, LAG-3, and CTLA-4 similar to exhausted T cells, which makes identification of anergic cells challenging. Finally, senescent T cells can be defined as having shortened telomeres, complete cell cycle arrest, express IL-2, TNF-α, and IFN-γ, and loss of CD28 expression (87). DNA damage has also been shown to trigger cellular senescence in T cells (88). Since dysfunctional T cells can express overlapping markers, use of one marker such as PD-1 clinically to identify patients with potential to respond to PD-1 directed therapy may contribute to challenges in identifying patients for treatment. Further, activation of T cells in these other states may reduce the efficacy of PD-1-directed therapies (89).

PD-1 Binding and Signaling with PD-L1 and PD-L2

PD-1 has two ligands PD-L1 and PD-L2. PD-L2 has a 2-6 fold higher binding affinity to PD-1 than PD-L1, and different binding kinetics may affect immune cells function (90). Although both PD-L1 and PD-L2 can be expressed on tumor cells, PD-L1 expression is more common. (91). Therapies targeting the PD-1 pathway are focused on PD-1 and PD-L1. PD-1 functions on multiple types of cells to balance immune regulation, self-antigen tolerance, and prevent abnormal immunopathology. A lack of PD-1 expression leads to autoimmunity in mice and leads to T cell proliferation, suggesting that

this pathway has potent effects on dampening T cell function (92). In the context of cancer, the PD-1 pathway dampens T cell function and ultimately leads to immune evasion of cancers due to upregulation of both PD-L1 and PD-L2 on cancer cells.

For PD-1 binding to limit T cell function, the T cell must bind to the MHCI receptor as well as PD-L1 or PD-L2 on an antigen-presenting cell, normal somatic cell, or tumor cell. Signaling in T cells due to PD-1 binding counteracts T cell receptor activation by MHCI and co-stimulation by CD28 and CD80. PD-1 signaling results in lower T cell proliferation, cytokine production, and reduces survival (91). PD-L1 can also interact with costimulatory molecule CD80 to diminish T cell responses (93). Studies show that PD-1 null T cells still have lower proliferation in the presence of PD-L1, which may indicate that PD-1 expression alone should not be used as a predictor of anti-PD-L1 therapy response in breast cancer (94).

Macrophages alter the function of CD8+ T cells by upregulating PD-L1 expression on tumor cells. In multiple breast cancer cells lines, TNF-α production by macrophages activated the NF-κB pathway and upregulated CNS5, a de-ubiquitination enzyme that stabilized PD-L1 in cancer cells (95). PD-L1 is also expressed on antigen presenting cells, like macrophages, dendritic cells as well as lymphocytes, T cells and B cells (96). PD-L1+ antigen presenting cells decrease IFN-γ, TNF-α and lL-2 expression by PD-1+ T cells (97), (98). IL-2 is particularly important for preventing T cell apoptosis and triggering T cell expansion, which may explain in part how macrophages contribute to lower CD8+ T cell numbers within tumors. In an orthotopic breast cancer model, progranulin upregulated PD-L1 on macrophages and as a consequence decreased infiltrating CD8+ T cells (99).

PD-L1 can also increase NO (nitric oxide) production by macrophages, another inhibitor of T cell proliferation (97).

In addition to tumor cells and antigen-presenting cells, PD-L1 is also expressed on endothelial cells. Expression of PD-L1 on endothelial cell reduces T cell recruitment into the tumor microenvironment by limiting T cell activity or proliferation. PD-L1 and PD-L2 are upregulated on endothelial cells in part due to increased concentrations of inflammatory cytokines like IFN-γ and TNF-α (100, 101). The density of PD-L1 expression on the endothelium could reduce the ability of PD-1+ T cells to invade intratumorally. As angiogenesis is increased in mammary tumors in mice (102), and macrophages demonstrate increased TNF-α expression in obesity (103), PD-L1 and PD-L2 expression by the endothelium could contribute to lower T cell recruitment and dampened effector function observed in breast tumors in obesity (101, 104). However, other mechanisms have been demonstrated to explained dampened T cell function in obese breast tumors including the role of other immunosuppressive myeloid cells and altered metabolism (105, 106).

Overall, in breast cancer, further studies are needed to define how PD-1 binding to PD-L1 and PD-L2 affects tumor cells, antigen presenting cells, and T cells. Signaling of PD-1 with PD-L1 or PD-L2 may be different within T cells and antigen presenting cells in the tumor and metastatic environment in the context of obesity. Further work is necessary to understand the mechanisms of how anti-PD-1 and anti-PD-L1 therapies alter cellular signaling to improve patient outcomes.

Identification of Immune Checkpoint Blockade Therapy Response

CD8+ T cells infiltrated into the tumor are valued as a positive predicter of responses to PD-1/PD-L1 therapy (107). Increased lymphocytes within the tumor are associated with better responses because contact between tumor cells and T cells is required to facilitate cytotoxicity and the destruction of tumors cells via the interaction of MHC antigens and T cell receptors. Increased levels of lymphocytes including cytokines in T cells in the periphery were associated with increased response to anti-PD-1 in patients with non-small cell lung cancer (NSCLC) (108). However, PD-1 expression on CD8+ T cells is not solely a strong predictor of response to anti-PD-1 therapy (109). In models of melanoma, some PD-1+ cells were less responsive to proliferation following ICB therapy (110), and stem-like T cell factor 1 (TCF1+) PD-1+ CD8+ T cells were identified as the target for ICB response (111). Other studies suggest that a higher number of circulating TIGIT+ PD-1+ T cells may predict response (81). The discovery of additional markers for response may improve selection of patients for ICB therapy (112).

Despite the focus on the CD8+ subset, other T cell subtypes could influence therapy response. CD4+ T cells are functionally divided into T helper cell 1 (Th1), Th2, Th17 and Treg cells. Recent studies demonstrated that CD4+ T cells, largely Th1 cells, supported the ability of CD8+ T to differentiate, form memory, have more migratory behavior, and support cytotoxic killing and survival (113). Increased circulating PD-1+ CD4+ cells in peripheral blood was associated with better responses to PD-1-directed ICB therapy in melanoma and NSCLC (114). CD4+ Th1 polarity was also associated with patient response, and polarization to Th17 rather than Th1 may be unfavorable for response in models of prostate cancer (115). Additionally, CD4+ Treg cells can have a

negative impact on ICB responses. PD-1+ Treg cells have immunosuppressive functions in response to ICB therapies. Therefore, a higher PD-1+ CD8+ T cell to PD-1+ Treg cell ratio may be more favorable for therapy response (116).

In addition to immune cells, PD-L1 expression on tumor cells has been correlated with improved responses to checkpoint therapy (117), (118). Different subtypes of breast cancer are known to have different levels of PD-L1 and PD-L2 expression. However, it has been shown that there is not a difference in PD-1 or PD-L1 expression between TNBC, Luminal A, Luminal B and HER2+ subtypes in one study either in the primary tumor or metastatic lymph nodes (119), although the sample sizes were limited. Certain breast cancer subtypes also have increased PD-L1 expression on tumor cells compared to other subtypes, including HER2+ and basal-like breast cancers (120) (117).

Increased mutational load in tumors have been attributed to improved efficacy of PD-1/PDL-1 therapy. Elevated mutations lead to more novel and abundant neoantigen presentation that allows T cells to recognize tumor cells more efficiently. Genetic characteristics that have been shown to enhance ICB therapy results include loss of tumor suppressor genes, activation of oncogenes, microsatellite instability, chromosome modifications, and BRCA1/2 mutations ((121); (122),(123);(124)). TNBC with BRCA1 mutations have shown to have improved ICB responses when dual anti-CTLA4 and anti-PD-1 therapies are combined with chemotherapy (125). TNBC identified with high mutational burdens have better pathological complete response with PD-L1 inhibitors in addition to anthracycline chemotherapy (126).

Combined therapies that increase tumor neoantigens may also increase the efficacy of ICB. For example, chemotherapy kills tumor cells and releases tumor

neoantigens. This can augment T cell immune responses. Chemotherapy also increases the availability of antigens presented by antigen presenting cells and facilitates immune cells recruitment, while ICB therapy can then reverse T cells exhaustion (127). Through a similar mechanism, radiation therapy could augment ICB responses, as radiation has also been shown to increase diverse intratumoral T cells(128).

Immune Checkpoint Blockade in Breast Cancer Subtypes

ERα+ breast cancers have a lower response rate to ICB than that of TNBC, and they are generally thought to be immunogenically “cold” due to limited infiltration of T cells (129, 130). The objective response rate of in patients with ERα+ breast cancer treated with anti-PD-1 therapy has been shown to be 12%, unlike 18.5% seen in TNBC (131). However, a subset of ERα+ tumors may have characteristics that may indicate they may be vulnerable to PD-1/PD-L1 inhibitors. Tumor infiltrating lymphocytes are present in poorer prognosis ERα+ tumors (132) which may indicate these patients could benefit from ICB. Further, one study found 33% of ERα+ cancers had elevated PD-L2 expression levels, which may indicate a potential response to anti PD-1 therapies or possibly future drugs targeting PD-L2 (133). A recently updated clinical trial will examine responses of patients with ERα+ breast cancer treated with pembrolizumab and neoadjuvant chemotherapy and adjuvant endocrine therapy. This study is set for completion in 2031 (134).

In early stage, high-risk, non-metastatic TNBC, pembrolizumab used with chemotherapy has been shown to have promising results for improved survival outcomes. Specifically, across cohorts which received the same dosage of ICB with different chemotherapy regimens, overall survival at twelve months ranged from 80-100% (135).

Interestingly, pembrolizumab as a monotherapy did not elicit a response better than chemotherapy alone, showing the importance for augmenting ICB with other standard of care regimens (136). Clinical trials examining atezolizumab (anti-PD-L1 antibody) with nab-paclitaxel chemotherapy in advanced TNBC have shown a progression-free survival rate of 29.1%. Further, patients with PD-L1+ tumors had a 58.9% response rate with 10.3% of patients demonstrating complete response. Patient survival was drastically improved in patients that received chemotherapy with ICB compared to the placebo which led to FDA approval of atezolizumab (118). This data shows that responses to ICB are not universal and need to be complimented with other interventions.

In HER2+ breast cancer, patients with trastuzumab-resistant HER-2+ breast cancer treated with pembrolizumab in conjunction with trastuzumab showed a 15% response in PD-L1+ patients and no response in PD-L1- patients (137). A subset of patients that have HER2 antagonist resistant breast cancers that express PD-L1 may be responsive to treatment with ICB. Currently, there is a study recruiting HER2+ breast cancer patients to receive pembrolizumab in combination with dual anti-HER2 blockade with trastuzumab and pertuzumab (138)

Macrophage Anti-CSFR1 Therapy

Macrophage depletion targeting the macrophage colony stimulating factor-1 (m-CSF/CSF-1) axis is a promising target currently used in cancer treatment. CSF-1R binds to both CSF-1 and IL-34 (139). Small molecule tyrosine kinase inhibitors prevent autophosphorylation of CSF-1R and stop cytosolic signaling transduction by targeting the intracellular domain of the receptor (140). Small molecules that have been developed

include PLX3397 (Pexidartinib), JNJ-40346527, PLX7486, ARRY-382 and BLZ945. PLX3397 gained FDA approved for the treatment of advanced tenosynovial giant cell tumors in 2019 (141). These small molecules have entered several clinical trials that have not yet reached completion or FDA approval, and results from these ongoing studies are limited (140). ARRY-382 is currently being investigated in combination with pembrolizumab for the treatment of TNBC and other solid tumors. While interim results of this study showed limited clinical benefit, the combination of therapy was tolerable (142). Antibodies targeting CSF-1R block the interaction of CSF-1R with CSF-1/IL-34 on its extracellular domain. Antibodies that target the receptor ligand binding domain include cabiralizumab (FPA008), AMB-05X (AMG 820), LY3022855/IMC-CS4, and axatilimab (SNDX-6352). Antibodies have also been developed that bind to the ligand CSF-1, including lacnotuzumab (MCS110) and PD-0360324 (143).

While CSF-1R is highly expressed on monocytes and macrophages (144, 145), CSF-1R is also expressed on other cell types that may inhibit the efficacy of this potential treatment. CSF-1R is expressed on myeloid dendritic cells (146), and depletion of these cells could also impact antigen presentation to T cells in PD-1 directed therapy. In addition, CSF-1R is also expressed on cells present in sites of potential metastasis including osteoclasts in bone, microglia in the brain, and alveolar cells in the lungs (147))(145, 148). These additional sites of expression of CSF-1R may contribute to off-target toxicities that will need to be monitored in clinical trials.

CSF-1R antibodies have been used successfully to deplete macrophages in breast cancer models. Blocking of CSF-1R increased the number of CD8+ T cells in the mouse mammary tumor virus-polyoma middle T antigen (MMTV-PyMT) model (149). In

combination with cyclophosphamide, antibody treatment against CSF-1R, and small molecule inhibition of CSF-1R lead to regression of multiple TNBC models and depletion of macrophages in T12 tumors (150). However, this response was dependent on elevated expression of *Csf1r.* This combination treatment was also successful in increasing central and effector memory CD8+ T cells within tumors compared to monotherapy alone (150). PLX3397 in combination with paclitaxel reduced metastasis and primary tumor growth by improving T cell responses in multiple TNBC models (151). Thus, multiple types of chemotherapy in combination with macrophage depletion therapy, either by agonist antibodies or small molecule inhibitors improved anti-tumor responses in breast cancer. Adding anti-PD-1/PD-L1 inhibitors to chemotherapy and anti-CSF-1R may be a robust strategy in treating some TNBC patients. However, CSF-1R treatments may not be limited to use in TNBC patients, since tumor CSF-1R expression has been associated with poorer prognosis in patients with ER+ disease (152).

In pre-clinical models, the use of CSF-1R directed therapy in combination with ICB improved therapy responses. Depleting macrophages via CSF-1R has been shown to improve T cell recruitment to tumors and metastasis in a model of osteosarcoma (153). Anti-CSF-1R treatment has also been shown to increase T cell activity and upregulate PD-1 on T cells (154). In a lung cancer model, treatment with combinations of anti-CSF-1R, anti-PD-1, anti-angiogenic therapy, or chemotherapy did not improve CD8+ T cell recruitment to tumors compared to the combination of PD-1 therapy and anti-angiogenic therapy (155). In some cancer types, anti-CSF-1R treatment may also reduce T regs which in higher numbers can negatively affect anti-PD-1 responses (156). In addition to upregulating PD-1 on T cells, targeting CSF-1R also increased PD-L1 on pancreatic

tumor cells (154). In a 4T1 mammary tumor model, PLX depletion of CSF-1R+ macrophages reduced metastasis and prolonged survival (157). Similarly in MET-1 mammary tumors, a combination PLX and anti-PD-1 therapy also reduced tumor size (158). The anti-tumor effects of combining CSF-1R treatment with anti-PD-1 therapies could further be augmented by adding additional immunotherapy targets. In a model of pancreatic cancer, a combination of anti-CSF-1R, anti-PD-1, and anti-CTLA4 therapy improved responses compared to either monotherapy alone or anti-CTLA-4 plus anti-PD-1 therapy (154). Overall, anti-CSF-1R depletion of macrophages increased T cell infiltration, activated T cell responses, and reduced immunosuppressive immune cells.

Obesity and Immune Checkpoint Blockade Therapy

The “obesity paradox” is the observation that, although obese patients have a worse prognosis when diagnosed with cancer, they have better ICB responses than patients with a BMI in the normal range. A cohort of patients with a BMI ≥30 kg/m^2 that had multiple types of cancer had a longer progression-free survival and overall survival compared to patients with a BMI ≤30 kg/m^2 when treated with anti-PD-L1 therapy (75). Another study examining 20 different stage IV metastatic cancer types, progression-free survival for patients with obesity (BMI >30 kg/m^2) on ICB was 479 days compared to 128 days for normal weight (BMI 18.5-25 kg/m^2) patients and 103 days for underweight (BMI<18.5 kg/m^2) patients (159). In men with NSCLC, a BMI in the obese range was associated with improved overall survival on atezolizumab (anti-PD-L1) but not in patients treated with docetaxel alone. The strongest association with BMI and improved overall survival was in patients with high PD-L1 expression including ≥50% of tumor cells or

≥10% of tumor-infiltrating immune cells (160). In melanoma, patients with a BMI in the obese range had longer progression free survival on anti-PD-1/PD-L1 therapy than patients with a BMI in the lean range, but only in male patients (7.6 vs. 2.7 months) (161). These results suggest that there may be sex differences in ICB therapy responses. In contrast, patients with renal cancer who have a BMI in the normal range have a better response to ICB therapy than patients with obesity, which may be due in part to elevated circulating IL-1β levels in patients with obesity (162). Although there is supported evidence that obese patients have better survival on ICB than lean patients, there is evidence that obese patients have an increase incidence of immune-related adverse events (IrAEs), such as myocarditis, colitis, or autoimmune diabetes, when treated with PD-1 therapy in a variety of malignancies (163, 164).

Preclinical models have provided some insight into these clinical observations. In a murine breast cancer model, obese mice had higher numbers of PD1+ CD8+ T cells in tumors, which expressed lower levels of *Ifnγ* and *Gzmb* (165). These results suggest that targeting the PD-1/PD-L1 pathway may be more efficacious in obesity due to elevated exhausted CD8+ T cells. Metabolically, obesity may also alter the function of immune cells. In the MMTV-PyMT model, elevated leptin levels in obese mice led to increased STAT3-mediated fatty oxidation in CD8+ T cells, which inhibits T cell function (105). Regardless of obesity, glucose restriction by tumors dampens glycolysis and the ability of T cells to produce IFN-γ, however glycolysis and T cell function is restored following treatment with anti-CTLA-4, PD-1, and PD-L1 antibodies (166). These results suggest that obesity may create an environment conducive to CD8+ T cells with the ability to respond to PD-1 directed therapy.

Obesity and Lung Metastatic Environment

In breast cancer, the immune cells in the tumor microenvironment (TME) differ from immune cells in the metastatic microenvironment (MME) (167). In contrast to primary mammary tumors, the metastatic site of the lungs has a greater number of neutrophils (168). Neutrophils have the ability to transfer lipid to metastatic cells, promoting proliferation and survival (169). Neutrophils also form neutrophil extracellular traps (NETs), which function as traps for pathogens like bacteria, and primary tumors at distal sites can promote the formation of NETs to facilitate metastasis in the lungs (170). While NETs can be thought of as traps for cancer cells, but they also induce signaling and attract cancer cells through CCDC25 (171). Under conditions of obesity, neutrophils are increased in the lungs of mice without mammary tumors as well as after tumor formation and metastatic growth (172, 173) Increased neutrophilia in the lung has been shown to be dependent on elevated levels of granulocyte macrophage-colony stimulating factor (GM-CSF) and IL-15 (174). One potential mechanism for increased metastasis in the lungs in obesity is through elevated NET formation from neutrophils in the lungs. NETs have been shown to diminish endothelial integrity leading to an influx of tumor cells into the lung parenchyma (173). However, further studies are needed to fully understand how neutrophils promote metastatic progression under conditions of obesity compared to metastasis under lean conditions.

Dendritic cells are another important myeloid lineage cell type present in the lungs that contributes to anti-metastatic immunity. Dendritic cells take up metastatic cell material in the lungs, travel to the mediastinal lymph nodes, and stimulate T cell responses. However, only CD103+ dendritic cells were able to stimulate CD8+ T cells

(175). In a melanoma model, monocyte-dendritic progenitor cells were found to be switched to an M2 macrophage-like phenotype in the lungs in an IL-6-dependent manner (176). Overall, this shows how dendritic cell precursors can contribute to metastasis.

Macrophages have been shown to be important for metastatic seeding, particularly to the lungs. There are two main resident populations of macrophages within the lungs: alveolar macrophages and interstitial macrophages. Alveolar macrophages are localized in the airway lumens and sample pathogens in the airways, which is critical for inflammatory responses and regulating fibrotic tissue repair (177, 178). In breast cancer metastasis, there has also been shown to be an abundance of lipid-associated macrophages, mostly alveolar macrophages (179). Alveolar macrophages promoted breast cancer metastasis to the lungs by suppressing anti-tumor T cells and increasing the polarization of T helper cells to Th2 (180). In obese mice, macrophages contribute to the formation of premetastatic niches in the lung (172, 181) and surround metastatic lesions (172). In both premetastatic niches and metastases, macrophages upregulated the SphK1/S1P/S1PR1 axis, leading to higher production of proinflammatory cytokines such as IL-6 in obesity (181). Although proinflammatory cytokines are produced by macrophages in the lungs with metastases in obese mice, other studies have found that immunosuppressive macrophages are elevated (182). Immunosuppressive macrophages are abundant lung metastases in lean mice. Macrophages have been shown to upregulate antigen presentation, interferon signaling, extracellular matrix remodeling, immunosuppression, and decreased capacity for phagocytosis (179). Although the metastasis promoting influence of macrophages has been documented in the primary tumor and metastatic sites like the lungs, there are also macrophage subtypes

that have been shown to be important in metastatic clearance. CD169+ macrophages in lymph nodes undergo proliferative expansion in response to tumor burden and have been shown to be protective against breast cancer metastasis (183).

T cells in the lungs can influence the formation and growth of breast cancer metastasis. Lung stromal cells may influence the polarization of Th2 helper T cells, which have been shown to promote breast cancer metastasis (184). CD4+ T cells such as Tregs can be recruited to the lungs in response to breast cancer metastasis. In lungs with 4T1 metastases, CCR4+ Tregs were increased through elevated CCL17/CCL22 expression. Elevated Treg recruitment resulted in reduced NK cells, which are important mediators of metastatic clearance (185). There are also populations of T cells in breast cancer that can contribute to metastatic dormancy. CD39+ PD1+ CD8+ T cells in tumors were associated with increased disease-free survival and decreased metastasis (186).

Much of the current understanding of obesity-related immune dysfunction in the lungs has been identified in the context of viral infections. In influenza infection, T cell metabolism was impaired and T cell memory subsets were decreased in the lungs of obese mice (187). In addition to metabolism, others have found impaired effector functions of CD8+ T cells in the lungs of influenza-infected obese mice (188). Obesity in both humans and mice caused impaired response to vaccination for influenza (189, 190), and more recently severe acute respiratory syndrome coronavirus 2 (SARS-CoV-2) (191), suggesting that T cell function in lung tissue is impaired in the context of obesity. Further studies are needed to understand how T cell impairment prior to cancer formation affects metastatic seeding to the lungs.

Literature Summary and Thesis Rational

Epidemiologically, obesity and breast density have been shown to increase breast cancer risk and contribute to more progressed disease of breast cancer patients. However, little is known about how these two risk factors interact together to modify the microenvironment of the mammary gland to promote breast cancer growth. In Chapter 2, we will compare and contrast changes that occur in the mammary gland as a consequence of obesity and breast density using a high-fat diet model to induce obesity and transgenic mice with increased collagen deposition. We will examine how these risk factors act together within the microenvironment of the mammary gland to enhance tumor growth and metastasis using the MMTV-PyMT mouse model of mammary tumorigenesis.

Obesity contributes to more advanced metastatic disease at the time of breast cancer diagnosis and obese patients have a higher risk of metastatic recurrence. A few studies have begun to investigate how obesity affects the lung niche before cancer development and the immune microenvironment after metastatic establishment. Most studies looking at lung immunity in obesity are in the context of viral infection. However, in the context of breast cancer metastasis adaptive immunity has been minimally explored. In many cancer types, CD8+ T cells become dysfunctional during the progression of disease. Overall, these altered T cell states can lead to immune evasion by cancer cells and poorer overall outcomes. Furthermore, ERα+ breast cancers were previously thought to be unsuitable for immunotherapy. However, evidence suggests that some ERα+ tumors, such as the luminal B subtype, may have favorable outcomes on ICB therapy. In Chapter 3, we will investigate how adaptive immune cell populations change

before and ERα+ metastases in lean and obese mice to understand how obesity alters the function of adaptive immune cells.

Evidence shows low efficacy of anti-PD-1 inhibitors alone in both human and animal studies. Higher tumor-associated macrophages (TAMs) within tumors are associated with poorer prognosis and CD8+ T cell exclusion from tumors. Potential therapies to increase tumor infiltrating lymphocytes could enhance anti-PD-1/PD-L1 responses. Therefore, combining strategies to deplete tumor-associated macrophages with anti-PD-1/PD-L1 inhibitors is a logical strategy to improve anti-tumor responses of CD8+T cells. However, important questions remain in understanding how obesity alters the function of both CD8+ T cells and macrophages in the metastatic microenvironment. Further, it is also unclear how anti-CSF-1R and anti-PD-1 therapies will affect ERα+ breast cancer lung metastasis in lean and obese mice. In Chapter 4, we will explore how combined immunotherapy targeting macrophages and T cells impacts ERα+ lung metastasis in lean and obese mouse models and how obesity changes the response of immune cell populations. Our goal was to understand how the lung immune system responded to these therapies with or without a co-morbidity like obesity that changes the immune response.

Chapter 5 is a summary of this dissertation's conclusions and discusses future directions into further investigating the interactions of obesity and breast density. Further, this chapter will summarize how we can further define T cell subtypes and other adaptive immune cells in the lungs before and after breast cancer metastasis under obese conditions to understand why obese patients have higher metastatic burdens. Lastly, to discuss the future of immunotherapy for obese breast cancer patients, especially those

with advanced ERα+ metastasis. In Chapter 6, this dissertation will be concluded with a science literacy chapter to communicate the conclusions of this dissertation and how it fits with what is known about obesity's effect on breast cancer risk, progression, metastasis, and immunotherapy responses for non-scientists.

References:

1. WHO. Prevalence of obesity among adults, BMI >= 30 (crude estimate) (%) [Available from: https://www.who.int/data/gho/data/indicators/indicator-details/GHO/prevalence-of-obesity-among-adults-bmi--30-(crude-estimate)-(-).

2. Avgerinos KI, Spyrou N, Mantzoros CS, Dalamaga M. Obesity and cancer risk: Emerging biological mechanisms and perspectives. Metabolism. 2019 Mar;92:121-35. PubMed PMID: 30445141. Epub 20181113. eng.

3. de Waard F, Baanders-van Halewijn EA. A prospective study in general practice on breast-cancer risk in postmenopausal women. Int J Cancer. 1974 Aug 15;14(2):153-60. PubMed PMID: 4378317. eng.

4. ML N, AK A, RL P, JE M, R C, CL C, et al. Overweight, Obesity, and Postmenopausal Invasive Breast Cancer Risk: A Secondary Analysis of the Women's Health Initiative Randomized Clinical Trials. JAMA oncology. 2015 2015 Aug;1(5). PubMed PMID: 26182172.

5. Michels KB, Terry KL, Willett WC. Longitudinal study on the role of body size in premenopausal breast cancer. Arch Intern Med. 2006 Nov 27;166(21):2395-402. PubMed PMID: 17130395. eng.

6. Schoemaker MJ, Nichols HB, Wright LB, Brook MN, Jones ME, O'Brien KM, et al. Association of Body Mass Index and Age With Subsequent Breast Cancer Risk in Premenopausal Women. JAMA Oncol. 2018 Nov 1;4(11):e181771. PubMed PMID: 29931120. PMCID: PMC6248078. Epub 20181108. eng.

7. Baer HJ, Colditz GA, Rosner B, Michels KB, Rich-Edwards JW, Hunter DJ, et al. Body fatness during childhood and adolescence and incidence of breast cancer in premenopausal women: a prospective cohort study. Breast Cancer Res. 2005;7(3):R314-25. PubMed PMID: 15987426. PMCID: PMC1143575. Epub 20050218. eng.

8. van den Brandt PA, Spiegelman D, Yaun SS, Adami HO, Beeson L, Folsom AR, et al. Pooled analysis of prospective cohort studies on height, weight, and breast cancer risk. Am J Epidemiol. 2000 Sep 15;152(6):514-27. PubMed PMID: 10997541. Epub 2000/09/21. eng.

9. Renehan AG, Tyson M, Egger M, Heller RF, Zwahlen M. Body-mass index and incidence of cancer: a systematic review and meta-analysis of prospective observational studies. Lancet. 2008 Feb 16;371(9612):569-78. PubMed PMID: 18280327. Epub 2008/02/19. eng.

10. Pierobon M, Frankenfeld CL. Obesity as a risk factor for triple-negative breast cancers: a systematic review and meta-analysis. Breast Cancer Res Treat. 2013 Jan;137(1):307-14. PubMed PMID: 23179600. Epub 2012/11/28. eng.

11. Kawai M, Malone KE, Tang MT, Li CI. Height, body mass index (BMI), BMI change, and the risk of estrogen receptor-positive, HER2-positive, and triple-negative breast cancer among women ages 20 to 44 years. Cancer. 2014 May 15;120(10):1548-56. PubMed PMID: 24500704. PMCID: PMC4013221. Epub 2014/02/07. eng.

12. Sellahewa C, Nightingale P, Carmichael AR. Obesity and HER 2 overexpression: a common factor for poor prognosis of breast cancer. Int Semin Surg Oncol. 2008 Feb 24;5:2. PubMed PMID: 18294401. PMCID: PMC2266765. Epub 20080224. eng.

13. Chan DS, Vieira AR, Aune D, Bandera EV, Greenwood DC, McTiernan A, et al. Body mass index and survival in women with breast cancer-systematic literature review and meta-analysis of 82 follow-up studies. Ann Oncol. 2014 Oct;25(10):1901-14. PubMed PMID: 24769692. PMCID: PMC4176449. Epub 2014/04/29. eng.

14. Majed B, Moreau T, Senouci K, Salmon RJ, Fourquet A, Asselain B. Is obesity an independent prognosis factor in woman breast cancer? Breast Cancer Res Treat. 2008 Sep;111(2):329-42. PubMed PMID: 17939036. Epub 20071016. eng.

15. Ewertz M, Jensen MB, Gunnarsdóttir K, Højris I, Jakobsen EH, Nielsen D, et al. Effect of obesity on prognosis after early-stage breast cancer. J Clin Oncol. 2011 Jan 1;29(1):25-31. PubMed PMID: 21115856. Epub 20101129. eng.

16. Sestak I, Distler W, Forbes JF, Dowsett M, Howell A, Cuzick J. Effect of body mass index on recurrences in tamoxifen and anastrozole treated women: an exploratory analysis from the ATAC trial. J Clin Oncol. 2010 Jul 20;28(21):3411-5. PubMed PMID: 20547990. Epub 2010/06/16. eng.

17. Blair CK, Wiggins CL, Nibbe AM, Storlie CB, Prossnitz ER, Royce M, et al. Obesity and survival among a cohort of breast cancer patients is partially mediated by tumor characteristics. NPJ Breast Cancer. 2019;5:33. PubMed PMID: 31602394. PMCID: PMC6775111. Epub 2019/10/12. eng.

18. Sparano JA, Wang M, Zhao F, Stearns V, Martino S, Ligibel JA, et al. Obesity at diagnosis is associated with inferior outcomes in hormone receptor-positive operable breast cancer. Cancer. 2012 Dec 1;118(23):5937-46. PubMed PMID: 22926690. PMCID: PMC3586227. Epub 2012/08/29. eng.

19. Biganzoli E, Desmedt C, Fornili M, de Azambuja E, Cornez N, Ries F, et al. Recurrence dynamics of breast cancer according to baseline body mass index. Eur J Cancer. 2017 Dec;87:10-20. PubMed PMID: 29096156. Epub 20171031. eng.

20. Kroenke CH, Chen WY, Rosner B, Holmes MD. Weight, weight gain, and survival after breast cancer diagnosis. J Clin Oncol. 2005 Mar 1;23(7):1370-8. PubMed PMID: 15684320. Epub 20050131. eng.

21. Litton JK, Gonzalez-Angulo AM, Warneke CL, Buzdar AU, Kau SW, Bondy M, et al. Relationship between obesity and pathologic response to neoadjuvant chemotherapy

among women with operable breast cancer. J Clin Oncol. 2008 Sep 1;26(25):4072-7. PubMed PMID: 18757321. PMCID: PMC6557586. Epub 2008/09/02. eng.

22. NCI. Dense Breasts: Answers to commonly asked questions 2024 [Available from: https://www.cancer.gov/types/breast/breast-changes/dense-breasts#:~:text=Breast%20density%20is%20a%20term,amounts%20of%20fatty%20breast%20tissue.

23. Boyd NF, Rommens JM, Vogt K, Lee V, Hopper JL, Yaffe MJ, et al. Mammographic breast density as an intermediate phenotype for breast cancer. Lancet Oncol. 2005 Oct;6(10):798-808. PubMed PMID: 16198986. eng.

24. Kim EY, Chang Y, Ahn J, Yun JS, Park YL, Park CH, et al. Mammographic breast density, its changes, and breast cancer risk in premenopausal and postmenopausal women. Cancer. 2020 Nov 1;126(21):4687-96. PubMed PMID: 32767699. Epub 20200807. eng.

25. Stomper PC, D'Souza DJ, DiNitto PA, Arredondo MA. Analysis of parenchymal density on mammograms in 1353 women 25-79 years old. AJR Am J Roentgenol. 1996 Nov;167(5):1261-5. PubMed PMID: 8911192. eng.

26. Breast cancer and hormone replacement therapy: collaborative reanalysis of data from 51 epidemiological studies of 52,705 women with breast cancer and 108,411 women without breast cancer. Collaborative Group on Hormonal Factors in Breast Cancer. Lancet. 1997 Oct 11;350(9084):1047-59. PubMed PMID: 10213546. eng.

27. Sprague BL, Gangnon RE, Burt V, Trentham-Dietz A, Hampton JM, Wellman RD, et al. Prevalence of mammographically dense breasts in the United States. J Natl Cancer Inst. 2014 Oct;106(10). PubMed PMID: 25217577. PMCID: PMC4200066. Epub 20140912. eng.

28. Bodewes FTH, van Asselt AA, Dorrius MD, Greuter MJW, de Bock GH. Mammographic breast density and the risk of breast cancer: A systematic review and meta-analysis. Breast. 2022 Dec;66:62-8. PubMed PMID: 36183671. PMCID: PMC9530665. Epub 20220926. eng.

29. Palomares MR, Machia JR, Lehman CD, Daling JR, McTiernan A. Mammographic density correlation with Gail model breast cancer risk estimates and component risk factors. Cancer Epidemiol Biomarkers Prev. 2006 Jul;15(7):1324-30. PubMed PMID: 16835331. eng.

30. Yamada D, Ohde S, Kajiura Y, Yagishita K, Nozaki F, Suzuki K, et al. Relationship Between Breast Density, Breast Cancer Subtypes, and Prognosis. Clin Breast Cancer. 2022 Aug;22(6):560-6. PubMed PMID: 35581133. Epub 20220422. eng.

31. Carney PA, Miglioretti DL, Yankaskas BC, Kerlikowske K, Rosenberg R, Rutter CM, et al. Individual and combined effects of age, breast density, and hormone

replacement therapy use on the accuracy of screening mammography. Ann Intern Med. 2003 Feb 4;138(3):168-75. PubMed PMID: 12558355. eng.

32. Kerlikowske K, Hubbard RA, Miglioretti DL, Geller BM, Yankaskas BC, Lehman CD, et al. Comparative effectiveness of digital versus film-screen mammography in community practice in the United States: a cohort study. Ann Intern Med. 2011 Oct 18;155(8):493-502. PubMed PMID: 22007043. PMCID: PMC3726800. eng.

33. Gur D, Klym AH, King JL, Bandos AI, Sumkin JH. Impact of the new density reporting laws: radiologist perceptions and actual behavior. Acad Radiol. 2015 Jun;22(6):679-83. PubMed PMID: 25837723. Epub 20150330. eng.

34. FDA. Important Information: Final

Rule to Amend the Mammography Quality Standards Act (MQSA) [Available from: https://www.fda.gov/radiation-emitting-products/mammography-quality-standards-act-and-program/important-information-final-rule-amend-mammography-quality-standards-act-mqsa#:~:text=On%20March%2010%2C%202023%2C%20the,later%20than%20September%2010%2C%202024.

35. Abrahamsson A, Rzepecka A, Romu T, Borga M, Leinhard OD, Lundberg P, et al. Dense breast tissue in postmenopausal women is associated with a pro-inflammatory microenvironment in vivo. Oncoimmunology. 2016;5(10):e1229723. PubMed PMID: 27853653. PMCID: PMC5087296. Epub 2016/11/18. eng.

36. Huo CW, Chew G, Hill P, Huang D, Ingman W, Hodson L, et al. High mammographic density is associated with an increase in stromal collagen and immune cells within the mammary epithelium. Breast Cancer Res. 2015 Jun 4;17(1):79. PubMed PMID: 26040322. PMCID: PMC4485361. Epub 20150604. eng.

37. Huo CW, Hill P, Chew G, Neeson PJ, Halse H, Williams ED, et al. High mammographic density in women is associated with protumor inflammation. Breast Cancer Research2018.

38. Hanahan D, Weinberg RA. Hallmarks of cancer: the next generation. Cell. 2011 Mar 4;144(5):646-74. PubMed PMID: 21376230. eng.

39. Hanahan D. Hallmarks of Cancer: New Dimensions. Cancer Discov. 2022 Jan;12(1):31-46. PubMed PMID: 35022204. eng.

40. García-Mendoza MG, Inman DR, Ponik SM, Jeffery JJ, Sheerar DS, Van Doorn RR, et al. Neutrophils drive accelerated tumor progression in the collagen-dense mammary tumor microenvironment. Breast Cancer Res. 2016 May 11;18(1):49. PubMed PMID: 27169366. PMCID: PMC4864897. Epub 20160511. eng.

41. Ghosh K, Brandt KR, Reynolds C, Scott CG, Pankratz VS, Riehle DL, et al. Tissue composition of mammographically dense and non-dense breast tissue. Breast

Cancer Res Treat. 2012 Jan;131(1):267-75. PubMed PMID: 21877142. PMCID: PMC3707294. Epub 20110830. eng.

42. Gabrielson M, Chiesa F, Paulsson J, Strell C, Behmer C, Rönnow K, et al. Amount of stroma is associated with mammographic density and stromal expression of oestrogen receptor in normal breast tissues. Breast Cancer Res Treat. 2016 Jul;158(2):253-61. PubMed PMID: 27349429. Epub 20160627. eng.

43. Cuzick J, Warwick J, Pinney E, Duffy SW, Cawthorn S, Howell A, et al. Tamoxifen-induced reduction in mammographic density and breast cancer risk reduction: a nested case-control study. J Natl Cancer Inst. 2011 May 4;103(9):744-52. PubMed PMID: 21483019. Epub 20110411. eng.

44. Northey JJ, Barrett AS, Acerbi I, Hayward MK, Talamantes S, Dean IS, et al. Stiff stroma increases breast cancer risk by inducing the oncogene ZNF217. J Clin Invest. 2020 Nov 2;130(11):5721-37. PubMed PMID: 32721948. PMCID: PMC7598051. eng.

45. Levental KR, Yu H, Kass L, Lakins JN, Egeblad M, Erler JT, et al. Matrix crosslinking forces tumor progression by enhancing integrin signaling. Cell. 2009 Nov 25;139(5):891-906. PubMed PMID: 19931152. PMCID: PMC2788004. eng.

46. Turashvili G, McKinney S, Martin L, Gelmon KA, Watson P, Boyd N, et al. Columnar cell lesions, mammographic density and breast cancer risk. Breast Cancer Res Treat. 2009 Jun;115(3):561-71. PubMed PMID: 18587641. Epub 20080628. eng.

47. Provenzano PP, Inman DR, Eliceiri KW, Knittel JG, Yan L, Rueden CT, et al. Collagen density promotes mammary tumor initiation and progression. BMC Med. 2008 Apr 28;6:11. PubMed PMID: 18442412. PMCID: PMC2386807. Epub 2008/04/30. eng.

48. Tran TXM, Moon SG, Kim S, Park B. Association of the Interaction Between Mammographic Breast Density, Body Mass Index, and Menopausal Status With Breast Cancer Risk Among Korean Women. JAMA Netw Open. 2021 Dec 1;4(12):e2139161. PubMed PMID: 34940866. PMCID: PMC8703253. Epub 20211201. eng.

49. Kerlikowske K, Bissell MCS, Sprague BL, Tice JA, Tossas KY, Bowles EJA, et al. Impact of BMI on Prevalence of Dense Breasts by Race and Ethnicity. Cancer Epidemiol Biomarkers Prev. 2023 Jun 7:Of1-of7. PubMed PMID: 37284771. Epub 20230607. eng.

50. Shieh Y, Scott CG, Jensen MR, Norman AD, Bertrand KA, Pankratz VS, et al. Body mass index, mammographic density, and breast cancer risk by estrogen receptor subtype. Breast Cancer Res. 2019 Apr 3;21(1):48. PubMed PMID: 30944014. PMCID: PMC6448282. Epub 20190403. eng.

51. Kim EY, Chang Y, Ahn J, Yun JS, Park YL, Park CH, et al. Menopausal Transition, Body Mass Index, and Prevalence of Mammographic Dense Breasts in Middle-Aged Women. J Clin Med. 2020 Jul 30;9(8). PubMed PMID: 32751482. PMCID: PMC7465213. Epub 20200730. eng.

52. Woolcott CG, Courneya KS, Boyd NF, Yaffe MJ, Terry T, McTiernan A, et al. Mammographic density change with 1 year of aerobic exercise among postmenopausal women: a randomized controlled trial. Cancer Epidemiol Biomarkers Prev. 2010 Apr;19(4):1112-21. PubMed PMID: 20332266. PMCID: PMC2945907. Epub 20100323. eng.

53. Wanders JO, Bakker MF, Veldhuis WB, Peeters PH, van Gils CH. The effect of weight change on changes in breast density measures over menopause in a breast cancer screening cohort. Breast Cancer Res. 2015 May 30;17(1):74. PubMed PMID: 26025139. PMCID: PMC4487974. Epub 20150530. eng.

54. Kanda H, Tateya S, Tamori Y, Kotani K, Hiasa K, Kitazawa R, et al. MCP-1 contributes to macrophage infiltration into adipose tissue, insulin resistance, and hepatic steatosis in obesity. J Clin Invest. 2006 Jun;116(6):1494-505. PubMed PMID: 16691291. PMCID: PMC1459069.

55. Gugliucci A. Biomarkers of dysfunctional visceral fat. Adv Clin Chem. 2022;109:1-30. PubMed PMID: 35953124. Epub 20220713. eng.

56. Blüher M. Adipose tissue dysfunction contributes to obesity related metabolic diseases. Best Pract Res Clin Endocrinol Metab. 2013 Apr;27(2):163-77. PubMed PMID: 23731879. Epub 20130306. eng.

57. Feng J, Lu S, Ou B, Liu Q, Dai J, Ji C, et al. The Role of JNk Signaling Pathway in Obesity-Driven Insulin Resistance. Diabetes Metab Syndr Obes. 2020;13:1399-406. PubMed PMID: 32425571. PMCID: PMC7196768. Epub 20200429. eng.

58. Priyanka A, Sindhu G, Shyni GL, Preetha Rani MR, Nisha VM, Raghu KG. Bilobalide abates inflammation, insulin resistance and secretion of angiogenic factors induced by hypoxia in 3T3-L1 adipocytes by controlling NF-κB and JNK activation. Int Immunopharmacol. 2017 Jan;42:209-17. PubMed PMID: 27936435. Epub 20161207. eng.

59. Carter JM, Hoskin TL, Pena MA, Brahmbhatt R, Winham SJ, Frost MH, et al. Macrophagic "Crown-like Structures" Are Associated with an Increased Risk of Breast Cancer in Benign Breast Disease. Cancer Prev Res (Phila). 2018 Feb;11(2):113-9. PubMed PMID: 29167285. Epub 2017/11/24. eng.

60. Pinteaux E, Inoue W, Schmidt L, Molina-Holgado F, Rothwell NJ, Luheshi GN. Leptin induces interleukin-1beta release from rat microglial cells through a caspase 1 independent mechanism. J Neurochem. 2007 Aug;102(3):826-33. PubMed PMID: 17419800. Epub 20070410. eng.

61. Chamberlin T, Clack M, Silvers C, Kuziel G, Thompson V, Johnson H, et al. Targeting Obesity-Induced Macrophages during Preneoplastic Growth Promotes Mammary Epithelial Stem/Progenitor Activity, DNA Damage, and Tumor Formation. Cancer Res. 2020 Oct 15;80(20):4465-75. PubMed PMID: 32868380. PMCID: PMC7572601. Epub 2020/09/02. eng.

62. Kuziel G, Moore BN, Arendt LM. Obesity and Fibrosis: Setting the Stage for Breast Cancer. Cancers (Basel). 2023 May 26;15(11). PubMed PMID: 37296891. PMCID: PMC10252103. Epub 20230526. eng.

63. Kuziel G, Moore BN, Haugstad GP, Arendt LM. Fibrocytes enhance mammary gland fibrosis in obesity. Faseb j. 2023 Jul;37(7):e23049. PubMed PMID: 37342915. PMCID: PMC10316715. Epub 2023/06/21. eng.

64. Lawler HM, Underkofler CM, Kern PA, Erickson C, Bredbeck B, Rasouli N. Adipose Tissue Hypoxia, Inflammation, and Fibrosis in Obese Insulin-Sensitive and Obese Insulin-Resistant Subjects. J Clin Endocrinol Metab. 2016 Apr;101(4):1422-8. PubMed PMID: 26871994. PMCID: PMC4880157. Epub 20160212. eng.

65. Spencer M, Yao-Borengasser A, Unal R, Rasouli N, Gurley CM, Zhu B, et al. Adipose tissue macrophages in insulin-resistant subjects are associated with collagen VI and fibrosis and demonstrate alternative activation. Am J Physiol Endocrinol Metab. 2010 Dec;299(6):E1016-27. PubMed PMID: 20841504. PMCID: PMC3006260. Epub 20100914. eng.

66. Kuziel G, Moore BN, Haugstad GP, Xiong Y, Williams AE, Arendt LM. Alterations in the mammary gland and tumor microenvironment of formerly obese mice. BMC Cancer. 2023 Dec 1;23(1):1183. PubMed PMID: 38041006. PMCID: PMC10693119. Epub 20231201. eng.

67. Wolfson B, Zhang Y, Gernapudi R, Duru N, Yao Y, Lo PK, et al. A High-Fat Diet Promotes Mammary Gland Myofibroblast Differentiation through MicroRNA 140 Downregulation. Mol Cell Biol. 2017 Feb 15;37(4). PubMed PMID: 27895151. PMCID: PMC5288574. Epub 20170201. eng.

68. Singh AK, McGuirk JP. CAR T cells: continuation in a revolution of immunotherapy. Lancet Oncol. 2020 Mar;21(3):e168-e78. PubMed PMID: 32135120. eng.

69. Bergman PJ. Cancer Immunotherapies. Vet Clin North Am Small Anim Pract. 2019 Sep;49(5):881-902. PubMed PMID: 31186125. Epub 2019/06/13. eng.

70. Verzoni E, Grassi P, Ratta R. Chapter 38 - Emerging Immunotherapies for Renal Cell Carcinoma. In: Dammacco F, Silvestris F, editors. Oncogenomics: Academic Press; 2019. p. 541-9.

71. Stanowska O, Kuczkiewicz-Siemion O, Dębowska M, Olszewski WP, Jagiełło-Gruszfeld A, Tysarowski A, et al. PD-L1-Positive High-Grade Triple-Negative Breast Cancer Patients Respond Better to Standard Neoadjuvant Treatment-A Retrospective Study of PD-L1 Expression in Relation to Different Clinicopathological Parameters. J Clin Med. 2022 Sep 21;11(19). PubMed PMID: 36233396. PMCID: PMC9573147. Epub 20220921. eng.

72. Markham A, Duggan S. Cemiplimab: First Global Approval. Drugs. 2018 Nov;78(17):1841-6. PubMed PMID: 30456447. Epub 2018/11/21. eng.

73. Twomey JD, Zhang B. Cancer Immunotherapy Update: FDA-Approved Checkpoint Inhibitors and Companion Diagnostics. Aaps j. 2021 Mar 7;23(2):39. PubMed PMID: 33677681. PMCID: PMC7937597. Epub 2021/03/08. eng.

74. Nanda R, Chow LQ, Dees EC, Berger R, Gupta S, Geva R, et al. Pembrolizumab in Patients With Advanced Triple-Negative Breast Cancer: Phase Ib KEYNOTE-012 Study. J Clin Oncol. 2016 Jul 20;34(21):2460-7. PubMed PMID: 27138582. PMCID: PMC6816000 online at www.jco.org. Author contributions are found at the end of this article. Epub 2016/05/04. eng.

75. Wang Z, Aguilar EG, Luna JI, Dunai C, Khuat LT, Le CT, et al. Paradoxical effects of obesity on T cell function during tumor progression and PD-1 checkpoint blockade. Nat Med. 2019 Jan;25(1):141-51. PubMed PMID: 30420753. PMCID: PMC6324991. Epub 2018/11/14. eng.

76. Cortellini A, Bersanelli M, Santini D, Buti S, Tiseo M, Cannita K, et al. Another side of the association between body mass index (BMI) and clinical outcomes of cancer patients receiving programmed cell death protein-1 (PD-1)/ Programmed cell death-ligand 1 (PD-L1) checkpoint inhibitors: A multicentre analysis of immune-related adverse events. Eur J Cancer. 2020 Mar;128:17-26. PubMed PMID: 32109847. Epub 2020/02/29. eng.

77. Pingili AK, Chaib M, Sipe LM, Miller EJ, Teng B, Sharma R, et al. Immune checkpoint blockade reprograms systemic immune landscape and tumor microenvironment in obesity-associated breast cancer. Cell Rep. 2021 Jun 22;35(12):109285. PubMed PMID: 34161764. PMCID: PMC8574993. eng.

78. Wherry EJ, Kurachi M. Molecular and cellular insights into T cell exhaustion. Nat Rev Immunol. 2015 Aug;15(8):486-99. PubMed PMID: 26205583. PMCID: PMC4889009. Epub 2015/07/25. eng.

79. Sen DR, Kaminski J, Barnitz RA, Kurachi M, Gerdemann U, Yates KB, et al. The epigenetic landscape of T cell exhaustion. Science2016. p. 1165-9.

80. JE K, F F, MD L, H Y, A W, SM A. PD-1 signalling in CD4(+) T cells restrains their clonal expansion to an immunogenic stimulus, but is not critically required for peptide-induced tolerance. Immunology. 2010 2010 May;130(1). PubMed PMID: 20113370.

81. Simon S, Voillet V, Vignard V, Wu Z, Dabrowski C, Jouand N, et al. PD-1 and TIGIT coexpression identifies a circulating CD8 T cell subset predictive of response to anti-PD-1 therapy. J Immunother Cancer. 2020 Nov;8(2). PubMed PMID: 33188038. PMCID: PMC7668369. eng.

82. Zhang Y, Hu J, Ji K, Jiang S, Dong Y, Sun L, et al. CD39 inhibition and VISTA blockade may overcome radiotherapy resistance by targeting exhausted CD8+ T cells and immunosuppressive myeloid cells. Cell Rep Med. 2023 Aug 15;4(8):101151. PubMed PMID: 37567173. PMCID: PMC10439278. Epub 20230810. eng.

83. Pardoll DM. The blockade of immune checkpoints in cancer immunotherapy. Nat Rev Cancer. 2012 Mar 22;12(4):252-64. PubMed PMID: 22437870. PMCID: PMC4856023. Epub 20120322. eng.

84. Schwartz RH. T cell anergy. Annu Rev Immunol. 2003;21:305-34. PubMed PMID: 12471050. Epub 20011219. eng.

85. Greenwald RJ, Boussiotis VA, Lorsbach RB, Abbas AK, Sharpe AH. CTLA-4 regulates induction of anergy in vivo. Immunity. 2001 Feb;14(2):145-55. PubMed PMID: 11239447. eng.

86. Wells AD, Walsh MC, Bluestone JA, Turka LA. Signaling through CD28 and CTLA-4 controls two distinct forms of T cell anergy. J Clin Invest. 2001 Sep;108(6):895-903. PubMed PMID: 11560959. PMCID: PMC200935. eng.

87. Tedeschi V, Paldino G, Kunkl M, Paroli M, Sorrentino R, Tuosto L, et al. CD8(+) T Cell Senescence: Lights and Shadows in Viral Infections, Autoimmune Disorders and Cancer. Int J Mol Sci. 2022 Mar 21;23(6). PubMed PMID: 35328795. PMCID: PMC8955595. Epub 20220321. eng.

88. Liu X, Si F, Bagley D, Ma F, Zhang Y, Tao Y, et al. Blockades of effector T cell senescence and exhaustion synergistically enhance antitumor immunity and immunotherapy. J Immunother Cancer. 2022 Oct;10(10). PubMed PMID: 36192086. PMCID: PMC9535198. eng.

89. Verma V, Shrimali RK, Ahmad S, Dai W, Wang H, Lu S, et al. PD-1 blockade in subprimed CD8 cells induces dysfunctional PD-1(+)CD38(hi) cells and anti-PD-1 resistance. Nat Immunol. 2019 Sep;20(9):1231-43. PubMed PMID: 31358999. PMCID: PMC7472661. Epub 20190729. eng.

90. Youngnak P, Kozono Y, Kozono H, Iwai H, Otsuki N, Jin H, et al. Differential binding properties of B7-H1 and B7-DC to programmed death-1. Biochem Biophys Res Commun. 2003 Aug 1;307(3):672-7. PubMed PMID: 12893276. eng.

91. Sharpe AH, Pauken KE. The diverse functions of the PD1 inhibitory pathway. Nat Rev Immunol. 2018 Mar;18(3):153-67. PubMed PMID: 28990585. Epub 2017/10/11. eng.

92. Nishimura H, Nose M, Hiai H, Minato N, Honjo T. Development of lupus-like autoimmune diseases by disruption of the PD-1 gene encoding an ITIM motif-carrying immunoreceptor. Immunity. 1999 Aug;11(2):141-51. PubMed PMID: 10485649. eng.

93. Sugiura D, Okazaki IM, Maeda TK, Maruhashi T, Shimizu K, Arakaki R, et al. PD-1 agonism by anti-CD80 inhibits T cell activation and alleviates autoimmunity. Nat Immunol. 2022 Mar;23(3):399-410. PubMed PMID: 35145298. Epub 20220210. eng.

94. Butte MJ, Keir ME, Phamduy TB, Sharpe AH, Freeman GJ. Programmed death-1 ligand 1 interacts specifically with the B7-1 costimulatory molecule to inhibit T cell responses. Immunity. 2007 Jul;27(1):111-22. PubMed PMID: 17629517. PMCID: PMC2707944. Epub 20070712. eng.

95. Lim SO, Li CW, Xia W, Cha JH, Chan LC, Wu Y, et al. Deubiquitination and Stabilization of PD-L1 by CSN5. Cancer Cell. 2016 Dec 12;30(6):925-39. PubMed PMID: 27866850. PMCID: PMC5171205. Epub 2016/11/22. eng.

96. Keir ME, Butte MJ, Freeman GJ, Sharpe AH. PD-1 and its ligands in tolerance and immunity. Annu Rev Immunol. 2008;26:677-704. PubMed PMID: 18173375. Epub 2008/01/05. eng.

97. Yamazaki T, Akiba H, Koyanagi A, Azuma M, Yagita H, Okumura K. Blockade of B7-H1 on macrophages suppresses CD4+ T cell proliferation by augmenting IFN-gamma-induced nitric oxide production. J Immunol. 2005 Aug 1;175(3):1586-92. PubMed PMID: 16034097. Epub 2005/07/22. eng.

98. Brown JA, Dorfman DM, Ma FR, Sullivan EL, Munoz O, Wood CR, et al. Blockade of programmed death-1 ligands on dendritic cells enhances T cell activation and cytokine production. J Immunol. 2003 Feb 1;170(3):1257-66. PubMed PMID: 12538684. Epub 2003/01/23. eng.

99. Fang W, Zhou T, Shi H, Yao M, Zhang D, Qian H, et al. Correction to: Progranulin induces immune escape in breast cancer via up-regulating PD-L1 expression on tumor-associated macrophages (TAMs) and promoting CD8(+) T cell exclusion. J Exp Clin Cancer Res. 41. England2022. p. 93.

100. Eppihimer MJ, Gunn J, Freeman GJ, Greenfield EA, Chernova T, Erickson J, et al. Expression and regulation of the PD-L1 immunoinhibitory molecule on microvascular endothelial cells. Microcirculation. 2002 Apr;9(2):133-45. PubMed PMID: 11932780. PMCID: PMC3740166. eng.

101. Rodig N, Ryan T, Allen JA, Pang H, Grabie N, Chernova T, et al. Endothelial expression of PD-L1 and PD-L2 down-regulates CD8+ T cell activation and cytolysis. Eur J Immunol. 2003 Nov;33(11):3117-26. PubMed PMID: 14579280. eng.

102. Hillers-Ziemer LE, McMahon RQ, Hietpas M, Paderta G, LeBeau J, McCready J, et al. Obesity Promotes Cooperation of Cancer Stem-Like Cells and Macrophages to Enhance Mammary Tumor Angiogenesis. Cancers (Basel). 2020 Feb 21;12(2). PubMed PMID: 32098183. PMCID: PMC7072330. Epub 2020/02/27. eng.

103. Castoldi A, Naffah de Souza C, Câmara NO, Moraes-Vieira PM. The Macrophage Switch in Obesity Development. Front Immunol. 2015;6:637. PubMed PMID: 26779183. PMCID: PMC4700258. Epub 20160105. eng.

104. Bracamonte-Baran W, Gilotra NA, Won T, Rodriguez KM, Talor MV, Oh BC, et al. Endothelial Stromal PD-L1 (Programmed Death Ligand 1) Modulates CD8(+) T-Cell Infiltration After Heart Transplantation. Circ Heart Fail. 2021 Oct;14(10):e007982. PubMed PMID: 34555935. PMCID: PMC8550427. Epub 20210924. eng.

105. Zhang C, Yue C, Herrmann A, Song J, Egelston C, Wang T, et al. STAT3 Activation-Induced Fatty Acid Oxidation in CD8(+) T Effector Cells Is Critical for Obesity-Promoted Breast Tumor Growth. Cell Metab. 2020 Jan 7;31(1):148-61.e5. PubMed PMID: 31761565. PMCID: PMC6949402. Epub 20191121. eng.

106. JT G, RM O, WJ T, M B, U M, RE S, et al. Obesity-Associated Myeloid-Derived Suppressor Cells Promote Apoptosis of Tumor-Infiltrating CD8 T Cells and Immunotherapy Resistance in Breast Cancer. Frontiers in immunology. 2020 10/06/2020;11. PubMed PMID: 33123173.

107. Linette GP, Carreno BM. Tumor-Infiltrating Lymphocytes in the Checkpoint Inhibitor Era. Curr Hematol Malig Rep. 2019 Aug;14(4):286-91. PubMed PMID: 31187421. PMCID: PMC6642683. eng.

108. Lao J, Xu H, Liang Z, Luo C, Shu L, Xie Y, et al. Peripheral changes in T cells predict efficacy of anti-PD-1 immunotherapy in non-small cell lung cancer. Immunobiology. 2023 May;228(3):152391. PubMed PMID: 37167681. Epub 20230428. eng.

109. Liang H, Li H, Xie Z, Jin T, Chen Y, Lv Z, et al. Quantitative multiplex immunofluorescence analysis identifies infiltrating PD1(+) CD8(+) and CD8(+) T cells as predictive of response to neoadjuvant chemotherapy in breast cancer. Thorac Cancer. 2020 Oct;11(10):2941-54. PubMed PMID: 32894006. PMCID: PMC7529566. Epub 20200907. eng.

110. Miller BC, Sen DR, Al Abosy R, Bi K, Virkud YV, LaFleur MW, et al. Subsets of exhausted CD8(+) T cells differentially mediate tumor control and respond to checkpoint blockade. Nat Immunol. 2019 Mar;20(3):326-36. PubMed PMID: 30778252. PMCID: PMC6673650. Epub 20190218. eng.

111. Siddiqui I, Schaeuble K, Chennupati V, Fuertes Marraco SA, Calderon-Copete S, Pais Ferreira D, et al. Intratumoral Tcf1(+)PD-1(+)CD8(+) T Cells with Stem-like Properties Promote Tumor Control in Response to Vaccination and Checkpoint Blockade Immunotherapy. Immunity. 2019 Jan 15;50(1):195-211.e10. PubMed PMID: 30635237. Epub 20190108. eng.

112. J C, H S, TH W, Z T, W Z. T cell anergy, exhaustion, senescence, and stemness in the tumor microenvironment. Current opinion in immunology. 2013 2013 Apr;25(2). PubMed PMID: 23298609.

113. Borst J, Ahrends T, Bąbała N, Melief CJM, Kastenmüller W. CD4(+) T cell help in cancer immunology and immunotherapy. Nat Rev Immunol. 2018 Oct;18(10):635-47. PubMed PMID: 30057419. Epub 2018/07/31. eng.

114. Inomata M, Kado T, Okazawa S, Imanishi S, Taka C, Kambara K, et al. Peripheral PD1-positive CD4 T-Lymphocyte Count Can Predict Progression-free Survival in Patients With Non-small Cell Lung Cancer Receiving Immune Checkpoint Inhibitor. Anticancer Res. 2019 Dec;39(12):6887-93. PubMed PMID: 31810958. Epub 2019/12/08. eng.

115. Jiao S, Subudhi SK, Aparicio A, Ge Z, Guan B, Miura Y, et al. Differences in Tumor Microenvironment Dictate T Helper Lineage Polarization and Response to Immune Checkpoint Therapy. Cell. 2019 Nov 14;179(5):1177-90.e13. PubMed PMID: 31730856. eng.

116. Kumagai S, Togashi Y, Kamada T, Sugiyama E, Nishinakamura H, Takeuchi Y, et al. The PD-1 expression balance between effector and regulatory T cells predicts the clinical efficacy of PD-1 blockade therapies. Nat Immunol. 2020 Nov;21(11):1346-58. PubMed PMID: 32868929. Epub 20200831. eng.

117. Sabatier R, Finetti P, Mamessier E, Adelaide J, Chaffanet M, Ali HR, et al. Prognostic and predictive value of PDL1 expression in breast cancer. Oncotarget. 2015 Mar 10;6(7):5449-64. PubMed PMID: 25669979. PMCID: PMC4467160. Epub 2015/02/12. eng.

118. P S, S A, HS R, A S, CH B, H I, et al. Atezolizumab and Nab-Paclitaxel in Advanced Triple-Negative Breast Cancer. The New England journal of medicine. 2018 11/29/2018;379(22). PubMed PMID: 30345906.

119. Yuan C, Liu Z, Yu Q, Wang X, Bian M, Yu Z, et al. Expression of PD-1/PD-L1 in primary breast tumours and metastatic axillary lymph nodes and its correlation with clinicopathological parameters. Sci Rep. 2019 Oct 7;9(1):14356. PubMed PMID: 31591439. PMCID: PMC6779893. Epub 20191007. eng.

120. Cimino-Mathews A, Thompson E, Taube J. PD-L1 (B7-H1) expression and the immune tumor microenvironment in

primary and metastatic breast carcinomas. Human Pathology2015. p. 52-63.

121. Peng W, Chen JQ, Liu C, Malu S, Creasy C, Tetzlaff MT, et al. Loss of PTEN Promotes Resistance to T Cell-Mediated Immunotherapy. Cancer Discov. 2016 Feb;6(2):202-16. PubMed PMID: 26645196. PMCID: PMC4744499. Epub 2015/12/10. eng.

122. Azuma K, Ota K, Kawahara A, Hattori S, Iwama E, Harada T, et al. Association of PD-L1 overexpression with activating EGFR mutations in surgically resected nonsmall-cell lung cancer. Ann Oncol. 2014 Oct;25(10):1935-40. PubMed PMID: 25009014. Epub 20140709. eng.

123. Le DT, Uram JN, Wang H, Bartlett BR, Kemberling H, Eyring AD, et al. PD-1 Blockade in Tumors with Mismatch-Repair Deficiency. N Engl J Med. 2015 Jun 25;372(26):2509-20. PubMed PMID: 26028255. PMCID: PMC4481136. Epub 2015/06/02. eng.

124. Davoli T, Uno H, Wooten EC, Elledge SJ. Tumor aneuploidy correlates with markers of immune evasion and with reduced response to immunotherapy. Science. 2017 Jan 20;355(6322). PubMed PMID: 28104840. PMCID: PMC5592794. Epub 2017/01/21. eng.

125. Nolan E, Savas P, Policheni AN, Darcy PK, Vaillant F, Mintoff CP, et al. Combined immune checkpoint blockade as a therapeutic strategy for BRCA1-mutated breast cancer. Sci Transl Med. 2017 Jun 7;9(393). PubMed PMID: 28592566. PMCID: PMC5822709. Epub 2017/06/09. eng.

126. Karn T, Denkert C, Weber KE, Holtrich U, Hanusch C, Sinn BV, et al. Tumor mutational burden and immune infiltration as independent predictors of response to neoadjuvant immune checkpoint inhibition in early TNBC in GeparNuevo. Ann Oncol. 2020 Sep;31(9):1216-22. PubMed PMID: 32461104. Epub 20200524. eng.

127. Gravara LD, Battiloro C, Cantile R, Letizia A, Vitiello F, Montesarchio V, et al. Chemotherapy and/or immune checkpoint inhibitors in NSCLC first-line setting: what is the best approach? Lung Cancer Manag. 2020 Feb 12;9(1):Lmt22. PubMed PMID: 32256708. PMCID: PMC7110571. Epub 2020/04/08. eng.

128. Twyman-Saint Victor C, Rech AJ, Maity A, Rengan R, Pauken KE, Stelekati E, et al. Radiation and dual checkpoint blockade activate non-redundant immune mechanisms in cancer. Nature. 2015 Apr 16;520(7547):373-7. PubMed PMID: 25754329. PMCID: PMC4401634. Epub 20150309. eng.

129. Goldberg J, Pastorello RG, Vallius T, Davis J, Cui YX, Agudo J, et al. The Immunology of Hormone Receptor Positive Breast Cancer. Front Immunol. 2021;12:674192. PubMed PMID: 34135901. PMCID: PMC8202289. Epub 20210511. eng.

130. O'Leary KA, Bates AM, Jin WJ, Burkel BM, Sriramaneni RN, Emma SE, et al. Estrogen receptor blockade and radiation therapy cooperate to enhance the response of immunologically cold ER+ breast cancer to immunotherapy. Breast Cancer Res. 2023 Jun 13;25(1):68. PubMed PMID: 37312163. PMCID: PMC10265911. Epub 20230613. eng.

131. Rugo HS, Delord JP, Im SA, Ott PA, Piha-Paul SA, Bedard PL, et al. Safety and Antitumor Activity of Pembrolizumab in Patients with Estrogen Receptor-Positive/Human Epidermal Growth Factor Receptor 2-Negative Advanced Breast Cancer. Clin Cancer Res. 2018 Jun 15;24(12):2804-11. PubMed PMID: 29559561. Epub 20180320. eng.

132. Criscitiello C, Vingiani A, Maisonneuve P, Viale G, Curigliano G. Tumor-infiltrating lymphocytes (TILs) in ER+/HER2- breast cancer. Breast Cancer Res Treat. 2020 Sep;183(2):347-54. PubMed PMID: 32621251. Epub 2020/07/06. eng.

133. Chervoneva I, Peck AR, Sun Y, Yi M, Udhane SS, Langenheim JF, et al. High PD-L2 Predicts Early Recurrence of ER-Positive Breast Cancer. JCO Precis Oncol. 2023 Jan;7:e2100498. PubMed PMID: 36652667. PMCID: PMC9928763. eng.

134. NCT03725059. <h2 _ngcontent-ng-c2037759435="" class="brief-title" style="box-sizing: inherit; font-size: 22px; line-height: 1.15; color: rgb(51, 51, 51); margin: 1.5rem 0px; font-family: Roboto, sans-serif; background-color: rgb(255, 255, 255);">Study of Pembrolizumab (MK-3475) Versus Placebo in Combination With Neoadjuvant Chemotherapy & Adjuvant Endocrine Therapy in the Treatment of Early-Stage Estrogen Receptor-Positive, Human Epidermal Growth Factor Receptor 2-Negative (ER+/HER2-) Breast Cancer (MK-3475-756/KEYNOTE-756) [Available from: https://clinicaltrials.gov/study/NCT03725059.

135. Schmid P, Salgado R, Park YH, Muñoz-Couselo E, Kim SB, Sohn J, et al. Pembrolizumab plus chemotherapy as neoadjuvant treatment of high-risk, early-stage triple-negative breast cancer: results from the phase 1b open-label, multicohort KEYNOTE-173 study. Ann Oncol. 2020 May;31(5):569-81. PubMed PMID: 32278621. Epub 2020/04/13. eng.

136. Simmons CE, Brezden-Masley C, McCarthy J, McLeod D, Joy AA. Positive progress: current and evolving role of immune checkpoint inhibitors in metastatic triple-negative breast cancer. Ther Adv Med Oncol. 2020;12:1758835920909091. PubMed PMID: 33014143. PMCID: PMC7517981. Epub 2020/10/06. eng.

137. Loi S, Giobbie-Hurder A, Gombos A, Bachelot T, Hui R, Curigliano G, et al. Pembrolizumab plus trastuzumab in trastuzumab-resistant, advanced, HER2-positive breast cancer (PANACEA): a single-arm, multicentre, phase 1b-2 trial. Lancet Oncol. 2019 Mar;20(3):371-82. PubMed PMID: 30765258. Epub 2019/02/16. eng.

138. NCT03988036. <h2 _ngcontent-ng-c2037759435="" class="brief-title" style="box-sizing: inherit; font-size: 22px; line-height: 1.15; color: rgb(51, 51, 51); margin: 1.5rem 0px; font-family: Roboto, sans-serif; background-color: rgb(255, 255, 255);">A Study With Pembrolizumab in Combination With Dual Anti-HER2 Blockade With Trastuzumab and Pertuzumab in Early Breast Cancer Patients With Molecular HER2-enriched Intrinsic Subtype (Keyriched-1) (Keyriched-1) [Available from: https://clinicaltrials.gov/study/NCT03988036.

139. Wei S, Nandi S, Chitu V, Yeung YG, Yu W, Huang M, et al. Functional overlap but differential expression of CSF-1 and IL-34 in their CSF-1 receptor-mediated regulation of myeloid cells. J Leukoc Biol. 2010 Sep;88(3):495-505. PubMed PMID: 20504948. PMCID: PMC2924605. Epub 20100526. eng.

140. Wen J, Wang S, Guo R, Liu D. CSF1R inhibitors are emerging immunotherapeutic drugs for cancer treatment. Eur J Med Chem. 2023 Jan 5;245(Pt 1):114884. PubMed PMID: 36335744. Epub 20221029. eng.

141. Azhar Z, Grose RP, Raza A, Raza Z. In silico targeting of colony-stimulating factor-1 receptor: delineating immunotherapy in cancer. Explor Target Antitumor Ther. 2023;4(4):727-42. PubMed PMID: 37711590. PMCID: PMC10497393. Epub 20230831. eng.

142. Johnson M, Dudek AZ, Sukari A, Call J, Kunk PR, Lewis K, et al. ARRY-382 in Combination with Pembrolizumab in Patients with Advanced Solid Tumors: Results from a Phase 1b/2 Study. Clin Cancer Res. 2022 Jun 13;28(12):2517-26. PubMed PMID: 35302585. PMCID: PMC9359741. eng.

143. Ordentlich P. Clinical evaluation of colony-stimulating factor 1 receptor inhibitors. Semin Immunol. 2021 Apr;54:101514. PubMed PMID: 34776301. Epub 20211112. eng.

144. Guilbert LJ, Stanley ER. Specific interaction of murine colony-stimulating factor with mononuclear phagocytic cells. J Cell Biol. 1980 Apr;85(1):153-9. PubMed PMID: 6965942. PMCID: PMC2110592. eng.

145. Byrne PV, Guilbert LJ, Stanley ER. Distribution of cells bearing receptors for a colony-stimulating factor (CSF-1) in murine tissues. J Cell Biol. 1981 Dec;91(3 Pt 1):848-53. PubMed PMID: 6276411. PMCID: PMC2112824. eng.

146. MacDonald KP, Rowe V, Bofinger HM, Thomas R, Sasmono T, Hume DA, et al. The colony-stimulating factor 1 receptor is expressed on dendritic cells during differentiation and regulates their expansion. J Immunol. 2005 Aug 1;175(3):1399-405. PubMed PMID: 16034075. eng.

147. Nandi S, Gokhan S, Dai XM, Wei S, Enikolopov G, Lin H, et al. The CSF-1 receptor ligands IL-34 and CSF-1 exhibit distinct developmental brain expression patterns and regulate neural progenitor cell maintenance and maturation. Dev Biol. 2012 Jul 15;367(2):100-13. PubMed PMID: 22542597. PMCID: PMC3388946. Epub 20120419. eng.

148. Mun SH, Park PSU, Park-Min KH. The M-CSF receptor in osteoclasts and beyond. Exp Mol Med. 2020 Aug;52(8):1239-54. PubMed PMID: 32801364. PMCID: PMC8080670. Epub 20200817. eng.

149. Strachan DC, Ruffell B, Oei Y, Bissell MJ, Coussens LM, Pryer N, et al. CSF1R inhibition delays cervical and mammary tumor growth in murine models by attenuating the turnover of tumor-associated macrophages and enhancing infiltration by CD8(+) T cells. Oncoimmunology. 2013 Dec 1;2(12):e26968. PubMed PMID: 24498562. PMCID: PMC3902121. Epub 2014/02/06. eng.

150. Singh S, Lee N, Pedroza DA, Bado IL, Hamor C, Zhang L, et al. Chemotherapy Coupled to Macrophage Inhibition Induces T-cell and B-cell Infiltration and Durable

Regression in Triple-Negative Breast Cancer. Cancer Res. 2022 Jun 15;82(12):2281-97. PubMed PMID: 35442423. PMCID: PMC9219596. eng.

151. Lim C, Hwang D, Yazdimamaghani M, Atkins HM, Hyun H, Shin Y, et al. High-Dose Paclitaxel and its Combination with CSF1R Inhibitor in Polymeric Micelles for Chemoimmunotherapy of Triple Negative Breast Cancer. Nano Today. 2023 Aug;51. PubMed PMID: 37484164. PMCID: PMC10357922. Epub 20230601. eng.

152. Riaz N, Burugu S, Cheng AS, Leung SCY, Gao D, Nielsen TO. Prognostic Significance of CSF-1R Expression in Early Invasive Breast Cancer. Cancers (Basel). 2021 Nov 18;13(22). PubMed PMID: 34830923. PMCID: PMC8616299. Epub 20211118. eng.

153. Fujiwara T, Yakoub MA, Chandler A, Christ AB, Yang G, Ouerfelli O, et al. CSF1/CSF1R Signaling Inhibitor Pexidartinib (PLX3397) Reprograms Tumor-Associated Macrophages and Stimulates T-cell Infiltration in the Sarcoma Microenvironment. Mol Cancer Ther. 2021 Aug;20(8):1388-99. PubMed PMID: 34088832. PMCID: PMC9336538. Epub 20210604. eng.

154. Zhu Y, Knolhoff BL, Meyer MA, Nywening TM, West BL, Luo J, et al. CSF1/CSF1R blockade reprograms tumor-infiltrating macrophages and improves response to T-cell checkpoint immunotherapy in pancreatic cancer models. Cancer Res. 2014 Sep 15;74(18):5057-69. PubMed PMID: 25082815. PMCID: PMC4182950. Epub 20140731. eng.

155. Martinez-Usatorre A, Kadioglu E, Boivin G, Cianciaruso C, Guichard A, Torchia B, et al. Overcoming microenvironmental resistance to PD-1 blockade in genetically engineered lung cancer models. Sci Transl Med. 2021 Aug 11;13(606). PubMed PMID: 34380768. PMCID: PMC7612153. eng.

156. Fattori S, Le Roy A, Houacine J, Robert L, Abes R, Gorvel L, et al. CD25high Effector Regulatory T Cells Hamper Responses to PD-1 Blockade in Triple-Negative Breast Cancer. Cancer Res. 2023 Sep 15;83(18):3026-44. PubMed PMID: 37379438. PMCID: PMC10502453. eng.

157. Li Z, Ding Y, Liu J, Wang J, Mo F, Wang Y, et al. Depletion of tumor associated macrophages enhances local and systemic platelet-mediated anti-PD-1 delivery for post-surgery tumor recurrence treatment. Nat Commun. 2022 Apr 6;13(1):1845. PubMed PMID: 35387972. PMCID: PMC8987059. Epub 20220406. eng.

158. Peranzoni E, Lemoine J, Vimeux L, Feuillet V, Barrin S, Kantari-Mimoun C, et al. Macrophages impede CD8 T cells from reaching tumor cells and limit the efficacy of anti-PD-1 treatment. Proc Natl Acad Sci U S A. 2018 Apr 24;115(17):E4041-e50. PubMed PMID: 29632196. PMCID: PMC5924916. Epub 2018/04/11. eng.

159. Maslov D, Tawagi K, Simenson V, Yuan H, Parent C, Bamnolker A, et al. Impact of body mass index on survival rates in patients receiving immune checkpoint inhibitors. Journal of Clinical Oncology. 2020 2020/05/20;38(15_suppl):e15108-e.

160. Kichenadasse G, Miners JO, Mangoni AA, Rowland A, Hopkins AM, Sorich MJ. Association Between Body Mass Index and Overall Survival With Immune Checkpoint Inhibitor Therapy for Advanced Non-Small Cell Lung Cancer. JAMA Oncol. 2020 Apr 1;6(4):512-8. PubMed PMID: 31876896. PMCID: PMC6990855. eng.

161. McQuade JL, Daniel CR, Hess KR, Mak C, Wang DY, Rai RR, et al. Association of body-mass index and outcomes in patients with metastatic melanoma treated with targeted therapy, immunotherapy, or chemotherapy: a retrospective, multicohort analysis. Lancet Oncol. 2018 Mar;19(3):310-22. PubMed PMID: 29449192. PMCID: PMC5840029. Epub 20180212. eng.

162. Boi SK, Orlandella RM, Gibson JT, Turbitt WJ, Wald G, Thomas L, et al. Obesity diminishes response to PD-1-based immunotherapies in renal cancer. J Immunother Cancer. 2020 Dec;8(2). PubMed PMID: 33427691. PMCID: PMC7757487. eng.

163. Eun Y, Kim IY, Sun JM, Lee J, Cha HS, Koh EM, et al. Risk factors for immune-related adverse events associated with anti-PD-1 pembrolizumab. Sci Rep. 2019 Oct 1;9(1):14039. PubMed PMID: 31575933. PMCID: PMC6773778. Epub 20191001. eng.

164. Martins F, Sofiya L, Sykiotis GP, Lamine F, Maillard M, Fraga M, et al. Adverse effects of immune-checkpoint inhibitors: epidemiology, management and surveillance. Nat Rev Clin Oncol. 2019 Sep;16(9):563-80. PubMed PMID: 31092901. eng.

165. Kado T, Nawaz A, Takikawa A, Usui I, Tobe K. Linkage of CD8+ t cell exhaustion with high-fat diet-induced tumourigenesis. Scientific Reports2019.

166. Chang CH, Qiu J, O'Sullivan D, Buck MD, Noguchi T, Curtis JD, et al. Metabolic Competition in the Tumor Microenvironment Is a Driver of Cancer Progression. Cell. 2015 Sep 10;162(6):1229-41. PubMed PMID: 26321679. PMCID: PMC4864363. Epub 20150827. eng.

167. Szekely B, Bossuyt V, Li X, Wali VB, Patwardhan GA, Frederick C, et al. Immunological differences between primary and metastatic breast cancer. Ann Oncol. 2018 Nov 1;29(11):2232-9. PubMed PMID: 30203045. eng.

168. Uribe-Querol E, Rosales C. Neutrophils in Cancer: Two Sides of the Same Coin. J Immunol Res. 2015;2015:983698. PubMed PMID: 26819959. PMCID: PMC4706937. Epub 20151224. eng.

169. Li P, Lu M, Shi J, Gong Z, Hua L, Li Q, et al. Lung mesenchymal cells elicit lipid storage in neutrophils that fuel breast cancer lung metastasis. Nat Immunol. 2020 Nov;21(11):1444-55. PubMed PMID: 32958928. PMCID: PMC7584447. Epub 20200921. eng.

170. Xiao Y, Cong M, Li J, He D, Wu Q, Tian P, et al. Cathepsin C promotes breast cancer lung metastasis by modulating neutrophil infiltration and neutrophil extracellular trap formation. Cancer Cell. 2021 Mar 8;39(3):423-37.e7. PubMed PMID: 33450198. Epub 20210114. eng.

171. Yang L, Liu Q, Zhang X, Liu X, Zhou B, Chen J, et al. DNA of neutrophil extracellular traps promotes cancer metastasis via CCDC25. Nature. 2020 Jul;583(7814):133-8. PubMed PMID: 32528174. Epub 20200611. eng.

172. Hillers-Ziemer LE, Williams AE, Janquart A, Grogan C, Thompson V, Sanchez A, et al. Obesity-Activated Lung Stromal Cells Promote Myeloid Lineage Cell Accumulation and Breast Cancer Metastasis. Cancers (Basel). 2021 Feb 28;13(5). PubMed PMID: 33670906. PMCID: PMC7957630. Epub 20210228. eng.

173. McDowell SAC, Luo RBE, Arabzadeh A, Doré S, Bennett NC, Breton V, et al. Neutrophil oxidative stress mediates obesity-associated vascular dysfunction and metastatic transmigration. Nat Cancer. 2021 May;2(5):545-62. PubMed PMID: 35122017. Epub 20210503. eng.

174. Quail DF, Olson OC, Bhardwaj P, Walsh LA, Akkari L, Quick ML, et al. Obesity alters the lung myeloid cell landscape to enhance breast cancer metastasis through IL5 and GM-CSF. Nat Cell Biol. 2017 Aug;19(8):974-87. PubMed PMID: 28737771. PMCID: PMC6759922. Epub 20170724. eng.

175. Headley MB, Bins A, Nip A, Roberts EW, Looney MR, Gerard A, et al. Visualization of immediate immune responses to pioneer metastatic cells in the lung. Nature. 2016 Mar 24;531(7595):513-7. PubMed PMID: 26982733. PMCID: PMC4892380. Epub 20160316. eng.

176. Magidey-Klein K, Cooper TJ, Kveler K, Normand R, Zhang T, Timaner M, et al. IL-6 contributes to metastatic switch via the differentiation of monocytic-dendritic progenitors into prometastatic immune cells. J Immunother Cancer. 2021 Jun;9(6). PubMed PMID: 34140316. PMCID: PMC8212411. eng.

177. Fels AO, Cohn ZA. The alveolar macrophage. J Appl Physiol (1985). 1986 Feb;60(2):353-69. PubMed PMID: 3005225. eng.

178. Kopf M, Schneider C, Nobs SP. The development and function of lung-resident macrophages and dendritic cells. Nat Immunol. 2015 Jan;16(1):36-44. PubMed PMID: 25521683. eng.

179. Huggins DN, LaRue RS, Wang Y, Knutson TP, Xu Y, Williams JW, et al. Characterizing Macrophage Diversity in Metastasis-Bearing Lungs Reveals a Lipid-Associated Macrophage Subset. Cancer Res. 2021 Oct 15;81(20):5284-95. PubMed PMID: 34389631. PMCID: PMC8530952. Epub 20210813. eng.

180. Sharma SK, Chintala NK, Vadrevu SK, Patel J, Karbowniczek M, Markiewski MM. Pulmonary alveolar macrophages contribute to the premetastatic niche by suppressing antitumor T cell responses in the lungs. J Immunol. 2015 Jun 1;194(11):5529-38. PubMed PMID: 25911761. Epub 20150424. eng.

181. Nagahashi M, Yamada A, Katsuta E, Aoyagi T, Huang WC, Terracina KP, et al. Targeting the SphK1/S1P/S1PR1 Axis That Links Obesity, Chronic Inflammation, and

Breast Cancer Metastasis. Cancer Res. 2018 Apr 1;78(7):1713-25. PubMed PMID: 29351902. PMCID: PMC6945803. Epub 20180119. eng.

182. Xing F, Zhao D, Wu SY, Tyagi A, Wu K, Sharma S, et al. Epigenetic and Posttranscriptional Modulation of SOS1 Can Promote Breast Cancer Metastasis through Obesity-Activated c-Met Signaling in African-American Women. Cancer Res. 2021 Jun 1;81(11):3008-21. PubMed PMID: 33446575. PMCID: PMC8178187. Epub 20210114. eng.

183. Tacconi C, Commerford CD, Dieterich LC, Schwager S, He Y, Ikenberg K, et al. CD169(+) lymph node macrophages have protective functions in mouse breast cancer metastasis. Cell Rep. 2021 Apr 13;35(2):108993. PubMed PMID: 33852863. eng.

184. Zheng Z, Li YN, Jia S, Zhu M, Cao L, Tao M, et al. Lung mesenchymal stromal cells influenced by Th2 cytokines mobilize neutrophils and facilitate metastasis by producing complement C3. Nat Commun. 2021 Oct 27;12(1):6202. PubMed PMID: 34707103. PMCID: PMC8551331. Epub 20211027. eng.

185. Olkhanud PB, Baatar D, Bodogai M, Hakim F, Gress R, Anderson RL, et al. Breast cancer lung metastasis requires expression of chemokine receptor CCR4 and regulatory T cells. Cancer Res. 2009 Jul 15;69(14):5996-6004. PubMed PMID: 19567680. PMCID: PMC2743688. Epub 20090630. eng.

186. Tallón de Lara P, Castañón H, Vermeer M, Núñez N, Silina K, Sobottka B, et al. CD39(+)PD-1(+)CD8(+) T cells mediate metastatic dormancy in breast cancer. Nat Commun. 2021 Feb 3;12(1):769. PubMed PMID: 33536445. PMCID: PMC7859213. Epub 20210203. eng.

187. Rebeles J, Green WD, Alwarawrah Y, Nichols AG, Eisner W, Danzaki K, et al. Obesity-Induced Changes in T-Cell Metabolism Are Associated With Impaired Memory T-Cell Response to Influenza and Are Not Reversed With Weight Loss. J Infect Dis. 2019 Apr 19;219(10):1652-61. PubMed PMID: 30535161. PMCID: PMC6473176. eng.

188. Green WD, Al-Shaer AE, Shi Q, Gowdy KM, MacIver NJ, Milner JJ, et al. Metabolic and functional impairment of CD8(+) T cells from the lungs of influenza-infected obese mice. J Leukoc Biol. 2022 Jan;111(1):147-59. PubMed PMID: 33847405. PMCID: PMC8787296. Epub 20210413. eng.

189. Kim YH, Kim JK, Kim DJ, Nam JH, Shim SM, Choi YK, et al. Diet-induced obesity dramatically reduces the efficacy of a 2009 pandemic H1N1 vaccine in a mouse model. J Infect Dis. 2012 Jan 15;205(2):244-51. PubMed PMID: 22147801. Epub 20111205. eng.

190. Dhakal S, Klein SL. Host Factors Impact Vaccine Efficacy: Implications for Seasonal and Universal Influenza Vaccine Programs. J Virol. 2019 Nov 1;93(21). PubMed PMID: 31391269. PMCID: PMC6803252. Epub 20191015. eng.

191. Watanabe M, Balena A, Tuccinardi D, Tozzi R, Risi R, Masi D, et al. Central obesity, smoking habit, and hypertension are associated with lower antibody titres in response to COVID-19 mRNA vaccine. Diabetes Metab Res Rev. 2022 Jan;38(1):e3465. PubMed PMID: 33955644. PMCID: PMC8209952. Epub 20210511. eng.

CHAPTER 2

Obesity and breast density together increase macrophage-driven inflammation and metastasis to the lungs

Abstract:

Recent epidemiological studies suggest that breast density and obesity together increase breast cancer risk. Although the underlying causes of increased risk associated with dense breasts and obesity have individually been explored, little is known about how these underlying risk factors interact together to promote breast cancer. To model breast density, we used heterozygous Col1a1^{tmjae} (Het) mice that have a mutation that limits collagen degradation, leading to increased mammary collagen deposition. Het and wild type (WT) littermates were fed either a low-fat diet (LFD) or a high-fat diet (HFD) to induce obesity. We observed significantly increased numbers of macrophages in mammary glands of HFD-fed WT and Het mice compared to LFD-fed WT mice. HFD-fed Het mice also had increased crown-like structures (CLS) at an early timepoint compared to other experimental groups. CD8+ T cells were decreased in mammary glands of mice fed HFD. We also observed significantly enhanced collagen surrounding mammary ducts from HFD-fed WT and Het mice compared to those from LFD-fed WT mice. When crossed with MMTV-PyMT mice to examine tumor growth, we did not see significant differences in tumor size. However, we did observe significantly increased pulmonary metastasis in HFD-fed Het mice compared to LFD-fed WT and Het mice. We also observed significant increases in macrophages surrounding tumors in LFD-fed Het and HFD-fed WT mice. Overall, we demonstrated breast density and obesity may cooperatively increase breast cancer risk.

Introduction:

Breast density and obesity individually are major risk factors for breast cancer (1, 2). Mammographic breast density is defined as having higher proportions of glandular and fibrous tissue in the breast with limited fatty tissue (3). Women with highly dense breasts have a 4 to 5-fold increase in breast cancer risk compared to women with low breast density (4). Breast tissue density widely varies based on a woman's age, menopausal status, body mass index (BMI), parity, and genetic predisposition. Percent density and BMI have been shown to be inversely related and are thought to act as confounders of each other's effects (5, 6). However, a recent large epidemiological study identified that obesity and breast density together increased breast cancer risk in Korean women (7). Further, increased breast density was associated with a higher risk for estrogen receptor negative breast tumors in women with obesity (8). These studies suggest that the risk factors of breast density and obesity may interact to enhance breast cancer risk, although the underlying mechanisms of these interactions have not been explored.

Areas of breast density are associated with increased fibrillar collagen deposition (9-11). Heterozygous Col1a1^{tm1jae} mice have a mutation in a crucial collagen I cleavage site causing resistance to degradation (12, 13), leading to increased fibrillar collagen in the mammary gland (14). Elevated collagen density in the mammary glands of Col1a1^{tm1jae} crossed with mice that expressed Polyomavirus middle-T under control of the MMTV promoter (MMTV-PyMT) promoted advanced tumor growth and more metastasis to the lung (15) (14, 16). Mice bearing the Col1a1^{tm1jae} mutation also had increased metastasis in an estrogen receptor positive breast tumor model (17). Using

this model in conjunction with a high-fat diet (HFD) model of obesity may provide insight into how the risk factors of mammographic density and obesity interact to enhance breast cancer risk.

Chronic inflammation has been implicated in the development of multiple types of cancer and may enhance breast cancer growth and progression. In humans, dense breast tissue is more inflammatory (18), having increased levels of extracellular IL-6, IL-8, and CCL5, as well as more CD45+ immune cells and CD68+ macrophages (19). Obesity also promotes increased inflammation in breast tissue through the chronic recruitment of macrophages.(20). Macrophages surround necrotic adipocytes and form crown-like structures (CLS), which are a hallmark of obesity, and secrete inflammatory cytokines including IL-6, intermediate nitrogen and oxygen species (iNOS), and TNF-α (21). While both breast density and obesity may enhance inflammation within breast tissue, the immune cells implicated in promoting inflammation and the contributions of each risk factor in modifying inflammation have not been identified.

To identify how breast density and obesity interact to enhance breast cancer risk, we examined immune cell recruitment into the mammary glands of obese and lean Col1a1^{tm1jae} mice. Further, we examined the impact of obesity and collagen density on mammary tumor growth and progression using the MMTV-PyMT mouse model. We observed that the risk factors together enhanced recruitment of immune cells and collagen deposition. In the MMTV-PyMT model, we observed an increase in PyMT+ tumor cells in the lungs from mice with both risk factors compared to lean wild type (WT) mice and lean heterozygous (Het) Col1a1^{tm1jae} mice. Our results suggest that the risk factors of breast density and obesity may collaboratively enhance inflammation within

breast tissue leading to increased risk for breast cancer in women with both dense breast tissue and obesity.

Materials and Methods:

Mouse Models

All animal procedures were conducted in compliance with a protocol approved by the University of Wisconsin Institutional Animal Care and Use Committee. Mice were housed and handled in accordance with the Guide for Care and Use of Laboratory Animals in AAALAC-accredited facilities (Animal Welfare Assurance Number: D16-00239). Mice were maintained and bred at the University of Wisconsin under the oversight of and with the ethical approval of the University of Wisconsin Animal Use and Care Committee. For this study, hemizygous male FVB/NJ MMTV-PyMT mice were crossed with female heterozygous Col1a1^{tm1jae} C57BL/6J mice. Beginning at 3 weeks of age, nulliparous female mice were genotyped and randomly divided into one of two treatment groups: low-fat diet (LFD) or HFD. The HFD (TestDiet 58Y1) consisted of 34.9% fat, 25.9% carbohydrates, and 23.1% protein (5.1 kcal/g) while the LFD (Envigo TD.2019) consisted of 9% fat, 44.9% carbohydrates, and 19.0% protein (3.3 kcal/g). The mice were allowed unrestricted access to their respective diets. Mice were weighed on a weekly basis. Mice were maintained on their respective diets for 9, 12, or 15 weeks before euthanasia and tissue collection.

Tissue Collection and Preparation

All mammary glands were collected, and total mammary gland weight was measured. One mammary gland per mouse was fixed in 10% neutral buffered formalin

for 48 hours and embedded in paraffin. A second mammary gland from each mouse was flash frozen and stored in liquid nitrogen. A third mammary gland from tumor-bearing mice was embedded in Optimal Cutting Temperature medium for cryosectioning. Lungs were dissected from tumor bearing mice. The largest lobe was flash frozen and stored in liquid nitrogen while the remaining lobes were fixed in 10% neutral buffered formalin for 48 hours and embedded in paraffin.

Immunohistochemistry

Paraffin embedded sections of mammary glands from PyMT- and PyMT+ mice were deparaffinized with xylenes and rehydrated with graded alcohols. Tissue sections were stained with anti-F4/80 (1:250; cat #123102; Biolegend), anti-CD8 (1:200; cat # NBP1-49045; NovusBio), or anti-PyMT (1:500, cat #NB100-2749) antibodies. Five images were used to quantify CD8+ cells, F4/80+ macrophages surrounding ducts, and F4/80+ crown-like structures (CLS) and then averaged. PyMT+ glands stained with F4/80 were quantified based on area of staining surrounding mammary intraepithelial neoplasia (MIN) lesions and tumor borders. Staining was normalized by lesion or tumor area in the image. Metastasis was defined as a minimum of 5 cells stained positive in the lung tissue in proximity. All images were taken with Nikon Eclipse E600 Microscope (RRID:SCR_018858) and QICAM Fast 1394 camera (Teledyne Photometrics, Tuscon, AZ, USA). All images were analyzed using ImageJ (NIH, RRID:SCR_003070).

Picrosirius red staining was completed as described (22). Picrosirius red was quantified as described (23). Five images of comparably sized ducts were used to

quantify picrosirius red staining from tissue from each mouse. Image values were then averaged per mouse.

Statistical Analysis

Results are reported as the mean ± standard error of the mean (s.e.m.). Statistical differences were determined using two-way analysis of variance (ANOVA) and Tukey's multiple comparisons posttest, unless otherwise noted. A p-value of ≤0.05 denotes significant value. All statistical analyses were performed with GraphPad Prism 9.4.1 (GraphPad Software).

Results:

Obesity increased adipocyte size and collagen deposition around mammary ducts

To model how the risk factor of obesity interacts with elevated collagen density, WT and Het littermates were randomized to receive either LFD or HFD for 9 weeks (early timepoint) or 12-15 weeks (late timepoint), then mammary glands and serum were collected (Figure 2-1A). Both WT and Het mice fed HFD gained significantly more weight than mice in both groups fed LFD starting at 8 weeks of age (Figure 2-1B). At the early and late timepoints, HFD-fed groups were significantly heavier than their LFD-fed counterparts (Figure S2-1A, B) and had increased mammary gland weights (Figure S2-1C, D). Consistent with increased mammary gland weights, HFD-fed WT and Het mice had significantly larger adipocyte diameters within their mammary glands at both early and late timepoints (Figure 2-1C).

Although mammographic density and obesity have an inverse relationship (5, 6), we recently observed that obesity enhances collagen deposition in the mammary gland (23). To understand how obesity contributes to collagen deposition in this model over time, we quantified collagen around mammary ducts. At the early timepoint, no significant differences in collagen deposition around mammary ducts were observed in LFD or HFD-fed mice of either genotype (Figure 2-1D). However, HFD-fed Het mice had significantly greater collagen deposition around ducts compared to LFD-fed WT mice ($p=0.004$, Figure 2-1D). Similar to the early timepoint, no differences in collagen deposition around ducts were present in LFD-fed mice of either genotype at the late timepoint (Figure 2-1D). No differences were also observed between WT and Het HFD-fed mice (Figure 2-1D). However, HFD-fed mice of both genotypes had significantly increased collagen deposition surrounding ducts compared to LFD-fed mice of both genotypes (Figure 2-1D). Overall, obesity increased mammary gland weight, adiposity and collagen around ducts.

Obesity increased macrophage-associated inflammation and decreased CD8+ T cells within the mammary gland

Macrophages surrounding dying adipocytes form F4/80+ CLS. At the early timepoint, no differences were observed between genotypes of LFD-fed mice (Figure 2-2A). In contrast, HFD-fed Het mice had significantly more CLS than HFD-fed WT mice ($p=0.02$, Figure 2-2A). HFD-fed Het mice also had significantly more CLS than LFD-fed WT mice ($p=0.005$, Figure 2-2A). At the late timepoint, no significant differences were observed between LFD-fed mice of both genotypes (Figure 2-2A). HFD-fed mice of both genotypes had significantly increased numbers of CLS compared to LFD-fed WT

mice (Figure 2-2A). However, both groups of HFD-fed mice were not significantly different from each other (Figure 2-2A).

After quantifying CLS in white adipose tissue of the mammary glands, we also examined macrophages directly in contact with the epithelial cells of the ducts. F4/80+ macrophages were not significantly different in any group at the early timepoint (Figure 2-2B). In the late timepoint, LFD-fed mice of both genotypes did not have significant differences in the number of macrophages surrounding ducts. In contrast, HFD-fed groups had more F4/80+ macrophages around mammary ducts compared LFD-fed WT mice (Figure 2-2B). No significant differences were identified between HFD-fed mice of both genotypes (Figure 2-2B).

Next, we examined CD8+ T cell recruitment within mammary glands of LFD and HFD-fed mice of both genotypes. At the early timepoint, no differences were present between LFD-fed mice of either genotype or HFD-fed mice of either genotype (Figure 2-2C). However, HFD-fed mice of both genotypes had significantly reduced numbers of CD8+ T cells than either LFD-fed WT or Het mice (Figure 2-2C). Similar to the early timepoint, no differences were observed between genotypes fed LFD or those fed HFD at the late timepoint (Figure 2-2C). Both LFD-fed WT and Het mice had significantly more CD8+ T cells that HFD-fed WT mice (Figure 2-2C). LFD-fed Het mice also had significantly more CD8+ T cells than HFD-fed Het mice ($p=0.04$, Figure 2-2C). This data shows that both risk factors together increased macrophage inflammation. However, at the late timepoint obesity suppressed CD8+ T cell recruitment to the mammary gland.

Impact of risk factors on MMTV-PyMT tumor progression

To model how the risk factors of obesity and elevated collagen impacted mammary tumor growth, MMTV-PyMT+ (PyMT+) mice were crossed with Col1a1^{tm1jae} mice, then PyMT+ collagen wildtype (WT) and PyMT+ collagen heterozygous (Het) littermates were randomized to receive either LFD or HFD for 9 or 15 weeks. At the 9 and 15-week timepoints, mammary glands, serum, and lungs were collected (Figure 2-3A). PyMT+ WT and Het mice fed HFD gained significantly more weight than mice in both groups of PyMT+ mice fed LFD starting at 6 weeks of age (Figure 2-3B). At the 9-week timepoint, PyMT+ mice of both genotypes fed HFD weighed significantly more than LFD-fed mice of both genotypes, and no significant differences were observed between either HFD-fed or LFD-fed groups (Figure S2-3A). The body weights of the PyMT+ mice at the 9-week timepoint were very similar to the body weights of the PyMT- mice (Figure S2-2B). Similarly, no significant differences were noted between the body weights of PyMT+ mice at the 15-week timepoint compared to 15-week-old PyMT- mice of either genotype (Figure S2-2C). These results show that PyMT transgene expression did not alter weight gain in the mice of any genotype.

Early in tumor progression, PyMT+ mice developed multifocal preneoplastic lesions within their mammary glands. At the 9-week timepoint, mammary gland weight was still consistent with body weights in all groups (Figure 2-3C). Variable numbers of ductal hyperplasias were observed in the mammary glands of all PyMT+ mice regardless of genotype (Figure 2-3D). Additionally, all PyMT+ mice had the formation of variable numbers of MIN, with no differences between mice fed LFD or HFD or genotype (Figure 2-3E). While multiple mice in each group had progression to

adenocarcinoma present, no significant differences in adenocarcinoma incidence were observed in any of the groups (Figure 2-3F).

At the 15-week timepoint, mammary gland weights were more variable, and no significant differences were observed based on diet or genotype (Figure 2-3G). All of the mice in each diet and genotype group had evidence of the formation of adenocarcinomas present in their mammary glands. Overall, risk factors did not affect the development of neoplastic lesions in the PyMT+ model.

Obesity and mammary density increased macrophage recruitment around tumors

Since we observed differences in immune cells in healthy mammary tissue, we hypothesized that differences in immune cells would be present during tumor progression. At 9 weeks, no differences were observed in F4/80+ macrophages surrounding MIN in any of the groups of PyMT+ mice (Figure 2-4A). With tumor progression to adenocarcinomas at 15 weeks, F4/80+ macrophages surrounding tumors were significantly higher in LFD-fed Het ($p=0.001$) and HFD-fed WT ($p=0.0007$) mice as compared to LFD-fed WT controls. Macrophages surrounding the tumors of HFD-fed Het mice were more variable (Figure 2-4B). No differences were observed in F4/80+ macrophages within the tumors of mice in any group (Figure S2-2D).

In the mammary tissue of PyMT- mice, we observed that obesity significantly reduced the recruitment of CD8+ T cells into the mammary glands (Figure 2-2C). However, in PyMT+ tumors, we did not observe any significant differences in CD8+ T cells (Figure 2-4C).

Obesity and breast density together increased metastasis to the lungs

To assess how the two risk factors contributed to pulmonary metastasis, we quantified metastases in the lungs of PyMT+ mice at 9- and 15-week timepoints. We saw no significant differences in the total number of PyMT+ metastases at 9 weeks (Figure 2-5). However, at 15 weeks, PyMT+ Het mice had significantly more metastasis within the lungs compared to either LFD-fed WT mice ($p=0.03$) or HFD-fed WT mice ($p=0.05$, Figure 2-5). Together, these results suggest that together increased collagen and obesity enhance metastasis during tumor progression.

Discussion

The relationship between breast density and obesity on breast cancer risk and progression are not well understood. Here we used an established model of mammary density with diet-induced obesity to assess mammary gland changes that may alter breast cancer risk. Understanding the immune cell and extracellular matrix changes that occur due to breast density and obesity will allow for better predictors of risk, identification of preventative strategies, and the development of unique approaches to breast cancer treatment.

Obesity enhanced macrophages within mammary glands in the mammary glands of non-tumor bearing mice. Adipocyte diameters and mammary gland weights were significantly larger at the early timepoint than LFD-fed WT mice. However, increased numbers of macrophages due to obesity were not seen until the late timepoint, suggesting that 5 weeks of exposure to the HFD was not sufficient induce mammary gland inflammation. We have previously observed mammary gland inflammation due to

obesity following consumption of HFD for 16 weeks (24). This observation is consistent with other studies showing that adipocyte stress and subsequent death due to hypertrophy correlates positively with obesity over time (25, 26). Adipocyte death also correlates with adipocyte size (25), which was highest at the late timepoint. One mechanism of macrophage recruitment into adipose tissue in obesity is through expression of monocyte chemoattractant protein-1 (MCP-1) /CC chemokine ligand 2 (CCL2) by adipocytes (27). Hypoxia also promotes macrophage recruitment. Adipose tissue with low oxygenation was found to have higher macrophage mRNA levels in human tissue in obesity (28). It is possible that increased collagen in the mammary glands of Het mice could exacerbate adipocyte death with obesity, leading to the elevated CLS that we observed in the mammary glands of HFD-fed Het mice at both early and late timepoints. Although we observed mildly elevated macrophages in the mammary glands of LFD-fed Het mice, similar to other studies looking at macrophages within high mammographic dense tissue (29), this difference did not reach significance. Overall, obesity and breast density together may enhance adipocyte stress and death creating an inflammatory environment.

Increased macrophages and collagen are thought to have suppressive effects on the recruitment of CD8+ T cells (30-32). Interestingly, we found that CD8+ T cells were reduced in non-tumor bearing HFD-fed mice at both the early and late timepoints, while we did not observe differences in CD8+ T cell recruitment with increased collagen density. Within the tumor microenvironment, we observed increased macrophages around the tumors of LFD-fed Het mice, and macrophages may have an immunosuppressive effect in the tumor microenvironment (33). However, LFD-fed Het

mice had similar levels of CD8+ T cells within tumors compared to LFD-fed WT mice. Although we observed similar patterns of macrophage recruitment between mammary density and obesity, the T cell responses appear to differ. This may suggest that there are functional differences in macrophages found in tumors associated with breast density and obesity, and further work is necessary to explore these differences in both macrophages and T cells.

In mice expressing the PyMT transgene, we did not see any differences in the frequency of hyperplasia or MIN at 9 weeks of age regardless of collagen genotype or diet. Although other groups have seen increased tumor progression in Col1a1^{tmjae} mice, the formation of early lesions was not explored (16). Diet-induced obesity has been shown to increase the tumor size in MMTV-PyMT mice, while MIN were seen mostly in LFD-fed mice, suggesting that the MIN progressed at a higher rate to tumors in the HFD-fed mice (34). Overall, we observed that the quantification of these early lesions was variable across collagen density and diet groups. We then sought to quantify macrophages surrounding early MIN lesions and tumors of MMTV-PyMT mice because of the known effects of macrophages on tumorigenesis. We previously observed that HFD-fed mice had increased macrophages surrounding hyperplasias and tumors in a trp53$^{-/-}$ model of mammary tumorigenesis (35). In this study, we did not observe significant difference in macrophages around MIN or within tumors. However, others have shown increased CD68+ macrophages in tumors of MMTV-PyMT mice on the FVB/N genetic background following feeding a HFD for 8 weeks (36). It is possible that the combination of risk factors could have a more pronounced impact on early

tumor formation and progression in a transgenic model with a greater latency to tumor formation or on a different genetic background of mice.

Mice expressing the PyMT transgene have detectible metastases to the lungs and lymph nodes around 13-14 weeks of age with a mean latency of 92 days (37). We hypothesized that these risk factors may accelerate this process, so we quantified metastasis at an early timepoint of 9 weeks. Interestingly, we observed metastases in all groups as early as 9 weeks, but no differences were observed among any groups. This data is consistent with a study showing no differences in pulmonary metastasis at 12 weeks of age in HFD-fed MMTV-PyMT mice compared to controls (36). In contrast, other studies have identified an increase in the size and number of metastases in HFD-fed mice (38) (39). The differences in metastasis in these models could be due to differences in mouse models or diet composition. Although we did not see a difference in metastasis with one risk factor alone, we saw significant increases in metastasis in HFD-fed Het mice compared to LFD-fed WT and Het mice.

Overall, our study shows that mammary gland density enhanced macrophage recruitment similar to mice fed HFD. However, over time, macrophage recruitment was associated with increased adiposity. Further, CD8+ T cell exclusion from mammary glands was dependent upon obesity. Interestingly, early induction of CLS and collagen deposition were seen in HFD-fed Het mice. These data suggest that both risk factors together may promote a maladaptive immune cell infiltration and extracellular matrix remodeling. Thus, breast density and obesity may cooperatively increase breast cancer risk. Obesity and breast density together promoted lung metastasis compared to mammary density alone. Future functional studies are needed to understand how

obesity and breast density alter inflammation. These studies suggest that women with dense breasts who become obese may have an increased risk for breast cancer and early progression to pulmonary metastasis.

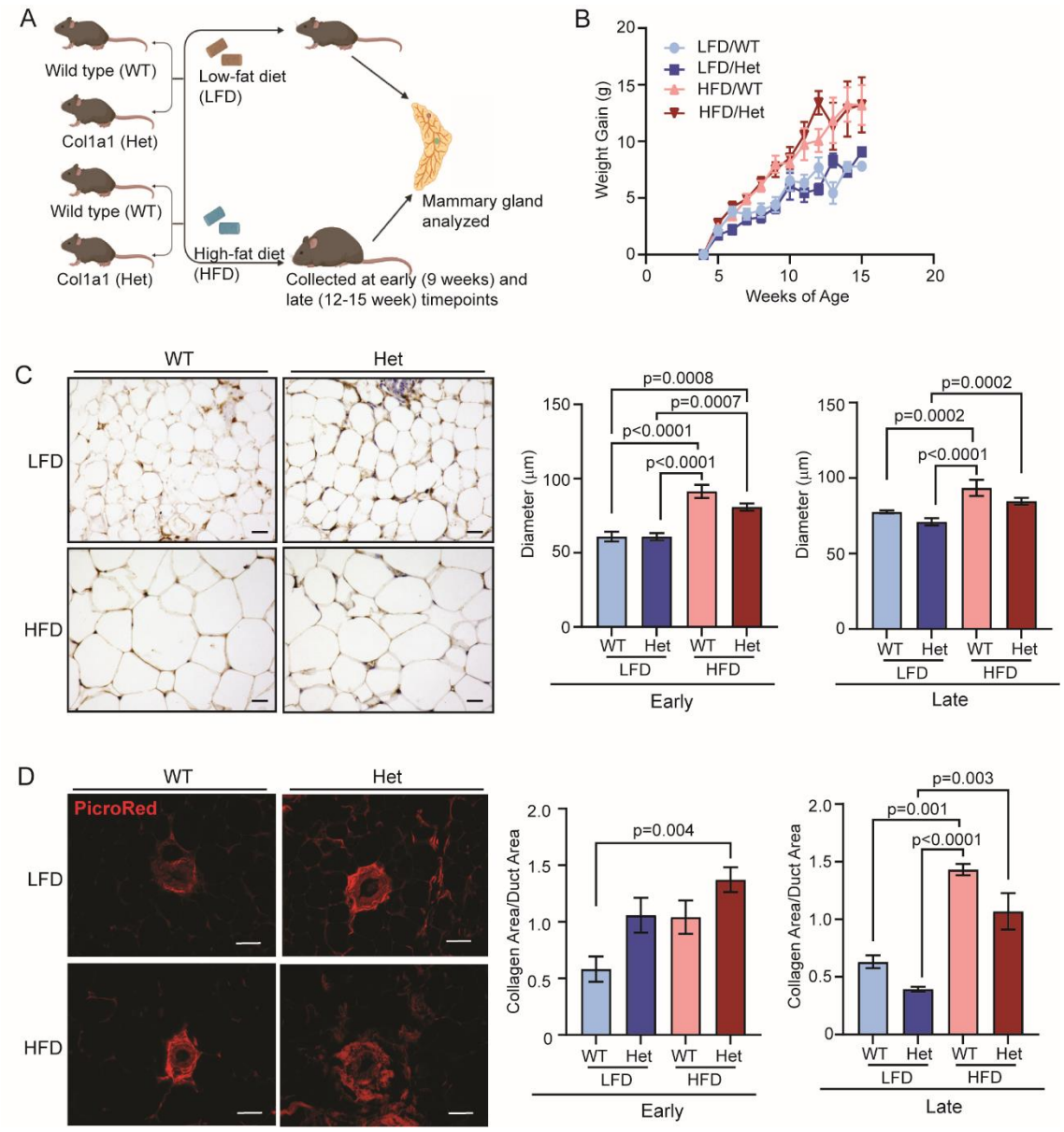

Figure 2-1: Obesity increased adipocyte size and collagen around mammary ducts. compared to mice from a model of breast density. A. Wild type (WT) mice were crossed with Col1a1^{tmjae} mice then WT and heterozygous (Het) littermates were fed low-fat diet (LFD) or high-fat diet (HFD). Mammary glands were collected from LFD/WT, LFD/Het, HFD/WT, or HFD/Het mice at the early (9 weeks) or late (12-15 weeks) timepoints. **B.** Weight gain of all four experimental groups (n=13-14 mice/group). **C.** Adipocyte diameter for early and late timepoints. Early timepoint (n= 6 mice/group) and late timepoint (n=6-8 mice/group). Representative images of mammary adipose tissue are from mice from the late timepoint. **D.** Quantified collagen around mammary ducts as a ratio of collagen area/ductal area, early timepoint (n= 4-6 mice/group) and late timepoint (n= 4-6 mice/group). Representative images are from mice from the late timepoint. Magnification bars **C**: 100 µm, **D**: 50 µm.

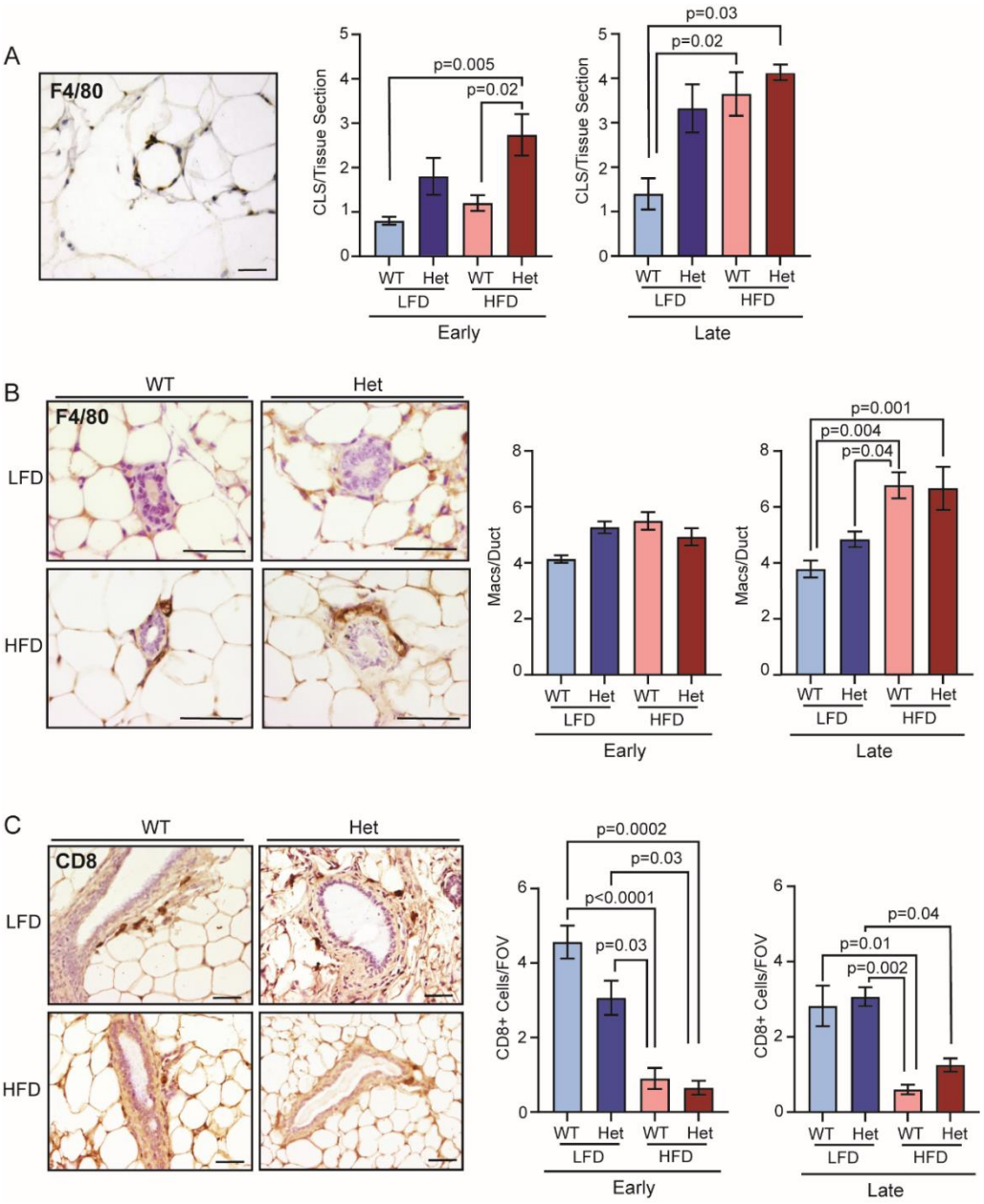

Figure 2-2: Obesity enhanced macrophage-driven inflammation and reduced CD8+ T cells compared to collagen dense mammary glands. A. Crown-like structures (CLS) of F4/80+ macrophages were quantified per tissue section in mammary glands from early timepoint (n=5-6 mice/group) and late timepoint (n=4-6 mice/group) mice. Representative images from each experimental group at the late timepoint. **B.** Quantification of F4/80+ macrophages around mammary ducts. Results are shown as an average count of macrophages at early timepoint (n= 6 mice/group) and late timepoint (n= 6-8 mice/group). Representative images are ducts from the late timepoint. **C.** Quantification of CD8+ T cells in the mammary gland. Early timepoint (n= 4-6 mice/group) and late timepoint (n= 4-8 mice/group). Data is represented as an average per field of view (FOV) in the adipose tissue of the gland. Magnification bars **A, C**: 50 µm, **B**: 25 µm.

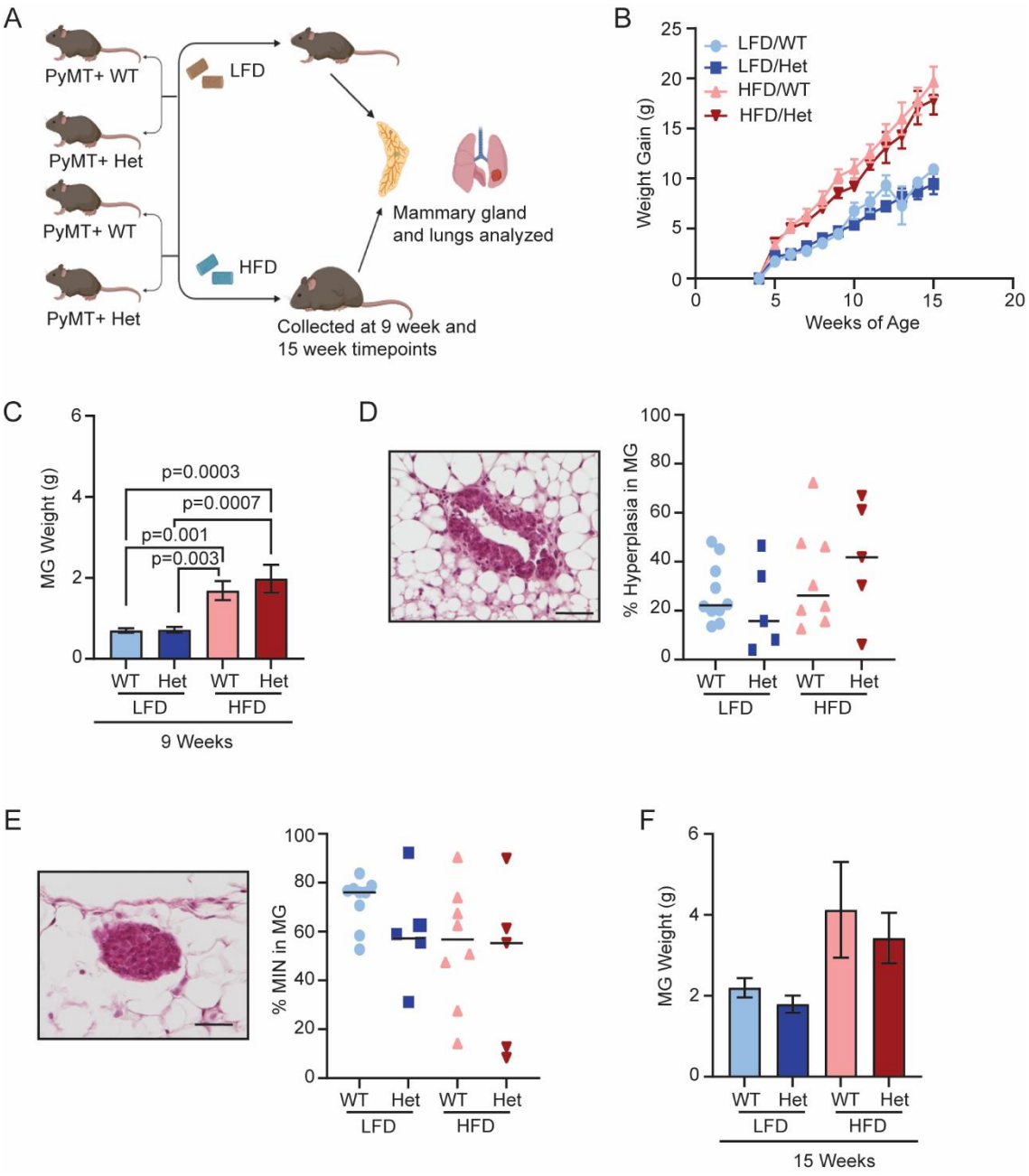

Figure 2-3: The effect of obesity and breast density on tumor stage and mammary gland weight in the MMTV-PyMT mouse model. A. MMTV-PyMT (PyMT+) mice were crossed with Col1a1^{tmjae} mice, and PyMT+ WT and PyMT+ Het littermates were fed either LFD or HFD. Mammary glands and lungs were collected from LFD-fed PyMT+ WT or PyMT+ Het mice or HFD-fed PyMT+ WT or PyMT+ Het mice at 9 or 15 weeks. **B.** Weight gain in grams (g) of all four experimental groups (n= 11-20 mice/group). HFD-fed groups were significantly heavier than LFD-fed groups by 6 weeks. **C.** Percentage of ducts in the mammary glands of each group that were hyperplastic (n=5-10 mice/group). Representative image shows a duct that depicts hyperplasia that was used as the standard for quantification. **D.** Percentage of ducts in the mammary gland that formed MIN. Representative image shows MIN that was used as standard for

quantification (n= 5-9 mice/group). **E.** Mammary gland weight of mice at 9-week timepoint (n= 6-10 mice/group). **F**. Number of mice with adenocarcinomas and no tumor formation at 9-week timepoint (n=5-9 mice/group). No differences observed among groups (Fishers exact test). **G**. Mammary gland weight of mice at 15-week timepoint (n= 6-10 mice/group). Magnification bars 50 µm.

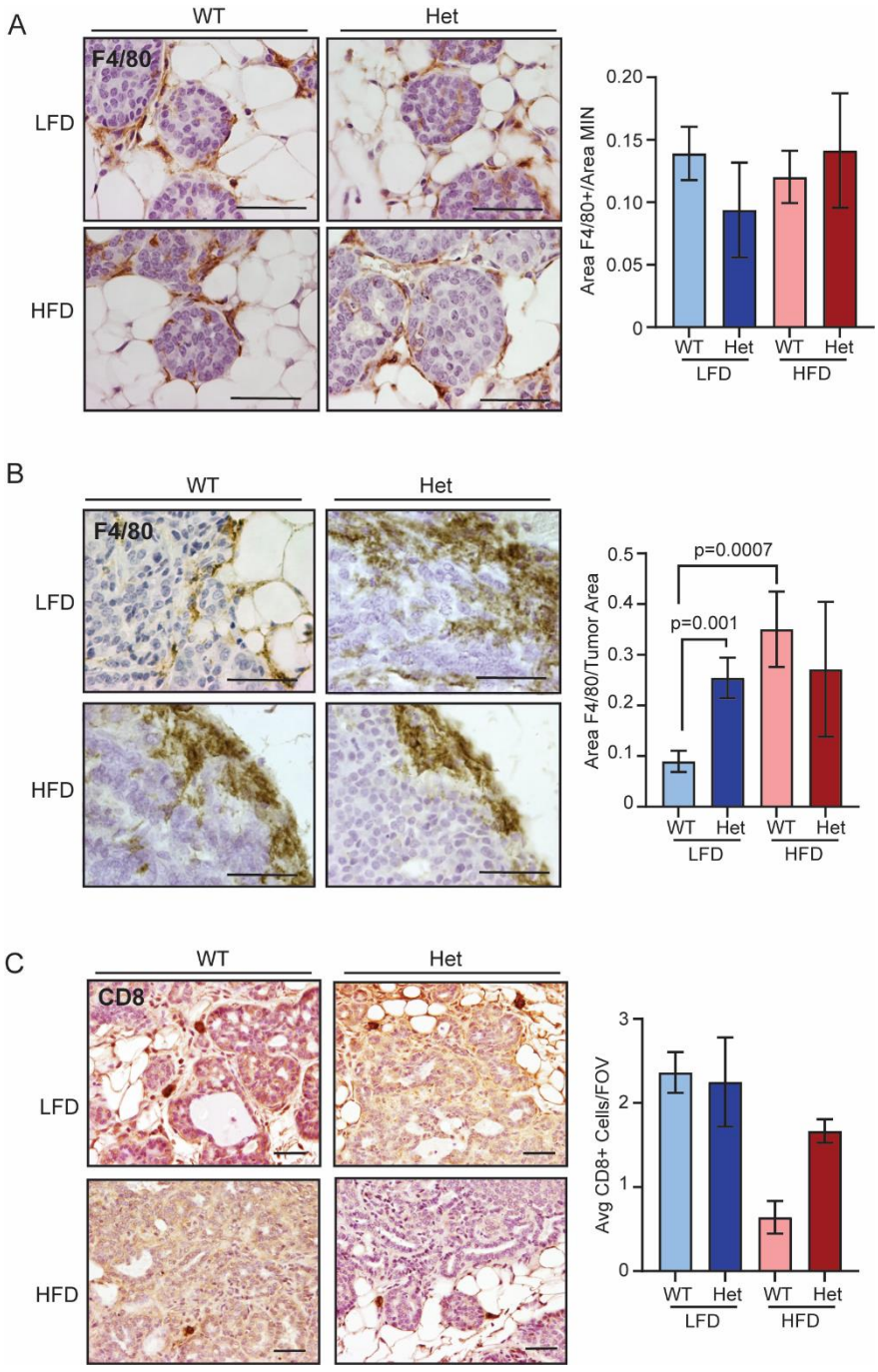

Figure 2-4: Obesity and mammary gland density increased macrophage recruitment around tumors. **A.** The ratio of F4/80+ macrophages area to MIN lesion area in mammary glands of mice at 9-week timepoint (n= 5-10 mice/group). **B.** The ratio of F4/80+ macrophage area on the tumor edge to tumor area (n= 5-10 mice/group) at the 15-week time point. **C.** Average number of CD8+ cells per field of view (FOV) per gland (n= 5-6 mice/group). Representative images of CD8+ T cells in adenocarcinomas from mice at 15-week timepoint. Magnification bars **A**, **B**: 25 µm, **C**: 50 µm.

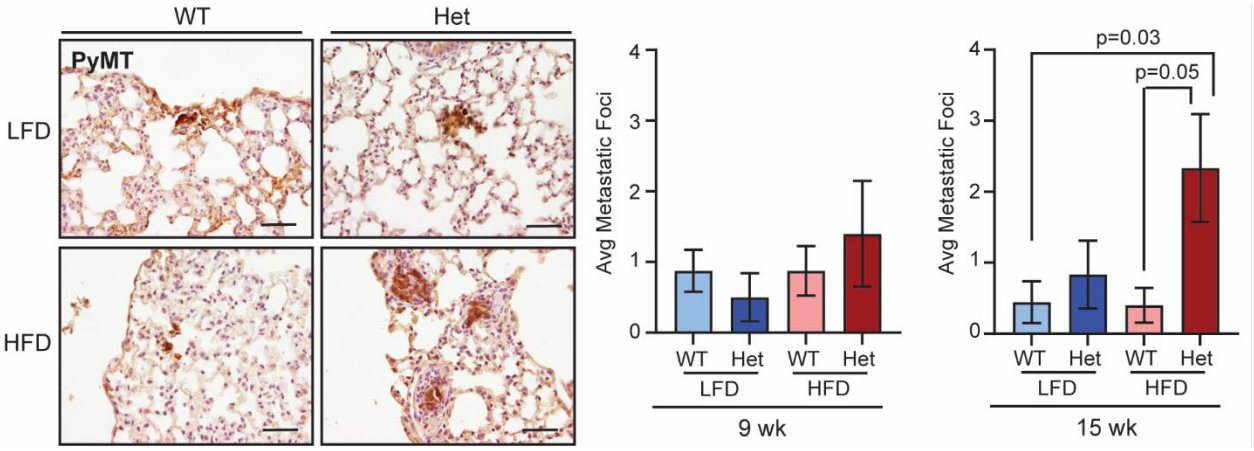

Figure 2-5: Lung metastasis was increased in mice with both obesity and breast density. A. Metastatic foci quantified in the lungs of PyMT+ mice at the 9 week timepoint (n=5-8 mice/group). **B.** Metastatic foci quantified in the lungs of PyMT+ mice at 15 week timepoint. (n= 5-9 mice/group). Magnification bars 50 µm.

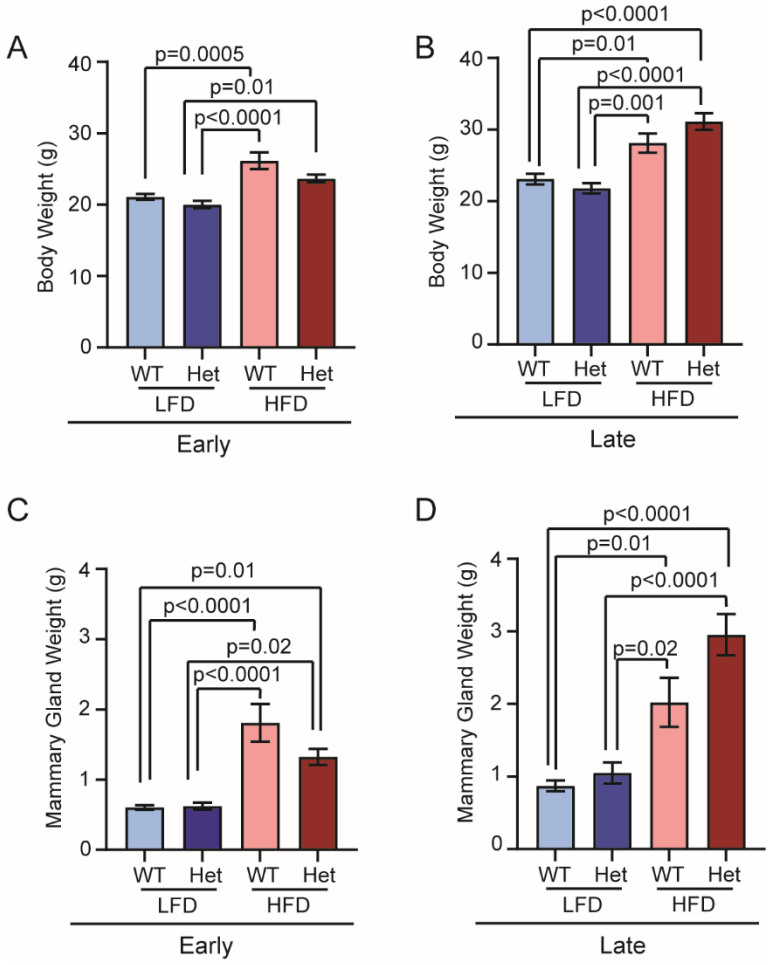

Supplementary Figure 2-1: Obesity increased mouse and mammary gland weight in non-tumor bearing mice. A. Body weight of mice in grams (g) at the early timepoint of 9 weeks (n= 6 mice/group). **B.** Mammary gland weight in g at the early timepoint (n= 6 mice/group). **C.** Body weight at the late timepoint of 12-15 weeks (n= 6 mice/group). **D.** Mammary gland weight of mice from late timepoint (n= 6-8 mice/group).

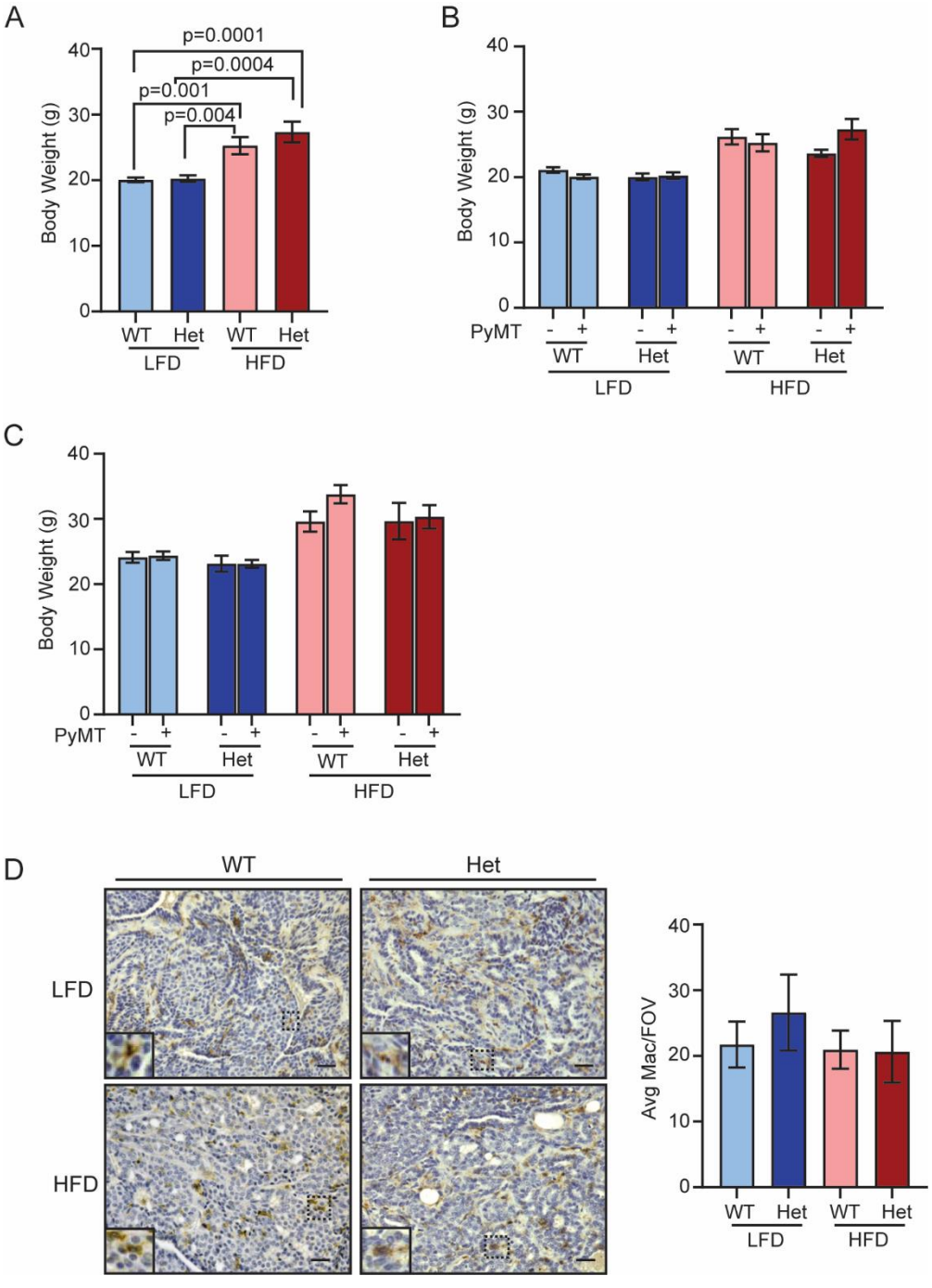

Supplementary Figure 2.2: MMTV-PyMT status did not affect body weight and risk factors did not affect intratumoral macrophage recruitment. A. Body weight of PyMT+ mice in grams (g) at 9-week timepoint (n= 5-10 mice/group). **B.** Comparison of final body weights of PyMT- and PyMT+ mice at 9-week timepoint (n= 6-10 mice/group). **C.** Comparison of final body weight of PyMT- and PyMT+ mice at 15-week timepoint (n= 6-8 mice/group). **D.** Quantification of F4/80+ macrophages within PyMT+ tumors per field of view (FOV) at 15-week timepoint (n= 4-6 mice/group). Magnification bar: 50 µm.

References:

1. Ewertz M, Jensen MB, Gunnarsdóttir K, Højris I, Jakobsen EH, Nielsen D, et al. Effect of obesity on prognosis after early-stage breast cancer. J Clin Oncol. 2011;29(1):25-31.

2. Sestak I, Distler W, Forbes JF, Dowsett M, Howell A, Cuzick J. Effect of body mass index on recurrences in tamoxifen and anastrozole treated women: an exploratory analysis from the ATAC trial. J Clin Oncol. 2010;28(21):3411-5.

3. NCI. Dense Breasts: Answers to commonly asked questions 2024 [Available from: https://www.cancer.gov/types/breast/breast-changes/dense-breasts#:~:text=Breast%20density%20is%20a%20term,amounts%20of%20fatty%20breast%20tissue.

4. Boyd NF, Rommens JM, Vogt K, Lee V, Hopper JL, Yaffe MJ, et al. Mammographic breast density as an intermediate phenotype for breast cancer. Lancet Oncol. 2005;6(10):798-808.

5. Pettersson A, Graff RE, Ursin G, Santos Silva ID, McCormack V, Baglietto L, et al. Mammographic density phenotypes and risk of breast cancer: a meta-analysis. J Natl Cancer Inst. 2014;106(5).

6. Boyd NF, Martin LJ, Sun L, Guo H, Chiarelli A, Hislop G, et al. Body size, mammographic density, and breast cancer risk. Cancer Epidemiol Biomarkers Prev. 2006;15(11):2086-92.

7. Tran TXM, Moon SG, Kim S, Park B. Association of the Interaction Between Mammographic Breast Density, Body Mass Index, and Menopausal Status With Breast Cancer Risk Among Korean Women. JAMA Netw Open. 2021;4(12):e2139161.

8. Shieh Y, Scott CG, Jensen MR, Norman AD, Bertrand KA, Pankratz VS, et al. Body mass index, mammographic density, and breast cancer risk by estrogen receptor subtype. Breast Cancer Res. 2019;21(1):48.

9. Alowami S, Troup S, Al-Haddad S, Kirkpatrick I, Watson PH. Mammographic density is related to stroma and stromal proteoglycan expression. Breast Cancer Res. 2003;5(5):R129-35.

10. Li T, Sun L, Miller N, Nicklee T, Woo J, Hulse-Smith L, et al. The association of measured breast tissue characteristics with mammographic density and other risk factors for breast cancer. Cancer Epidemiol Biomarkers Prev. 2005;14(2):343-9.

11. Guo YP, Martin LJ, Hanna W, Banerjee D, Miller N, Fishell E, et al. Growth factors and stromal matrix proteins associated with mammographic densities. Cancer Epidemiol Biomarkers Prev. 2001;10(3):243-8.

12. Beare AH, O'Kane S, Krane SM, Ferguson MW. Severely impaired wound healing in the collagenase-resistant mouse. J Invest Dermatol. 2003;120(1):153-63.

13. Liu X, Wu H, Byrne M, Jeffrey J, Krane S, Jaenisch R. A targeted mutation at the known collagenase cleavage site in mouse type I collagen impairs tissue remodeling. J Cell Biol. 1995;130(1):227-37.

14. Provenzano PP, Inman DR, Eliceiri KW, Knittel JG, Yan L, Rueden CT, et al. Collagen density promotes mammary tumor initiation and progression. BMC Med. 2008;6:11.

15. García-Mendoza MG, Inman DR, Ponik SM, Jeffery JJ, Sheerar DS, Van Doorn RR, et al. Neutrophils drive accelerated tumor progression in the collagen-dense mammary tumor microenvironment. Breast Cancer Res. 2016;18(1):49.

16. Esbona K, Inman D, Saha S, Jeffery J, Schedin P, Wilke L, et al. COX-2 modulates mammary tumor progression in response to collagen density. Breast Cancer Res. 2016;18(1):35.

17. Barcus CE, O'Leary KA, Brockman JL, Rugowski DE, Liu Y, Garcia N, et al. Elevated collagen-I augments tumor progressive signals, intravasation and metastasis of prolactin-induced estrogen receptor alpha positive mammary tumor cells. Breast Cancer Research2017.

18. Danforth DN. The Role of Chronic Inflammation in the Development of Breast Cancer. Cancers (Basel). 2021;13(15).

19. Abrahamsson A, Rzepecka A, Romu T, Borga M, Leinhard OD, Lundberg P, et al. Dense breast tissue in postmenopausal women is associated with a pro-inflammatory microenvironment in vivo. Oncoimmunology. 2016;5(10):e1229723.

20. Maliniak ML, Miller-Kleinhenz J, Cronin-Fenton DP, Lash TL, Gogineni K, Janssen EAM, et al. Crown-Like Structures in Breast Adipose Tissue: Early Evidence and Current Issues in Breast Cancer. Cancers (Basel). 2021;13(9).

21. Weisberg SP, McCann D, Desai M, Rosenbaum M, Leibel RL, Ferrante AW, Jr. Obesity is associated with macrophage accumulation in adipose tissue. J Clin Invest. 2003;112(12):1796-808.

22. Wegner KA, Keikhosravi A, Eliceiri KW, Vezina CM. Fluorescence of Picrosirius Red Multiplexed With Immunohistochemistry for the Quantitative Assessment of Collagen in Tissue Sections. The journal of histochemistry and cytochemistry : official journal of the Histochemistry Society. 2017;65(8):479-90.

23. Kuziel G, Moore BN, Haugstad GP, Arendt LM. Fibrocytes enhance mammary gland fibrosis in obesity. Faseb j. 2023;37(7):e23049.

24. Chamberlin T, Thompson V, Hillers-Ziemer LE, Walton BN, Arendt LM. Obesity reduces mammary epithelial cell TGFβ1 activity through macrophage-mediated extracellular matrix remodeling. Faseb j. 2020.

25. Cinti S, Mitchell G, Barbatelli G, Murano I, Ceresi E, Faloia E, et al. Adipocyte death defines macrophage localization and function in adipose tissue of obese mice and humans. J Lipid Res. 2005;46(11):2347-55.

26. Engin AB. Adipocyte-Macrophage Cross-Talk in Obesity. Adv Exp Med Biol. 2017;960:327-43.

27. Kanda H, Tateya S, Tamori Y, Kotani K, Hiasa K, Kitazawa R, et al. MCP-1 contributes to macrophage infiltration into adipose tissue, insulin resistance, and hepatic steatosis in obesity. J Clin Invest. 2006;116(6):1494-505.

28. Pasarica M, Sereda OR, Redman LM, Albarado DC, Hymel DT, Roan LE, et al. Reduced adipose tissue oxygenation in human obesity: evidence for rarefaction, macrophage chemotaxis, and inflammation without an angiogenic response. Diabetes. 2009;58(3):718-25.

29. Huo CW, Hill P, Chew G, Neeson PJ, Halse H, Williams ED, et al. High mammographic density in women is associated with protumor inflammation. Breast Cancer Research2018.

30. Zhang W, Zhang Q, Yang N, Shi Q, Su H, Lin T, et al. Crosstalk between IL-15Rα(+) tumor-associated macrophages and breast cancer cells reduces CD8(+) T cell recruitment. Cancer Commun (Lond). 2022;42(6):536-57.

31. Hillers-Ziemer LE, McMahon RQ, Hietpas M, Paderta G, LeBeau J, McCready J, et al. Obesity Promotes Cooperation of Cancer Stem-Like Cells and Macrophages to Enhance Mammary Tumor Angiogenesis. Cancers (Basel). 2020;12(2).

32. DH P, BL R, L D, L C, J W, LA B, et al. Collagen promotes anti-PD-1/PD-L1 resistance in cancer through LAIR1-dependent CD8 + T cell exhaustion. Nature communications. 2020;11(1).

33. Peranzoni E, Lemoine J, Vimeux L, Feuillet V, Barrin S, Kantari-Mimoun C, et al. Macrophages impede CD8 T cells from reaching tumor cells and limit the efficacy of anti-PD-1 treatment. Proc Natl Acad Sci U S A. 2018;115(17):E4041-e50.

34. Cranford TL, Velázquez KT, Enos RT, Sougiannis AT, Bader JE, Carson MS, et al. Effects of high fat diet-induced obesity on mammary tumorigenesis in the PyMT/MMTV murine model. Cancer Biol Ther. 2019;20(4):487-96.

35. Chamberlin T, Clack M, Silvers C, Kuziel G, Thompson V, Johnson H, et al. Targeting Obesity-Induced Macrophages during Preneoplastic Growth Promotes Mammary Epithelial Stem/Progenitor Activity, DNA Damage, and Tumor Formation. Cancer Res. 2020;80(20):4465-75.

36. Cowen S, McLaughlin SL, Hobbs G, Coad J, Martin KH, Olfert IM, et al. High-Fat, High-Calorie Diet Enhances Mammary Carcinogenesis and Local Inflammation in MMTV-PyMT Mouse Model of Breast Cancer. Cancers (Basel). 2015;7(3):1125-42.

37. Bharadwaj AG, Dahn ML, Liu RZ, Colp P, Thomas LN, Holloway RW, et al. S100A10 Has a Critical Regulatory Function in Mammary Tumor Growth and Metastasis: Insights Using MMTV-PyMT Oncomice and Clinical Patient Sample Analysis. Cancers (Basel). 2020;12(12).

38. Sundaram S, Yan L. Adipose monocyte chemotactic protein-1 deficiency reduces high-fat diet-enhanced mammary tumorigenesis in MMTV-PyMT mice. J Nutr Biochem. 2020;77:108313.

39. Sundaram S, Yan L. High-fat Diet Enhances Mammary Tumorigenesis and Pulmonary Metastasis and Alters Inflammatory and Angiogenic Profiles in MMTV-PyMT Mice. Anticancer Res. 2016;36(12):6279-87.

CHAPTER 3:

Obesity contributes to CD8+ T cell dysfunction in the lungs before and after ERα+ breast cancer metastasis.

Abstract:

Breast cancer patients with obesity have an increased risk for metastases following diagnosis. We have previously observed that obesity enhances macrophages surrounding breast cancer metastasis, however little is known about how obesity alters the function of adaptive immune cells in the metastatic niche of the lungs in obesity. To test adaptive immune function in the lungs, we fed female mice either a low-fat diet (LFD) or high-fat diet (HFD) to induce obesity, then we transplanted estrogen receptor alpha positive (ERα+) TC2 cells into the mammary fat pads. Tumors grew to 0.5 cm in diameter then were surgically removed to model metastatic growth. Eight weeks after tumor removal, T cell populations were quantified in metastatic lung tissue or lung tissue from non-tumor bearing mice using flow cytometry. To assess how obesity alters the functional state of T cells, CD45+ cells were sorted from lungs from lean and obese mice with and without metastasis, and gene expression was examined using the Nanostring nCounter Immune Exhaustion panel. We also disassociated whole lung tissue from LFD and HFD-fed mice and stimulated CD8+ T cells to measure cytokine expression. In the lungs of non-tumor bearing mice, CD8+ T cells from obese mice expressed higher levels of PD-1, and immune cells from the lungs of obese mice had increased expression of genes associated with T cell receptor signaling. Stimulated T cells from obese mice produced less cytokines compared to lean mice. In metastatic lungs from obese mice, immune cells had higher expression of genes associated with T cell receptor signaling and reduced expression of genes associated with interferon and tumor necrosis factor alpha (TNFα) signaling. Following stimulation, CD8+ T cells from metastatic lungs of obese mice secreted significantly higher levels of TNFα in response

to stimulation. These results suggest that obesity increases T cell dysfunction in ERα+ breast cancer lung metastasis, but stimulation of CD8+ T cells uncovers increased functional responses despite PD-1 expression.

Introduction:

Obesity rates are increasing worldwide, and the rates of obesity in women are higher or equal to men depending on ethnicity (1). As more women are considered obese, the higher the risk for cancer amongst women, particularly an increased risk for postmenopausal breast cancer (2-5). After the diagnosis of breast cancer, women with a body mass index (BMI) ≥30 kg/m^2 have worse disease outcomes and resistance to most therapeutic interventions (6). Obese breast cancer patients also have more advanced disease at the time of diagnosis, specifically higher-grade tumors, and more distant metastasis, particularly to the lungs (7). Patients who are obese also develop metastasis more frequently than their lean counterparts and have a higher risk of dying from their disease (8-10). ERα+ breast cancer accounts for most cancer subtypes diagnosed in women (11). Obese patients are at risk for developing ERα+ Luminal B breast cancer (12), which has an elevated expression of proliferation markers and higher histologic grade (13). Women who are obese with ERα+ tumors have decreased overall survival and an increased risk for metastasis (14, 15). Although ERα+ tumors are removed as part of standard of care, metastasis can occur decades after resection (16). While there have been studies identifying poor adaptive immune responses in the lungs in response to infectious respiratory diseases and vaccines under conditions of obesity (17), little is known how obesity affects the response to breast cancer metastasis in the lungs.

Obesity has been characterized as a chronic inflammatory disease (18). However, adaptive immune cell dysfunction or exclusion, particularly impaired CD8+ T cell function, has been reported under conditions of obesity in primary breast tumors,

visceral fat, spleen, and in circulation (19-22). Exhaustion is a type of T cell dysfunction caused by abundant and chronic antigen stimulation and inflammatory signals (23). T cell exhaustion is often defined by programmed cell death-1 (PD-1) expression on T cells along with other checkpoint marker expression, such as Lag-3 and Tim-3 (24). It was thought that T cell exhaustion led to a homogenous population that lost effector function progressively over time. However, now it's known that this population of CD8+ T cells is heterogenous and includes some subsets of exhausted CD8+ T cells that have stem cell function (25). T cell dysfunction has been identified in the lungs of obese patients and is attributed to poorer outcomes in respiratory infectious disease (26). However, the impact of obesity on T cell dysfunction before and after metastatic disease has not been examined.

Recent clinical studies suggest that patients with obesity that received immune checkpoint blockade (ICB) targeting the PD-1/PD-L1 axis for melanoma and lung cancer had improved outcomes.(27-29). However, these improved responses in patients with obesity were observed more frequently in men (27). ICB has not been well-explored as a treatment for patients with ERα+ breast cancer, because ERα+ breast cancer is considered immunologically "cold" compared to other breast cancer subtypes (30) (31) In order to enhance ICB efficacy and improve outcomes for more patients, it is crucial to understand how obesity alters the function of adaptive immune cells in the metastatic environment.

In metastasis, CD8+ T cells have shown to be reduced compared to levels in primary tumors (32). Our lab and others have shown a shift in the myeloid population in the lungs under conditions of obesity that may contribute to increased metastasis (33,

34). However, adaptive immune cells like CD8+ T cells have not been widely explored in lung metastasis under obese conditions. In our study, we used ERα+ TC2 mammary tumor cells to study ERα+ breast cancer metastasis, which has been previously challenging to model in mice (35). Here we investigate CD8+ T cell function in non-tumor bearing mice and mice with ERα+ lung metastasis under conditions of obesity. We discovered that obese mice have increased PD-1+ CD8+ T cells in the lungs before and after metastasis. After metastasis, CD8+ T cells retain function to produce cytokines after stimulation. These results provide new insight into CD8+ T cell function in the lungs under conditions of obesity.

Methods:

Mouse Models

All animal procedures were approved by the University of Wisconsin Institutional Animal Care and Use Committee, per guidelines published by the NIH Guide for the Care and Use of Laboratory Animals (Animal protocol number V005188). All mice were housed in AAALAC-accredited facilities. Three-week-old-female FVB/N (FVB/NTac, Taconic Biosciences) mice were fed either a purified chow low-fat diet (LFD; 16% kcal from fat; 2920X; Teklad Global; ENVIGO) or a high-fat diet (HFD; 60% kcal from fat; Test Diet 58Y1; 0056833) for 16 weeks to induce obesity. Food and water were provided *ad libitum.* Body weights were measured weekly. Non-tumor-bearing mice were used as controls, and lungs were collected after 16 weeks on the diets. For metastases, LFD and HFD-fed mice were orthotopically transplanted with ERα+ green fluorescence protein (GFP) expressing TC2 cells. TC2 cells have previously been reported as ERα+ (36). 75,000 TC2 cells suspended in PBS were injected into bilateral

fourth inguinal mammary glands. Tumor diameters were measured each week using calipers. Tumor volume was calculated using the formula (L*W*W)/2. Once tumors reached a diameter of 0.5 cm, tumors were resected. If tumors recurred at the surgical site, mice were excluded from the study. Mice were fed their respective diets for another 8 weeks before collection. Mice were then euthanized with CO_2 asphyxiation.

Cell Culture

TC2 cells were provided by Dr. Linda Schuler at the University of Wisconsin-Madison. TC2 cells were cultured in DMEM (Corning; 10-017-CV, Corning, NY, USA) supplemented with 10% FBS and 1 mg/mL G418 (ThermoFisher Scientific; 11811023, Waltham, MA, USA). All media contained 1% antibiotic/antimycotic solution, and cells were maintained at 37°C in 5% CO_2. Tumor cell lines were not further validated and were tested for mycoplasma prior to use in experiments (Idexx BioAnalytics, Columbia, MO, USA). Before transplantation TC2 cells were trypsinized with 0.25% trypsin for 5 minutes at 37 °C in 5% CO_2. Cells were then counted and suspended in PBS at 2.5 $x10^3$ cells/mL.

Tissue Collection

Blood was removed from lungs via cardiac puncture following euthanasia. The three largest lobes of the lungs from each mouse were manually minced in 1 mL of DMEM (Corning, 10-017-CV) supplemented with 10% FBS (Gibco, A52567-01), 1% antibiotic-antimycotic solution (Corning, 30-004-CI), 10 µg/mL insulin (Sigma-Aldrich, I0516), 5 ng/mL human epidermal growth factor (Sigma-Aldrich, E9644), 0.5 µg/mL hydrocortisone (Sigma-Aldrich, H0888), 3 mg/mL collagenase A (Sigma-Aldrich, 11088793001),100 U/mL hyaluronidase (Sigma-Aldrich, H3506), and 0.1 mg/mL DNase I (Sigma-Aldrich,

10104159001) and digested for 45 mins at 37°C. The two smaller lobes of the lungs were fixed for 2 hours in 4% paraformalin at 4°C, followed by rinsing with PBS three times for 30 min. Lungs were incubated in 20% sucrose/PBS at 4°C overnight. The following day, the lungs were incubated in 30% sucrose/PBS for 1 hr prior to snap-freezing in Optimal cutting temperature (OCT) compound (Thermo Fisher; 4585) in a bath of methanol and dry ice.

Immunofluorescence and Histology

The lung tissue was sectioned using a cryostat at the Experimental Pathology Laboratory (Carbone Cancer Center, University of Wisconsin-Madison). Frozen sections of lung tissue were incubated in cold methanol for 5 min and then rinsed with PBS before blocking and incubating with primary antibodies as Table S1. Nuclei were counterstained with DAPI, then mounted with TrueVIEW Autofluorescence Quenching Kit (Vector Laboratories, SP-8400-15). All tissues were imaged on the Nikon Eclipse E600. All images were quantified using ImageJ (NIH). Five 200X images were taken in random areas of lung tissue with similar densities in nuclei. An average cell count of each image was recorded for each individual mouse. If lungs were stained with one marker, tissue was imaged in multiple channels to identify auto fluorescent cells. These cells were then excluded from analysis. H&Es of lungs were used to identify and quantify breast cancer metastasis. H&E's were scanned at 200X and 400X using the Nikon Eclipse E600 to identify metastasis. Two of five lung lobes were used to quantify metastasis.

Flow Cytometry

After digestion, lungs were mechanically dissociated using a 20-gauge needle in 5% bovine calf serum (BCS) in PBS to achieve a cell suspension. Samples were then incubated for 2 mins in Ammonium–chloride–potassium (ACK) lysis buffer (Quality Biological; 118-156-101, Gaithersburg, MD, USA) to lyse red blood cells. Next, samples were filtered 100 µm (Falcon; 352360) and 40 µm cell strainers (Falcon; 352340) to isolate single cells. For each mouse, 500,000 lung cells were blocked with Fc blocking antibody (CD16/32, ThermoFisher; 14-0161-82) for 20 minutes. To assess viability, each lung sample was stained with live/dead UV blue dye (ThermoFisher; L34961) in PBS for 30 minutes at 4°C in the dark. A sample spiked with cells heat-killed at 60°C for 5 mins was included as a control. Antibodies for flow cytometry analysis are listed in Table S1. Samples were incubated with antibodies for 20 min in 2% BCS/PBS at 4°C. Cells were fixed with Cyofix/CytoPerm Plus kit with Golgi Plug (BD Biosciences; 555028) for 25 minutes, then stored in 2% BCS/PBS at 4°C overnight. Flow cytometry was conducted on a Cytek Aurora Cytometer using SpectroFlo software. Fluorescence minus one (FMO) and single color controls were included. Single color controls conjugated to UltraComp ebeads (ThermoFisher; 01-2222-42), and a sample of unstained cells and beads were used to determine fluorophore unmixing. Samples and FMOs were analyzed using FlowJo (version 10.1).

CD8+ T cell stimulation experiments

Whole lung tissue isolated from mice with TC2 tumors was digested and separated into a single cell suspension. 500,000 cells from non-tumor-bearing and TC2 metastatic lungs were incubated in RPMI media (Corning; 10-040-CV) with 10% FBS, (100 ng/mL) IL-2 (ThermoFisher; PIRP8605), and (1 µ/mL) Golgi Plug from BD Cytofix/Cytoperm Plus (BD Biosciences; 555028). Stimulated samples received (10 ng/mL) (ThermoFisher; BP6851) phorbol myristate acetate and (1 µg/mL) (ThermoFisher; I24222) ionomycin (PMAI). Stimulated and unstimulated lungs were incubated for 5 hours at 37°C in the presence of CO_2. After 5 hours cells were stained for cell surface markers CD8α and PD-1 (Table S1). Cells were then permeabilized and stained for intracellular cytokines TNFα and IFNγ (Table S1). Cells were stored overnight at 4°C and analyzed the next day on a Cytek Aurora Cytometer. Each individual data point represents a separate mouse.

NanoString Analysis

RNA was collected from CD45+ cells isolated from lungs tissue with or without TC2 metastasis. Anti-Rat IgG Dynabeads (ThermoFisher; 11035) were incubated with CD45 (Biolegend; 103101) antibodies at a 1:10 ratio for 30 minutes at 4°C. Beads conjugated to CD45 antibodies were incubated with dissociated lung tissue for 30 minutes at 4°C as described by the manufacturer. RNA was extracted using Qiagen RNA Microkit (Qiagen; 74004). Samples were tested for quality control by the Biotechnology Center (University of Wisconsin-Madison) using a NanoDrop One Spectrophotometer and Agilent 2100 Bioanalyzer. RNA with DV200 greater than 70% were sent to the Translational Research Initiatives in Pathology (TRIP) Laboratory (Carbone Cancer Center, University of

Wisconsin-Madison) for analysis on the nCounter MAX System using the nCounter NanoString Immune Exhaustion Panel (NanoString; XT-H-EXHAUST-12). If samples failed quality control from either the UW-Madison Biotechnology Center or ROSALIND Analysis Software, the samples were excluded from the study. nCounter NanoString data was analyzed using ROSALIND software.

Statistical Analysis

Results are reported as the mean ± standard error of the mean (s.e.m.). Statistical differences were determined using two-way analysis of variance (ANOVA) and Tukey's multiple comparisons posttest, unless otherwise noted. A p-value of ≤0.05 denotes significant value. All statistical analyses were performed with GraphPad Prism 9.4.1 (GraphPad Software).

Results:

Obesity increases immune cell recruitment and PD-1 expression on CD8+ T cells in non-tumor bearing mice

To investigate how obesity changes the immune microenvironment in the lungs to create an environment vulnerable to metastatic growth, we fed 3-week-old female FVB/N mice HFD or LFD diet for 16 weeks. HFD-fed mice were significantly heavier at 16 weeks than LFD-fed mice (Figure 3-1A). We then collected the lung tissue and digested the tissue into a single cell suspension, stained the cells with antibodies to investigate T cell populations, and quantified cells using flow cytometry (Figure S3-1). CD45+ immune cells were increased in lungs from HFD-fed mice compared to LFD-fed mice (Figure 3-1B). However, CD3+, CD4+, and CD8+ cells were unchanged in the

lungs of mice fed either diet (Figure 3-1C-E). Obesity has been shown to promote PD-1 expression in T cells in other contexts (19), so we examined PD-1 expression in the lungs. PD-1 was not significantly increased on CD4+ cells in lungs of LFD and HFD-fed mice (Figure 3-1F). However, PD-1 was significantly increased on CD8+ T cells in lungs of HFD-fed mice (Figure 3-1G). These results suggest that CD8+ T cells rather than CD4+ T cells could be dysfunctional in the lungs of HFD-fed mice prior to tumor formation.

CD8+ T cells from lungs of HFD-fed mice show signs of exhaustion

Since we observed PD-1+ CD8+ T cells in the lungs of obese mice, we hypothesized that obesity may promote T cell dysfunction. We sorted CD45+ total immune cells from lungs non-tumor bearing mice fed LFD or HFD for 16 weeks, then examined gene expression using the NanoString Immune Cell Exhaustion Panel. Immune cells from the lungs of HFD-fed mice had significant differences in gene expression compared to those from LFD-fed mice (Figure 3-2A, Table S3-2). Genes associated with T cell receptor (TCR) signaling (Figure 3-2B) and a T cell checkpoint signaling signature (Figure 3-2C) were mostly upregulated in immune cells from the lungs of HFD-fed mice. Upregulation of expression of other checkpoints, such as *Tigit* (Figure 3-2C), suggest an exhausted-like signature.

Since CD8+ T cells in the lungs of non-tumor bearing mice showed evidence of dysfunction, we tested their function *in vitro* using IL-2 and PMAI stimulation. We incubated isolated cells from the whole spleen and whole lungs without (Un) or with PMAI (Stim) and quantified changes in cytokines and PD-1 expression using flow cytometry (Figure S3-2). In the spleen, CD8+ T cells from LFD and HFD-fed mice

responded to stimulation to produce significantly higher levels of TNF-α and IFN-γ compared to unstimulated CD8+ T cells (Figure 3-2D, E). Additionally, PD-1 expression of CD8+ T cells was unaffected by diet or stimulation in the spleen (Figure 3-2F). In the lungs of LFD-fed mice, CD8+ T cells responded to stimulation with PMAI by significantly increasing TNF-α expression ($p=0.0006$, Figure 3-2G). While CD8+ T cells from HFD-fed mice had elevated expression of TNF-α compared to unstimulated cells ($p=0.01$), the level of TNF-α was significantly lower than stimulated cells from LFD-fed mice ($p=0.02$, Figure 3-2G). In contrast to the spleen (Figure 3-2E), CD8+ T cells from the lungs of LFD or HFD-fed mice did not produce more IFN-γ in response to stimulation (Figure 3-2H). Similar to the spleen (Figure 3-2F), stimulation of CD8+ T cells in the lungs of LFD-fed mice did not alter expression levels of PD-1 (Figure 3-2I). However, stimulation of CD8+ T cells in the lungs of HFD-fed mice led to significantly increased levels of PD-1 ($p=0.007$, Figure 3-2I). Together, these results suggest that CD8+ T cells from the lungs of HFD-fed mice have evidence of chronic stimulation leading to increased exhaustion prior to tumor formation.

Obesity promotes tumorigenesis and more advanced metastatic disease in a model of ERα+ breast cancer

To model metastasis of ERα+ mammary tumors to the lungs, mice were randomized to receive LFD or HFD for 16 weeks. LFD and HFD-fed mice were injected with TC2 cells, then tumors were resected following growth to 0.5 cm in diameter. Eight weeks following tumor resection, mice were euthanized, and lung tissue was collected for analysis (Figure 3-3A). HFD-fed mice orthotopically injected with TC2 ERα+ mammary tumor cells gained significantly more weight than LFD-fed mice (Figure 3-3B).

TC2 tumors grew faster in HFD mice but were resected at similar volumes as tumors from LFD-fed mice (Figure S3-3). TC2 tumors expressed ERα in both LFD and HFD-fed mice (Figure 3-3C), and we previously observed no significant differences in ERα expression in mice fed either diet (33). TC2 metastases were increased in HFD-fed lungs compared to mice that were fed LFD (p=0.04, Figure 3-3D). Obesity overall increased metastasis to the lungs in a ERα+ mammary tumor model.

Obesity increased inflammation and upregulated PD-1 expression on CD8+ T cells within ERα+ lung metastases

To assess how obesity altered adaptive T cells within the metastatic environment, we digested metastatic lungs from LFD and HFD-fed mice into a single cell suspension and quantified T cells using flow cytometry. Like non-tumor bearing mice (Figure 3-1B), metastatic lungs of HFD-fed mice had significantly more CD45+ cells than LFD-fed mice (p=0.02, Figure 3-4A). No significant differences were observed in CD3+ cells in the lungs of mice either diet group (Figure 3-4B). Similarly, no significant differences were observed in total CD4+ cells (Figure 3-4C) or PD-1+ CD4+ T cells (Figure 3-4D). However, immunofluorescent staining of metastatic lungs showed a significant increase in immunosuppressive FOXP3+CD4+ Tregs in the metastatic lungs of HFD-fed mice (p=0.03, Figure 3-4E). No significant differences in CD8+ T cells were observed in the metastatic lungs of LFD or HFD-fed mice quantified either by flow cytometry (Figure 3-4F) or using immunofluorescence (Figure 3-4G). However, PD-1+ CD8+ T cells were significantly elevated in the metastatic lungs of HFD-fed mice (p=0.02, Figure 3-4H). Together, these results suggest that obesity enhances immunosuppressive CD4+ T regs and immune checkpoint expression on CD8+ T cells.

CD8+ T cells from obese lung metastasis retain function despite increased levels of PD-1

To assess functional changes in the immune cells, we sorted CD45+ cells from metastatic lungs and examined gene expression before and after metastasis using the NanoString Immune Exhaustion Panel. Immune cells from LFD-fed mice showed multiple gene expression changes before and after metastases (Figures S3-4A and Table S3-4). Immune cells from the metastatic lungs of LFD-fed mice demonstrated downregulation of multiple genes associated with TCR signaling (Figure S3-4B) and cytotoxicity (Figure S3-4C). However, immune cells from metastatic lungs of LFD-fed mice had significant upregulation of genes associated with type II interferon signaling (Figure S3-4D) and TNF signaling (Figure S3-4E). In contrast, immune cells from non-tumor bearing and metastatic lungs of LFD-fed mice showed greater differences in gene expression (Figure S3-4A and Table S3-4) compared to HFD-fed mice (Figure S3-5A and Table S3-5). While genes associated with TCR signaling and cytotoxicity were also downregulated in immune cells from metastatic lungs of HFD-fed mice (Figure S3-5B and S3-5C), fewer genes were down regulated and fold change differences of genes associated with these pathways were smaller than in immune cells from metastatic lungs of LFD-fed mice (Figure S3-4B and S3-4C). Further, tumor necrosis factor (TNF) signaling was down regulated in immune cells from metastases of HFD-fed mice compared to non-tumor bearing HFD-fed mice (Figure S3-5D), and no differences in interferon II signaling were detected. Together, these results suggest that metastases cause a greater change in function of immune cells in LFD-fed mice compared to HFD-fed mice.

With direct comparison of gene expression of immune cells isolated from metastatic lungs of LFD and HFD-fed mice, a number of genes were differentially expressed (Figure 3-5A, Table S3-3). Similar to the comparison of immune cells in non-tumor bearing mice (Figure 3-2B), genes associated with TCR signaling were significantly upregulated in immune cells from HFD-fed mice (Figure 3-5B). We also observed increased expression of genes associated with cytotoxicity (Figure 4-5C). Surprisingly, genes associated with interferon type II signaling (Figure 3-5D) and TNF signaling were downregulated in immune cells from metastatic lungs of HFD-fed mice (Figure 3-5E). In addition to gene expression changes associated with CD8+ T cells, we also observed a significant increase in a gene expression signature of natural killer (NK) cell exhaustion (Figure 3-5F), as well as B cell receptor (BCR) signaling (Figure 3-5G) in immune cells from metastatic lungs of HFD-fed mice. These gene signatures suggest that obesity may also alter the function of NK and B cells in the metastatic environment.

To directly test the function of CD8+ T cells from LFD and HFD-fed mice with metastases, we stimulated cells from the whole spleen and lungs with PMAI and IL-2. CD8+ T cells from the spleen of LFD-fed mice significantly upregulated TNF-α in response to stimulation ($p=0.01$, Figure 3-5H). Similarly, CD8+ cells from the spleen of HFD-fed mice showed increased expression of TNF-α ($p<0.0001$), and the degree of stimulation was significantly greater in CD8+ T cells from the spleen of HFD-fed mice compared to LFD-fed mice ($p=0.03$, Figure 3-5H). PMAI and IL-2 stimulation did not affect PD-1 expression in CD8+ T cells of the spleen in either LFD or HFD-fed mice (Figure 3-5I). Similar to the spleen, CD8+ T cells in the lungs of LFD-fed mice with

metastases showed increased expression of TNF-α in response to stimulation (p=0.05, Figure 3-5J). CD8+ T cells from HFD-fed mice also showed a significant elevation of TNFα expression compared to unstimulated cells (p=0.0003) as well as stimulated CD8+ T cells from LFD-fed mice (p=0.007, Figure 3-5J). Unlike in non-tumor bearing mice (Figure 3-2I), stimulation of CD8+ T cells in metastatic lungs did not increase PD-1 expression in CD8+ T cells. Together, these results suggest that although CD8+ T cells from metastatic lungs of HFD-fed mice show expression of PD-1, CD8+ T cells are capable of a more robust response following stimulation than CD8+ T cells from LFD-fed mice.

Discussion:

Patients with obesity and breast cancer are at risk for developing ERα+ Luminal B breast cancer (12), which have a higher risk for relapse following initial treatment (37). Here we used a diet-induced obesity model to simulate obesity and orthotopically injected syngeneic ERα+ TC2 mouse mammary cells into the mammary glands of obese and lean mice, to model ERα+ metastasis. We compared immune cells from lungs from LFD and HFD fed non-tumor bearing mice and mice who have previously had TC2 tumors to identify changes in the lung microenvironment before and after tumor burden in lean and obese mice. We discovered that CD8+ T cells before metastasis have impaired ability to respond to stimulus in obese mice and express higher levels of PD-1. Further, CD8+ T cells in obese mice have higher expression of genes associated with TCR stimulation before and after metastasis. After metastasis, CD8+ cells from obese mice responded to stimulation and produced higher levels of TNFα than CD8+ T cells from metastatic lungs of LFD-fed mice despite higher PD-1

expression. Together, these results suggest that CD8+ T cells in the lungs of obese mice may have better responses to immune checkpoint inhibitors targeting PD-1/PD-L1.

In healthy, non-tumor-bearing mice, we showed that obesity increased total immune recruitment of CD45+ cells, as we observed previously (33). Percentages of CD3+, CD4+, CD8+ cells were unchanged in the lungs of non-tumor bearing mice. However, analysis of CD45+ cells suggests that non-tumor bearing obese mice had increased expression of genes related to TCR signaling and T cell checkpoint signaling, including the gene for T cell immunoglobulin and ITIM domain (TIGIT), *Tigit*. PD-1 expression and upregulation of *Tigit* may indicate CD8+ T cells moved into a more exhausted signature. Functionally, stimulation of CD8+ T cells revealed that CD8+ T cells from the lungs of HFD-fed mice had reduced ability to produce significant amounts of TNFα compared to CD8+ T cells from the lungs of LFD-fed mice. Interestingly, stimulation also increased PD-1 expression only on CD8+ T cells derived from lungs of HFD-fed mice. These data may indicate that chronic TCR stimulation due to obesity *in vivo* may prime CD8+ T cells for upregulation of PD-1 expression with acute stimulation *in vitro.* Other immune cells cultured with the CD8+ T cells from the lung support this upregulation of PD-1 with TCR stimulation and this supportive cellular environment is different in HFD-fed mice. Overall, this data supports the idea that CD8+ T cells in non-tumor bearing HFD-fed mice have a dysfunctional signature similar to exhaustion prior to tumor formation (38). Recent work suggests that T cell dysfunction within sarcomas in obesity lead to decreased immunosurveillance (39). Additional work is necessary to determine whether dysfunctional T cells in the lungs promote metastatic growth in this site.

Following metastatic growth, we observed increased CD45+ immune cells within lungs from obese mice. Despite increased inflammation, HFD-fed mice had elevated metastases. Based on data showing lower CD8+ T cell infiltration in primary tumors of obese mice (20, 40), we hypothesized CD8+ T cells would be reduced in the lungs of HFD-fed mice with metastasis. However, similar to non-tumor bearing mice, we did not see differences in CD3+, CD4+, and CD8+ cells. PD-1 expression was significantly upregulated on CD8+ cells in lungs from HFD-fed mice. While we observed significantly increased expression of genes associated with T cell receptor signaling and cytotoxicity, genes associated with Type II interferon and TNF signaling pathways were down regulated. When TNF-α and IFN-γ are expressed by CD8+ T cells, these cytokines are both cytotoxic to cancer cells and can activate other cells in the immune system (41). Decreased pathways associated with TNF-α and IFN-γ could indicate T cell exhaustion (42). Together these data suggest that T cells in metastases of obese mice show more stimulation than those from LFD-fed mice and may retain some cytotoxicity but have the potential to become more exhausted with higher PD-1 expression. To investigate the function of CD8+ T cells, we quantified TNF-α following acute stimulation. Similar to non-tumor bearing mice, in the spleen both LFD-fed and HFD-fed derived CD8+ T cells responded to stimulation and produced significantly more TNF-α. In isolated cells from metastatic lungs, there were clearly different responses. Prior to metastasis, CD8+ T cells from HFD-fed mice were unable to respond to PMAI stimulation and produced less TNF-α than stimulated cells from LFD-fed mice. However, after metastatic establishment, CD8+ T cells from HFD-fed mice were able to respond to stimulation and produce more TNFα than stimulated lean CD8+ T cells. Despite PD-1 expression,

obese CD8+ T cells area able to retain function and respond more robustly to stimulation. These observations are consistent with CD8+ T cells observed in human breast tumors, which retained functionality while expressing markers of exhaustion, in contrast to similar cells in melanomas (43) Recent work has shown that subsets of exhausted CD8+ T cells exist, some of which retain polyfunctionality,(44) and further work is necessary to define CD8+ T cell populations within metastatic niches.

Immunosuppressive Tregs may play a role in the elevated metastases observed in the lungs of obese mice. We observed increased CD4+FOXP3+ cells in the metastatic lungs of HFD-fed mice. Tregs are known to affect the activation of both CD4+ and CD8+ T cells, in addition to impairing the function of NK cells and antigen presenting cells (45). An increase in Tregs in HFD-fed mice may result in dysfunction of other immune cells leading to immune evasion by metastasis in obese mice. This data is in contrast to work by McDowell *et. al*. that showed no differences in Tregs in the metastatic lungs of obese mice in the MMTV-PyMT mammary tumor model. Differences in these results may be due to the different subtypes of breast cancer modeled as well as the presence of primary tumors in MMTV-PyMT mice.

Gene expression profiling also revealed differences in function of other cell types, including NK and B cells, that might enhance metastatic growth in obese mice. NK cells have been found to not directly clear metastasis in the lungs in melanoma, but rather reduce metastatic disease by supporting CD4+ and CD8+ T cell recruitment to the lungs and supporting T cell activation (46) In this same study, it was established NK cells prevent lung metastasis by eliminating circulating tumors cells.(46) NK cells however, can become exhausted and this may affect their ability in the lung to mitigate T cell

immune responses. NK cells are exhausted through chronic stimulation of activating receptors NKp46 and NKG2D and can be reversed through balancing inhibitory signals (47). Like exhausted T cells, NK cells can also produce less TNF-α and IFN-γ (48) Although consensus on the regulatory mechanisms behind NK cell exhaustion are not as well defined as T cell exhaustion (49). Obesity led to enhanced expression of genes associated with NK exhaustion, suggesting that NK cells may have chronic unbalanced activating and inhibitory signals, leading to immune evasion by metastasis. Exhausted NK cells could also contribute to the lower expression of genes associated with TNF and IFN signaling seen in obese metastatic lungs. Dysfunctional NK cells within lung metastasis have been found to contribute to ICB resistance in melanoma (50). Interestingly, B cell receptor (BCR) signaling was also upregulated. B cell memory signatures have been associated with responses to ICB therapy (51). Further work is necessary to understand how these different cell types interact together in metastases and how this activity might be dysregulated in obesity.

Our study shows that despite ERα+ cancers notoriously being labeled as “cold”, obese patients with ERα+ lung metastasis may benefit for ICB targeting PD-1/PD-L1. In recent clinical trials, a cohort of patients with endocrine therapy resistant ERα+ metastatic breast cancer responded to ICB therapy.(52, 53) While multiple variables can exist for response to ICB therapy, the role of obesity was not considered as a variable for patient outcomes. We identified an exhausted-like state for CD8+ T cells in metastatic lungs under obese conditions. A recent small clinical trial showed that CD8+ PD-1+ exhausted T cells were present in the blood or tumors of patients with ERα+ metastases that responded to ICB (54). Understanding how obesity alters the function

of CD8+ T cells could identify biomarkers for patient response to ICB or identify patients that would benefit from IBC for metastatic ERα+ breast cancer.

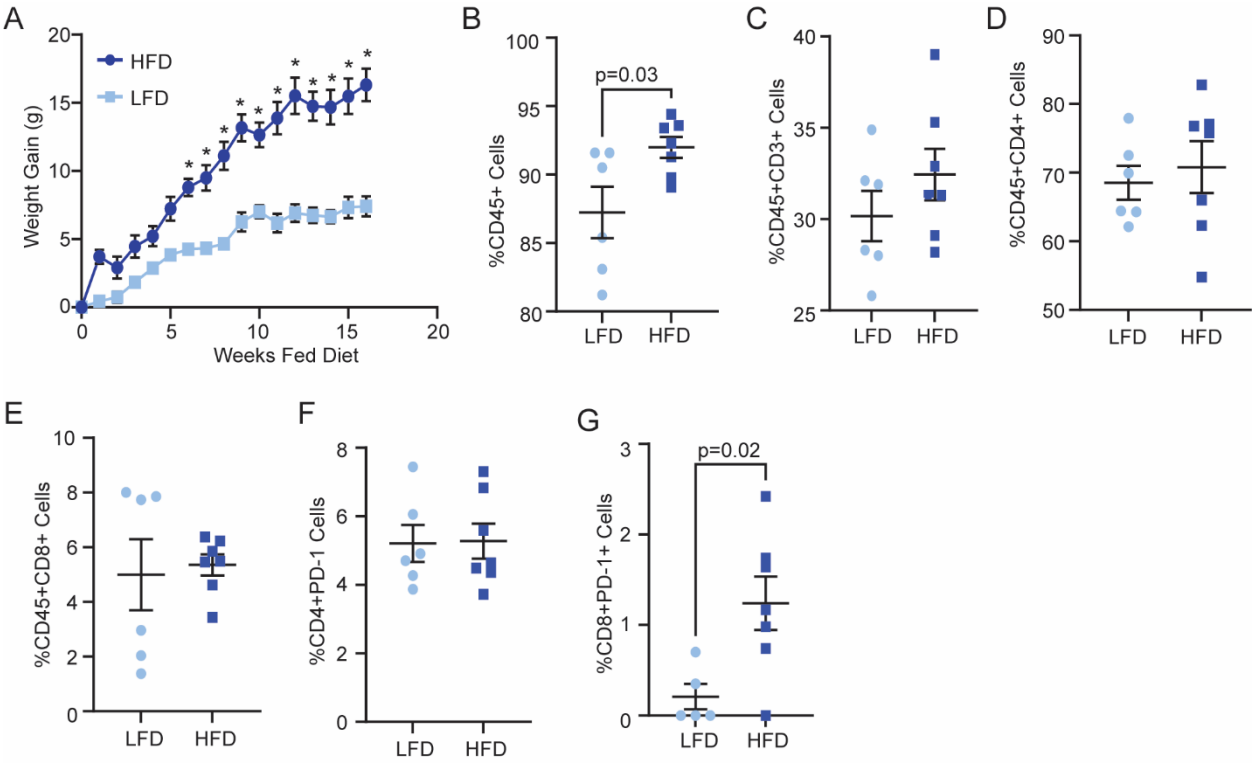

Figure 3-1: Obesity increases immune cell infiltration and PD-1 expression on CD8+ T cells in lungs of non-tumor bearing mice. A. Weight gain over time of LFD and HFD mice over 16 weeks. Significance was determined with a multiple t-test at $p<0.05$. Flow cytometry quantification of total CD45+ cells (**B**), CD3+ cells (**C**), CD4+ T cells (**D**), PD1+ CD4+ cells (**E**), CD8 + T cells (**F**), and PD1+ CD8+ T cells **(G)** in lungs of LFD and HFD-fed non-tumor bearing mice. **B-G.** Data was quantified using flow cytometry, and significance was determined using a t- test ($p<0.05$). Error bars represent s.e.m.

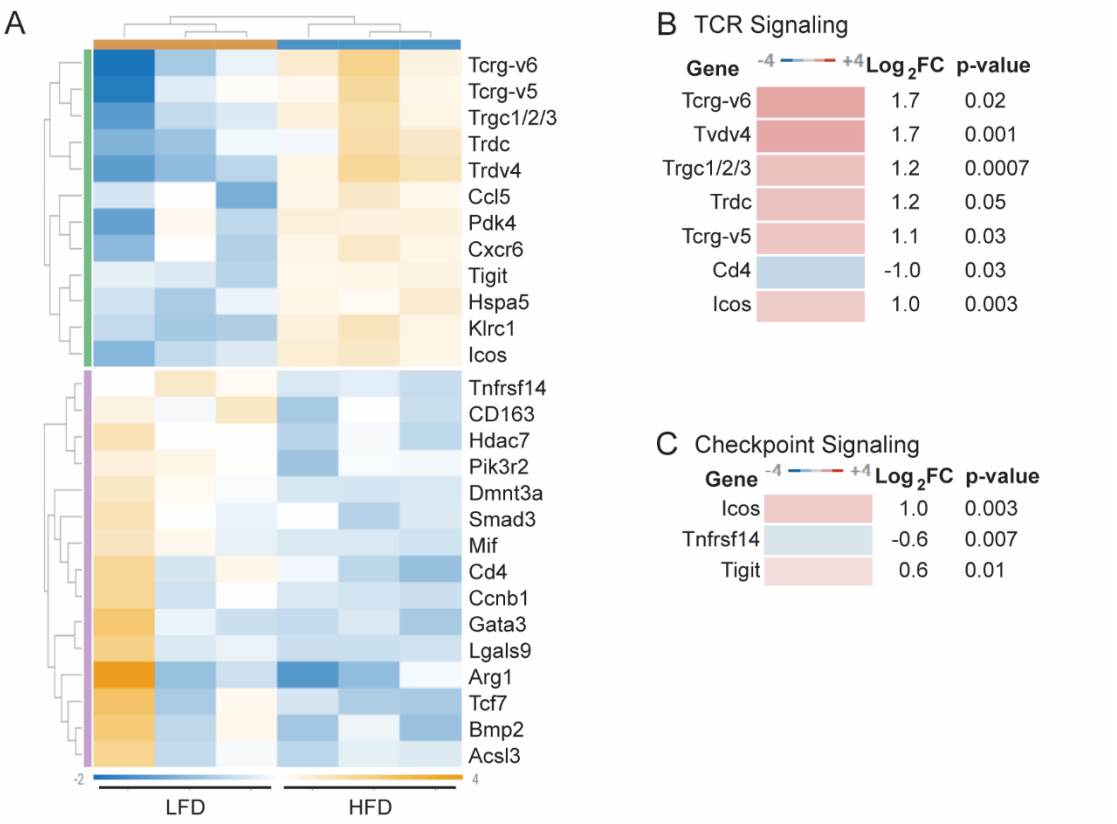
A
Tcrg-v6
Tcrg-v5
Trgc1/2/3
Trdc
Trdv4
Ccl5
Pdk4
Cxcr6
Tigit
Hspa5
Klrc1
Icos
Tnfrsf14
CD163
Hdac7
Pik3r2
Dmnt3a
Smad3
Mif
Cd4
Ccnb1
Gata3
Lgals9
Arg1
Tcf7
Bmp2
Acsl3
-2
4
LFD
HFD
B TCR Signaling
Gene
-4
+4
Log2FC
p-value
Tcrg-v6 1.7 0.02
Tvdv4 1.7 0.001
Trgc1/2/3 1.2 0.0007
Trdc 1.2 0.05
Tcrg-v5 1.1 0.03
Cd4 -1.0 0.03
Icos 1.0 0.003
C Checkpoint Signaling
Gene
-4
+4
Log2FC
p-value
Icos 1.0 0.003
Tnfrsf14 -0.6 0.007
Tigit 0.6 0.01

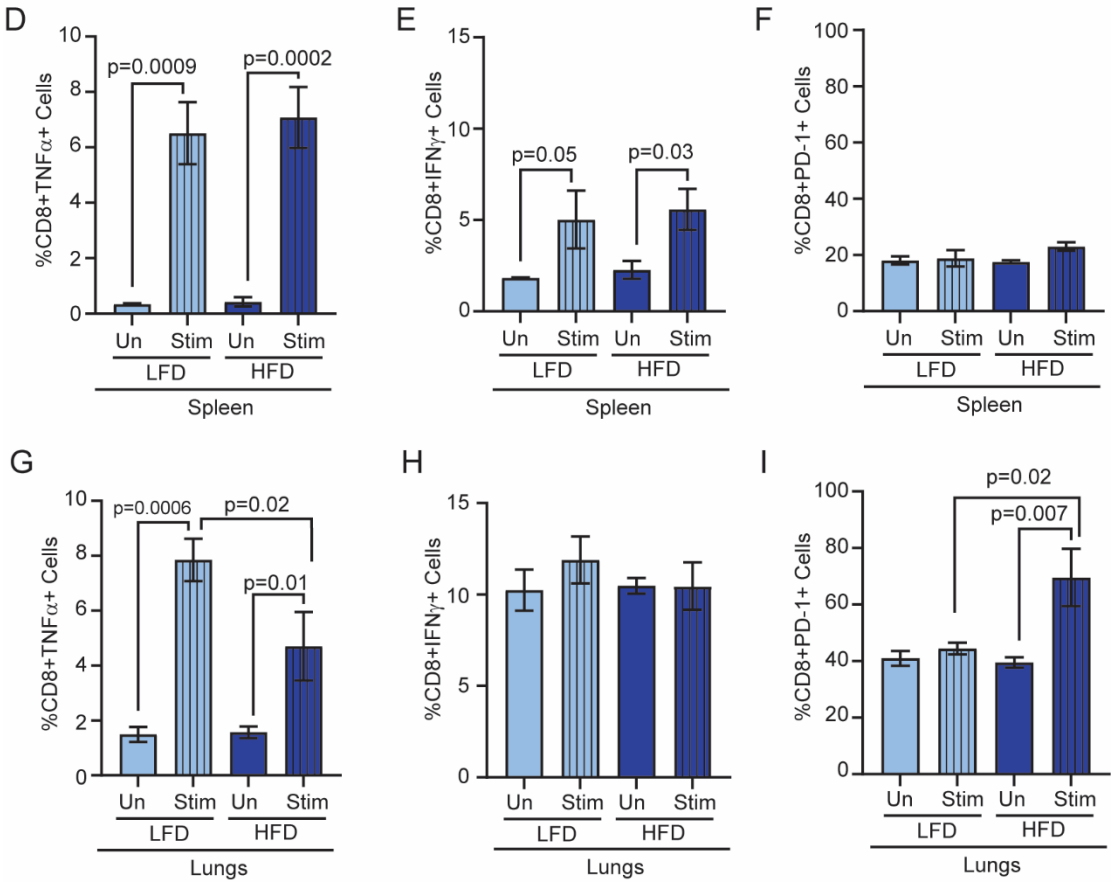
D
%CD8+TNFα+ Cells
p=0.0009
p=0.0002
Un
Stim
Un
Stim
LFD
HFD
Spleen
E
%CD8+IFNγ+ Cells
p=0.05
p=0.03
Un
Stim
Un
Stim
LFD
HFD
Spleen
F
%CD8+PD-1+ Cells
Un
Stim
Un
Stim
LFD
HFD
Spleen
G
%CD8+TNFα+ Cells
p=0.0006
p=0.02
p=0.01
Un
Stim
Un
Stim
LFD
HFD
Lungs
H
%CD8+IFNγ+ Cells
Un
Stim
Un
Stim
LFD
HFD
Lungs
I
%CD8+PD-1+ Cells
p=0.02
p=0.007
Un
Stim
Un
Stim
LFD
HFD
Lungs

Figure 3-2: Obesity increases gene expression associated with T cell receptor signaling, but impaired response to stimulation in CD8+ T cells in lungs. A. Heatmap representing all genes found to be significantly different between CD45+ immune cells sorted from the lungs of LFD and HFD-fed non-tumor bearing mice. Gene expression quantified using NanoString Immune Exhaustion panel (n=3/group). **B.** Genes associated with T cell receptor (TCR) signaling signature in HFD-fed mice that were upregulated (red) and downregulated (blue). **C.** Genes associated with T cell checkpoint signaling signature that were upregulated and downregulated in HFD-fed mice. Cells from the whole spleens of LFD and HFD-fed mice were treated with vehicle (Un) or stimulated (Stim) with IL-2 and PMAI and CD8+ T cells expressing TNFα (**D**), IFNγ (**E**), and PD-1 (**F**) were quantified using flow cytometry (n=5/group). Cells from whole lung tissue were treated with vehicle (Un) or stimulated with IL-2 and PMAI, and CD8+ T cells expressing TNFα (**G**), IFNγ (**H**), and PD-1 (**I**) were quantified (n=5/group). Statistical significance was determined by 2-way ANOVA with Tukey's multiple comparison post-test, and error bars represent s.e.m.

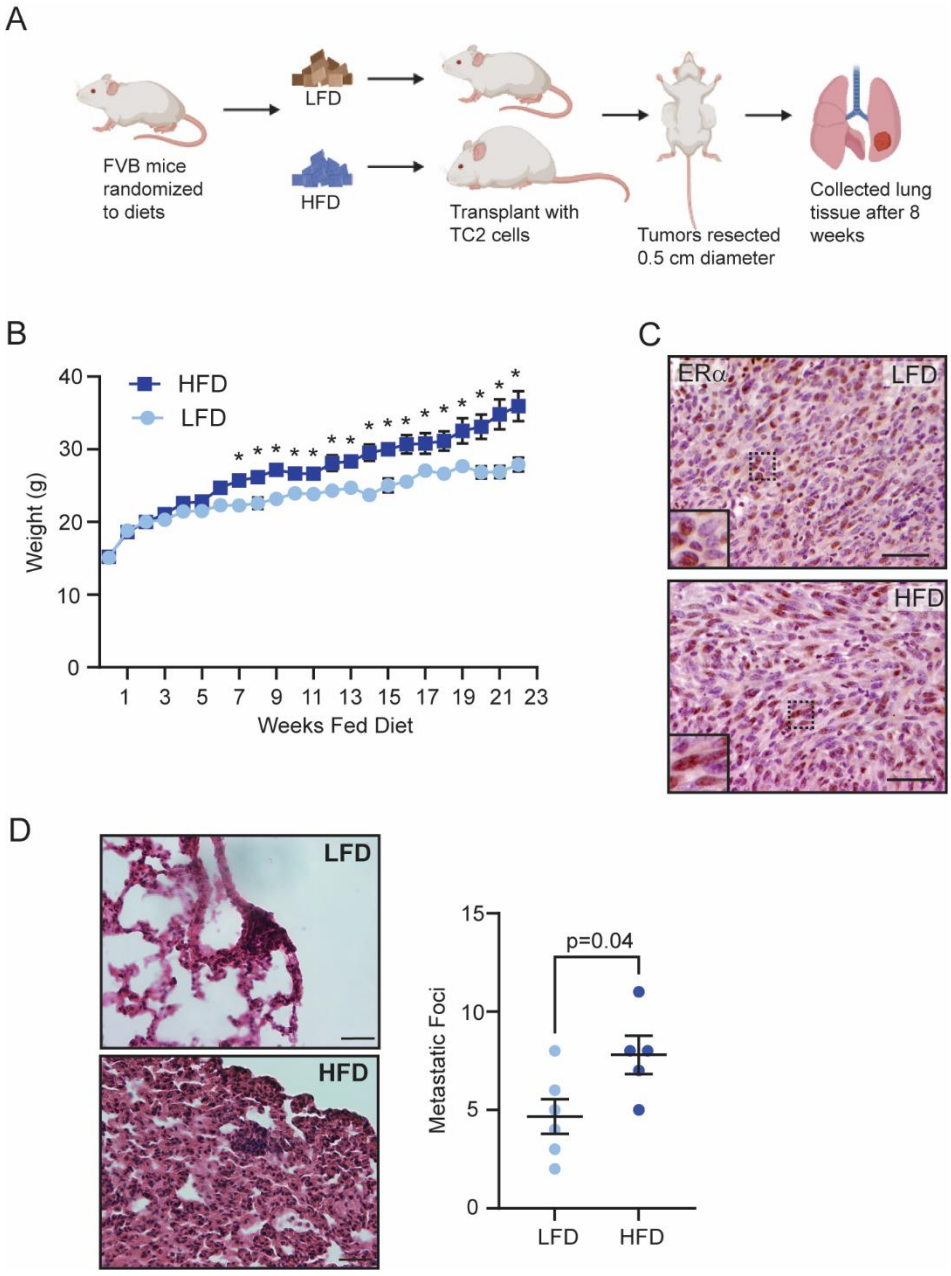

Figure 3-3: TC2 tumor cell model of ERα+ metastasis in obese and lean mice. A. Mice were randomized to receive LFD or HFD for 16 weeks. LFD and HFD-fed mice were injected with TC2 cells, then tumors were resected following growth to 0.5 cm in diameter. Eight weeks following tumor resection, mice were euthanized, and lung tissue was collected for analysis. **B.** Weight gain of mice fed LFD or HFD during experiment. Significance was determined using multiple t tests. **C.** Representative images of ERα expression in TC2 tumors in mammary glands of LFD and HFD-fed mice**. D.** Quantification of ERα+ TC2 metastasis in the lung of LFD and HFD mice after tumor removal with representative images. Significance was determined using t-test. Magnification bars 50 μm.

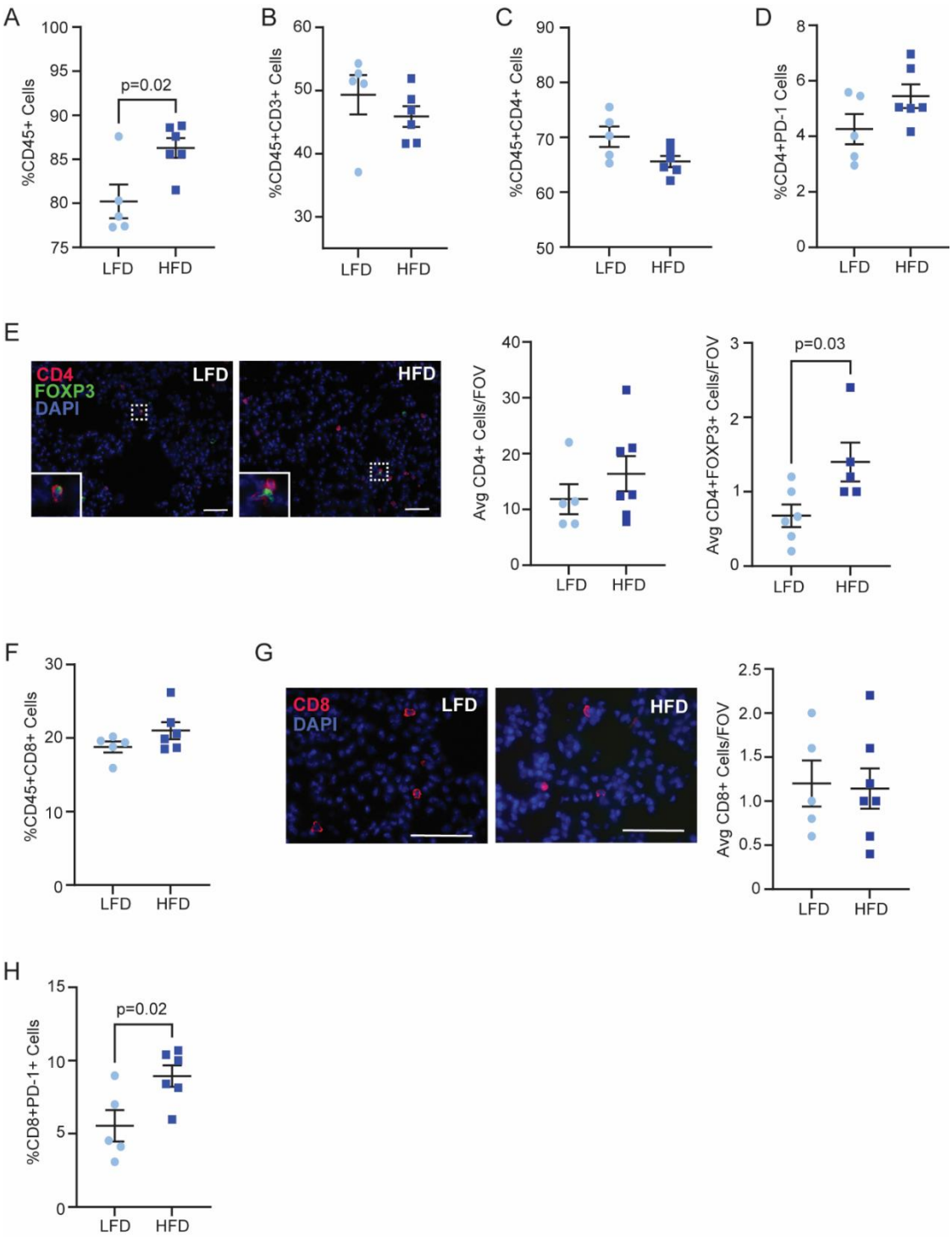

Figure 3-4: Obesity increases PD-1 expression and immunosuppressive Tregs in TC2 ERα+ metastatic lungs. Flow cytometry quantification of total CD45+ immune cells (**A**), CD3+ cells (**B.**), CD4+ T cells (**C**) and PD1+ CD4+ cells (**D**) in TC2 ERα+ metastatic lungs of LFD and HFD-fed mice. **E.** Representative images of CD4+ FoxP3+ Treg cells in LFD and HFD TC2 ERα+ metastatic lungs. Quantification of CD4+ T cells and CD4+ FOXP3+ Tregs per field of view (FOV). Flow cytometry quantification of

CD8+ T cells (**F**) and PD1+ CD8+ T cells (**G**) in TC2 ERα+ metastatic lungs of LFD and HFD-fed mice. **H.** Representative images and quantification of CD8+ T cells in metastatic lungs of LFD and HFD-fed mice. Significance was determined using a t- test, and error bars represent s.e.m. Magnification bars 50 μm

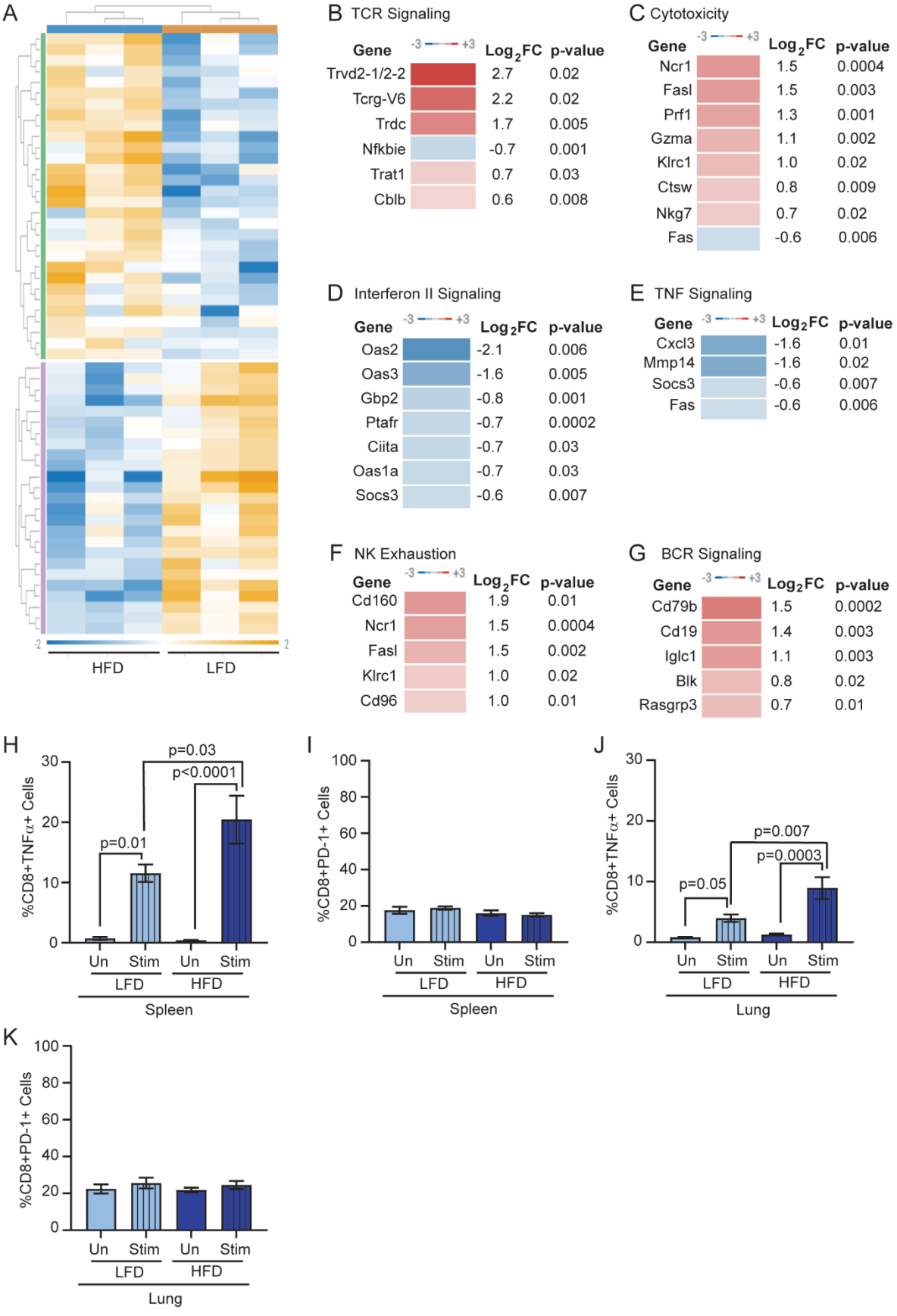
A
HFD
LFD
B TCR Signaling
Gene
Log2FC
p-value
Trvd2-1/2-2 2.7 0.02
Tcrg-V6 2.2 0.02
Trdc 1.7 0.005
Nfkbie -0.7 0.001
Trat1 0.7 0.03
Cblb 0.6 0.008
C Cytotoxicity
Ncr1 1.5 0.0004
Fasl 1.5 0.003
Prf1 1.3 0.001
Gzma 1.1 0.002
Klrc1 1.0 0.02
Ctsw 0.8 0.009
Nkg7 0.7 0.02
Fas -0.6 0.006
D Interferon II Signaling
Oas2 -2.1 0.006
Oas3 -1.6 0.005
Gbp2 -0.8 0.001
Ptafr -0.7 0.0002
Ciita -0.7 0.03
Oas1a -0.7 0.03
Socs3 -0.6 0.007
E TNF Signaling
Cxcl3 -1.6 0.01
Mmp14 -1.6 0.02
Socs3 -0.6 0.007
Fas -0.6 0.006
F NK Exhaustion
Cd160 1.9 0.01
Ncr1 1.5 0.0004
Fasl 1.5 0.002
Klrc1 1.0 0.02
Cd96 1.0 0.01
G BCR Signaling
Cd79b 1.5 0.0002
Cd19 1.4 0.003
Iglc1 1.1 0.003
Blk 0.8 0.02
Rasgrp3 0.7 0.01
H
%CD8+TNFα+ Cells
p=0.03
p<0.0001
p=0.01
Un Stim Un Stim
LFD HFD
Spleen
I
%CD8+PD-1+ Cells
Spleen
J
%CD8+TNFα+ Cells
p=0.007
p=0.0003
p=0.05
Lung
K
%CD8+PD-1+ Cells
Lung

Figure 3-5: CD8+ T cells from metastatic lungs of obese show increased levels of activity despite PD-1 expression. A. Heatmap representing all genes found to be significantly different between CD45+ immune cells sorted from TC2 ERα+ metastatic lungs from LFD and HFD-fed mice. Gene expression quantified using NanoString Immune Exhaustion panel (n=3/group). Genes associated with signatures of TCR signaling (**B**), Cytotoxicity (**C**), Interferon type II signaling (**D**), TNF signaling (**E**), NK cell exhaustion (**F**), and BCR cell signaling (**G**). Genes upregulated in red or downregulated in blue in HFD-fed mice. **H-I.** Cells from the whole spleens of LFD and HFD-fed mice were treated with vehicle (Un) or stimulated (Stim) with IL-2 and PMAI and CD8+ T cells expressing TNFα (**H**) and PD-1 (**I**) were quantified using flow cytometry (n=5/group). Cells from whole lung tissue were treated with vehicle (Un) or stimulated with IL-2 and PMAI, and CD8+ T cells expressing TNFα (**J**) and PD-1 (**K**) were quantified (n=5/group). Statistical significance was determined by 2-way ANOVA with Tukey's multiple comparison post-test, and error bars represent s.e.m.

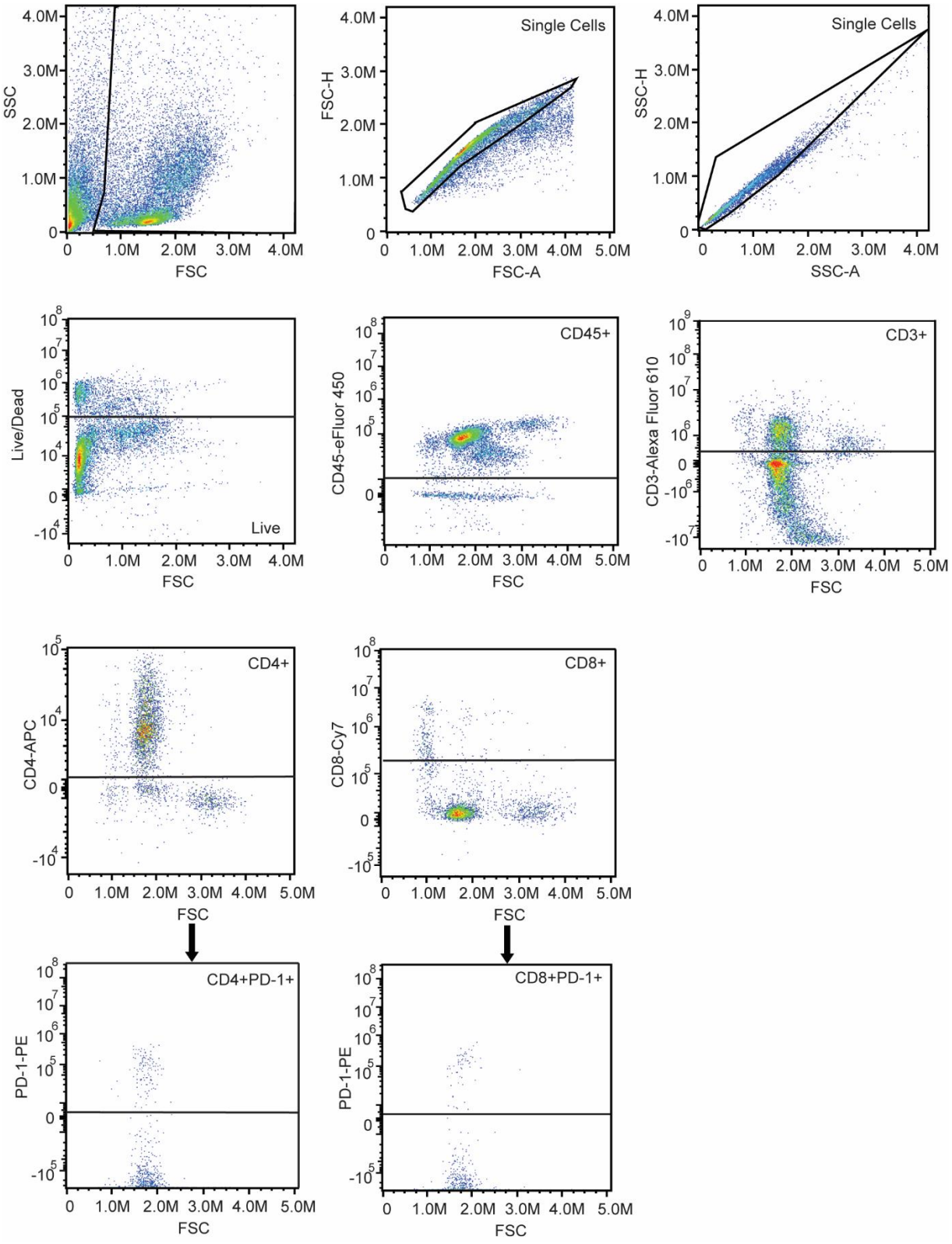

Supplementary Figure 3-1: Gating strategy for flow cytometry experiments in lungs. Gates for live cells, CD45+, CD3+, CD4+, CD8+, PD-1+ cells were all determined with fluorescence minus one (FMO) samples.

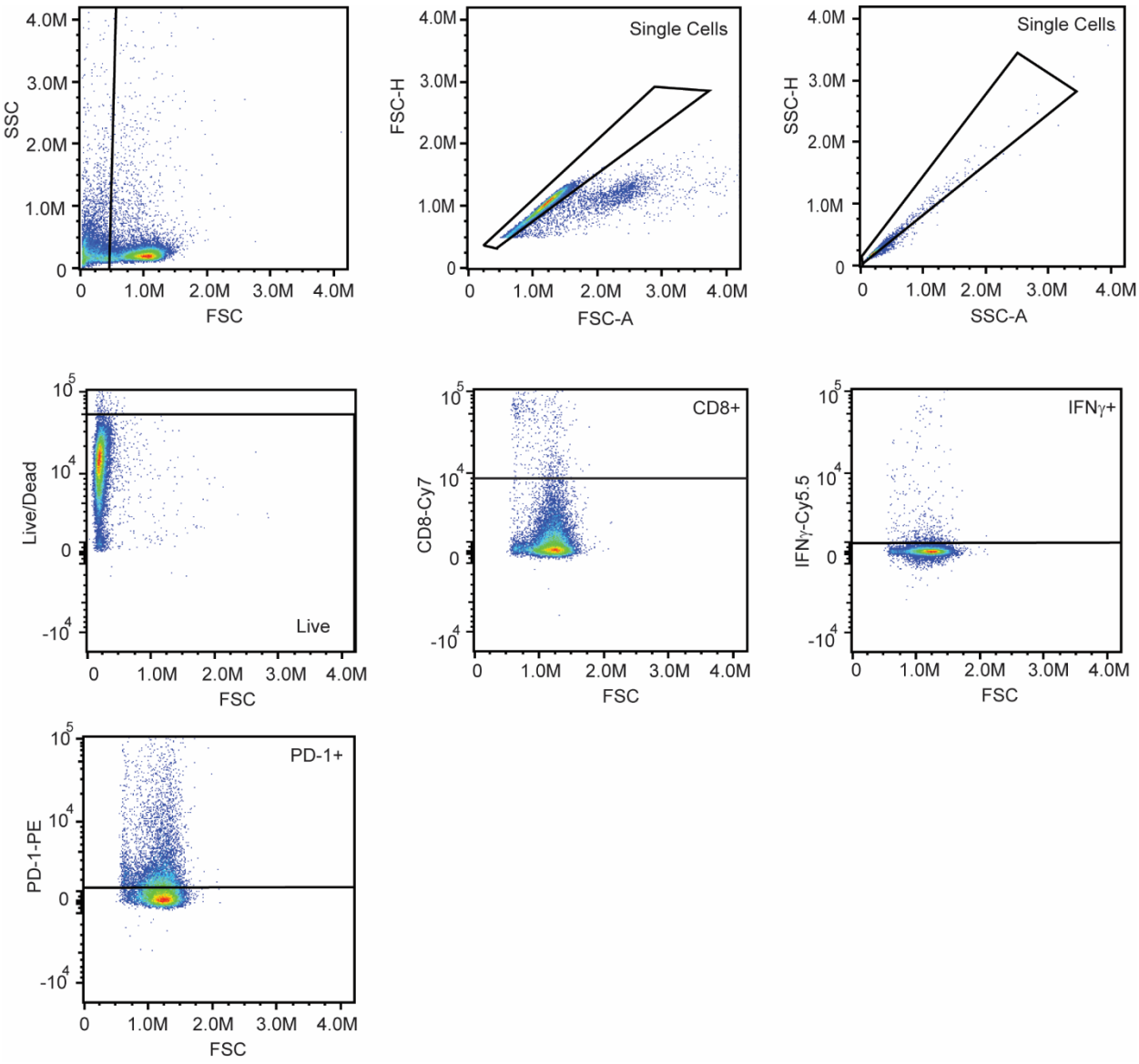

Supplementary Figure 3-2: Gating strategy for T cell stimulation experiments of cells in spleen and lungs. Gates for live cells, CD45+, CD8+, PD-1+, TNFα+, IFNγ+ cells were all determined with FMO samples.

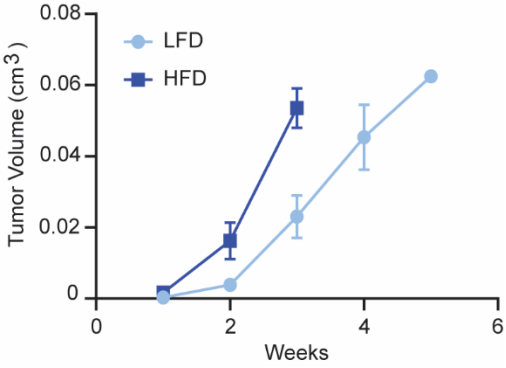

Supplementary Figure 3-3: TC2 tumors grow faster in HFD-fed mice. Tume growth curve for TC2 ERα+ tumors. Tumors were removed when tumors reached a diameter of 0.5 cm. Tumor volumes were reported as cm^3. Significance was determined with a multiple t-test at $p<0.05$.

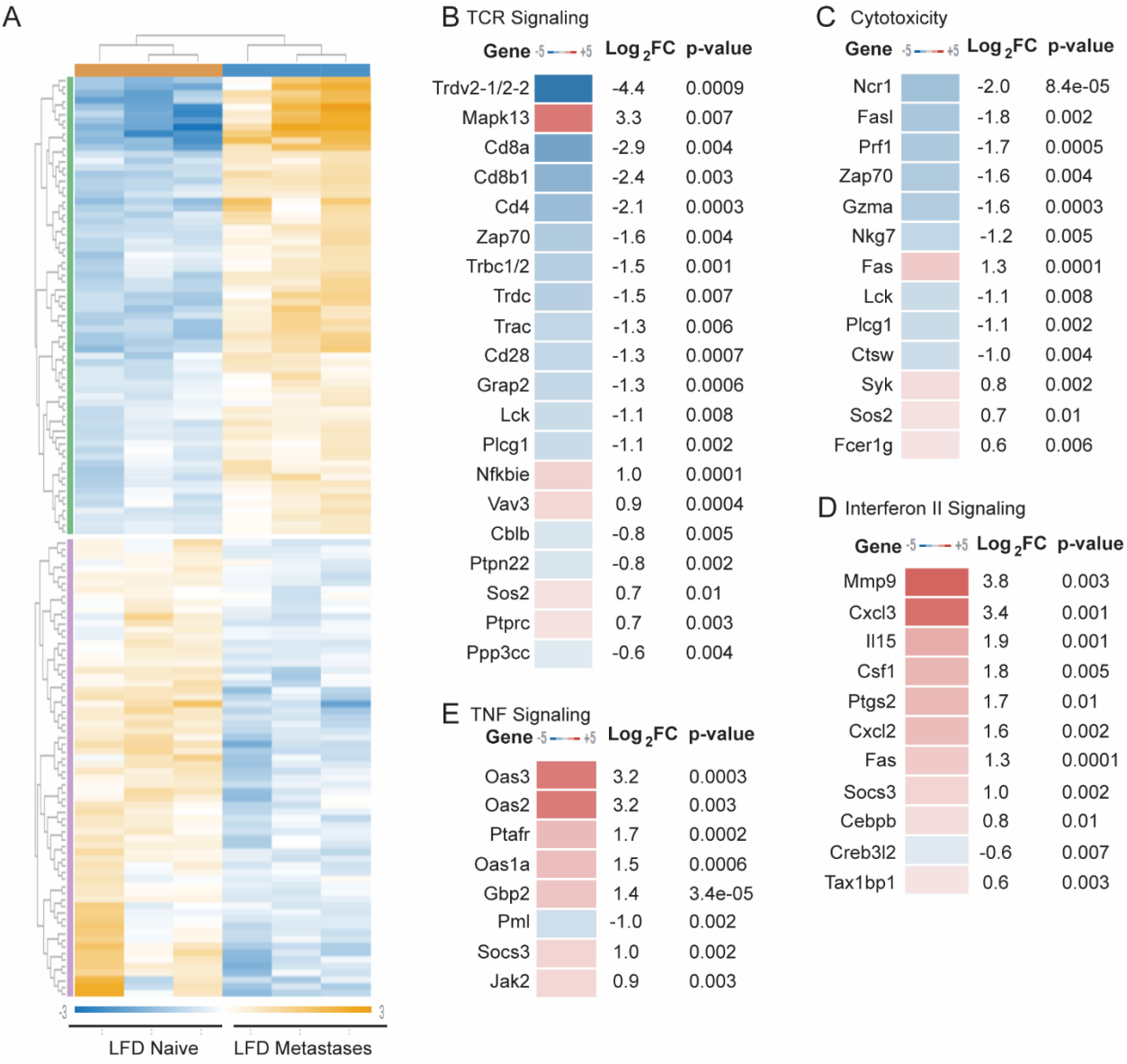

Supplementary Figure 3-4: TNF and IFN signaling is upregulated in LFD-fed mice with metastasis compared to non-tumor bearing LFD-fed mice. A. Heatmap representing all genes found to be significantly different between CD45+ immune cells sorted from lungs of non-tumor bearing LFD-fed mice and TC2 ERα+ metastatic lungs of LFD-fed mice. Gene expression quantified using NanoString Immune Exhaustion panel (n=3/group). Genes associated with signatures of TCR signaling (**B**), Cytotoxicity (**C**), Type II Interferon (**D**), and TNF signaling (**E**). Genes upregulated in red or downregulated in blue from lungs of LFD-fed mice with TC2 cell metastases compared to lungs from non-tumor bearing LFD-fed mice.

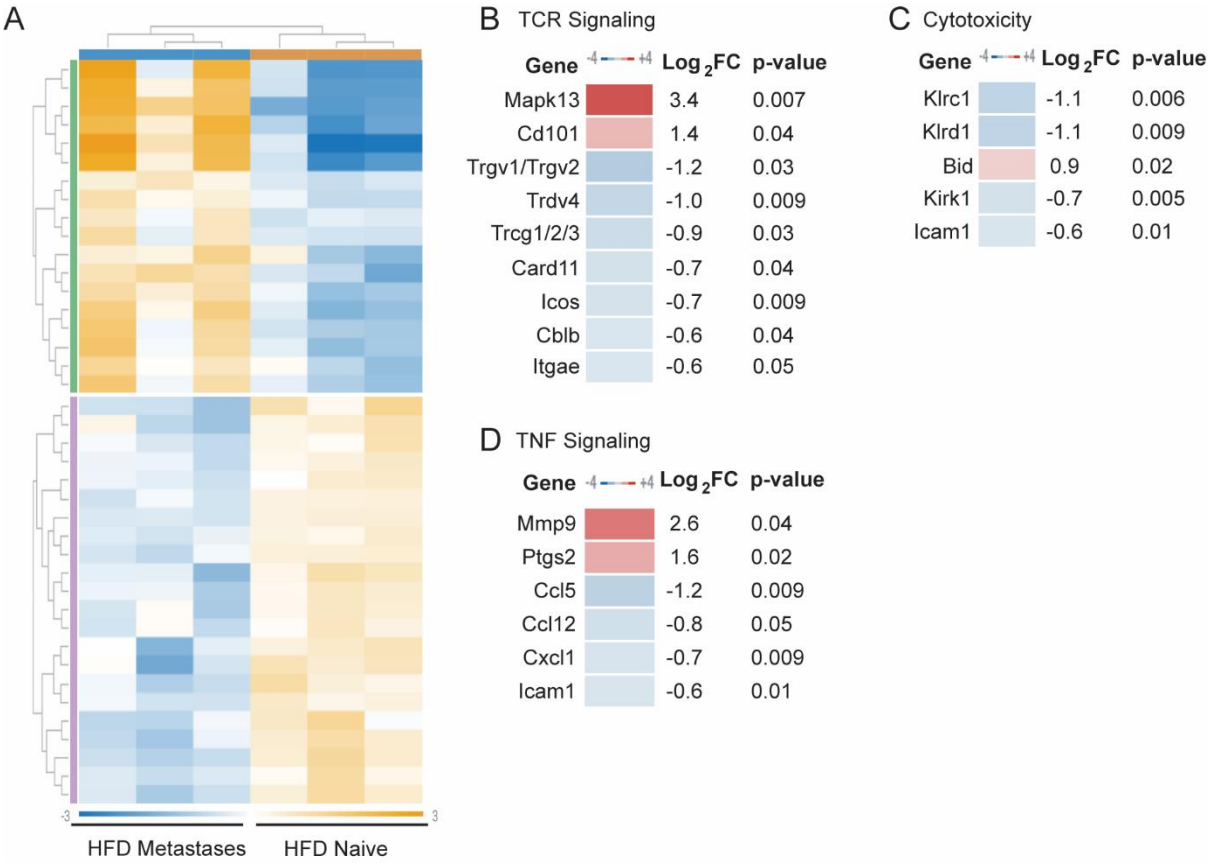

Supplementary Figure 3-5: A. T cell activity is suppressed in HFD-fed mice with metastasis compared to HFD-fed non-tumor bearing lungs Heatmap representing all genes found to be significantly different between CD45+ immune cells sorted from lungs of non-tumor bearing HFD-fed mice and TC2 ERα+ metastatic lungs of HFD-fed mice. Gene expression quantified using NanoString Immune Exhaustion panel (n=3/group). Genes associated with signatures of TCR signaling (**B**), Cytotoxicity (**C**), and TNF signaling (**D**). Genes upregulated in red or downregulated in blue from lungs of HFD-fed mice with TC2 cell metastases compared to lungs from non-tumor bearing HFD-fed mice.

Antibody	Dilution	Manufacturer	Catalog Number
Fc Receptor	1 µg/mL	ThermoFisher	14-0161-86
CD8	4 µg/mL	Novus	NBP1-49045
FoxP3	0.2 µg/mL	Cell Signaling	12653T
CD4	2 µg/mL	Biolegend	100402
Anti-Rabbit Secondary green	8 µg/mL	ThermoFisher	A-11008
Anti-Rat Secondary red	8 µg/mL	ThermoFisher	A-11081
CD45	5 µg/mL	Biolegend	103101
CD45-eFluor 450	5 µg/mL	ThermoFisher	48-0453-82
CD3 PE-efluor610	20 µg/mL	ThermoFisher	61-0031-82
CD4 APC	2 µg/mL	BioLegend	100515
CD8α-PE/Cy7	Lung (4 µg/mL) Spleen (1 µg/mL)	BioLegend	100721
CD115-Brilliant Violet 711	10 µg/mL	BioLegend	135515
CD11b-Brilliant Violet 605	5 µg/mL	BioLegend	101237
PD-1-PE	Lung (10 µg/mL) Spleen (2.5 µg/mL)	BioLegend	135205
PD-L1-PerCP-eFluor 710	2.5 µg/mL	ThermoFisher	46-5982-82
TNFα-eFluor 450	Lung (5 µg/mL) Spleen (5 µg/mL)	ThermoFisher	48-7321-82
IFNγ-PerCP/Cy5.5	Lung (1.25 µg/mL) Spleen (1.25 µg/mL)	BioLegend	505822

Table S3-1: A summary of antibodies used in staining immunofluorescence (IF), flow cytometry, and cell sorting.

Table S3-2. Comparison of gene expression from non-tumor bearing LFD and HFD-fed

Gene Name	LFD Naïve #1	LFD Naïve #2	LFD Naïve #3	HFD Naïve #1	HFD Naïve #2	HFD Naïve #3
Tcrg-V6	-1.58814	-0.61647	-0.13805	0.592267	1.389797	0.360607
Tcrg-V5	-1.51059	-0.21699	0.084555	0.178165	1.204325	0.260525
Trgc1/2/3	-1.14962	-0.41963	-0.2268	0.43249	1.02486	0.3387
Trdc	-0.86882	-0.68596	-0.0968	-0.07762	1.074363	0.654823
Trdv4	-1.13049	-0.77492	-0.47395	0.29045	1.25592	0.83299
Ccl5	-0.28313	0.013267	-0.92553	0.260667	0.705667	0.229067
Pdk4	-1.06565	0.199175	-0.45175	0.460165	0.411665	0.446385
Cxcr6	-0.79204	0.062347	-0.52828	0.271087	0.663837	0.323057
Tigit	-0.17815	-0.23871	-0.49924	0.240993	0.310753	0.364343
Hspa5	-0.3372	-0.5894	-0.1216	0.3229	0.1634	0.5619
Klrc1	-0.4086	-0.62551	-0.55191	0.42558	0.81221	0.34823
Icos	-0.84478	-0.41611	-0.22761	0.539595	0.656155	0.292735
Tnfrsf14	-0.00378	0.660145	0.172435	-0.2548	-0.19067	-0.38335
Cd163	0.365918	-0.06185	0.702998	-0.61731	-0.01814	-0.37161
Hdac7	0.88766	0.04431	0.05878	-0.48392	-0.05722	-0.44961
Pik3r2	0.43599	0.31361	0.06505	-0.6703	-0.05095	-0.0934
Dnmt3a	0.693173	0.146323	-0.03162	-0.26965	-0.28237	-0.25587
Smad3	0.88063	-0.01418	-0.12741	-0.0007	-0.5126	-0.22574
Mif	0.756318	0.229108	-0.16419	-0.23675	-0.24997	-0.33451
Cd4	1.258968	-0.27671	0.278328	-0.08115	-0.45685	-0.72258
Ccnb1	1.280578	-0.33068	-0.02971	-0.25815	-0.29984	-0.36219
Gata3	1.750935	-0.12443	-0.36046	-0.40708	-0.25602	-0.60297
Lgals9	1.41957	-0.23652	-0.14928	-0.35611	-0.36057	-0.31709
Arg1	3.09219	-0.72012	-0.34719	-1.18945	-0.76275	-0.07268
Tcf7	1.8501	-0.59584	0.19298	-0.28163	-0.55839	-0.60722
Bmp2	1.65679	-0.44646	0.24294	-0.64372	-0.11268	-0.69687
Acsl3	1.335705	-0.4151	-0.05216	-0.45948	-0.17821	-0.23078

Table S3-2: Genes significantly different in CD45+ cells isolated from naïve lungs from LFD and HFD-fed mice.

Table S3-3. Comparison of gene expression from metastatic lungs of LFD and HFD-fed mice.

Gene Name	HFD TC2 #1	HFD TC2 #2	HFD TC2 #2	LFD TC2 #1	LFD TC2 #2	LFD TC2 #3
Cd19	0.385533	0.376223	0.977993	-1.10219	0.041833	-0.6794
Itga6	0.593733	0.148543	0.676653	-0.91759	0.025883	-0.52723
Cd96	0.207487	0.024877	0.674177	-0.7695	-0.14694	0.009907
Cd160	0.664737	-0.27132	0.367917	-0.45427	-0.34268	0.035627
Nkg7	0.645883	0.024803	0.361163	-0.80201	-0.17256	-0.05729
Fasl	0.42629	0.41494	0.54639	-0.57536	-0.14184	-0.67042
Klrc1	0.485395	0.164755	0.633485	-0.5207	-0.41568	-0.34727
Bcl2	0.710153	0.306913	0.439893	-1.0038	-0.18438	-0.26879
Ctsw	0.416247	0.374397	0.257247	-0.87268	0.042517	-0.21772
Cd79b	0.287522	0.632752	1.191132	-0.80502	-0.31844	-0.98795
Iglc1	-0.12636	0.513082	0.822352	-0.2933	-0.15085	-0.76493
Ms4a1	-0.04332	0.696238	1.138538	-0.68773	-0.21074	-0.89298
Tcrg-V6	0.808335	0.230285	0.670225	-1.09951	-0.77735	0.168005
Trdc	0.897868	0.295208	0.705968	-0.68525	-0.94805	-0.26574
Ncr1	1.207105	0.334925	0.542435	-1.34486	-0.2997	-0.43992
Gzma	1.077953	0.172353	0.189513	-0.68713	-0.41303	-0.33967
Spib	-0.4922	0.522843	0.743213	-0.51809	-0.03494	-0.22084
Blk	-0.092	0.217055	0.548185	-0.22893	-0.45376	0.009435
Trat1	-0.1879	0.250442	0.678352	-0.06179	-0.32961	-0.3495
Rasgrp3	0.105775	0.113745	0.503665	-0.01543	-0.14661	-0.56116
Foxo1	0.060355	0.379465	0.378965	-0.04861	-0.22919	-0.541
Trdv2-1/2-2	0.9872	0.60558	-0.07418	-0.01794	-0.16526	-1.3354
Prf1	1.191705	0.090415	0.391795	-0.60444	-0.20006	-0.86943
Ehhadh	0.72094	-0.23672	0.27455	0.04427	-0.28831	-0.51473
Sesn1	0.507847	-0.05561	0.350437	-0.13472	-0.17513	-0.49281
Tgfb2	0.607373	-0.33261	0.678833	0.282813	-1.27217	0.035753
Pctp	0.388118	-0.02452	0.006208	0.004028	-0.4958	0.121968
Cblb	0.354945	0.159165	0.274495	-0.22212	-0.30882	-0.25768
Clcf1	-0.01179	0.56812	-0.21068	-0.12385	-0.05734	-0.16446
Taf6l	0.331272	0.190092	0.168432	-0.37851	-0.22337	-0.08792
Cd33	-0.13846	-0.97775	-0.25266	-0.07539	0.468017	0.976257
Gk	-0.18558	-1.07693	0.173158	-0.05456	0.509498	0.634418
Cd14	-0.18005	-0.92675	-0.11175	0.13495	0.40105	0.68255
Il1r2	-0.27545	-1.19995	-0.72365	0.28645	1.01065	0.90195
Socs3	-0.31353	-0.29518	-0.31801	-0.10677	0.441197	0.592307
Sesn2	-0.42423	-0.54127	0.044945	-0.11723	0.305765	0.732005
Fas	-0.33389	-0.62998	-0.01278	0.124795	0.216085	0.635755

Stat3	-0.21685	-0.51295	-0.17465	0.00315	0.34635	0.55495
Entpd1	-0.64518	-0.40896	-0.09945	0.247113	0.347933	0.558533
Ptafr	-0.77632	-0.19065	-0.18012	0.227998	0.340398	0.578698
Oas2	-1.40632	-0.12326	-1.33645	0.234365	1.184915	1.446735
Oas3	-1.11663	-0.25299	-0.69885	0.257398	0.583778	1.227298
Ciita	-0.88932	0.07509	-0.35051	0.33271	0.2276	0.60443
H2-Eb1	-1.10106	0.185273	-0.68328	0.752963	-0.06117	0.907263
Cxcl9	-1.03099	-0.13697	-0.48227	0.869115	0.007045	0.774055
Oas1a	-0.7524	0.282762	-0.65654	0.194732	0.073862	0.857582
Nfkbie	-0.7097	0.037843	-0.45223	0.556173	0.190453	0.377453
Gbp2	-0.68247	-0.29672	-0.27717	0.362643	0.369683	0.524023
Cd86	-0.50495	-0.15546	-0.46411	0.927557	-0.1454	0.342377
Cd80	-0.1889	-0.1843	-0.47666	0.727612	0.059652	0.062592
Mmp14	-0.60092	-0.55163	-1.01321	0.972645	0.324555	0.868545
Cxcl3	-0.39323	-1.11303	-0.76329	1.077483	0.053843	1.138213
Il1rn	-0.32943	-0.48063	-0.19563	0.650467	0.102467	0.252767
Ccnt2	-0.31356	-0.38712	-0.24668	0.364338	0.067588	0.515438
Nfe2l2	-0.31495	-0.44995	-0.13795	0.39945	0.07895	0.42445

Table S3-3: Genes significantly different in CD45+ cells isolated from TC2 ERα+ metastatic lungs from LFD and HFD-fed mice.

Table S3-4. Comparison of gene expression from lungs of non-tumor bearing and metastatic LFD-fed mice.

Gene Name	LFD Naïve #1	LFD Naïve #2	LFD Naïve #3	LFD TC2 #1	LFD TC2 #2	LFD TC2 #3
Slc2a3	-1.03321	-1.4014	-1.06158	0.081978	1.479768	1.934448
Hdc	-1.05879	-1.5066	-1.70291	-0.0339	2.028257	2.273957
Oas3	-1.40959	-1.8585	-0.92298	0.96493	1.29131	1.93483
Oas2	-1.81152	-1.79093	-0.71887	0.719468	1.670018	1.931838
Mmp9	-1.1457	-1.71295	-2.23188	0.110025	2.133895	2.846595
Mapk13	-0.73703	-1.59092	-2.34728	0.559493	1.748153	2.367573
Csf3r	-1.10393	-1.65909	-1.94852	0.418475	1.992375	2.300675
Il1f9	-1.46546	-1.69816	-2.69156	0.94842	2.48543	2.42133
Il1r2	-1.25965	-2.31328	-2.06858	1.433938	2.158138	2.049438
Cxcl3	-1.40322	-1.25139	-2.139	1.91884	0.8952	1.97957
Il1b	-1.0416	-1.3267	-1.8647	0.737	1.7981	1.6979
Gbp2	-0.51197	-0.65983	-0.92463	0.64267	0.64971	0.80405
Pdcd1lg2	-0.20783	-0.99085	-0.49239	0.633023	0.231513	0.826523
Fas	-0.5634	-0.66835	-0.65532	0.428272	0.519562	0.939232
Lilra6	-1.04187	-0.96117	-0.58236	0.985473	0.682023	0.917893
Ptafr	-0.85879	-0.74343	-0.86967	0.669593	0.781993	1.020293
Entpd1	-0.87418	-0.76348	-0.42286	0.549423	0.650243	0.860843
Il13ra1	-0.99174	-0.51042	-0.26481	0.522027	0.455727	0.789227
Adora2b	-1.2728	-0.86519	-1.2578	1.738322	0.107312	1.550152
Fcgr2b	-0.89736	-0.6105	-1.02881	1.471163	0.010833	1.054663
Cxcl9	-0.73751	-0.93932	-0.36476	0.999577	0.137507	0.904517
Ahr	-0.90186	-0.64266	-0.46944	0.822618	0.306778	0.884568
Gk	-0.68791	-0.65065	-0.55074	0.212088	0.776148	0.901068
Gng12	-0.60655	-0.54839	-0.63572	0.247892	0.509732	1.033032
Ccr2	-0.83581	-0.31005	-0.5787	0.391352	0.264752	1.068452
Pira1	-0.78774	-0.40441	-0.39522	0.180753	0.549953	0.856653
Plscr1	-1.12734	-0.07322	-0.24714	0.238307	0.388607	0.820797
Socs3	-0.9169	-0.20166	-0.3821	0.084538	0.632508	0.783618
Pirb	-0.85568	-0.26217	-0.45705	0.132963	0.662613	0.779313
Nfil3	-0.98001	-0.31131	-0.97828	0.615895	0.648895	1.004795
Oas1a	-0.85572	-0.57086	-0.82181	0.568807	0.447937	1.231657
Ncf4	-0.76702	-0.53732	-0.80392	0.261483	0.685983	1.160783
Gadd45a	-0.60159	-0.9361	-1.01216	-0.00961	1.261178	1.298288
Sell	-0.60967	-0.8367	-1.1066	0.472027	0.866327	1.214627
Csf1	-0.61765	-1.12878	-0.78757	0.351507	1.484047	0.698457
Cxcl2	-0.90655	-0.89345	-0.51085	0.44465	1.21085	0.65535
Ccr1	-0.95851	-0.64153	-1.14239	0.478578	1.242768	1.021088
Ptgs2	-0.64796	-0.66528	-1.17342	0.457437	1.216047	0.813187

Cd14	-1.06163	-0.81473	-1.19113	0.751267	1.017367	1.298867
Il15	-1.05169	-0.94705	-0.79108	0.531715	0.900425	1.357665
Cd33	-1.30825	-0.82103	-0.73829	0.42417	0.96758	1.47582
Jak2	-0.31232	-1.05965	-0.05952	0.760095	0.589795	0.081585
Il1rl1	-0.81918	-0.6199	-0.27812	0.697457	0.629577	0.390177
Hspa5	-0.4162	-0.6684	-0.2005	0.6023	0.545	0.1378
St3gal6	-0.39463	-0.6477	-0.34973	0.10582	1.04561	0.24063
Sos2	-0.38318	-0.41188	-0.23814	0.007125	0.655475	0.370585
Il6ra	-0.49289	-0.48202	-0.18669	0.125568	0.496068	0.539968
Tax1bp1	-0.24371	-0.55703	-0.12578	0.102043	0.253433	0.571033
Ptprc	-0.4025	-0.3539	-0.2115	-0.0718	0.3667	0.673
Cd200r1	-0.70328	-0.26252	-0.14628	0.558475	0.314325	0.239265
Cd84	-0.71115	-0.27131	-0.10071	0.37189	0.34519	0.36609
Nfkbie	-0.63195	-0.35535	-0.60662	0.712783	0.347063	0.534063
Vav3	-0.72592	-0.31131	-0.43365	0.446157	0.359527	0.665207
Nfe2l2	-0.65852	-0.37012	-0.45182	0.591983	0.271483	0.616983
Fcer1g	-0.52655	-0.09505	-0.32005	0.24565	0.04895	0.64705
Batf	-0.77422	0.033185	-0.48593	0.354355	0.149025	0.723575
Scp2	-0.54989	-0.10189	-0.52894	0.355347	0.182137	0.643247
Cd80	-0.88997	-0.17208	-0.30142	0.898813	0.230853	0.233793
Il1rn	-1.00524	-0.26908	-0.41494	0.87832	0.33032	0.48062
Osm	-0.94429	-0.30422	-0.65382	0.610817	1.097017	0.194507
Mcl1	-0.89215	-0.36095	-0.36305	0.28665	0.62285	0.70665
Syk	-0.815	-0.1028	-0.2978	0.1466	0.5916	0.4774
Sesn2	-0.62945	-0.06188	-0.66984	0.029645	0.452635	0.878875
Cebpb	-0.74672	0.045583	-0.48022	0.160983	0.385183	0.635183
Bcl6	-0.26255	-0.52611	-0.59797	0.009582	0.504102	0.872942
4632428N05Rik	-0.48829	-0.42286	-0.46445	0.118837	0.637137	0.619637
Nfkb2	-0.41169	-0.27109	-0.36652	0.084292	0.359452	0.605552
Stat3	-0.4707	-0.2846	-0.4445	0.1016	0.4448	0.6534
Siglech	0.297625	-0.11328	0.983315	-0.17926	-0.51665	-0.47177
Cd163	0.310625	-0.11716	0.647705	-0.37323	-0.37517	-0.09279
Cd180	0.26347	0.17315	0.41832	-0.35826	-0.31553	-0.18115
Il27ra	-0.16843	0.232763	0.404053	0.155063	-0.21397	-0.40949
Atm	0.0568	0.13143	0.56257	-0.09513	-0.16591	-0.48976
Rasgrp3	0.357567	0.336637	0.366417	-0.1279	-0.25908	-0.67363
Il6st	0.256938	0.336658	0.430468	-0.17748	-0.311	-0.53558
Pik3r2	0.418708	0.296338	0.047768	-0.1058	-0.59366	-0.06335
Cd276	0.108638	0.314768	-0.00036	0.054658	-0.60723	0.129528
Pvrig	-0.05475	0.509465	0.304125	-0.0559	-0.55199	-0.15097
Blk	0.068352	0.590332	0.101962	-0.25806	-0.48289	-0.0197
Cd22	-0.32709	1.26005	0.51325	-0.34467	-0.65202	-0.44952

Il7r	-0.09127	0.826705	0.432245	-0.50456	-0.52072	-0.14242
Hdac9	-0.24457	0.287512	0.501242	-0.18071	-0.25764	-0.10584
Creb3l2	-0.27312	0.546128	0.321488	-0.1435	-0.2394	-0.21159
Clcf1	0.087703	0.734473	0.468613	-0.4389	-0.37239	-0.47951
Cblb	-0.03046	0.50675	0.5415	-0.29851	-0.38521	-0.33407
Ptprs	0.111038	0.440568	0.456378	-0.4886	-0.39515	-0.12423
Ppp3cc	0.185405	0.314305	0.259435	-0.31326	-0.27924	-0.16666
Lef1	0.612613	0.567233	0.692223	-0.59741	-0.97124	-0.30343
Pmepa1	0.162832	0.565882	0.566602	-0.17808	-1.06649	-0.05075
Trdc	0.166477	0.349327	0.938497	-0.537	-0.7998	-0.11749
Cd19	0.638678	0.749678	0.814098	-1.25642	-0.1124	-0.83363
Cd79b	0.851963	0.714013	0.462923	-0.77752	-0.29094	-0.96045
Trdv2-1/2-2	0.206538	0.898498	1.693158	-0.44447	-0.59179	-1.76193
Prf1	0.535267	1.167517	0.613217	-0.81846	-0.41408	-1.08345
Sesn1	0.554818	0.627768	0.635698	-0.47326	-0.51367	-0.83135
Fasl	0.319465	0.891845	0.470775	-0.67352	-0.24	-0.76858
Grap2	0.496322	0.593332	0.599322	-0.75522	-0.4054	-0.52836
Nkg7	0.5601	1.00871	0.22748	-1.05682	-0.42737	-0.3121
Ncr1	0.927142	1.090592	0.810622	-1.59282	-0.54766	-0.68788
Gzma	0.614907	1.153957	0.463247	-0.95122	-0.67712	-0.60376
Zbtb16	-0.11902	0.723058	1.279458	-1.09551	-0.12097	-0.66701
Bcl2	0.323015	0.787905	0.758475	-1.14128	-0.32186	-0.40627
Cd28	0.683418	0.394218	0.774548	-1.00129	-0.60047	-0.25042
Cd96	0.251388	0.462788	0.618418	-0.91152	-0.28896	-0.13211
Ptpn22	0.150063	0.472863	0.532193	-0.63285	-0.19367	-0.32861
S1pr1	0.062975	1.050575	0.767605	-1.25014	-0.50467	-0.12636
Tnfrsf14	0.257083	0.921013	0.433293	-1.31238	-0.3297	0.030683
Eomes	0.733075	0.542155	0.131825	-0.84488	-0.62225	0.060065
Mif	0.925367	0.398157	0.004847	-0.79405	-0.29289	-0.24142
Ms4a1	0.651202	0.490542	0.235852	-0.54978	-0.07279	-0.75503
Spib	0.600393	0.471223	0.151583	-0.66787	-0.18472	-0.37062
Taf6l	0.40819	0.65537	0.11299	-0.54076	-0.38562	-0.25017
Ctsw	0.776668	0.220278	0.310588	-0.95923	-0.04403	-0.30427
Pml	0.562102	0.427092	0.404362	-0.93954	0.028042	-0.48206
Foxo1	1.015117	0.301647	0.246857	-0.29688	-0.47746	-0.78927
Gnas	0.643645	0.360645	0.245945	-0.29238	-0.59313	-0.36474
Plcg1	0.811953	-0.05812	0.491033	-0.52266	-0.13926	-0.58296
Acaca	0.637108	-0.11283	0.272168	-0.22391	-0.08561	-0.48692
Cd160	0.797425	-0.27314	-0.07328	-0.35084	-0.23925	0.139065
Ptpn7	0.682185	0.057265	0.095315	-0.28829	-0.41023	-0.13626
Mcm5	0.656538	0.121658	0.210128	-0.40102	-0.50371	-0.08359
Dgkz	0.498488	0.307558	0.314878	-0.44892	-0.38933	-0.28267

Acsl3	1.396298	-0.35449	0.008448	-0.12918	-0.47444	-0.44663
Chek1	1.321478	-0.19228	-0.16637	-0.31489	-0.17087	-0.47706
Pycr2	1.376613	-0.16209	-0.03309	-0.4484	-0.35952	-0.37353
Trac	1.557118	-0.10724	0.104748	-0.77883	-0.40743	-0.36836
Mcm7	1.438295	-0.06174	0.297575	-0.64741	-0.39432	-0.63242
Lck	1.296508	-0.11687	0.214838	-0.73015	-0.14844	-0.51588
Cd4	1.704203	0.168523	0.723563	-0.97934	-0.67686	-0.9401
Itga6	1.417197	0.226177	1.087057	-1.35475	-0.41128	-0.96439
Trbc1/2	1.425045	0.076045	0.696065	-1.40858	-0.63725	-0.15134
Hdac7	1.378368	0.535008	0.549478	-1.51098	-0.51576	-0.43611
Zap70	1.15965	0.32319	0.52891	-1.32144	-0.11031	-0.58
Cd8a	2.101313	-0.83747	0.628573	-0.61598	-1.0349	-0.24155
Cd8b1	2.391653	-0.66241	0.804423	-1.11918	-0.45264	-0.96186
Tcf7	2.346488	-0.09939	0.689438	-1.31638	-0.87252	-0.74763

Table S3-4: Genes significantly different in CD45+ cells isolated from TC2 ERα+ metastatic lungs and naïve lungs from LFD-fed mice.

Table S3-5. Comparison of gene expression from lungs of non-tumor bearing and metastatic HFD-fed mice.

Gene Name	HFD TC2 #1	HFD TC2 #2	HFD TC2 #3	HFD Naïve #1	HFD Naïve #2	HFD Naïve #3
Mmp9	2.091517	-0.24962	1.698477	-0.3791	-1.58933	-1.57193
Il1b	1.826	0.2449	1.3371	-0.4377	-1.489	-1.4813
Mapk13	1.76257	1.0352	1.36195	-1.23442	-1.52901	-1.39629
Hdc	1.570212	0.388532	1.718912	-0.66521	-1.67721	-1.33524
Il1f9	2.21698	0.64582	1.54492	-0.30289	-2.08178	-2.02305
Csf3r	1.871578	0.315498	1.511778	-0.41275	-1.76366	-1.52244
Pdcd1lg2	0.347857	0.584617	0.221117	-0.31875	-0.50187	-0.33296
Bid	0.710098	0.169048	0.342938	-0.14297	-0.55371	-0.5254
Fos	0.512783	-0.11202	0.565683	-0.44472	-0.22322	-0.29852
Dusp1	0.8186	-0.2352	0.5521	-0.3031	-0.4087	-0.4237
Ms4a4a	0.369843	0.238033	0.998623	0.279733	-0.81716	-1.06908
Lilra6	0.634957	0.890637	0.697057	-0.3435	-0.57025	-1.30889
Sell	0.789847	0.368147	0.764447	-0.14005	-0.95642	-0.82596
Ptgs2	1.103253	0.182783	1.078473	-0.27636	-1.12917	-0.95899
Gadd45a	1.2288	-0.13205	0.84906	-0.3925	-0.73415	-0.81916
Ccr1	1.30131	-0.0723	0.80052	-0.2381	-0.98266	-0.80877
Cebpd	0.909198	0.032648	0.543888	0.089738	-0.60794	-0.96753
Cd101	1.218777	-0.11465	0.753997	-0.22303	-0.7134	-0.92168
Il12b	-0.43744	-0.45154	-0.89657	0.687842	0.140052	0.957652
Il10	0.216645	-0.60579	-0.89574	0.228415	0.386335	0.670125
Cxcl1	-0.06763	-0.34123	-0.55503	0.210367	0.086067	0.667467
Cd276	-0.17633	-0.15953	-0.55105	0.132108	0.290028	0.464778
Itgae	-0.15182	-0.24347	-0.45236	-0.01953	0.418503	0.448663
Icam1	-0.42979	-0.07909	-0.38814	0.261475	0.310455	0.325075
Klrk1	-0.32549	-0.29753	-0.39237	0.281388	0.365598	0.368408
Cblb	-0.28067	-0.396	-0.20022	0.255322	0.187282	0.434282
Card11	-0.38386	-0.5857	-0.10815	0.325318	0.358148	0.394248
Cyp8b1	-0.22567	-0.23487	-1.03577	0.198798	0.735228	0.562288
Ccl12	-0.16575	-0.14757	-0.75346	0.134093	0.525213	0.407463
Icos	-0.36149	0.083795	-0.78108	0.149495	0.512915	0.396355
Rora	-0.40483	0.069607	-0.56018	0.055647	0.571657	0.268107
Trgv1/Trgv2/Trgv3	-0.00206	-1.11079	-0.24581	0.294857	0.452777	0.611037
Ccl3	0.046912	-1.29121	-0.38344	0.644112	0.398612	0.585012
Ccl2	-0.1166	-0.71145	-0.51145	0.781107	0.335587	0.222817
H2-Ob	-0.11079	-0.42961	-0.42038	0.475495	0.198555	0.286715
Trdv4	-0.61479	-0.64408	-0.09753	0.492002	0.914932	-0.05054
Klrd1	-0.5695	-0.83023	-0.16755	0.407507	0.749847	0.409937
Ccl5	-0.46863	-0.68823	-0.50103	0.383267	0.859767	0.414867

Trgc1/2/3	-0.29937	-0.49383	-0.31605	0.109762	0.795932	0.203552
Klrc1	-0.31444	-0.78317	-0.46253	0.339608	0.803578	0.416958

Table S3-5: Genes significantly different in CD45+ cells isolated from TC2 ERα+ metastatic lungs and naïve lungs from HFD-fed mice.

References:

1. Purnell JQ. Definitions, Classification, and Epidemiology of Obesity. In: Feingold KR, Anawalt B, Blackman MR, Boyce A, Chrousos G, Corpas E, et al., editors. Endotext. South Dartmouth (MA): MDText.com, Inc.

2. Avgerinos KI, Spyrou N, Mantzoros CS, Dalamaga M. Obesity and cancer risk: Emerging biological mechanisms and perspectives. Metabolism. 2019;92:121-35.

3. de Waard F, Baanders-van Halewijn EA. A prospective study in general practice on breast-cancer risk in postmenopausal women. Int J Cancer. 1974;14(2):153-60.

4. Pierobon M, Frankenfeld CL. Obesity as a risk factor for triple-negative breast cancers: a systematic review and meta-analysis. Breast Cancer Res Treat. 2013;137(1):307-14.

5. Renehan AG, Tyson M, Egger M, Heller RF, Zwahlen M. Body-mass index and incidence of cancer: a systematic review and meta-analysis of prospective observational studies. Lancet. 2008;371(9612):569-78.

6. Chan DS, Vieira AR, Aune D, Bandera EV, Greenwood DC, McTiernan A, et al. Body mass index and survival in women with breast cancer-systematic literature review and meta-analysis of 82 follow-up studies. Ann Oncol. 2014;25(10):1901-14.

7. Majed B, Moreau T, Senouci K, Salmon RJ, Fourquet A, Asselain B. Is obesity an independent prognosis factor in woman breast cancer? Breast Cancer Res Treat. 2008;111(2):329-42.

8. Ewertz M, Jensen MB, Gunnarsdóttir K, Højris I, Jakobsen EH, Nielsen D, et al. Effect of obesity on prognosis after early-stage breast cancer. J Clin Oncol. 2011;29(1):25-31.

9. Sestak I, Distler W, Forbes JF, Dowsett M, Howell A, Cuzick J. Effect of body mass index on recurrences in tamoxifen and anastrozole treated women: an exploratory analysis from the ATAC trial. J Clin Oncol. 2010;28(21):3411-5.

10. Harborg S, Cronin-Fenton D, Jensen MR, Ahern TP, Ewertz M, Borgquist S. Obesity and Risk of Recurrence in Patients With Breast Cancer Treated With Aromatase Inhibitors. JAMA Netw Open. 2023;6(10):e2337780.

11. Raheem F, Karikalan SA, Batalini F, El Masry A, Mina L. Metastatic ER+ Breast Cancer: Mechanisms of Resistance and Future Therapeutic Approaches. Int J Mol Sci. 2023;24(22).

12. Menikdiwela KR, Kahathuduwa C, Bolner ML, Rahman RL, Moustaid-Moussa N. Association between Obesity, Race or Ethnicity, and Luminal Subtypes of Breast Cancer. Biomedicines. 2022;10(11).

13. Ades F, Zardavas D, Bozovic-Spasojevic I, Pugliano L, Fumagalli D, de Azambuja E, et al. Luminal B breast cancer: molecular characterization, clinical management, and future perspectives. J Clin Oncol. 2014;32(25):2794-803.

14. Sparano JA, Wang M, Zhao F, Stearns V, Martino S, Ligibel JA, et al. Obesity at diagnosis is associated with inferior outcomes in hormone receptor-positive operable breast cancer. Cancer. 2012;118(23):5937-46.

15. Biganzoli E, Desmedt C, Fornili M, de Azambuja E, Cornez N, Ries F, et al. Recurrence dynamics of breast cancer according to baseline body mass index. Eur J Cancer. 2017;87:10-20.

16. Zhang XH, Giuliano M, Trivedi MV, Schiff R, Osborne CK. Metastasis dormancy in estrogen receptor-positive breast cancer. Clin Cancer Res. 2013;19(23):6389-97.

17. Almond M, Farne HA, Jackson MM, Jha A, Katsoulis O, Pitts O, et al. Obesity dysregulates the pulmonary antiviral immune response. Nat Commun. 2023;14(1):6607.

18. Saltiel AR, Olefsky JM. Inflammatory mechanisms linking obesity and metabolic disease. J Clin Invest. 2017;127(1):1-4.

19. Porsche CE, Delproposto JB, Geletka L, O'Rourke R, Lumeng CN. Obesity results in adipose tissue T cell exhaustion. JCI insight. 2021;6(8).

20. Núñez-Ruiz A, Sánchez-Brena F, López-Pacheco C, Acevedo-Domínguez NA, Soldevila G. Obesity modulates the immune macroenvironment associated with breast cancer development. PLoS One. 2022;17(4):e0266827.

21. Wogsland CE, Lien HE, Pedersen L, Hanjra P, Grondal SM, Brekken RA, et al. High-dimensional immunotyping of tumors grown in obese and non-obese mice. Disease models & mechanisms. 2021;14(4).

22. Misumi I, Starmer J, Uchimura T, Beck MA, Magnuson T, Whitmire JK. Obesity Expands a Distinct Population of T Cells in Adipose Tissue and Increases Vulnerability to Infection. Cell Rep. 2019;27(2):514-24.e5.

23. Wherry EJ, Kurachi M. Molecular and cellular insights into T cell exhaustion. Nat Rev Immunol. 2015;15(8):486-99.

24. Pichler AC, Carrié N, Cuisinier M, Ghazali S, Voisin A, Axisa PP, et al. TCR-independent CD137 (4-1BB) signaling promotes CD8(+)-exhausted T cell proliferation and terminal differentiation. Immunity. 2023;56(7):1631-48.e10.

25. Dolina JS, Van Braeckel-Budimir N, Thomas GD, Salek-Ardakani S. CD8(+) T Cell Exhaustion in Cancer. Front Immunol. 2021;12:715234.

26. Green WD, Al-Shaer AE, Shi Q, Gowdy KM, MacIver NJ, Milner JJ, et al. Metabolic and functional impairment of CD8(+) T cells from the lungs of influenza-infected obese mice. J Leukoc Biol. 2022;111(1):147-59.

27. McQuade JL, Daniel CR, Hess KR, Mak C, Wang DY, Rai RR, et al. Association of body-mass index and outcomes in patients with metastatic melanoma treated with targeted therapy, immunotherapy, or chemotherapy: a retrospective, multicohort analysis. Lancet Oncol. 2018;19(3):310-22.

28. Richtig G, Hoeller C, Wolf M, Wolf I, Rainer BM, Schulter G, et al. Body mass index may predict the response to ipilimumab in metastatic melanoma: An observational multi-centre study. PLoS One. 2018;13(10):e0204729.

29. Cortellini A, Bersanelli M, Santini D, Buti S, Tiseo M, Cannita K, et al. Another side of the association between body mass index (BMI) and clinical outcomes of cancer patients receiving programmed cell death protein-1 (PD-1)/ Programmed cell death-ligand 1 (PD-L1) checkpoint inhibitors: A multicentre analysis of immune-related adverse events. Eur J Cancer. 2020;128:17-26.

30. Chakraborty B, Byemerwa J, Krebs T, Lim F, Chang CY, McDonnell DP. Estrogen Receptor Signaling in the Immune System. Endocr Rev. 2023;44(1):117-41.

31. Schuler LA, Murdoch FE. Endogenous and Therapeutic Estrogens: Maestro Conductors of the Microenvironment of ER+ Breast Cancers. Cancers (Basel). 2021;13(15).

32. Zhu L, Narloch JL, Onkar S, Joy M, Broadwater G, Luedke C, et al. Metastatic breast cancers have reduced immune cell recruitment but harbor increased macrophages relative to their matched primary tumors. J Immunother Cancer. 2019;7(1):265.

33. Hillers-Ziemer LE, Williams AE, Janquart A, Grogan C, Thompson V, Sanchez A, et al. Obesity-Activated Lung Stromal Cells Promote Myeloid Lineage Cell Accumulation and Breast Cancer Metastasis. Cancers (Basel). 2021;13(5).

34. McDowell SAC, Milette S, Doré S, Yu MW, Sorin M, Wilson L, et al. Obesity alters monocyte developmental trajectories to enhance metastasis. J Exp Med. 2023;220(8).

35. Özdemir BC, Sflomos G, Brisken C. The challenges of modeling hormone receptor-positive breast cancer in mice. Endocr Relat Cancer. 2018;25(5):R319-r30.

36. Barcus CE, O'Leary KA, Brockman JL, Rugowski DE, Liu Y, Garcia N, et al. Elevated collagen-I augments tumor progressive signals, intravasation and metastasis of prolactin-induced estrogen receptor alpha positive mammary tumor cells. Breast Cancer Research2017.

37. Szostakowska M, Trębińska-Stryjewska A, Grzybowska EA, Fabisiewicz A. Resistance to endocrine therapy in breast cancer: molecular mechanisms and future goals. Breast Cancer Res Treat. 2019;173(3):489-97.

38. Simon S, Labarriere N. PD-1 expression on tumor-specific T cells: Friend or foe for immunotherapy? Oncoimmunology. 2017;7(1):e1364828.

39. Piening A, Ebert E, Gottlieb C, Khojandi N, Kuehm LM, Hoft SG, et al. Obesity-related T cell dysfunction impairs immunosurveillance and increases cancer risk. Nat Commun. 2024;15(1):2835.

40. Hillers-Ziemer LE, McMahon RQ, Hietpas M, Paderta G, LeBeau J, McCready J, et al. Obesity Promotes Cooperation of Cancer Stem-Like Cells and Macrophages to Enhance Mammary Tumor Angiogenesis. Cancers (Basel). 2020;12(2).

41. Hoekstra ME, Vijver SV, Schumacher TN. Modulation of the tumor micro-environment by CD8(+) T cell-derived cytokines. Curr Opin Immunol. 2021;69:65-71.

42. Zhang Z, Chen L, Chen H, Zhao J, Li K, Sun J, et al. Pan-cancer landscape of T-cell exhaustion heterogeneity within the tumor microenvironment revealed a progressive roadmap of hierarchical dysfunction associated with prognosis and therapeutic efficacy. EBioMedicine. 2022;83:104207.

43. Egelston CA, Avalos C, Tu TY, Simons DL, Jimenez G, Jung JY, et al. Human breast tumor-infiltrating CD8(+) T cells retain polyfunctionality despite PD-1 expression. Nat Commun. 2018;9(1):4297.

44. Miller BC, Sen DR, Al Abosy R, Bi K, Virkud YV, LaFleur MW, et al. Subsets of exhausted CD8(+) T cells differentially mediate tumor control and respond to checkpoint blockade. Nat Immunol. 2019;20(3):326-36.

45. Geng X, Li M, Cui B, Lu C, Liu X, Zhang P, et al. CD4+CD25+Foxp3+ regulatory T cells suppress NKG2D-mediated NK cell cytotoxicity in peripheral blood. Medicine (Baltimore). 2019;98(22):e15722.

46. Vyas M, Requesens M, Nguyen TH, Peigney D, Azin M, Demehri S. Natural killer cells suppress cancer metastasis by eliminating circulating cancer cells. Front Immunol. 2022;13:1098445.

47. Myers JA, Schirm D, Bendzick L, Hopps R, Selleck C, Hinderlie P, et al. Balanced engagement of activating and inhibitory receptors mitigates human NK cell exhaustion. JCI Insight. 2022;7(15).

48. Lee EHC, Wong DCP, Ding JL. NK Cells in a Tug-of-War With Cancer: The Roles of Transcription Factors and Cytoskeleton. Front Immunol. 2021;12:734551.

49. Roe K. NK-cell exhaustion, B-cell exhaustion and T-cell exhaustion-the differences and similarities. Immunology. 2022;166(2):155-68.

50. Nakamura T, Sato T, Endo R, Sasaki S, Takahashi N, Sato Y, et al. STING agonist loaded lipid nanoparticles overcome anti-PD-1 resistance in melanoma lung metastasis via NK cell activation. J Immunother Cancer. 2021;9(7).

51. Helmink BA, Reddy SM, Gao J, Zhang S, Basar R, Thakur R, et al. B cells and tertiary lymphoid structures promote immunotherapy response. Nature. 2020;577(7791):549-55.

52. Rugo HS, Delord JP, Im SA, Ott PA, Piha-Paul SA, Bedard PL, et al. Safety and Antitumor Activity of Pembrolizumab in Patients with Estrogen Receptor-Positive/Human Epidermal Growth Factor Receptor 2-Negative Advanced Breast Cancer. Clin Cancer Res. 2018;24(12):2804-11.

53. Waks AG, Stover DG, Guerriero JL, Dillon D, Barry WT, Gjini E, et al. The Immune Microenvironment in Hormone Receptor-Positive Breast Cancer Before and After Preoperative Chemotherapy. Clin Cancer Res. 2019;25(15):4644-55.

54. Terranova-Barberio M, Pawlowska N, Dhawan M, Moasser M, Chien AJ, Melisko ME, et al. Exhausted T cell signature predicts immunotherapy response in ER-positive breast cancer. Nature communications. 2020;11(1):3584.

CHAPTER 4:

Obesity increases the efficacy of anti-CSF-1R inhibitors combined with anti-PD-1 immune checkpoint blockade therapy in a model of ERα+ breast cancer metastasis.

Abstract:

Breast cancer patients with a body mass index (BMI) of ≥30 kg/m^2 have an increased risk for metastatic disease compared to patients with a BMI in the normal range. We have previously observed elevated CSF-1R+ macrophages surrounding estrogen receptor (ER)+ metastases in obese mice and increased PD-1+ CD8+ T cells. These results are suggestive that immunotherapy targeting CSF-1R and PD-1 may be beneficial to reduce metastases. To test this hypothesis, we fed 3-week-old female FVB/N mice either a low-fat diet (LFD) or high-fat diet (HFD) for 16 weeks to induce obesity, then injected estrogen receptor alpha positive (ERα+) TC2 cells into the mammary fat pads. Tumors grew to 0.5 cm in diameter then were surgically removed to model metastatic growth. LFD and HFD-fed mice bearing metastasis were treated with anti-PD-1 antibodies with or without anti-CSF-1R therapy. In response to anti-PD-1 therapy, obese mice had an influx of T cells into metastatic lungs, and NanoString analysis showed that cytotoxic gene expression was upregulated in lean mice, while obese mice had upregulated expression of genes associated with T cell checkpoints. Obese mice had reduced metastasis in response to treatment with anti-CSF-1R antibodies and decreased numbers of PD-L1+ myeloid cells. Obese mice treated with combined CSF-1R and PD-1 therapies showed increased inflammation and elevated PD-1+ CD8+ T cells in obese mice. Additionally, obese mice had less metastasis compared to lean mice on dual therapy. Our results show that macrophage depletion in combination with anti-PD-1 inhibitors reduces ERα+ metastases in obese mice.

Introduction:

Patients with breast cancer and obesity are more likely to have metastasis at the time of diagnosis (1-3). Further, obese patients have worse overall survival when treated with standard of care therapy (4). Luminal B breast cancer expresses estrogen receptor alpha (ERα+) and are associated with higher histological grade (5). ERα+ disease accounts for 70% of breast cancers diagnosed in women (6) Luminal B breast cancer is associated with obesity and obese women with ERα+ have increased risk for metastasis and have lower levels of survival (7) (8, 9). Although ERα+ tumors are removed as part of standard of care, metastasis can occur 20 years after resection (10, 11).

Immune checkpoint blockade (ICB) has emerged as a new tool in cancer treatment. However, ICB therapy targeting programmed cell death-1 (PD-1) and its ligand PD-L1 are not efficacious in all patients. In ERα+ breast cancer, the responses to ICB are very low, with objective response rates equaling 12% (12). Strategies have emerged to increase the efficacity of ICB targeting PD-1/PD-L1 in several cancers, including breast cancer (13). Methods to increase tumor infiltrating lymphocytes have improved ICB responses in immunogenically cold tumors (14, 15). To increase tumor infiltrating lymphocytes, one strategy is to deplete macrophages within the mammary tumors (16). Macrophages can limit the infiltration of lymphocytes like CD8+ T cells within tumors. Within breast cancer metastasis, higher levels of macrophages around lung metastasis have been seen under obese conditions (17) Therefore, combining macrophage depletion strategies with checkpoint inhibitors may improve overall anti-tumor immune responses. Colony stimulating factor-1 receptor (CSF-1R) inhibitors have

been used clinically to deplete macrophages and monocytes in the tumor microenvironment. In pre-clinical models, combining CSF-1R inhibitors with anti-PD-1 inhibitors in mammary tumors in mice have improved CD8+ T cell infiltration and decreased tumor volume compared to each therapy alone (18). However, it is unknown what effects these two immunotherapies will have in a model of ERα+ breast metastasis under conditions of obesity.

Obesity is associated with chronic inflammation and adaptive immune cell dysfunction (19). Obesity causes macrophage driven inflammation within fat and the mammary gland (20, 21). Macrophages have been shown to promote breast cancer growth and suppress CD8 +T cells in primary tumors in obesity (22), and we have previously shown that there is an increase of CSF-1R+ macrophages within metastasis in the lungs of obese mice (17). Others have shown an increase in monocytes and PD-1+ CD8+ T cells within lung metastasis in obese mice (23). Together, these studies suggest that depletion of CSF-1R+ macrophages may enhance anti-PD-1 therapies in obese mice in ERα+ metastatic breast cancer.

Here we feed female FVB/N mice a low-fat diet (LFD) or high-fat-diet (HFD) to model obesity. We orthotopically injected TC2 ERα+ mammary cells into the mammary fat pad to model ERα+ breast cancer. Mice were treated with either IgG control, anti-PD-1 or anti-CSF-1R antibodies or a combination of both therapies to answer how the metastatic immune microenvironment in the lungs responds under lean and obese conditions. Our work may identify a new therapeutic opportunity to reduce metastasis for patients with stage IV ERα+ breast cancer.

Materials and Methods:

Mouse Models

All animal procedures were approved by the University of Wisconsin Institutional Animal Care and Use Committee, per guidelines published by the NIH Guide for the Care and Use of Laboratory Animals (Animal protocol number V005188). All mice were housed in AAALAC-accredited facilities. Three-week-old-female FVB/N (FVB/NTac, Taconic Biosciences) mice were fed either a purified chow low-fat diet (LFD; 16% kcal from fat; 2920X; Teklad Global; ENVIGO) or high-fat diet (HFD; 60% kcal from fat; Test Diet 58Y1; 0056833) for 16 weeks to induce obesity. Food and water were provided *ad libitum.* Body weights were measured weekly. LFD and HFD-fed mice were orthotopically transplanted with $ER\alpha^{+}$ GFP^{+} TC2 cells. 75,000 TC2 cells suspended in 1X PBS were injected into bilateral fourth inguinal mammary glands. Tumor diameters were measured each week using calipers. Tumor volume was calculated using the formula (L*W*W)/2. Once tumors reached a diameter of 0.5 cm, tumors were resected. If tumors recurred at the surgical site, mice were excluded from the study. Mice were fed their respective diets for another 8 weeks before beginning immunotherapy regimens.

After 8 weeks, mice were randomized to receive either immunoglobulin G (IgG) control (BioCell; BE0089), anti-CSF-1R (BioCell; BE0146), anti-PD-1 (BioCell; BE0146), or anti-CSF-1R, and ant-PD-1 antibodies. IgG and anti-PD-1 were injected intraperitoneally with 250 µg/0.2 mL in sterile PBS every 3 days for 2 weeks. Anti-CSF-1R treated mice were given a 1.0 mg loading dose in sterile PBS then 0.5 mg doses every 5 days for a total of 2.5 mg per mouse. Mice treated anti-CSF-1R and anti-PD-1

antibodies were given a 1.0 mg loading dose of anti-CSF-1R then began anti-PD-1 treatment the next day. For NanoString analysis, mice were treated with IgG, anti-PD-1, and anti-CSF-1R antibodies once tumors reached 0.7 cm in diameter. Mice were collected a day after the last antibody treatment. At the end of treatment, mice were humanely euthanized with CO_2 asphyxiation.

Cell culture

TC2 cells were provided by Dr. Linda Schuler at the University of Wisconsin-Madison (24). TC2 cells were cultured in DMEM (Corning; 10-017-CV, Corning, NY, USA) supplemented with 10% FBS and 1 mg/mL G418 (ThermoFisher Scientific; 11811023, Waltham, MA, USA). All media contained 1% antibiotic/antimycotic solution, and cells were maintained at 37°C in 5% CO_2. Tumor cell lines were not further validated and were tested for mycoplasma prior to use in experiments (Idexx BioAnalytics, Columbia, MO, USA). Before transplantation, TC2 cells were trypsinized with 0.25% trypsin for 5 minutes at 37°C in 5% CO_2. Cells were then counted and suspended in PBS at 2.5 $x10^3$ cells/mL.

Tissue Collection

Blood was removed from lungs via cardiac puncture following euthanasia. The three largest lobes of the lungs from each mouse were manually minced in 1 mL of DMEM (Corning, 10-017-CV) supplemented with 10% FBS (Gibco, A52567-01), 1% antibiotic-antimycotic solution (Corning, 30-004-CI), 10 µg/mL insulin (Sigma-Aldrich, I0516), 5 ng/mL human epidermal growth factor (Sigma-Aldrich, E9644), 0.5 µg/mL hydrocortisone (Sigma-Aldrich, H0888), 3 mg/mL collagenase A (Sigma-Aldrich), and 0.1 mg/mL DNase

I (Sigma-Aldrich, 10104159001) and digested for 45 mins at 37°C. Tissue was not frozen prior to RNA extraction or flow cytometry staining.

Flow Cytometry

After digestion, lungs were mechanically dissociated through a 20-gauge needle in 5% bovine calf serum (BCS) in PBS to achieve a cell suspension. Samples were then incubated for 2 mins in Ammonium–chloride–potassium (ACK) lysis buffer (Quality Biological; 118-156-101, Gaithersburg, MD, USA) to lyse red blood cells. Next, samples were filtered 100 μm (Falcon; 352360) and 40 μm cell strainers (Falcon; 352340) to isolate single cells. For each mouse, 500,000 lung cells were blocked with Fc blocking antibody (CD16/32, ThermoFisher; 14-0161-82) for 20 minutes. To assess viability, each lung sample was stained with live/dead UV blue dye (ThermoFisher; L34961) in PBS for 30 minutes at 4°C in the dark. A sample spiked with cells heat-killed at 60°C for 5 mins was included as a control. Antibodies for flow cytometry analysis are listed in Table S1. Samples were incubated with antibodies for 20 min in 2% BCS/PBS at 4°C. Cells were fixed with Cyofix/CytoPerm Plus kit with Golgi Plug (BD Biosciences; 555028) for 25 minutes, then stored in 2% BCS/PBS at 4°C overnight. Flow cytometry was conducted on a Cytek Aurora Cytometer using SpectroFlo software. Fluorescence minus one (FMO) and single-color controls were included. Single color controls conjugated to UltraComp ebeads (ThermoFisher; 01-2222-42), and a sample of unstained cells and beads were used to determine fluorophore unmixing. Samples and FMOs were analyzed using FlowJo (version 10.1).

CD8+ T cell stimulation experiments

Whole lung tissue isolated from mice with TC2 tumors was digested and separated into a single cell suspension. F4/80+ macrophages were FACS sorted from LFD and HFD-fed tumor bearing mice (ThermoFisher; 17-4801-82). CD8+ T cells were isolated from a spleen from a LFD-fed mouse using the EasySep Mouse CD8+ T cell Isolation Kit (Stemcell Technologies; 19853). 24 well plates were coated with (1 µg/mL) CD3 antibodies (eBioscience; 16-0032-82) for 2 hours in 1X PBS at °C in 5% CO2. PBS was then removed from wells. T cells and macrophages were incubated at a 1:3 ratio (macrophages/CD8+T cells) in RPMI media (Corning; 10-040-CV) in CD3 antibody coated wells with 10% FBS, with or without (5 µg/mL) CD28 antibodies (eBioscience; 16-0281-82) for 24 hours. After 19 hours Golgi Plug from BD Cytofix/Cytoperm Plus (BD Biosciences; 555028) was added to wells for 5 hours. After 5 hours cells were stained for cell surface markers CD8α and F4/80 (Table S1). Cells were then permeabilized and stained for intracellular cytokines TNFα and IFNγ (Table S1). Cells were stored overnight at 4°C and analyzed the next day on a Cytek Aurora Cytometer. Each individual data point represents a replicate from macrophages sorted from LFD and HFD-fed mice.

NanoString RNA Analysis

RNA was collected from CD45+ cells isolated from lung tissue with TC2 metastasis treated with either IgG, anti-PD-1 or anti-CSF-1R antibodies. Anti-Rat IgG Dynabeads (ThermoFisher; 11035) were incubated with CD45 (Biolegend; 103101) antibodies at a 1:10 ratio for 30 minutes at 4°C. Beads conjugated to CD45 antibodies were incubated

with dissociated lung tissue for 30 minutes at 4°C as described by the manufacturer. RNA was extracted using Qiagen RNA Microkit (Qiagen; 74004). Samples were tested for RNA quality by the UW Biotechnology Center (University of Wisconsin-Madison) using a NanoDrop One Spectrophotometer and Agilent 2100 Bioanalyzer. RNA with DV200 greater than 70% were sent to the Translational Research Initiatives in Pathology (TRIP) Laboratory (UW Carbone Cancer Center, University of Wisconsin-Madison) for analysis on the nCounter MAX System. RNA from IgG and anti-PD-1 treated mice were analyzed on the nCounter NanoString Immune Exhaustion Panel (NanoString; XT-H-EXHAUST-12) and an additional set of RNA from IgG mice and anti-CSF-1R treated mice were analyzed on the nCounter NanoString Myeloid Innate Immunity Panel (NanoString; XT_PGX_MmV2_Myeloid_CSO). If samples failed quality control during testing from the UW-Madison Biotechnology Center or ROSALIND Analysis Software, samples were excluded from the study. nCounter NanoString data was analyzed using ROSALIND software.

Statistical Analysis

Results are reported as the mean ± standard error of the mean (s.e.m.). Statistical differences were determined using two-way analysis of variance (ANOVA) and Tukey's multiple comparisons posttest, unless otherwise noted. A p-value of ≤0.05 denotes significant value. All statistical analyses were performed with GraphPad Prism 9.4.1 (GraphPad Software).

Results:

Anti-PD-1 treatment upregulates immune checkpoints in HFD-fed mice

To investigate how ERα+ tumors and metastasis respond to anti-PD-1 ICB therapy in lean and obese mice, 3-week-old female FVB/N mice were fed either a LFD or a HFD for 16 weeks, then TC2 ERα+ mammary tumor cells were orthotopically injected into mammary fat pads. Once tumors reached 0.7 in diameter, mice were randomized to receive IgG or anti-PD-1 antibodies (Figure 4-1A). As observed previously, HFD-fed mice gained significantly more weight than LFD-fed mice (Figure 4-1B) (17, 25, 26). Interestingly, HFD-fed mice treated with anti-PD-1 antibodies had a mild, although not significant, decrease in tumor growth compared to HFD-fed IgG treated mice (Figure 4-1C).

As the major cause of breast cancer mortality is due to metastasis, we examined how targeting PD-1 altered immune cell function in the lung metastatic site. To do this, we sorted CD45+ cells from metastatic lungs, extracted RNA, and analyzed gene expression using the NanoString Immune Exhaustion Panel. In immune cells from IgG-treated mice, we observed a number of genes that were differentially expressed (Figure S4-1A, Table S4-2). In particular, expression of genes associated with T cell receptor (TCR) signaling were upregulated in HFD-fed mice compared to LFD-fed mice (Figure S4-1B). We also observed that expression of genes involved with myeloid immune evasion pathways were also altered (Figure S4-1C). *Nos2* was significantly upregulated in immune cells from obese mice (4.3 fold, p=0.01, Figure S4-1C), which plays a role in enhancing macrophage migration and survival and has been associated with lung carcinogenesis (27).

Immune cells from LFD-fed mice had the largest number of genes expression differences in mice treated either with IgG or anti-PD-1 antibodies (Figure 4-1D, Table S4-3). As expected, anti-PD-1 treatment increased genes associated with cytotoxicity (Figure 1E). Genes associated with IL-10 signaling were mostly upregulated in LFD-fed mice treated with anti-PD-1 inhibitors (Figure 4-1F); IL-10 signaling has been shown to increase immunosuppression with PD-1 therapy (28). We also observed elevated expression of genes involved in NFκB signaling in mice treated with anti-PD-1 antibodies (Figure 4-1G). In particular, CCL21 expression, which was upregulated 3-fold (p=0.04, Figure 4-1G), was increased hepatocellular carcinoma and enhanced ICB response (29). We also saw a decrease in genes associated with myeloid cell immune evasion in LFD-fed mice treated with anti-PD-1 antibodies (Figure 4-1H). *Arg1,* which is expressed by immunosuppressive myeloid cells *(30)*, was downregulated 5-fold compared to IgG treated LFD-fed mice (p=0.01, Figure 4-1H).

Like in LFD-fed mice, multiple genes were differentially expressed in immune cells from metastatic lungs of HFD-fed mice (Figure 4-1I, Table S4-4). In contrast to LFD-fed mice, HFD-fed mice treated with anti-PD-1 antibodies had increased expression of other genes associated with T cell checkpoint signaling, including *Lag3* and *Tigit* (Figure 4-1J). Similar to LFD-fed mice, genes involved in NFκB signaling were upregulated in HFD-fed mice treated with anti-PD-1 antibodies (Figure 4-1K). Unlike in LFD-fed mice, *Vcam1* expression was upregulated 4-fold (p=0.002), and VCAM1 has been shown to enhance T cell infiltration in other preclinical models (31).

Unexpectedly, there were only six genes differentially expressed between LFD and HFD-fed mice treated with anti-PD-1 antibodies (Figure S4-1D, Table S4-5). *Gzmb*

is the most pro-apoptotic of the granzyme family (32) and was upregulated in immune cells from LFD-fed mice (Figure S4-1D). In contrast, *Gzmd*, which was upregulated in immune cells from HFD-fed mice (Figure S4-1D), may be produced by multiple cell types including activated mast cells (33). Overall, immune cells in TC2 ER+ lung metastasis from obese mice show increased in T cell receptor activation and signs of myeloid cell immune dysfunction.

Anti-PD-1 treatment reduced metastasis in LFD-fed mice

ERα+ breast cancer can recur with distal metastasis up to 20 years after the initial diagnosis and treatment (11). To examined immune responses to anti-PD-1 antibodies for metastatic diseases, we fed FVB/N female mice LFD or HFD for 16 weeks. We orthotopically injected ERα+ GFP+ TC2 mammary cells into the fat pads of LFD and HFD-fed mice then surgically removed tumors when they reached 0.5 cm in diameter. We allowed 8 weeks for metastatic progression, then treated mice with anti-PD-1 or IgG control antibodies (Figure 4-2A). Tumors in HFD-fed mice grew significantly faster than in LFD-fed mice prior to tumor removal (Figure 24-B). After 8 weeks, we quantified cell populations using flow cytometry (Figure S4-2). Flow cytometry analysis revealed no differences in CD45+ total immune cells or CD4+ cells between LFD or HFD-fed mice treated with IgG or anti-PD-1 antibodies (Figure 4-2C, D). No differences were observed in the percentage of CD8+ T cells following anti-PD-1 treatment in LFD-fed mice (Figure 4-2E). However, anti-PD-1 treatment significantly increased CD8+ T cell recruitment into the lungs in HFD-fed mice compared to HFD-fed mice treated with IgG control antibodies ($p=0.02$, Figure 4-2E). No significant differences in PD-1

expression on CD8+ T cells were observed in any of the treatment groups (Figure 4-2F).

Obesity has been shown to increase myeloid lineage cells in metastasis in multiple contexts (17, 23). However, we did not see any differences in CD11b+ cells or CD115/CSF-1R+ cells regardless of diet or treatment (Figure 4-2G, H). PD-L1 expression on myeloid cells has been associated with increased responses to ICB in triple negative breast cancer (34). Although we saw a trending increase in PD-L1+ CD11b+ cells in HFD-fed mice, we did not see any significant differences in PD-L1 expression due to treatment with anti-PD-1 antibodies (Figure 4-2I).

To measure metastatic burden in the lungs of LFD and HFD-fed mice, we quantified GFP+ cells. There was a significant reduction in GFP+ metastasis in LFD-fed mice treated with anti-PD-1 antibodies compared to LFD-fed mice treated with an IgG control ($p=0.05$, Figure 4-2J). Anti-PD-1 treatment did not reduce GFP+ metastatic cells in HFD-fed mice (Figure 4-2J). PD-L1 is also expressed on tumor cells within metastatic lesions (35). Although there seemed to be an increase of PD-L1 expression on TC2 cells within LFD-fed mice treated with anti-PD-1 antibodies compared to IgG controls, this was not significant, and no differences were observed in HFD-fed mice in either group (Figure 4-2K). Overall, only LFD-fed mice showed a reduction in GFP+ metastasis within the lungs, and obesity did not significantly alter immune cells recruitment to the lungs in response to anti-PD-1 therapy.

Macrophages from obese lung metastasis are immunosuppressive

To understand how macrophages from lung metastasis altered the function of CD8+ T cells, we cultured CD8+ T cells sorted from the spleen of LFD-fed mice with FACS-isolated macrophages from LFD and HFD-fed mice with TC2 ERα+ metastasis. Cells were cultured with CD3 alone (unstimulated) or stimulated with CD28 and CD3 antibodies for 24 hours. Using flow cytometry, we quantified changes in expression of TNF-α and IFN-γ in CD8+ T cells (Figure S4-3A). First, we confirmed similar numbers of macrophages in our co-culture conditions (Figure S4-3B). Macrophages from HFD-fed mice significantly decreased basal expression of TNF-α in unstimulated CD8+ T cells compared to macrophages from LFD-fed mice ($p=0.03$, Figure S4-3C). Stimulation did not further enhance expression of TNF-α or induce IFN-γ in CD8+ T cells when cultured with macrophages from metastatic lungs (Figure S4-3C, D). Overall, macrophages from HFD-fed mice had an immunosuppressive effect to limit cytokine expression in CD8+ T cells.

Given the immunosuppressive effects of macrophages isolated from metastatic lungs, we investigated the impact of anti-CSF-1R antibodies to inhibit macrophages in the lungs of mice with metastasis. We fed female mice LFD or HFD for 16 weeks, then orthotopically injected ERα+ GFP+ TC2 mammary cells into mammary fat pads. We then treated mice with IgG or anti-CSF-1R antibodies when tumors reach 0.7 cm in diameter (Figure 4-3A). Within primary tumors, we did not observe any impact on tumor growth in either LFD or HFD-fed mice treated with IgG or anti-CSF-1R antibodies (Figure 4-3B).

To assess functional changes in myeloid lineage cells within the metastatic environment, we isolated CD45+ immune cells from the lungs of LFD and HFD-fed mice bearing TC2 tumors. We then compared gene expression using the NanoString Myeloid Innate Immunity Panel. In IgG treated mice, there were a number of genes with differential expression (Figure S4-4A, Table S4-6). Expression of genes associated with chemokine signaling were significantly reduced in IgG treated HFD-fed mice (Figure S4-4B). Elevated expression of CXCL13 has been shown to promote the expansion and activation of CD8+ T cells in multiple different types of cancer (36) and diminished expression of *Cxcl13* in metastatic lungs from HFD-fed mice may reduce the ability to recruit CD8+ T cells.

We observed multiple genes differentially expressed in LFD-fed mice treated either with IgG or anti-CSF-1R antibodies (Figure 4-3C, Table S4-7). Treatment of LFD-fed mice with anti-CSF-1R antibodies led to increased expression of genes associated with lymphocyte activation (Figure 4-3D). *Nr4a1* expression was upregulated in CSF-1R treated mice, which is increased upon TCR stimulation and is involved in self-tolerance (37). Chemokine signaling was also downregulated in LFD-fed mice treated with anti-CSF-1R antibodies (Figure 4-3E). Interestingly, *Ccr2* expression was upregulated in immune cells from anti-CSF-1R treated mice (1.0-fold, p=0.005, Figure 4-3E). CCR2 expression is associated with pro-inflammatory macrophages (38). Although targeting CSF-1R depletes macrophages in the tumor microenvironment, it has been found to polarize other macrophages to M1 in colorectal cancer (39).

Fewer genes were differentially expressed in HFD-fed mice treated with control IgG compared to anti-CSF1R antibodies than observed in LFD-fed mice (Figure 4-3G,

Table S8). In HFD-fed mice treated with anti-CSF-1R antibodies, a number of cytokine signaling pathways were reduced (Figure 4-3G). Expression of *Kitl*, as known as stem cell factor, and its receptor *Kit* were both significantly downregulated (Figure 4-3G), and this cognate receptor and ligand have been associated with mobilizing immature myeloid cells to promote metastasis (40). Chemokine signaling was downregulated in immune cells from HFD-fed mice (Figure 4-3H), however, not as many chemokines were downregulated compared to LFD-fed mice treated with anti-CSF-1R antibodies (Figure 4-3E). Expression of *Cxcl12* was downregulated in HFD-fed mice treated with anti-CSF-1R antibodies (-3.8 fold, p=0.004, Figure 4-3H). Inhibition of CXCR4, the receptor for CXCL12, with a peptide antagonist led to reduced T regulatory cells (Tregs) and improved responses to anti-PD-1 therapy in a model of colon cancer (41).

In immune cells from mice treated with anti-CSF-1R antibodies, HFD-fed mice had a number of genes that were downregulated compared to LFD-fed mice (Figure S4-4D, Table S4-9). Genes associated with cytokine signaling were also downregulated in HFD-fed mice treated with anti-CSF-1R antibodies compared control anti-CSF-1R treated mice (Figure S4-4D). Interestingly, *Tnfrsf4* was upregulated in immune cells from HFD-fed mice treated with anti-CSF-1R antibodies (1.2-fold, p=0.03, Figure S4-4D). TNFRSF4, also known as OX40, is a costimulatory receptor that enhances CD8+ T cell responses to antigens (42).

Anti-CSF-1R treatment increases inflammation and reduces PD-L1+ myeloid cells in lung metastasis of HFD-fed mice

To investigate how anti-CSF-1R antibodies alter immune responses in the metastatic lungs of LFD and HFD-fed mice, we fed female mice LFD or HFD for 16

weeks. We orthotopically injected ERα+ GFP+ TC2 mammary tumor cells into the fat pads of LFD and HFD-fed mice, then surgically removed tumors when they reached 0.5 cm in diameter. Eight weeks after tumor removal, we treated mice with anti-CSF-1R or IgG control antibodies (Figure 4-4A).

Flow cytometry analysis of metastatic lungs showed an increase in total CD45+ immune cells in HFD-fed mice treated with ant-CSF-1R antibodies compared to all other treatment groups (Figure 4-4B). No differences were observed in CD4+ and CD8+ T cells in LFD or HFD-fed mice regardless of immunotherapy treatment (Figure 4-4C, D). No significant differences were observed in PD-1 expression on CD8+ T cells in LFD-fed mice (Figure 4-4E). In contrast, HFD-fed mice treated with anti-CSF-1R therapy had significantly increased amounts of PD-1+ CD8+ T cells compared to either LFD or HFD-fed mice treated with IgG control antibodies (Figure 4-4E).

To investigate how anti-CSF-1R antibodies impacted myeloid lineage cells, we quantified CD11b+ cells. No significant difference was observed in CD11b+ cells in LFD-fed mice in either treatment group (Figure 4-4F). However, HFD-fed mice treated with anti-CSF-1R antibodies had significantly increased myeloid cells compared to both LFD and HFD-fed mice treated with IgG (Figure 4-4F). CD115/CSF-1R+ macrophages were reduced in both LFD and HFD-fed mice treated with anti-CSF-1R antibodies, however, these differences did not reach significance (Figure 4-4G). We then sought to quantify PD-L1+ myeloid cells to see if immunosuppressive innate cells were decreased with anti-CSF-1R antibodies. No significant differences were observed in LFD-fed mice treated with anti-CSF-1R antibodies (Figure 4-4H). In HFD-fed mice, anti-CSF-1R

treatment significantly decreased PD-L1 CD11b+ myeloid cells compared to IgG treatment (p=0.03, Figure 4H).

To quantify metastasis, we measured GFP+ cells in the lungs of LFD and HFD-fed mice. No significant differences in GFP+ cells were observed in LFD-fed mice (Figure 4-4I). In contrast, HFD-fed mice treated with anti-CSF-1R antibodies had significantly less GFP+ metastatic cells than both LFD-fed groups, although HFD-fed mice treated with anti-CSF-1R antibodies did not have significantly decreased GFP+ metastatic cells compared to HFD-fed controls (Figure 4-4I). We did not observe any significant differences in PD-L1+ GFP+ cells in LFD-fed groups (Figure 4-4J). However, PD-L1+GFP+ cells were significantly increased in HFD-fed mice treated with anti-CSF-1R antibodies compared to LFD and HFD-fed mice treated with IgG controls (Figure 4-4J). Together these data suggest that depletion of CSF-1R+ myeloid cells in HFD-fed mice promoted a more robust immune response to diminish metastasis in the lungs.

Dual anti-CSF-1R and anti-PD-1 immunotherapy is more robust in metastatic lungs from obese mice

We hypothesized that HFD-fed mice might benefit from a combination of anti-PD-1 inhibitors in addition to macrophage depletion via anti-CSF-1R antibodies. To test this hypothesis, we injected TC2 tumor cells into the mammary glands of LFD and HFD-fed mice, and treated mice with metastases with anti-PD-1 and anti-CSF-1R (dual) or IgG control antibodies 8 weeks after tumor removal (Figure 4-5A). Using flow cytometry, we observed that LFD-fed mice did not have significant differences in CD45+ cells,

however, HFD-fed mice treated with both antibodies had significantly higher levels of total CD45+ immune cells compared to all other treatment groups (Figure 4-5B). No differences were observed in CD4+ or CD8+ T cells in any treatment group (Figure 4-5C, D). Although CD8+ T cell numbers were not different, PD-1 expression was significantly increased on CD8+ T cells in both LFD and HFD mice that received dual treatment compared to IgG controls (Figure 4-5E).

We then quantified myeloid lineage cells. No differences were detected in total CD11b+ cells in any of the treatment groups (Figure 4-5F). IgG-treated LFD-fed mice had significantly decreased CD115+ macrophages compared to LFD-fed mice that received dual treatment ($p=0.03$, Figure 4-5G). Similarly, IgG-treated HFD-fed mice showed a significant decrease in CD115+ macrophages compared to dual-treated HFD-fed mice ($p=0.04$, Figure 4-5G). These data show that the treatment with the anti-CSF-1R antibodies reduced macrophages in metastatic lungs of both groups. PD-L1 expression was variable across all groups, and no significant differences in CD11b+PD-L1+ cells were detected among any of the treatment groups (Figure 4-5H).

To identify changes in metastasis, we quantified GFP+ tumor cells. No significant difference was observed between IgG-treated LFD-fed mice and dual antibody treated LFD-fed mice (Figure 4-5I). However, dual antibody-treated LFD-fed mice had significantly higher GFP+ tumor cells than IgG-treated HFD-fed mice ($p=0.03$) and dual antibody treated HFD-fed mice ($p=0.003$, Figure 4-5I). No differences were observed between IgG-treated HFD-fed mice and dual antibody treated HFD-fed mice (Figure 4-5I). GFP+ PD-L1+ tumor cells were not significantly different between IgG-treated LFD-fed mice and dual antibody-treated LFD-fed mice (Figure 4-5J). However, both IgG-

treated LFD and HFD-fed mice had significantly less GFP+ PD-L1+ cells compared to dual antibody-treated HFD-fed mice (Figure 4-5J). Overall, HFD-fed mice had a more robust response to dual anti-PD-1 and anti-CSF-1R therapy through increased levels of checkpoint markers, immune cells, and reduced GFP+ metastasis.

Discussion:

The use of ICB therapies targeting the PD-1/PD-L1 axis have had low rates of efficacy ERα+ breast cancer (12). However, combining ICB therapies with other immunotherapies or other therapeutics have potential to improve responses in these patients (43). While immune responses in the primary tumors have been examined, less is known about how ICB impacts the metastatic microenvironment (44). We explored anti-CSF-1R antibodies to deplete macrophages with the goal of increasing infiltrating lymphocytes within metastasis and response to ICB therapy. Here we demonstrated that anti-PD-1 treatment alone reduced ERα+ breast cancer metastasis in LFD-fed mice, but not obese mice, and increased expression of genes associated with cytotoxicity in immune cells. Anti-PD-1 therapy increased CD8+ T cells in metastatic lungs of HFD-fed mice, but these T cells had gene expression associated with exhaustion. In contrast to LFD-fed mice, anti-CSF-1R antibodies increased inflammation, reduced PD-L1+ cells, and increased PD-1 expression in HFD-fed mice, evident of a more robust increase in immune activity. These results suggest that the metastatic microenvironment in HFD-fed mice may be more favorable after macrophage depletion. In fact, dual anti-CSF-1R and anti-PD-1 antibodies led to a more robust reduction of metastasis in HFD-fed mice. This study provides evidence that ERα+

breast cancer lung metastasis can respond to dual macrophage depletion and anti-PD-1 inhibitors under conditions of obesity.

In response to anti-PD-1 antibodies, we observed a significant decrease in GFP+ metastatic cells in LFD-fed mice. Analysis of gene expression of CD45+ cells from metastasis in LFD-fed mice treated with anti-PD-1 or IgG antibodies revealed an increase in genes associated with cytotoxicity, including *Gzmb*, and a decrease in genes associated with myeloid cell immune evasion such as *Arg1*. Interestingly, anti-PD-1 antibody treated LFD-fed mice did not show significant increases in CD8+ PD-1+ T cells, which was associated with ICB responses in a small clinical trial of patients with highly treated metastatic ERα+ breast cancer (45). In contrast, the CD45+ cells from the metastatic lungs of anti-PD-1 antibody-treated HFD-fed mice showed upregulation of genes associated with terminal exhaustion, including *Lag-3* and *Tigit*.(46). Further, expression of *Tnfrsf14*, a member of the TNFα superfamily, was downregulated in response to anti-PD-1 antibodies. Reduced expression of *Tnfrsf14* has been associated with poorer prognosis in multiple types of cancer when downregulated (47). Overall, these results point to a reduced response to anti-PD-1 antibodies as a single agent in lungs with ERα+ metastases under conditions of obesity.

Compared with primary breast cancers, breast cancer metastases have greater recruitment of macrophages.(48, 49). Macrophages in the lungs have been shown to suppress T cell responses (50), which may contribute to the increased metastases observed in this environment. Obesity also enhances myeloid lineage cells in the bone marrow, resulting in expansion of myeloid cells in metastatic sites (17, 23). Co-culture of macrophages isolated from the metastatic environment of the lungs with CD8+ T cells

from the spleens of non-tumor bearing mice showed that macrophages from HFD-fed mice reduced basal levels of TNFα production in CD8+ T cells, and stimulation of the CD8+ T cells did not enhance TNFα expression levels. These results demonstrate significant immunosuppression by macrophages from metastases in mice fed HFD. In comparison of gene expression from immune cells from IgG controls, HFD-fed mice had decreased expression of *Cxcl13* compared to LFD-fed mice. Since CXCL13 has been shown to be involved in T cell activation, decreased CXCL13 play a role in the observed reduction of T cell function when exposed to macrophages isolated from metastasis from HFD-fed mice (36). Additional studies are necessary to identify differences in macrophages from obese mice that promote immunosuppression in CD8+ T cells.

Anti-CSF-1R treatment increased anti-metastasis inflammation. Gene expression of CD45+ cells from metastasis of anti-CSF-1R antibody treated LFD-fed mice increased lymphocyte activation and decreased chemokine signaling compared to LFD-fed IgG controls. Increased lymphocyte activation matches data that supports CSF-1R+ cells diminish lymphocyte mediated immunity in cancer (51). However, only HFD-fed mice revealed differences in immune cell recruitment, including an increase in CD45+ and CD11b+ cells. Downregulation of cytokines related to angiogenesis and anti-inflammation in HFD-fed mice may aid in more immune recruitment after anti-CSF-1R treatment. For example, inhibition of *Sptbn1* expression in hepatocellular carcinoma led to upregulation of expression of inflammatory cytokines (52). This gene was found to be downregulated in HFD-fed mice treated with anti-CSF-1R antibodies and may partially explain increased immune recruitment to the lungs of these mice.

Treatment with anti-CSF-1R antibodies may improve anti-PD-1 responses in lung metastasis of obese mice. Other studies have documented that macrophages can lead to anti-PD-1 resistance (53). We observed reduced TNF-α expression in CD8+ T cells when incubated with macrophages from metastatic lungs of HFD-fed mice, showing that the macrophages from obese mice are more immunosuppressive. Depletion of CSF-1R+ macrophages also decreased PD-L1+ myeloid cells. However, both M1, inflammatory macrophages, and M2, anti-inflammatory macrophages, can express PD-L1 (54), and it is unclear whether M1 or M2 macrophages are being reduced in HFD-fed mice. PD-L1 high/+ macrophages have also been shown to be T cell activating compared to PD-L1 low/- macrophages which were immunosuppressive. In the same study, higher tumor associated macrophage PD-L1+/PD-L1- ratio was associated with better clinical outcomes in a ERα-/ERα+ mixed cohort of breast cancer patients (55). These studies are recent and further investigation is needed into the heterogeneity of PD-L1+ macrophages. Anti-CSF-1R therapies are also thought to reprogram macrophages to an M1 phenotype (39), but more studies are needed to confirm this in obesity. In obese mice PD-1+ CD8+ T cells were increased with anti-CSF-1R treatment. An increase in PD-1+ CD8+ T cells in response to anti-CSF-1R inhibitors has been seen in models of other types of cancer (56). PD-L1+ tumor cells were increased with anti-CSF-1R treatment in HFD-fed mice, which could coincide with an increase of inflammation, particularly M1 macrophages, or a resistance to the clearing of PD-L1+ tumor cells (57). Thus, macrophages within ERα+ breast cancer metastasis are different in HFD-fed mice than in lean controls and removing the CSF-1R+ macrophage population reduces metastasis under obese conditions.

Dual anti-CSF-1R and anti-PD-1 treatment reduced metastasis in HFD-fed mice. Flow cytometry data revealed an increase in total immune infiltration only in HFD-fed mice. HFD-fed mice that received dual treatment diminished metastasis that was significantly lower than LFD-fed dual treated mice. However, dual treatment was not curative in either diet after 2-weeks, and a significant level of PD-L1+ metastasis remained in HFD-fed dual treated mice compared to IgG treated HFD-fed mice. Additional investigation into duration and timing of anti-CSF-1R and anti-PD-1 inhibitors is needed to identify if this combination could be curative. Treating PD-L1+ metastasis could be done with the addition of anti-PD-L1 treatment. Overall, dual treatment was more efficacious in HFD-fed mice as it reduced lung metastasis.

Further studies are needed to identify what changes in the lung prior to treatment may be biomarkers for response to anti-CSF1R and anti-PD1 therapies. Patients with advanced metastatic disease may receive immunotherapy treat patients after resistance to standard of care. Therefore, it is important to understand how standard of care may influence the lung environment prior to immunotherapy to better predict patient outcomes. The standard of care for ERα+ breast cancer are estrogen/ER inhibitors coupled with cyclin-dependent kinases (CDK) 4/6 inhibitors after primary tumor removal (58, 59). In our study, we did not treat mice with standard of care before investigating the effects of CSF-1R+ macrophage/monocyte depletion or anti-PD-1 inhibitors. Estrogen signaling has been shown to influence macrophages and immune responses (60), and treatment of mice with anti-estrogen therapies may alter the function of macrophages and CD8+ T cells. Further studies are needed on how obesity affects

immunotherapy response when coupled with standard of care treatment to enhance the ability to translate this work for patients with obesity.

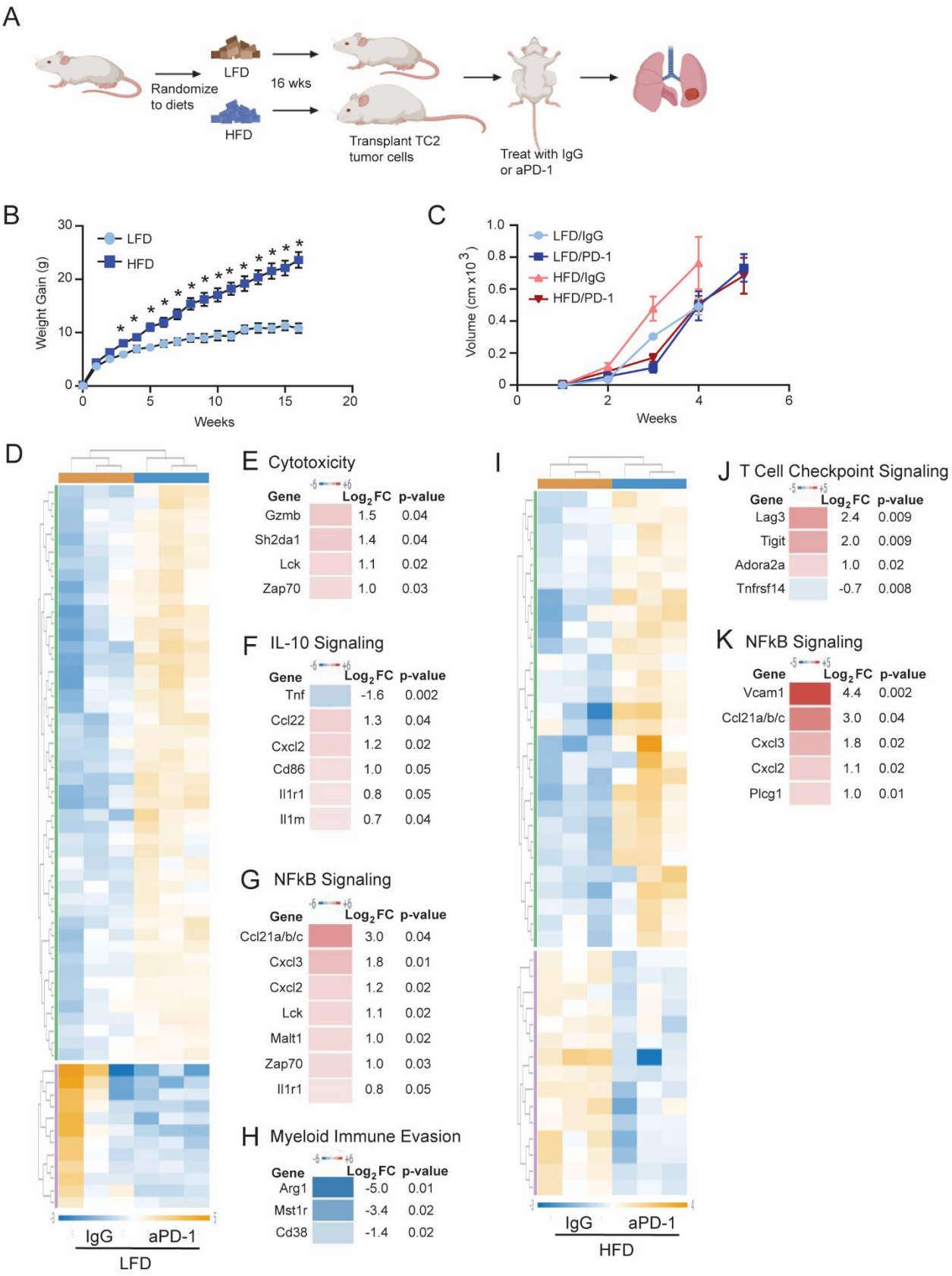
A
Randomize to diets
LFD
HFD
16 wks
Transplant TC2 tumor cells
Treat with IgG or aPD-1
B
LFD
HFD
Weight Gain (g)
Weeks
C
LFD/IgG
LFD/PD-1
HFD/IgG
HFD/PD-1
Volume (cm x10^3)
Weeks
D
IgG
aPD-1
LFD
E Cytotoxicity
Gene Log2FC p-value
Gzmb 1.5 0.04
Sh2da1 1.4 0.04
Lck 1.1 0.02
Zap70 1.0 0.03
F IL-10 Signaling
Gene Log2FC p-value
Tnf -1.6 0.002
Ccl22 1.3 0.04
Cxcl2 1.2 0.02
Cd86 1.0 0.05
Il1r1 0.8 0.05
Il1m 0.7 0.04
G NFkB Signaling
Gene Log2FC p-value
Ccl21a/b/c 3.0 0.04
Cxcl3 1.8 0.01
Cxcl2 1.2 0.02
Lck 1.1 0.02
Malt1 1.0 0.02
Zap70 1.0 0.03
Il1r1 0.8 0.05
H Myeloid Immune Evasion
Gene Log2FC p-value
Arg1 -5.0 0.01
Mst1r -3.4 0.02
Cd38 -1.4 0.02
I
IgG
aPD-1
HFD
J T Cell Checkpoint Signaling
Gene Log2FC p-value
Lag3 2.4 0.009
Tigit 2.0 0.009
Adora2a 1.0 0.02
Tnfrsf14 -0.7 0.008
K NFkB Signaling
Gene Log2FC p-value
Vcam1 4.4 0.002
Ccl21a/b/c 3.0 0.04
Cxcl3 1.8 0.02
Cxcl2 1.1 0.02
Plcg1 1.0 0.01

Figure 4-1: Anti-PD1 treatment increased cytotoxicity in LFD-fed mice and T cell exhaustion in HFD-fed mice (**A**) Experimental design for treating mice with ER+ mammary tumors and metastases with anti-PD-1 antibodies. Mice were fed LFD or HFD, then TC2 ER+ mammary tumor cells were transplanted into mammary fat pads. Once tumors reached 0.7 cm in diameter, LFD and HFD-fed mice were randomized to receive IgG or anti-PD-1 antibodies. (**B**) Weight gain of LFD and HFD-fed mice (n=22, 30 mice/group). (**C**) Tumor growth of mice treated with IgG or anti-PD-1 antibodies (n=6 tumors/group). (**D**) Heatmap representing all genes that were significantly different in CD45+ cells from metastatic lungs of LFD-fed mice treated with IgG or anti-PD1 antibodies (n=3/group). Genes associated with signatures of Cytotoxicity (**E**), IL-10 Signaling (**F**), NF-kB Signaling (**G**), and Myeloid Immune Evasion (**H**). (**I**) Heatmap representing all genes that were significantly different between CD45+ cells sorted from metastatic lungs from HFD-fed mice treated with either IgG or anti-PD-1 antibodies (n=3/group). Genes associated with signatures of T Cell Checkpoint Signaling (**J**), and NF-kB Signaling (**K**).

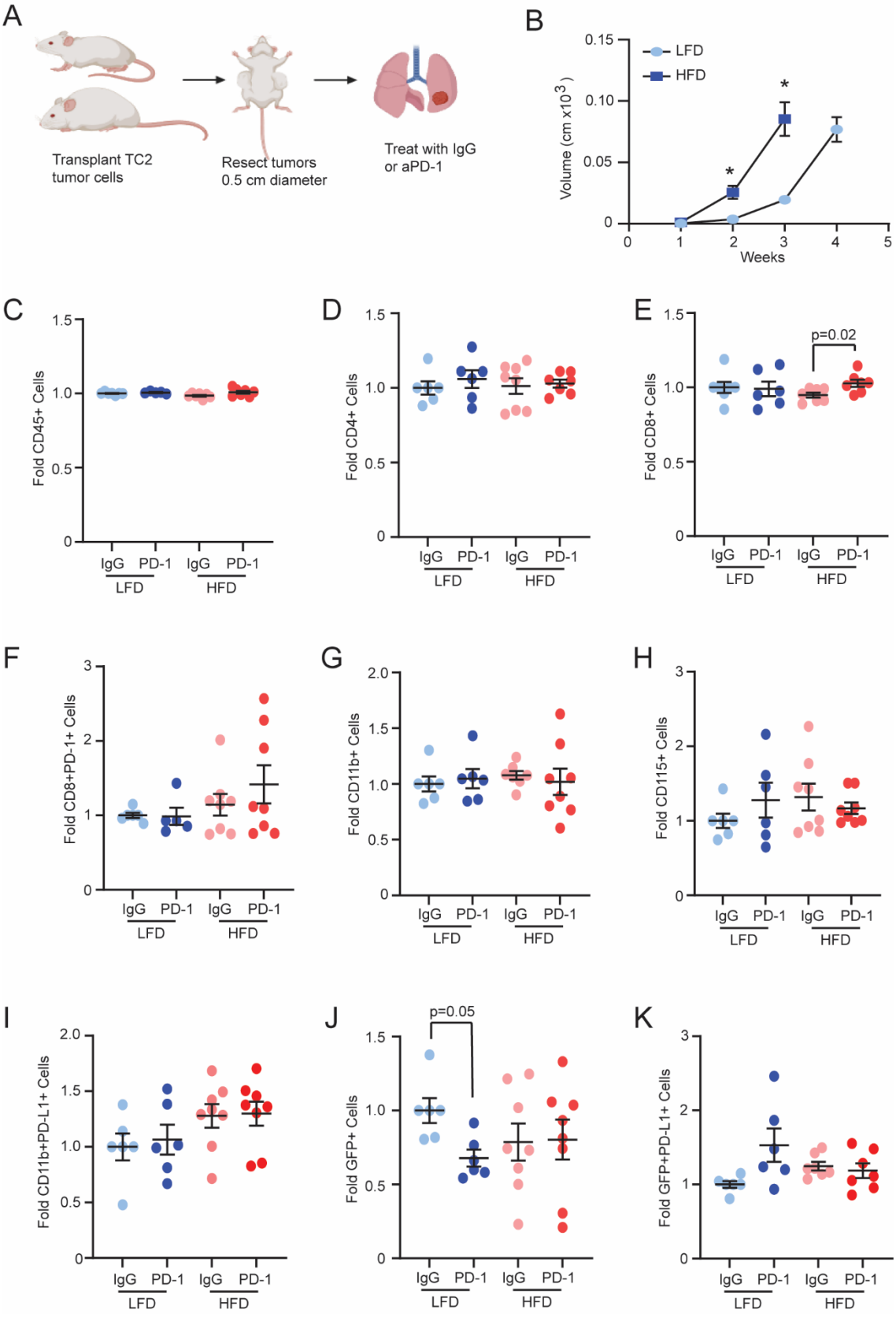
A
Transplant TC2 tumor cells
Resect tumors 0.5 cm diameter
Treat with IgG or aPD-1
B
LFD
HFD
Volume (cm x10^3)
Weeks
C
Fold CD45+ Cells
D
Fold CD4+ Cells
E
Fold CD8+ Cells
p=0.02
F
Fold CD8+PD-1+ Cells
G
Fold CD11b+ Cells
H
Fold CD115+ Cells
I
Fold CD11b+PD-L1+ Cells
J
Fold GFP+ Cells
p=0.05
K
Fold GFP+PD-L1+ Cells
IgG PD-1 IgG PD-1
LFD HFD

Figure 4-2: Anti-PD1 decreases metastasis in LFD-fed mice (**A**) Experimental design for treating mice with ER+ metastasis with anti-PD-1 antibodies. Mice were fed LFD or HFD, then TC2 ER+ mammary tumor cells were transplanted into mammary fat pads. Once tumors reached 0.5 cm in diameter, tumors were resected. After 8 weeks, LFD and HFD-fed mice were randomized to receive IgG or anti-PD-1 antibodies. (**B**) Tumor growth curves of TC2 tumors prior to resection. Flow cytometry analysis of CD45+ (**C**), CD4+ (**D**), CD8+ (**E**), CD8+ PD1+ (**F**), CD11b+ (**G**), CD115+ (**H**), CD11b PDL1+ (**I**), GFP+ (**J**), GFP+ PDL1+ (**K**) cells from metastatic lungs of LFD-fed and HFD-fed mice treated with IgG or anti-PD1 antibodies. Statistical significance was determined by 2-way ANOVA with Tukey's multiple comparison post-test, and error bars represent s.e.m.

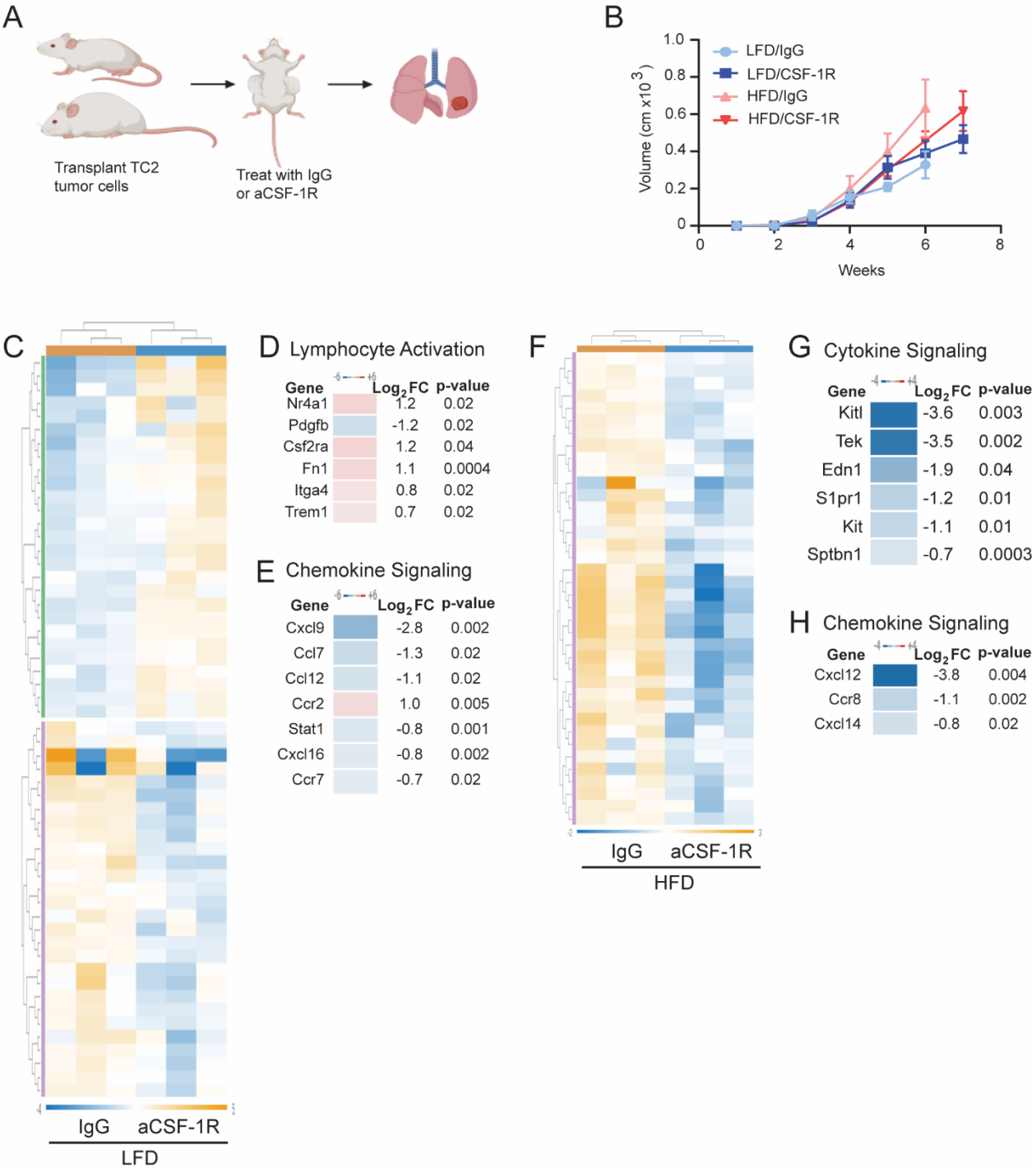

Figure 4-3: Anti-CSF1R primes metastasis for anti-PD1 treatment (**A**) Experimental design for treating mice with ER+ mammary tumors and metastasis with anti-CSF-1R antibodies. Mice were fed LFD or HFD, then TC2 mammary tumor cells were transplanted into mammary fat pads. Once tumors reached 0.7 cm in diameter, LFD and HFD-fed mice were randomized to receive IgG or anti-CSF-1R antibodies. (**B**) Tumor growth of LFD and HFD-fed mice treated with either IgG control or anti-CSF-1R

antibodies (6 tumors/group). (**C**) Heatmap representing all genes that were significantly different in CD45+ cells sorted from metastatic lungs from LFD-fed mice treated with IgG or anti-CSF-1R antibodies (n=3/group). Genes associated with signatures of Lymphocyte Activation (**D**), Chemokine Signaling (**E**). (**F**) Heatmap representing all genes that were significantly different in CD45+ cells sorted from metastatic lungs from HFD-fed mice treated with either IgG or anti-CSF-1R antibodies (n=3/group). Genes associated with signatures of Cytokine Signaling (**G**) and Chemokine Signaling (**H**).

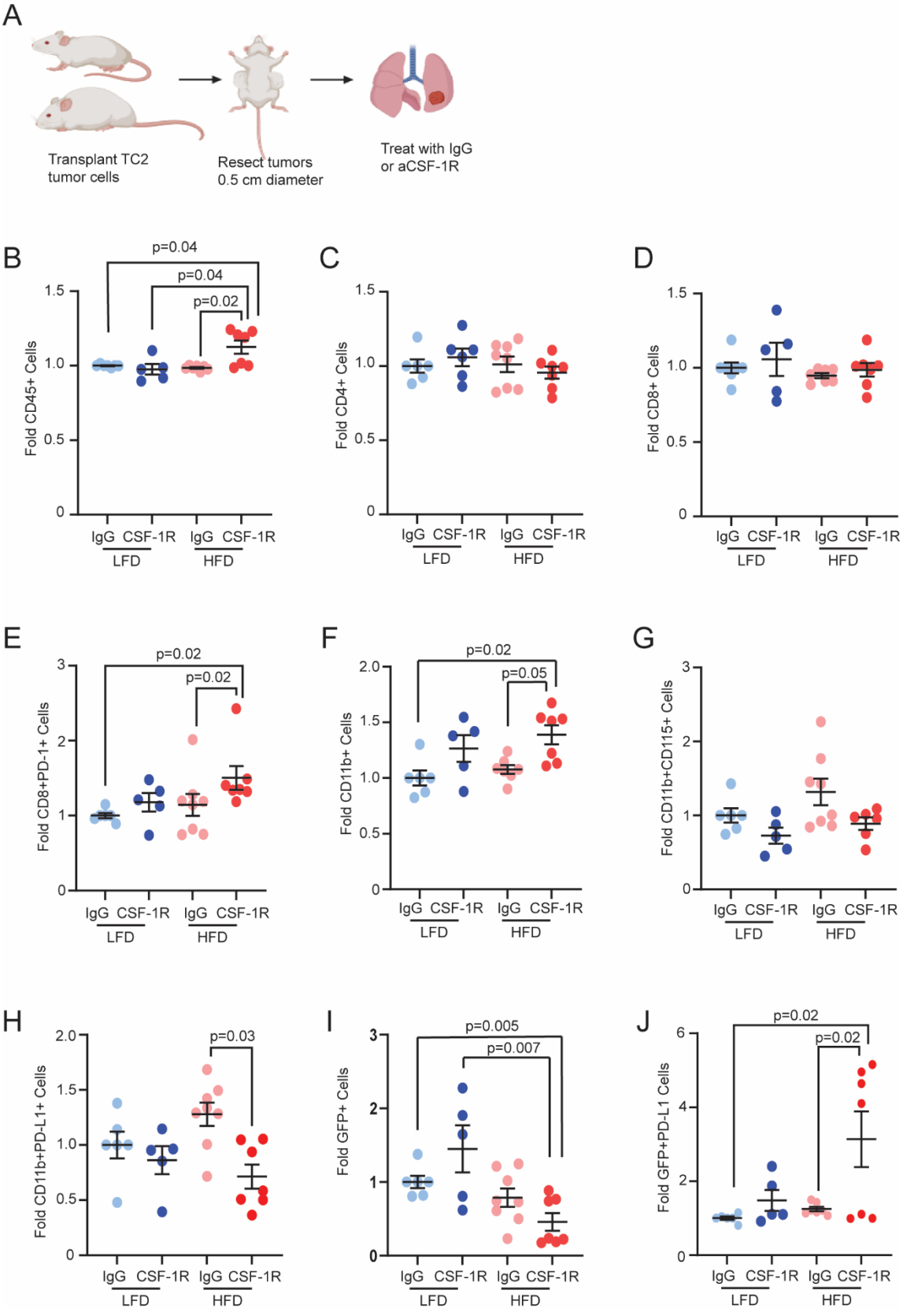
A
Transplant TC2 tumor cells
Resect tumors 0.5 cm diameter
Treat with IgG or aCSF-1R
B
Fold CD45+ Cells
p=0.04
p=0.04
p=0.02
C
Fold CD4+ Cells
D
Fold CD8+ Cells
E
Fold CD8+PD-1+ Cells
p=0.02
p=0.02
F
Fold CD11b+ Cells
p=0.02
p=0.05
G
Fold CD11b+CD115+ Cells
H
Fold CD11b+PD-L1+ Cells
p=0.03
I
Fold GFP+ Cells
p=0.005
p=0.007
J
Fold GFP+PD-L1 Cells
p=0.02
p=0.02
IgG CSF-1R IgG CSF-1R
LFD HFD

Figure 4-4: Anti-CSF1R increases inflammation in HFD-fed metastasis (**A**) Experimental design for treating mice ER+ metastasis with anti-CSF-1R antibodies. Mice were fed LFD or HFD, then TC2 ER+ tumor cells were transplanted into mammary fat pads. Once tumors reached a diameter of 0.5 cm, tumors were resected. LFD and HFD-fed mice were randomized to receive IgG or anti-CSF-1R antibodies. Flow cytometry analysis of CD45+ (**B**), CD4+ (**C**), CD8+ (**D**), CD8+ PD1+ (**E**), CD11b+ (**F**), CD115+ (**G**), CD11b PDL1+ (**H**), GFP+ (**I**), GFP+ PDL1+ (**J**) cells from metastatic lungs of LFD-fed and HFD-fed mice treated with IgG or anti-CSF-1R antibodies. Statistical significance was determined by 2-way ANOVA with Tukey's multiple comparison post-test, and error bars represent s.e.m.

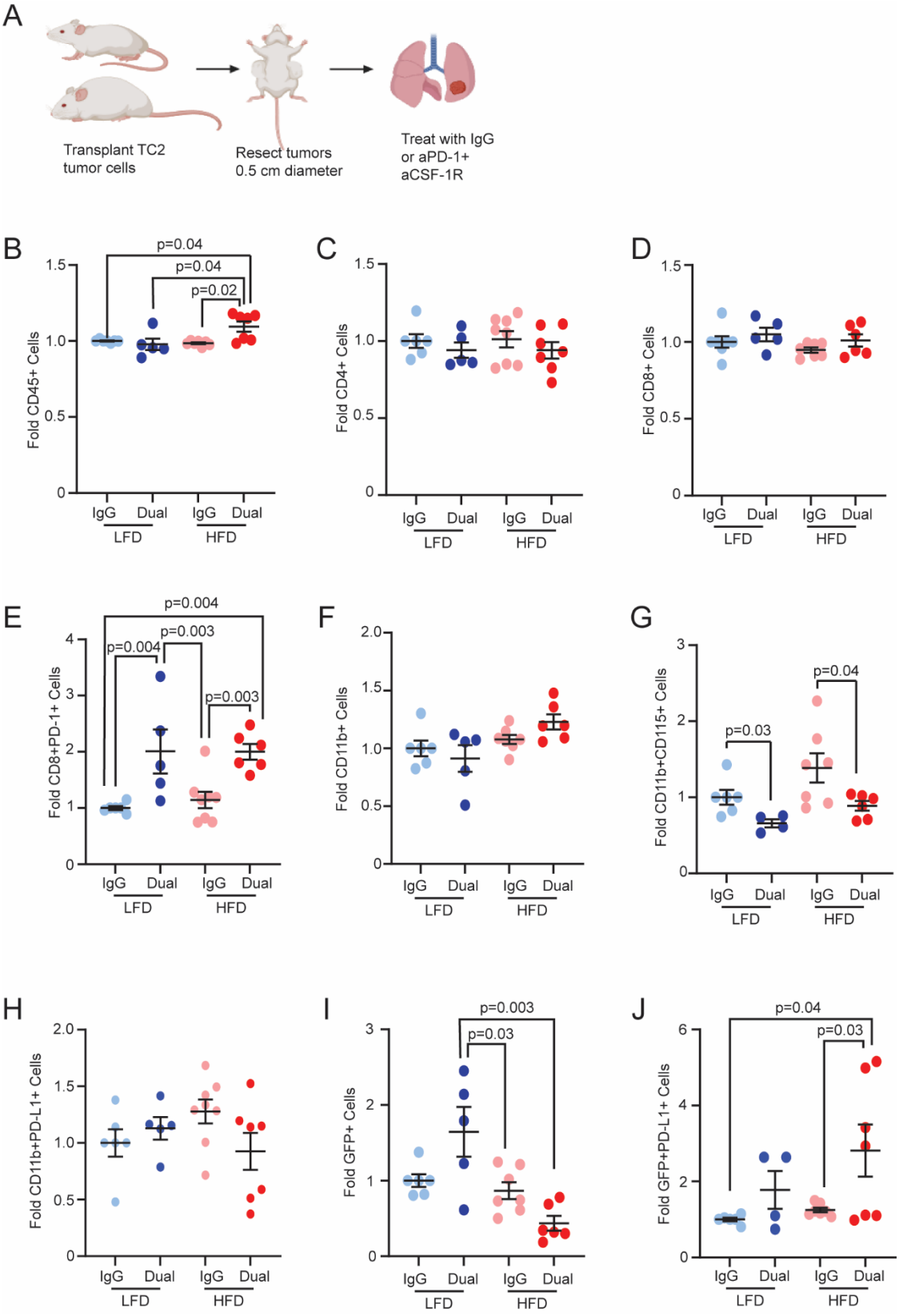
A
Transplant TC2 tumor cells
Resect tumors 0.5 cm diameter
Treat with IgG or aPD-1+ aCSF-1R
B
Fold CD45+ Cells
p=0.04
p=0.04
p=0.02
C
Fold CD4+ Cells
D
Fold CD8+ Cells
E
Fold CD8+PD-1+ Cells
p=0.004
p=0.003
p=0.004
p=0.003
F
Fold CD11b+ Cells
G
Fold CD11b+CD115+ Cells
p=0.04
p=0.03
H
Fold CD11b+PD-L1+ Cells
I
Fold GFP+ Cells
p=0.003
p=0.03
J
Fold GFP+PD-L1+ Cells
p=0.04
p=0.03
IgG
Dual
LFD
HFD

Figure 4-5: Dual anti CSF1R and anti-PD1 treatment is more efficacious in HFD-fed mice (**A**) Experimental design for treating mice with ER+ metastasis with anti-PD-1 and anti-CSF-1R antibodies. Mice were fed LFD or HFD, then TC2 mammary tumor cells were transplanted into mammary fat pads. Once tumors reached 0.5 cm in diameter, tumors were resected. LFD and HFD-fed mice were randomized to receive either IgG or anti-PD-1 and anti-CSF-1R antibodies (Dual). Flow cytometry analysis of CD45+ (**B**), CD4+ (**C**), CD8+ cells (**D**), CD8+ PD1+ (**E**), CD11b+ (**F**), CD115+ (**G**), CD11b PDL1+ (**H**), GFP+ (**I**), GFP+ PDL1+ (**J**) cells from metastatic lungs from LFD and HFD-fed mice treated with IgG or dual antibodies. Statistical significance was determined by 2-way ANOVA with Tukey's multiple comparison post-test, and error bars represent s.e.m.

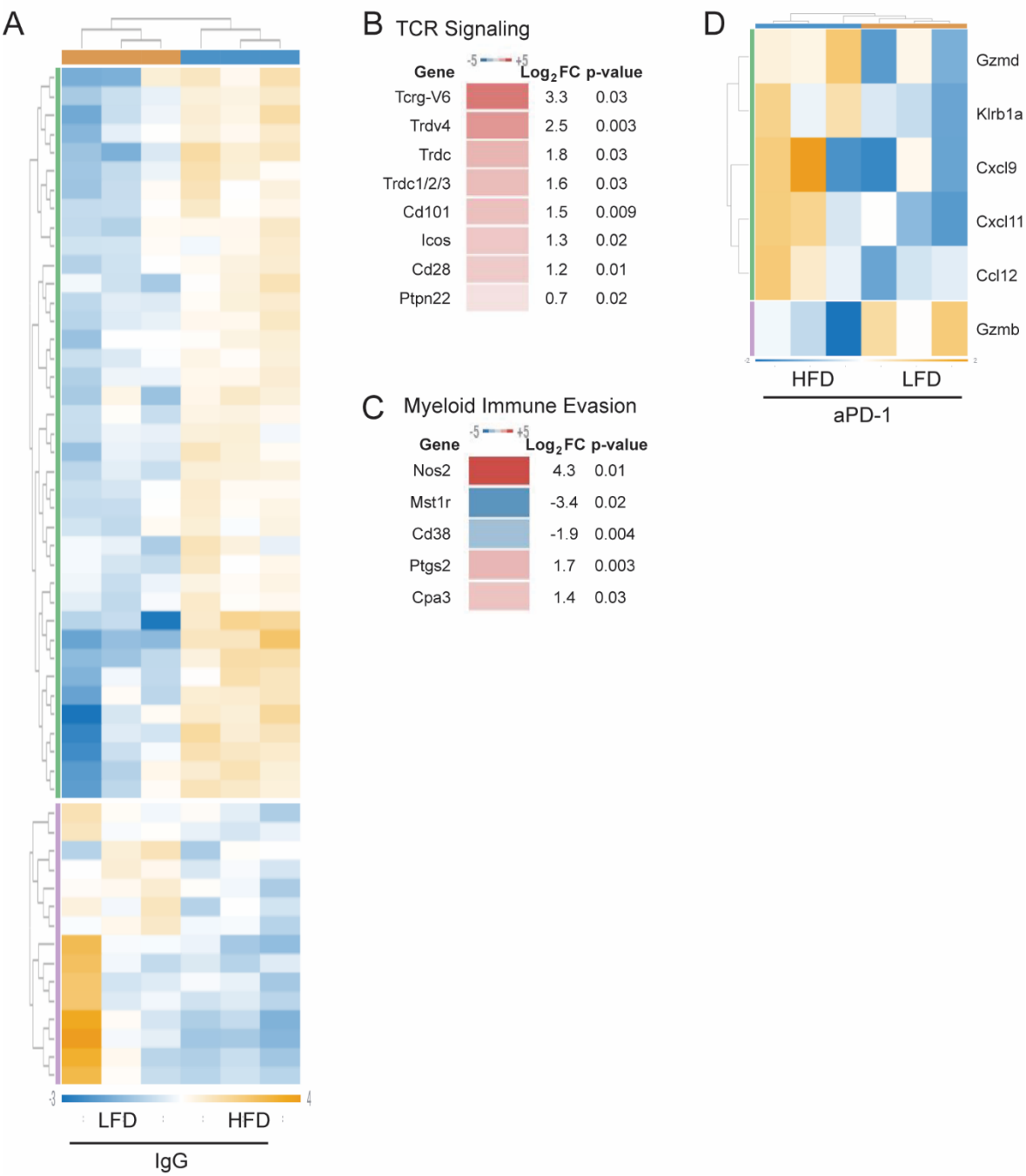

Supplementary Figure 4-1 Obese metastasis has increased TCR signaling and myeloid Immune evasion: (**A**) Heatmap representing all genes that were significantly different in CD45+ cells sorted from ER+ metastatic lungs from LFD or HFD-fed mice treated with IgG antibodies (n=3/group). Genes associated with signatures of TCR Signaling (**B**) and Myeloid Immune Evasion (**C**). (**D**) Heatmap representing all genes

that were significantly different in CD45+ cells sorted from ER+ metastatic lungs from LFD or HFD-fed mice treated with anti-PD-1 antibodies (n=3/group).

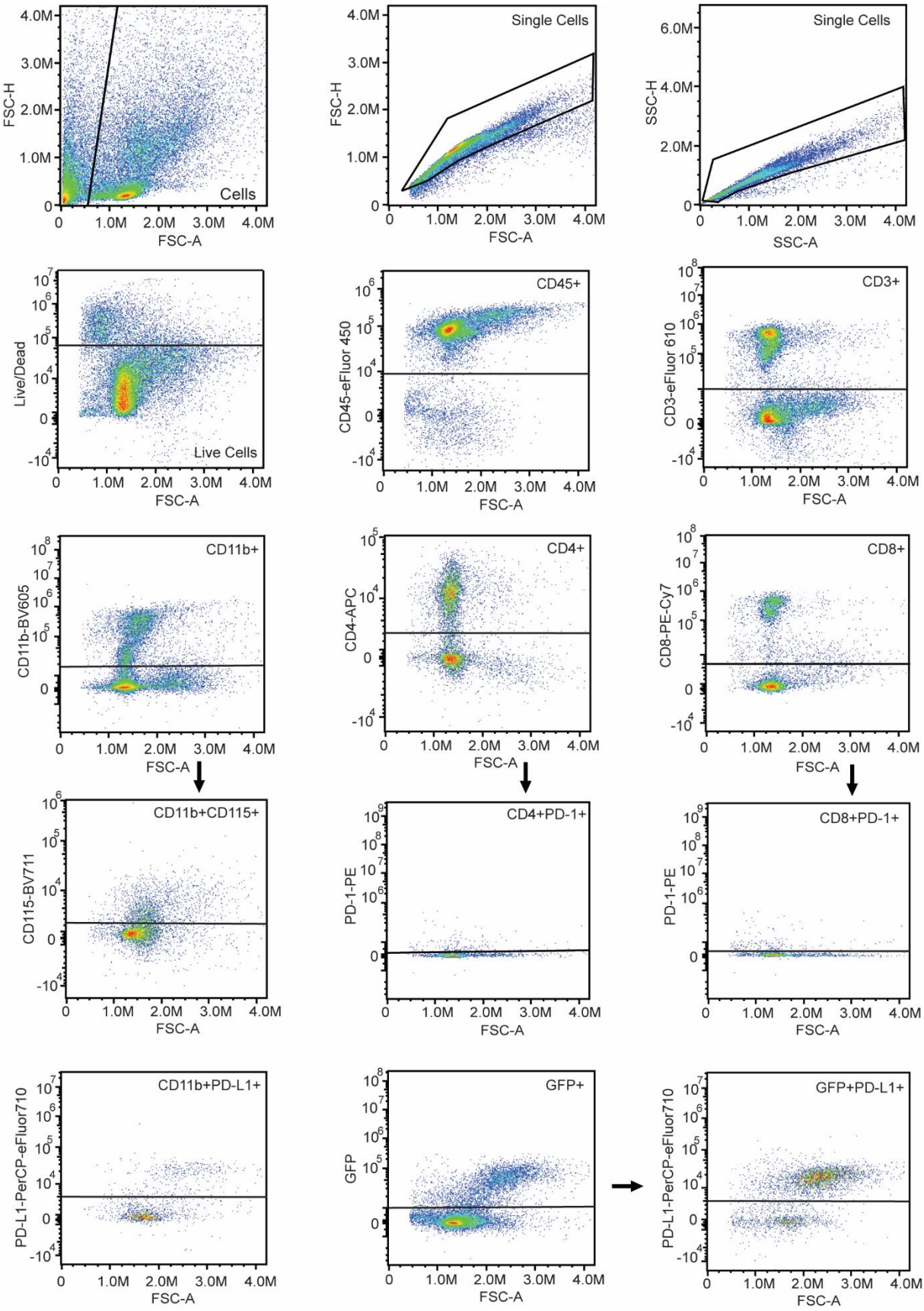
Cells
FSC-H
FSC-A
Single Cells
SSC-H
SSC-A
Live Cells
Live/Dead
CD45+
CD45-eFluor 450
CD3+
CD3-eFluor 610
CD11b+
CD11b-BV605
CD4+
CD4-APC
CD8+
CD8-PE-Cy7
CD11b+CD115+
CD115-BV711
CD4+PD-1+
CD8+PD-1+
PD-1-PE
CD11b+PD-L1+
PD-L1-PerCP-eFluor710
GFP+
GFP
GFP+PD-L1+

Supplementary Figure 4-2: Gating strategy for flow cytometry panel for metastatic lungs. Cells were gated to remove debris (cells), single cells, and live cells. Immune cells were gated for CD45, then CD3. CD3+ cells were gated for CD4 and CD8, then CD4 and CD8+ cells were gated for PD-1. CD3- cells were gated for CD11b. CD11b+ cells were gated for CD115 and PD-L1. Live cells were gated for GFP, and GFP cells were gated for PD-1L1.

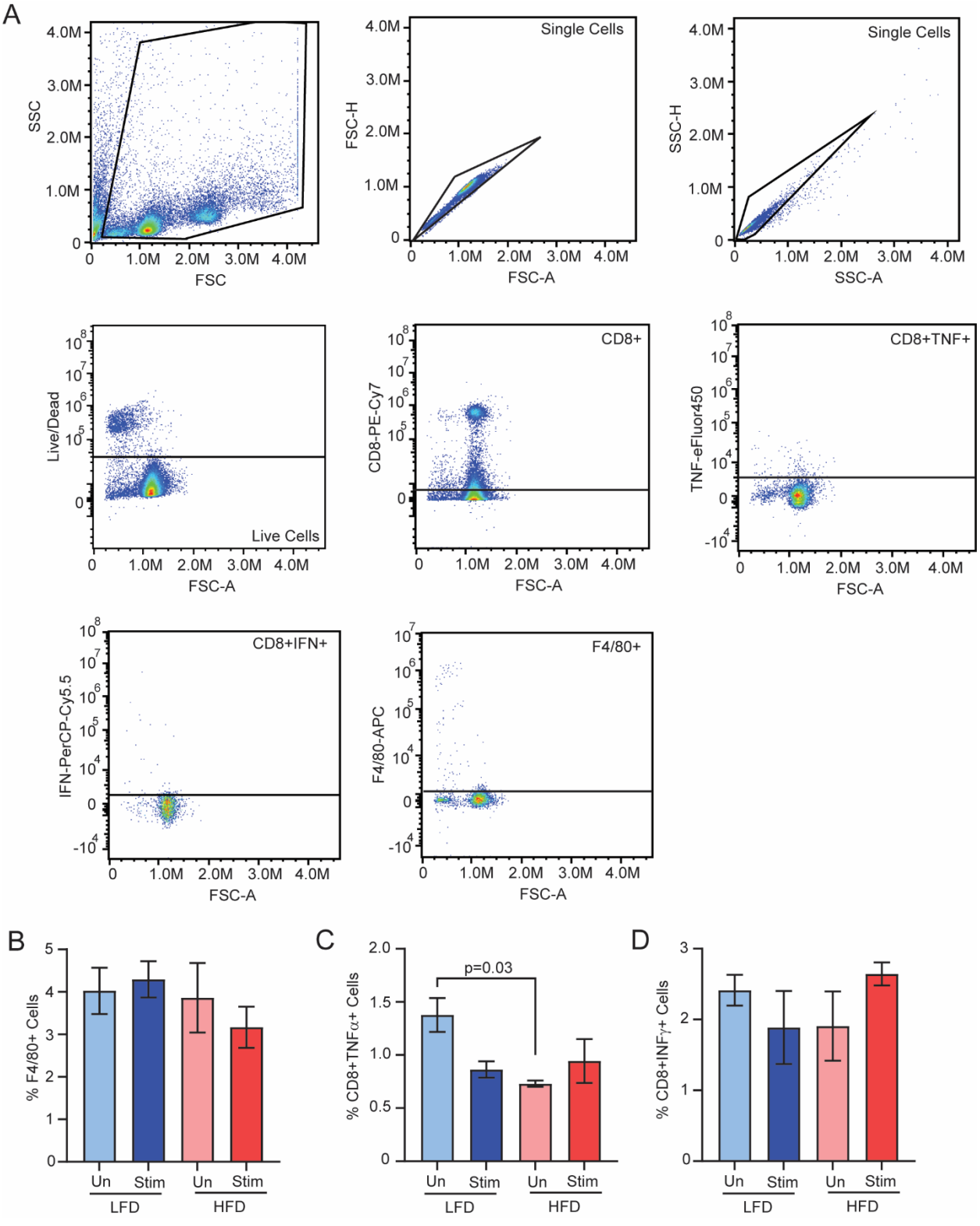
A
SSC
FSC
Single Cells
FSC-H
FSC-A
Single Cells
SSC-H
SSC-A
Live/Dead
Live Cells
FSC-A
CD8+
CD8-PE-Cy7
FSC-A
CD8+TNF+
TNF-eFluor450
FSC-A
CD8+IFN+
IFN-PerCP-Cy5.5
FSC-A
F4/80+
F4/80-APC
FSC-A
B
% F4/80+ Cells
Un
Stim
Un
Stim
LFD
HFD
C
% CD8+TNFα+ Cells
p=0.03
Un
Stim
Un
Stim
LFD
HFD
D
% CD8+INFγ+ Cells
Un
Stim
Un
Stim
LFD
HFD

Supplementary Figure 4-3: F4/80+ macrophages from metastatic lungs of obese mice decreased TNFα production in CD8+ T cells (**A**) Gating strategy for co-culture experiments between F4/80+ macrophages isolated from metastatic lungs and splenic CD8+ T cells. Debris was removed (cells), then gated for single cells and live cells. Gates were set for CD8 cells, then TNFα and IFNγ. Live cells were also gated for F4/80 macrophages. F4/80+ macrophages from metastatic lungs of LFD and HFD-fed mice were co-cultured with CD8+ T cells isolated from the spleen of LFD-fed mice. Cells were unstimulated (Un) or stimulated (Stim) with CD28+ antibodies. Quantification of CD8+TNFα+ (**B**), CD8+IFNγ (**C**), and total F4/80+ macrophages (**D**). Statistical significance was determined by 2-way ANOVA with Tukey's multiple comparison post-test, and error bars represent s.e.m.

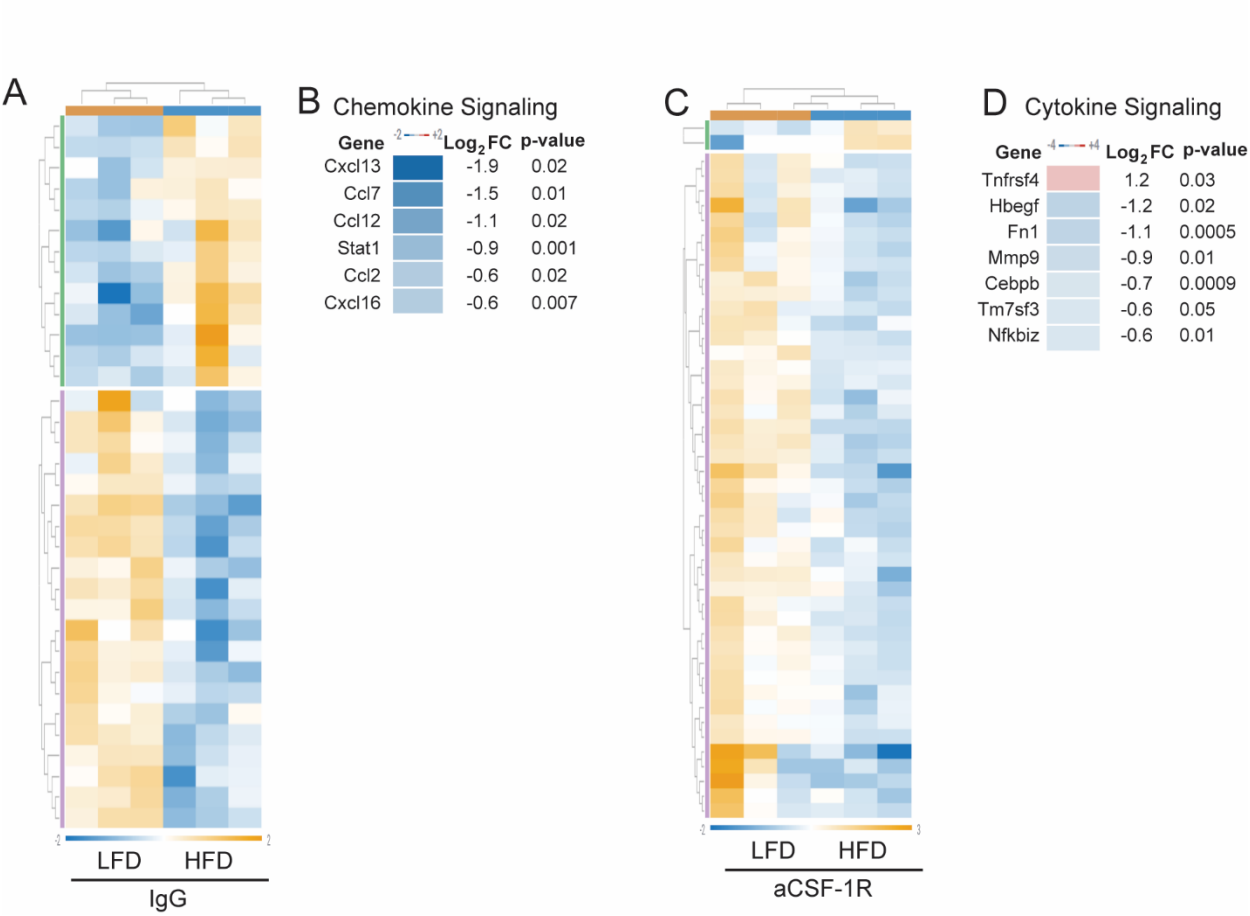

Supplementary Figure 4-4: Obese mice have lower expression of chemokines involved in T cell activation (**A**) Heatmap representing all genes that were significantly different in CD45+ cells from metastatic lungs from mice treated with IgG antibodies (n=3/group). Genes associated with signatures of Chemokine Signaling (**B**). (**C**) Heatmap representing all genes that were significantly different in CD45+ cells sorted from metastatic lungs from mice treated with anti-CSF-1R antibodies (n=3/group). Genes associated with signatures of Cytokine Signaling (**D**).

Table S4-1. Antibodies for T cell stimulation and flow cytometry.

Antibody	Dilution	Manufacturer	Catalog Number
Fc Receptor	1 µg/mL	ThermoFisher	14-0161-86
CD3	1 µg/mL	ThermoFisher	16-0032-82
CD28	5 µg/mL	ThermoFisher	16-0281-82
CD45	5 µg/mL	Biolegend	103101
CD45-eFluor 450	5 µg/mL	ThermoFisher	48-0453-82
CD3 PE-efluor610	20 µg/mL	ThermoFisher	61-0031-82
CD4 APC	2 µg/mL	BioLegend	100515
CD8α-PE/Cy7	4 µg/mL	BioLegend	100721
CD115-Brilliant Violet 711	10 µg/mL	BioLegend	135515
CD11b-Brilliant Violet 605	5 µg/mL	BioLegend	101237
PD-1-PE	10 µg/mL	BioLegend	135205
PD-L1-PerCP-eFluor 710	2.5 µg/mL	ThermoFisher	46-5982-82
F4/80 APC	12.5 µg/mL	ThermoFisher	17-4801-82
TNFα-eFluor 450	5 µg/mL	ThermoFisher	48-7321-82
IFNγ-PerCP/Cy5.5	1.25 µg/mL	BioLegend	505822

Supplementary Table 4-1: Antibodies used for flow cytometry and CD8+ T cell stimulation.

Table S4-2. Comparison of gene expression of LFD and HFD-fed mice with metastases treated with IgG antibodies.

Gene Name	LFD IgG 1	LFD IgG 2	LFD IgG 3	HFD IgG 1	HFD IgG 2	HFD IgG 3	Cluster
Hdc	-1.3647167	-1.33338	0.576323	0.833523	0.206623	1.081623	1
Plscr1	-0.874065	-0.53854	-0.23599	0.516635	0.394535	0.737435	1
Il15	-1.4351467	-0.54854	-0.16682	0.584123	0.358443	1.207933	1
Il1b	-1.22675	-0.25005	0.04455	0.52365	0.21295	0.69565	1
Tcrg-V6	-1.0006683	-1.34034	-0.36588	1.224452	0.613942	0.868492	1
Cd28	-0.9515417	-0.61173	-0.1932	1.067378	0.579178	0.109918	1
Vegfa	-0.9843983	-0.56508	0.128762	0.970272	-0.0069	0.457342	1
Junb	-0.5954333	-0.56423	0.053967	0.751967	0.053167	0.300567	1
Gadd45a	-0.625485	-0.77793	0.169385	0.240035	0.236415	0.757575	1
Pbx1	-0.4792633	-0.46047	0.130657	-0.11807	0.252797	0.674357	1
Sema4d	-0.7678417	-0.48458	0.021358	0.166498	0.429268	0.635298	1
Oas2	-0.1202233	-0.49769	-0.906	0.059177	0.477067	0.987677	1
Cpa3	-0.6610983	-0.29027	-0.33373	0.121672	0.507892	0.655532	1
Bcl6	-0.73188	-0.32361	-0.24379	0.26595	0.24559	0.78774	1
Hgf	-1.037725	-0.00053	-0.01323	0.073285	0.399075	0.579135	1
E2f2	-0.544735	-0.35388	-0.04521	0.346965	0.076035	0.520835	1
Fos	-0.7845333	-0.17463	-0.18563	0.255767	0.269667	0.619367	1
Cd40	-0.8808133	0.346887	-1.01739	0.299917	0.733797	0.517607	1
Psmb9	-0.5469567	0.064003	-0.55873	0.373573	0.428753	0.239353	1
Tapbp	-0.5706767	-0.16805	-0.22892	0.510993	0.568753	-0.11211	1
Btla	-1.033435	-0.21877	-0.31819	0.881345	0.543085	0.145975	1
Cd180	-0.687445	-0.27449	-0.55272	0.560405	0.517725	0.436535	1
Ptpn22	-0.5390267	-0.41567	-0.03406	0.667103	0.160103	0.161543	1
Lrrk2	-0.58666	-0.58387	0.04613	0.64891	0.12067	0.35482	1
Nfe2l2	-0.4554333	-0.64573	0.167567	0.578367	-0.04623	0.401467	1
Iglc1	-0.1028183	-0.23099	-0.83603	0.943542	0.455212	-0.22892	1
Jak3	-0.10305	-0.43356	-0.56648	0.80146	0.00836	0.29327	1
Scp2	-0.1566267	-0.55977	-0.18176	0.400303	0.126193	0.371653	1
Nfkb2	-0.2749733	-0.64179	-0.06433	0.694167	0.071467	0.215467	1
Mx2	-0.7302642	-0.5845	-2.2654	0.687506	1.505836	1.386826	1
Nos2	-1.5385917	-1.0709	-1.16683	0.864068	0.867438	2.044818	1
Trdv4	-1.1499167	-0.97501	-0.64691	0.445393	1.185723	1.140713	1
Trdc	-1.2821433	-0.12704	-0.63285	0.057017	1.109237	0.875787	1
Tlr1	-1.5531733	0.124507	-0.68715	0.595727	0.641617	0.878477	1

Cd101	-2.3278517	-0.41226	0.148598	0.686468	0.561378	1.343668	1
Ptgs2	-2.0555	-0.31341	-0.44756	1.30789	0.59529	0.91329	1
Cxcr6	-1.931685	-0.52511	-0.07672	1.043635	0.809645	0.680245	1
Trgc1/2/3	-1.693115	-0.76976	0.295315	0.631545	1.002415	0.533595	1
Icos	-1.6383767	-0.66872	0.127363	0.943113	0.737133	0.499483	1
Socs2	1.00981833	0.118508	-0.12894	0.095508	-0.27315	-0.82174	2
Lifr	0.87884667	-0.06544	0.052097	-0.22906	-0.42012	-0.21631	2
Cd160	-0.756255	0.567045	0.969145	-0.86456	0.064815	0.019805	2
Ccr5	0.00393833	0.594608	0.264808	-0.38522	-0.05941	-0.41872	2
Il1rl2	0.09836667	0.201317	0.629907	0.062837	-0.13544	-0.85698	2
Vcam1	0.46415	-0.11653	0.87243	-0.75963	-0.00019	-0.46023	2
Lpl	-0.0506283	0.269372	0.724872	-0.11876	-0.07783	-0.74703	2
Cd38	2.344455	-0.06302	-0.06861	-0.18333	-0.92063	-1.10884	2
Itga6	2.16709833	-0.12828	-0.62072	-0.3597	-0.74611	-0.31228	2
Lpar1	1.967035	-0.44791	-0.32145	-0.06043	-0.22007	-0.91715	2
Fabp4	1.96044833	-0.33774	-0.12622	-0.46978	-0.32663	-0.70007	2
Ucp1	2.99448	0.1243	-0.41666	-0.81426	-0.59539	-1.29247	2
Lepr	3.44636	-0.09304	-0.26675	-0.94874	-0.90859	-1.22924	2
Mst1r	2.78633667	0.228757	-0.7089	-0.8004	-0.5491	-0.95668	2
Cmklr1	2.44146667	0.076657	-0.57218	-0.72477	-0.49239	-0.72877	2

Supplementary Table 4-2: Comparison of gene expression of LFD-fed mice with metastasis treated with IgG or anti-PD-1 antibodies from the NanoString Immune Exhaustion Panel.

Table S4-3. Comparison of gene expression of LFD-fed mice with metastasis treated with IgG or anti-PD-1 antibodies.

Gene Name	LFD IgG 1	LFD IgG 2	LFD IgG 3	LFD aPD-1 1	LFD aPD-1 2	LFD aPD-1 3	Cluster
Tnfrsf9	-0.943095	-0.50207	-0.88711	0.245455	1.134835	0.951995	1
Ccl22	-1.083055	-0.36079	-0.32609	-0.214585	1.307205	0.677325	1
Zap70	-1.166396667	0.014773	-0.3182	0.30908333	0.76331333	0.39742333	1
Lck	-1.13452	-0.29258	-0.17389	0.46982	0.90049	0.23068	1
Trat1	-1.352286667	-0.35854	0.076053	0.27000333	0.84414333	0.52062333	1
Il9r	-1.100953333	-0.48368	-0.19216	0.32030667	1.00498667	0.45150667	1
Rora	-0.873715	-0.64001	-0.11606	0.242685	0.864205	0.522895	1
Cd3e	-1.181298333	-0.66298	0.009222	0.56931167	1.16221167	0.10353167	1
Cd4	-1.671218333	-0.47839	0.319452	0.56857167	1.18115167	0.08043167	1
Sesn3	-1.389385	-0.20333	0.197645	0.491085	0.817045	0.086935	1
Ccr7	-1.869388333	-0.59887	0.116722	0.34833167	1.26115167	0.74205167	1
Wnt11	-1.665486667	-0.63432	-0.09282	0.87833333	0.84827333	0.66601333	1
Icos	-1.835818333	-0.86616	-0.07008	0.85505167	1.31628167	0.60072167	1
Tnfrsf4	-1.479103333	-0.62083	-1.02488	0.54983667	1.56873667	1.00624667	1
Dcn	-1.699878333	-0.71762	-0.74316	1.17141167	1.24559167	0.74365167	1
Ctla4	-1.793173333	-0.51243	-0.69743	0.71656667	1.55585667	0.73061667	1
Cd5	-1.802811667	-0.14248	-0.36965	0.50426833	1.45830833	0.35236833	1
Sh2d1a	-1.477413333	-0.23212	-0.26435	0.78873667	1.02264667	0.16250667	1
Cd3g	-1.415163333	-0.31521	-0.06155	0.49304667	1.01250667	0.28637667	1
Pdcd1	-0.798823333	-1.2056	-0.262	0.21569667	0.99099667	1.05973667	1
Id2	-0.6344	-1.0002	-0.1615	0.5372	0.575	0.6839	1
Tnfrsf18	-0.720505	-0.82843	0.206775	0.589905	0.529305	0.222955	1
Il21r	-0.79626	-0.77552	-0.34855	0.5619	0.95099	0.40744	1
Cd28	-0.974581667	-0.63477	-0.21624	0.79645833	0.73576833	0.29336833	1
Ccl21a/b/c	-0.832676667	-1.04682	-0.80487	1.21661333	0.65336333	0.81438333	1
Vegfa	-1.4317	-1.01238	-0.31854	1.12995	0.63946	0.99321	1
Cxcl3	-1.485458333	-1.17305	-0.21324	0.81968167	0.80178167	1.25028167	1
Havcr2	-0.85557	-0.4334	-1.20002	1.65613	0.52054	0.31232	1
Trbc1/2	-0.903243333	-0.83692	-0.21921	1.25316667	0.55318667	0.15302667	1
Slamf6	-0.466145	-0.66832	-0.04709	0.771265	0.532435	-0.122155	1
S1pr1	-0.516868333	-0.71452	-0.2305	1.04533167	0.64744167	-0.2308883	1
Trim2	-0.09695	-0.68455	-0.55808	0.81591	-0.07748	0.60115	1
Cd86	-0.31415	-0.60576	-0.41696	0.72586	0.20705	0.40396	1
Psmb9	-0.560436667	0.050523	-0.57221	0.70066333	0.51166333	-0.1302067	1
Tox4	-0.275518333	-0.229	-0.4465	0.77138167	0.13586167	0.04377167	1

Ptger4	-0.506115	-0.41798	-0.30794	0.632095	0.406025	0.193925	1
Cxcl2	-0.9663	-0.6072	-0.1961	0.3933	0.3417	1.0346	1
Gzmb	-1.231153333	-0.0403	-0.44435	0.66952667	0.12936667	0.91691667	1
Hgf	-1.123906667	-0.08672	-0.09942	0.35266333	0.34044333	0.61693333	1
Gbp2	-0.840275	-0.12623	-0.29087	0.530835	0.510235	0.216315	1
Malt1	-0.95028	-0.32071	-0.32302	0.64267	0.51717	0.43417	1
Nfil3	-0.9387	-0.0293	-0.0159	0.3906	0.2623	0.331	1
Il1r1	-0.92968	-0.33254	0.06769	0.41499	0.41008	0.36946	1
Nfkbie	-1.13365	-0.26345	0.20697	0.28086	0.44227	0.467	1
Itgb3	-0.754361667	-0.26215	-0.27157	0.12756833	0.59164833	0.56886833	1
Cul2	-0.464171667	-0.03779	-0.38865	0.13888833	0.27750833	0.47421833	1
Ptpn22	-0.527196667	-0.40384	-0.02223	0.38438333	0.19706333	0.37181333	1
Il1rn	-0.841166667	-0.37657	0.089433	0.21543333	0.27703333	0.63583333	1
Arg1	4.352553333	2.569833	-2.81677	-1.67980667	-0.4881667	-1.9376467	2
Ltbp1	3.934606667	1.311297	-1.78463	-1.03999333	-1.6259533	-0.7953233	2
Gata6	2.886656667	0.731417	-1.78597	-1.13444333	-0.3053733	-0.3922833	2
Mst1r	2.864478333	0.306898	-0.63076	-0.76059167	-0.7615917	-1.0184317	2
Lepr	3.19457	-0.34483	-0.51854	-1.53063	-0.28341	-0.51716	2
Ucp1	3.174528333	0.304348	-0.23661	-0.82455167	-1.1654017	-1.2523117	2
Itga6	2.33015	0.03477	-0.45767	-0.54311	-0.34081	-1.02333	2
Cmklr1	2.308748333	-0.05606	-0.7049	-0.38224167	-0.5324117	-0.6331317	2
Acaca	1.617815	0.014445	-0.48275	-0.359115	-0.263435	-0.526965	2
Cd38	2.04996	-0.35752	-0.36311	-0.53562	-0.45553	-0.33818	2
Tnf	1.634918333	-0.17987	0.567178	-0.77520167	-0.7248117	-0.5222117	2
Lifr	0.908496667	-0.03579	0.081747	-0.17810333	-0.3671233	-0.4092233	2

Supplementary Table 4-3: Comparison of gene expression of HFD-fed mice with metastases treated with IgG or anti-PD-1 antibodies from the NanoString Immune Exhaustion Panel.

Table S4-4. Comparison of gene expression of HFD-fed mice with metastases treated with IgG o anti-PD-1 antibodies.

Gene Name	HFD IgG 1	HFD IgG 2	HFD IgG 3	HFD aPD-1 1	HFD aPD-1 2	HFD aPD-1 3	Cluster
Bcl2l1	-0.688075	-0.634385	-0.045215	0.895795	0.340975	0.130905	1
Il1rn	-0.8073333	-0.1595333	-0.1619333	0.355966667	0.331366667	0.441466667	1
Plcg1	-0.566955	-0.392475	-0.241095	-0.093255	0.927105	0.366675	1
Naa50	-0.584475	-0.046005	-0.290785	-0.005735	0.652425	0.274575	1
Ccr5	-0.42835	-0.10254	-0.46185	0.35958	0.25288	0.38028	1
Jak2	-0.3307167	-0.2045167	-0.3766167	0.199783333	0.602883333	0.109183333	1
Cxcl3	-1.5484283	-0.5335883	-0.5981783	1.130831667	0.490831667	1.058531667	1
Ifng	-1.6082633	-0.8264533	0.28607667	0.144296667	0.829216667	1.175126667	1
Pmepa1	-1.4873517	0.00904833	-0.5765317	0.390738333	1.043228333	0.620868333	1
Cxcl2	-1.1051833	-0.5054833	-0.1460833	0.764916667	0.627216667	0.364616667	1
Il1rl2	0.06307167	-0.1352083	-0.8567483	0.472171667	0.527001667	-0.07028833	1
Trim35	-0.278395	-0.366955	-0.657075	0.130205	0.837155	0.335065	1
Lpl	-0.2858417	-0.2449117	-0.9141117	0.435688333	0.654488333	0.354688333	1
Lag3	-0.0631933	-1.0213533	-2.4289333	1.429866667	1.663076667	0.420536667	1
Mras	0.34604333	-0.6232167	-1.5824967	0.755193333	0.909993333	0.194483333	1
Sftpa1	-1.1919417	-1.6080717	-0.7405517	0.216658333	3.295738333	0.028168333	1
Ccl21a/b/c	-1.1667283	-0.2552883	-0.5998583	-0.72159833	2.171211667	0.572261667	1
Dcn	-1.1968233	-0.2853833	-1.1604633	0.013836667	1.556156667	1.072676667	1
Vcam1	-1.3940617	-0.6346217	-1.0946617	1.220998333	1.487028333	0.415318333	1
Klrk1	-0.91908	-0.59214	-0.82443	0.73413	1.3481	0.25342	1
Id2	-0.4153667	-0.6820667	-1.1490667	0.818233333	1.080933333	0.347333333	1
Klrb1a	-0.5001117	-0.3077117	-1.1076117	0.763868333	0.971578333	0.179988333	1
H2-DMb2	-0.6539333	-0.3916033	-0.9528633	1.043756667	1.007256667	-0.05261333	1
Cxcl9	-0.3031067	-0.6261267	-0.6711367	-0.80139667	0.828383333	1.573383333	1
Tigit	-0.4843483	-0.6607783	-1.4219883	-0.08993833	1.442301667	1.214751667	1
Pparg	-0.2042733	-0.3197033	-0.7146533	-0.23549333	1.114176667	0.359946667	1
Tslp	-0.5256517	0.06267833	-0.9298617	0.043108333	1.174858333	0.174868333	1
Adora2a	-0.3282017	0.02617833	-1.0188317	-0.06545167	0.916628333	0.469678333	1
Tnfrsf14	0.375175	-0.006625	0.553785	-0.714705	-0.113045	-0.094585	2
Il1b	0.44186667	0.13116667	0.61386667	-0.58403333	-0.237733333	-0.36513333	2
Tapbp	0.47932833	0.53708833	-0.1437717	-0.69991167	0.154638333	-0.32737167	2
Atr	0.53129833	0.03287833	0.29419833	-0.62209167	0.186108333	-0.42239167	2
Cpa3	0.00464333	0.39086333	0.53850333	-0.33026667	0.280653333	-0.88439667	2
Pik3cd	0.524215	0.169415	0.312715	-0.519605	-0.081925	-0.404815	2
Mx2	0.71370467	1.53203467	1.41302467	-0.57813533	-2.755713333	-0.32491533	2

Tlr1	0.34606167	0.39195167	0.62881167	-0.48899833	-0.591938333	-0.28588833	2
Cd180	0.61882667	0.57614667	0.49495667	-1.17244333	-0.081203333	-0.43628333	2
Oas2	0.12742	0.54531	1.05592	-1.70721	-0.29983	0.27839	2
Rnf213	0.17769	0.54594	0.57019	-0.92511	-0.18069	-0.18802	2
Tgfb2	1.21253167	-0.1211383	0.83385167	-1.49434833	-0.256888333	-0.17400833	2
Cdc14b	1.20643167	0.05076167	0.52032167	-1.22290833	-0.262988333	-0.29161833	2
Rara	0.81115833	0.18113833	0.44045833	-0.56491167	-0.365931667	-0.50191167	2
Nr4a1	0.85821667	-0.0393833	0.19881667	-0.43338333	-0.143583333	-0.44068333	2

Supplementary Table 4-4: Comparison of gene expression of LFD and HFD-fed mice with metastases treated with IgG from the NanoString Immune Exhaustion Panel.

Table S4-5. Comparison of gene expression of LFD and HFD-fed mice with metastases treated with anti-PD-1 antibodies.

Gene Name	HFD aPD-1 1	HFD aPD-1 2	HFD aPD-1 3	LFD aPD-1 1	LFD aPD-1 2	LFD aPD-1 3	Cluster
Gzmd	0.217536667	0.16290667	0.854546667	-0.766423333	-0.140656667	-0.60922333	1
Klrb1a	-0.704063333	-0.08752667	0.496353333	-0.164416667	-0.263186667	-0.68528667	1
Cxcl9	0.794728333	1.53972833	-0.835051667	-0.912751667	-0.111868333	-0.69852167	1
Cxcl11	0.791973333	0.67845333	-0.182446667	-0.016603333	-0.532836667	-0.77174667	1
Ccl12	0.826515	0.309775	-0.106935	-0.689935	-0.208785	-0.130635	1
Gzmb	-0.063581667	-0.28814167	-1.055931667	0.566808333	0.026648333	0.81419833	2

Supplementary Table 4-5: Comparison of gene expression of LFD and HFD-fed mice with metastases treated with anti-PD-1 antibodies from the NanoString Immune Exhaustion Panel.

Table S4-6. Comparison of LFD and HFD-fed mice with metastasis treated with IgG antibodies.

Gene Name	LFD IgG 1	LFD IgG 2	LFD IgG 3	HFD IgG 1	HFD IgG2	HFD IgG3
Cdh5	-0.23786	-0.5303	-0.54843	0.92468	-0.0485	0.44041
Cd34	-0.35737	-0.37255	-0.30886	0.469727	0.070777	0.498287
Tnfrsf11a	-0.00035	-0.60418	-0.26219	0.246945	0.300675	0.319085
Kit	-0.42566	-0.60434	0.241765	0.269655	0.453705	0.064865
Btg2	-0.37493	-0.44083	-0.10773	0.127767	0.429267	0.366467
Nr4a1	-0.60535	-0.97865	0.14205	-0.26685	1.25505	0.45375
Nfatc2	-0.3971	-0.42257	-0.20547	-0.14469	0.857552	0.312272
Lta4h	-0.25698	-0.56574	-0.45358	0.205507	0.858297	0.212507
Il1r1	-0.09385	-1.32316	-0.61792	0.217093	1.239113	0.578713
Lag3	-0.21586	-0.60563	-0.85541	-0.00728	1.27428	0.4099
Fgfr1	-0.58337	-0.60747	-0.58166	-0.15887	1.766933	0.164423
Plau	-0.39	-0.47039	-0.23653	-0.11646	1.40116	-0.18778
Mmp12	-0.354	-0.2052	-0.4832	-0.2227	1.0651	0.2
Chil4	-0.13682	1.632683	-0.32372	-0.00552	-0.67842	-0.48822
Marco	0.450248	1.006088	0.173918	-0.22107	-0.78808	-0.6211
C4a	0.452137	0.643397	0.048127	-0.09928	-0.71687	-0.3275
Top2a	-0.12077	0.802118	0.342768	-0.21968	-0.67221	-0.13222
C3	0.087167	0.404367	0.415667	-0.11083	-0.43153	-0.36483
Cxcl13	0.478258	0.838548	0.752058	-0.48293	-0.64528	-0.94065
Mmp13	0.657922	0.636572	0.451172	-0.36298	-0.89457	-0.48812
C1qc	0.547405	0.722395	0.477995	-0.39531	-1.03477	-0.31773
Stat1	0.246823	0.123523	0.826913	-0.11112	-0.47473	-0.61142
Irf7	0.472888	0.322018	0.635358	-0.21427	-1.05997	-0.15602
Isg15	0.188732	0.182802	0.891372	-0.24872	-0.68164	-0.33255
Ccl7	1.125293	-0.00383	0.532693	0.001703	-1.08124	-0.57463
Gpr183	0.719302	0.220902	0.251232	-0.14262	-0.96446	-0.08436
Ccl12	0.779947	0.233447	0.328027	-0.21629	-0.48247	-0.64265
Ccl2	0.73692	0.17069	-0.03354	-0.13971	-0.39219	-0.34217
Cxcl16	0.580455	0.063595	0.292285	-0.44724	-0.57446	0.085355
Mmp19	0.56564	0.38444	0.27347	-0.67155	-0.36452	-0.18748
C1qb	0.182652	0.443712	0.429292	-0.63464	-0.29151	-0.12951
Timd4	0.04394	0.56321	0.72508	-1.05745	-0.15381	-0.12097
Flt3	0.296073	0.344973	0.678323	-0.74473	-0.4642	-0.11045
C1qa	0.233627	0.583267	0.602687	-0.6411	-0.47883	-0.29964

Supplementary Table 4-6: Comparison of gene expression of LFD-fed mice with metastasis treated with IgG or anti-CSF-1R antibodies from the NanoString Myeloid Innate Immunity Panel.

Table S4-7. Comparison of gene expression of LFD-fed mice with metastasis treated with IgG or anti-CSF-1R antibodies.

Gene Name	LFD IgG 1	LFD IgG 2	LFD IgG 3	LFD aCSF1R 1	LFD aCSF1R 2	LFD aCSF1R 3
Prg2	-2.05912	-1.09341	-1.01061	1.879487	-0.26501	2.548677
Ear6	-1.82304	-0.85733	-0.71564	1.106475	0.523615	1.765905
Camp	-1.73112	-0.00985	-0.7899	0.625727	0.506327	1.398827
Csf2ra	-0.73905	-0.74942	0.092483	1.411253	-0.85063	0.835353
Nr4a1	-0.69502	-1.06832	0.052383	1.137983	-0.29412	0.867083
Prok2	-1.23672	-0.63495	0.089082	-0.68701	0.848812	1.620782
Ly6g	-1.47246	-0.4119	-0.13891	0.170667	0.551617	1.300997
Mmp8	-0.97141	-0.33923	-0.15376	-0.19455	0.352015	1.306915
Gata1	-0.94112	-0.40837	0.10739	0.22893	0.16849	0.84468
S100a8	-1.06487	-0.41677	-0.08167	0.212433	0.085833	1.265033
Trem1	-0.48243	-0.35339	-0.07423	-0.07243	9.00E-05	0.98239
S100a9	-0.63808	-0.33338	-0.14988	-0.21208	0.296617	1.036817
Ptgs1	-0.6765	-0.07336	-0.23568	-0.02841	0.458652	0.555292
Selp	-0.49944	-0.28044	-0.22854	-0.08522	0.528262	0.565372
Mmp9	-0.65601	-0.27245	-0.34966	-0.4146	0.69091	1.00181
Pglyrp1	-0.55466	-0.20225	-0.19407	-0.31847	0.360922	0.908522
Ceacam1	-0.0005	-0.43742	-0.55009	-0.06938	0.862223	0.195153
Lta4h	-0.18303	-0.49179	-0.37963	0.53128	0.67059	-0.14742
Fn1	-0.6515	-0.4514	-0.5361	0.4158	0.4372	0.786
Ikbke	-0.59013	-0.35694	-0.17239	0.34545	0.39863	0.37538
Fut4	-0.07694	-0.66705	-0.25083	0.313448	0.304088	0.377288
Krba1	-0.29562	-0.31541	-0.24711	0.156077	0.086367	0.615707
Tm7sf3	-0.41174	-0.25926	-0.1662	0.196277	0.024817	0.616117
S100a4	-0.04027	-0.73527	-0.28087	0.788033	0.297533	-0.02917
Ccr2	-0.5242	-0.7187	-0.18264	0.77472	0.26209	0.38873
Itga4	-0.41205	-0.29235	-0.27667	0.641092	-0.17727	0.517242
C3ar1	-0.35125	-0.64051	-0.16769	0.769035	-0.17759	0.567985
Ptprb	1.24123	0.009	-0.08878	-0.54808	-0.40207	-0.2113
Ccl7	0.983398	-0.14572	0.390798	-0.05797	-0.67095	-0.49955
Irf8	4.444531	-2.54977	2.872881	0.280181	-2.45833	-2.58949
Cyr61	2.94658	-3.37312	2.27192	1.04179	-3.28168	0.39451
Col14a1	1.205933	0.645573	0.917403	-0.84642	-1.58492	-0.33758
Mmp13	0.938817	0.917467	0.732067	-1.25259	-1.21349	-0.12226
C1qa	0.3009	0.65054	0.66996	-0.51603	-1.34811	0.24274
C1qc	0.60837	0.78336	0.53896	-0.69291	-1.05331	-0.18447

C1qb	0.345812	0.606872	0.592452	-0.50621	-1.1773	0.138372
Stat1	0.213792	0.090492	0.793882	-0.47722	-0.42951	-0.19144
Cxcl9	0.359443	0.325153	1.470963	-0.33033	-0.88827	-0.93697
Tnfrsf4	-0.02817	0.229718	0.763178	-0.14679	-0.47026	-0.34767
Ttk	0.315327	0.368017	-0.05937	0.135227	-0.28778	-0.47141
Ccr7	0.579	0.16166	0.26745	0.06429	-0.37585	-0.69655
Top2a	-0.08123	0.841657	0.382307	-0.45551	0.157967	-0.84518
Ccl12	0.7565	0.21	0.30458	-1.08344	0.3249	-0.51254
Fzd4	0.436675	0.396845	0.251695	-0.30373	-0.36417	-0.41733
Cxcl16	0.619478	0.102618	0.331308	-0.14965	-0.52757	-0.37618
Chil4	0.1008	1.8703	-0.0861	-0.9355	-1.013	0.0635
Chil3	-0.07997	2.001633	-0.06377	-0.89967	-1.18967	0.231433
Marco	0.337992	0.893832	0.061662	-0.62415	-0.78647	0.117132
Pdgfb	0.373683	0.814543	-0.02388	-0.47837	-0.4608	-0.22519
Ear3	0.313683	0.949683	-0.17432	-0.36002	-0.55532	-0.17372
Kif20a	-0.26783	0.920267	0.950597	0.312087	-1.57326	-0.34185
Cldn1	0.2406	0.61408	0.38041	-0.04578	-1.01695	-0.17236
Mrc1	0.224208	0.792268	0.171878	-0.09778	-1.16386	0.073288
C4a	0.379297	0.570557	-0.02471	-0.02299	-0.88549	-0.01665
Adgre1	0.512207	0.507387	0.165557	-0.32022	-1.00539	0.140467

Supplementary Table 4-7: Comparison of gene expression of HFD-fed mice with metastasis treated with IgG or anti-CSF-1R antibodies from the NanoString Myeloid Innate Immunity Panel.

Table S4-8. Comparison of gene expression of HFD-fed mice with metastasis treated with IgG or anti-CSF-1R antibodies.

Gene Name	HFD IgG 1	HFD IgG 2	HFD IgG 3	HFD aCSF1R 1	HFD aCSF1R 2	HFD a CSF1R 3
Ercc1	0.203787	0.038897	0.174167	-0.14902	-0.07889	-0.18893
Kit	0.234052	0.418102	0.029262	-0.19112	-0.2415	-0.2488
Nr2f6	0.239577	0.299317	0.116857	-0.39275	0.029797	-0.29279
Cxcl14	0.511602	0.122112	0.108522	-0.36122	-0.27328	-0.10774
Mx1	0.29431	0.44861	0.25945	-0.45279	-0.56457	0.01499
Prkca	0.476278	0.331018	0.119488	-0.49321	-0.3826	-0.05097
Adamts2	0.44376	0.19089	0.15373	-0.47347	-0.21657	-0.09834
Siglec1	0.588195	0.470535	0.374485	-0.05462	-0.48125	-0.89736
Rhoc	0.104292	0.363202	0.471512	0.037772	-0.30479	-0.67199
Ccr8	0.111607	0.268647	0.321457	-0.24942	0.041237	-0.49352
Arg1	-0.65039	2.764455	-0.06857	-0.09631	-1.24623	-0.70298
Cd163	-0.42663	0.826743	0.804683	-0.02142	-0.91354	-0.26985
Col3a1	-0.06488	1.109562	0.459902	-0.39275	-0.82646	-0.28538
Slc16a6	-0.07737	0.718345	0.271795	-0.10825	-0.49083	-0.31371
Mob3c	-0.16002	0.347927	0.415367	-0.37533	-0.13919	-0.08874
Flt1	0.188932	0.822412	0.533712	-0.84195	-0.42893	-0.27418
Cdh1	0.002788	0.459658	0.262678	-0.44732	-0.22584	-0.05196
Tspan7	1.280052	0.216842	0.746392	-0.3358	-1.80534	-0.10215
Kitl	1.408838	0.219708	1.293578	-0.60863	-1.73207	-0.58142
Timp3	1.518658	0.331458	1.071908	-0.23511	-1.94225	-0.74466
Tek	1.502143	0.422213	0.919843	-0.52875	-1.50358	-0.81188
Cxcl12	1.48522	0.27001	0.8691	-0.78667	-1.37365	-0.46401
Cdh5	1.459683	0.486503	0.975413	-0.88241	-1.55839	-0.48081
Col4a2	0.927085	0.425245	0.714485	-0.26887	-0.97133	-0.82663
Ptprb	1.254588	0.185228	1.054408	-0.33088	-1.25198	-0.91136
Adamts1	1.020153	0.010373	1.240963	-0.28928	-1.28719	-0.69503
Cav1	0.836757	0.317627	0.575927	-0.12604	-1.26069	-0.34357
Col1a2	0.397818	0.160578	1.144698	-0.44864	-0.83302	-0.42143
S1pr1	0.565783	0.321113	0.531163	-0.10831	-1.01971	-0.29005
Hpgd	1.293137	0.339587	0.305147	-0.95676	-0.59654	-0.38456
Hc	0.813473	0.020033	0.634473	-0.97823	-0.06925	-0.42051
Stab1	0.763643	-0.44602	0.251483	-0.30678	-0.13477	-0.12757
Cd34	0.337762	-0.06119	0.366322	-0.40362	-0.05878	-0.1805
Edn1	0.96906	-0.56607	0.6858	-0.44885	-0.51785	-0.12209

Tgfbr3	0.71721	-0.0184	0.43696	-0.21881	-0.69888	-0.21808
Fzd4	0.795652	0.130372	0.186322	-0.28888	-0.83933	0.015862
Enc1	0.40697	0.45257	0.12205	0.09431	-0.88254	-0.19336
Sptbn1	0.455542	0.182972	0.282832	-0.22576	-0.45064	-0.24495

Supplementary Table 4-8: Comparison of HFD-fed mice with metastasis treated with IgG or snit-CSF1R from the NanoString Myeloid Innate Immunity Panel.

Table S4-9. Comparison of LFD and HFD-fed mice with metastasis treated with anti-CSF-1R antibodies.

Gene Name	LFD aCSF1R 1	LFD aCSF1R 2	LFD aCSF1R 3	HFD aCSF1R 1	HFD aCSF1R 2	HFD aCSF1R 3
Tnfrsf4	-0.35504	-0.15416	-0.47763	-0.08733	0.61972	0.45444
Tuba1a	-1.32262	-0.0154	-0.00102	-0.01023	0.637238	0.712038
C5ar1	0.785932	-0.3298	0.414032	0.044122	-0.47193	-0.44236
Tlr13	0.773215	-0.30189	0.428415	-0.28696	-0.2286	-0.3842
Pglyrp1	0.846608	-0.38038	0.299008	-0.10301	-0.2478	-0.41442
Arg1	1.831627	-0.32039	0.651597	-0.13541	-1.28533	-0.74208
Mmp9	0.955745	-0.46067	0.644845	-0.05931	-0.4653	-0.61533
Mmp8	1.130055	-0.37141	0.175155	-0.09345	-0.36775	-0.47262
Ly6g	1.003613	-0.12672	0.254233	-0.1331	-0.39362	-0.60442
Csf3r	0.880233	-0.17857	0.175033	-0.12557	-0.34307	-0.40807
Hbegf	0.365543	0.760303	0.183543	-0.08104	-0.75338	-0.47498
Fcgr1	0.410837	0.372277	0.318897	-0.1126	-0.58326	-0.40614
C3ar1	0.535858	0.736908	-0.20971	-0.18227	-0.36799	-0.51279
Mx1	0.653913	0.639053	-0.09945	-0.51651	-0.62829	-0.04873
Mafb	0.630423	0.407703	0.023713	-0.27852	-0.32825	-0.45508
Tlr4	0.045023	0.168443	0.659743	-0.28083	-0.29126	-0.30113
Golim4	0.502725	0.211935	0.048935	-0.33066	-0.22903	-0.20392
Grn	0.473597	0.152367	0.248107	-0.35914	-0.19132	-0.3236
Ptgs1	0.707402	0.123702	0.610762	-0.40626	-0.90167	-0.13394
Selp	0.592912	-0.05768	0.555802	-0.17577	-0.64118	-0.27409
Fn1	0.762517	0.392317	0.413717	-0.51068	-0.50008	-0.55778
Cd38	0.618743	0.397813	0.562633	-0.24451	-0.71962	-0.61507
Slc16a6	0.52673	0.43145	0.35652	-0.24222	-0.6248	-0.44768
Ear6	1.441378	0.781948	0.199088	-0.46239	-0.52484	-1.43518
Camp	0.957797	0.184697	0.065297	-0.0889	-0.46041	-0.65847
Tgm2	1.086357	0.422857	-0.18955	-0.05204	-0.74929	-0.51832
Maff	0.798688	0.454038	-0.35372	0.160228	-0.502	-0.55723
Ier3	0.689298	0.446698	-0.0513	0.036298	-0.4939	-0.62709
Ccrl2	0.934983	-0.07762	0.135683	-0.44872	-0.07422	-0.47012
Cebpb	0.5803	0.0669	0.2563	-0.3428	-0.1784	-0.3823
Fut4	0.490247	0.426407	0.417047	-0.03057	-0.19169	-1.11143
Ikbke	0.304648	0.274718	0.327898	0.161818	-0.30117	-0.76791

Runx2	0.856762	0.215472	-0.09007	-0.15948	-0.33894	-0.48375
Irf7	0.829163	0.340783	0.022393	-0.3572	-0.31447	-0.52068
Sell	0.687183	0.057583	0.376083	-0.22282	-0.42002	-0.47802
C3	0.611017	0.087817	0.182117	-0.15748	-0.27208	-0.45138
Alox5	0.675207	-0.06903	0.235677	-0.05312	-0.34105	-0.44767
Nfkbiz	0.768633	-0.02417	0.079733	-0.10387	-0.35727	-0.36307
Cd163	0.774177	0.178177	0.047357	0.046947	-0.84517	-0.20148
Egr3	0.828822	-0.04775	0.117532	-0.0945	-0.63298	-0.17113
Tm7sf3	0.543443	0.123603	-0.04786	-0.06087	-0.3642	-0.19413
Ly6c1	0.599347	0.189077	0.156017	-0.06492	-0.4417	-0.43781
Prg2	2.202603	1.533413	-0.61109	-0.2346	-0.96305	-1.92729
Serpinb2	2.043093	0.647413	-0.79153	-0.79194	-0.3106	-0.79645
Apoe	2.33876	0.23405	-0.48264	-0.81064	-0.73173	-0.5478
Siglec1	1.509018	0.010538	-0.39934	0.049718	-0.37691	-0.79302
Trem2	1.380388	0.052828	-0.32209	-0.25635	-0.35498	-0.49979

Supplementary Table 4-9: Comparison of LFD and HFD-fed mice with metastasis treated with anti-CSF-1R antibodies from the NanoString Myeloid Innate Immunity Panel.

References:

1. Majed B, Moreau T, Senouci K, Salmon RJ, Fourquet A, Asselain B. Is obesity an independent prognosis factor in woman breast cancer? Breast Cancer Res Treat. 2008;111(2):329-42.

2. Ewertz M, Jensen MB, Gunnarsdóttir K, Højris I, Jakobsen EH, Nielsen D, et al. Effect of obesity on prognosis after early-stage breast cancer. J Clin Oncol. 2011;29(1):25-31.

3. Sestak I, Distler W, Forbes JF, Dowsett M, Howell A, Cuzick J. Effect of body mass index on recurrences in tamoxifen and anastrozole treated women: an exploratory analysis from the ATAC trial. J Clin Oncol. 2010;28(21):3411-5.

4. LeVee A, Mortimer J. The Challenges of Treating Patients with Breast Cancer and Obesity. Cancers (Basel). 2023;15(9).

5. Ades F, Zardavas D, Bozovic-Spasojevic I, Pugliano L, Fumagalli D, de Azambuja E, et al. Luminal B breast cancer: molecular characterization, clinical management, and future perspectives. J Clin Oncol. 2014;32(25):2794-803.

6. Raheem F, Karikalan SA, Batalini F, El Masry A, Mina L. Metastatic ER+ Breast Cancer: Mechanisms of Resistance and Future Therapeutic Approaches. Int J Mol Sci. 2023;24(22).

7. Menikdiwela KR, Kahathuduwa C, Bolner ML, Rahman RL, Moustaid-Moussa N. Association between Obesity, Race or Ethnicity, and Luminal Subtypes of Breast Cancer. Biomedicines. 2022;10(11).

8. Sparano JA, Wang M, Zhao F, Stearns V, Martino S, Ligibel JA, et al. Obesity at diagnosis is associated with inferior outcomes in hormone receptor-positive operable breast cancer. Cancer. 2012;118(23):5937-46.

9. Biganzoli E, Desmedt C, Fornili M, de Azambuja E, Cornez N, Ries F, et al. Recurrence dynamics of breast cancer according to baseline body mass index. Eur J Cancer. 2017;87:10-20.

10. Zhang XH, Giuliano M, Trivedi MV, Schiff R, Osborne CK. Metastasis dormancy in estrogen receptor-positive breast cancer. Clin Cancer Res. 2013;19(23):6389-97.

11. Pan H, Gray R, Braybrooke J, Davies C, Taylor C, McGale P, et al. 20-Year Risks of Breast-Cancer Recurrence after Stopping Endocrine Therapy at 5 Years. N Engl J Med. 2017;377(19):1836-46.

12. Rugo HS, Delord JP, Im SA, Ott PA, Piha-Paul SA, Bedard PL, et al. Safety and Antitumor Activity of Pembrolizumab in Patients with Estrogen Receptor-Positive/Human Epidermal Growth Factor Receptor 2-Negative Advanced Breast Cancer. Clin Cancer Res. 2018;24(12):2804-11.

13. Huang R, Wang Z, Hong J, Wu J, Huang O, He J, et al. Targeting cancer-associated adipocyte-derived CXCL8 inhibits triple-negative breast cancer progression and enhances the efficacy of anti-PD-1 immunotherapy. Cell Death Dis. 2023;14(10):703.

14. Hiltbrunner S, Cords L, Kasser S, Freiberger SN, Kreutzer S, Toussaint NC, et al. Acquired resistance to anti-PD1 therapy in patients with NSCLC associates with immunosuppressive T cell phenotype. Nat Commun. 2023;14(1):5154.

15. Fitzgerald AA, Wang S, Agarwal V, Marcisak EF, Zuo A, Jablonski SA, et al. DPP inhibition alters the CXCR3 axis and enhances NK and CD8+ T cell infiltration to improve anti-PD1 efficacy in murine models of pancreatic ductal adenocarcinoma. J Immunother Cancer. 2021;9(11).

16. Strachan DC, Ruffell B, Oei Y, Bissell MJ, Coussens LM, Pryer N, et al. CSF1R inhibition delays cervical and mammary tumor growth in murine models by attenuating the turnover of tumor-associated macrophages and enhancing infiltration by CD8(+) T cells. Oncoimmunology. 2013;2(12):e26968.

17. Hillers-Ziemer LE, Williams AE, Janquart A, Grogan C, Thompson V, Sanchez A, et al. Obesity-Activated Lung Stromal Cells Promote Myeloid Lineage Cell Accumulation and Breast Cancer Metastasis. Cancers (Basel). 2021;13(5).

18. Peranzoni E, Lemoine J, Vimeux L, Feuillet V, Barrin S, Kantari-Mimoun C, et al. Macrophages impede CD8 T cells from reaching tumor cells and limit the efficacy of anti-PD-1 treatment. Proc Natl Acad Sci U S A. 2018;115(17):E4041-e50.

19. Kawai T, Autieri MV, Scalia R. Adipose tissue inflammation and metabolic dysfunction in obesity. Am J Physiol Cell Physiol. 2021;320(3):C375-c91.

20. Cancello R, Henegar C, Viguerie N, Taleb S, Poitou C, Rouault C, et al. Reduction of macrophage infiltration and chemoattractant gene expression changes in white adipose tissue of morbidly obese subjects after surgery-induced weight loss. Diabetes. 2005;54(8):2277-86.

21. Chamberlin T, Thompson V, Hillers-Ziemer LE, Walton BN, Arendt LM. Obesity reduces mammary epithelial cell TGFβ1 activity through macrophage-mediated extracellular matrix remodeling. Faseb j. 2020.

22. Hillers-Ziemer LE, McMahon RQ, Hietpas M, Paderta G, LeBeau J, McCready J, et al. Obesity Promotes Cooperation of Cancer Stem-Like Cells and Macrophages to Enhance Mammary Tumor Angiogenesis. Cancers (Basel). 2020;12(2).

23. McDowell SAC, Milette S, Doré S, Yu MW, Sorin M, Wilson L, et al. Obesity alters monocyte developmental trajectories to enhance metastasis. J Exp Med. 2023;220(8).

24. Barcus CE, O'Leary KA, Brockman JL, Rugowski DE, Liu Y, Garcia N, et al. Elevated collagen-I augments tumor progressive signals, intravasation and metastasis of prolactin-induced estrogen receptor alpha positive mammary tumor cells. Breast Cancer Research2017.

25. Chamberlin T, Clack M, Silvers C, Kuziel G, Thompson V, Johnson H, et al. Targeting Obesity-Induced Macrophages during Preneoplastic Growth Promotes Mammary Epithelial Stem/Progenitor Activity, DNA Damage, and Tumor Formation. Cancer Res. 2020;80(20):4465-75.

26. Kuziel G, Moore BN, Haugstad GP, Arendt LM. Fibrocytes enhance mammary gland fibrosis in obesity. Faseb j. 2023;37(7):e23049.

27. Wang X, Gray Z, Willette-Brown J, Zhu F, Shi G, Jiang Q, et al. Macrophage inducible nitric oxide synthase circulates inflammation and promotes lung carcinogenesis. Cell Death Discov. 2018;4:46.

28. Lamichhane P, Karyampudi L, Shreeder B, Krempski J, Bahr D, Daum J, et al. IL10 Release upon PD-1 Blockade Sustains Immunosuppression in Ovarian Cancer. Cancer Res. 2017;77(23):6667-78.

29. Xu W, Weng J, Xu M, Zhou Q, Liu S, Hu Z, et al. Chemokine CCL21 determines immunotherapy response in hepatocellular carcinoma by affecting neutrophil polarization. Cancer Immunol Immunother. 2024;73(3):56.

30. Grzywa TM, Sosnowska A, Matryba P, Rydzynska Z, Jasinski M, Nowis D, et al. Myeloid Cell-Derived Arginase in Cancer Immune Response. Front Immunol. 2020;11:938.

31. Riegler J, Gill H, Ogasawara A, Hedehus M, Javinal V, Oeh J, et al. VCAM-1 Density and Tumor Perfusion Predict T-cell Infiltration and Treatment Response in Preclinical Models. Neoplasia. 2019;21(10):1036-50.

32. Trapani JA. Granzymes: a family of lymphocyte granule serine proteases. Genome Biol. 2001;2(12):Reviews3014.

33. Rönnberg E, Calounova G, Guss B, Lundequist A, Pejler G. Granzyme D is a novel murine mast cell protease that is highly induced by multiple pathways of mast cell activation. Infect Immun. 2013;81(6):2085-94.

34. Ahmed FS, Gaule P, McGuire J, Patel K, Blenman K, Pusztai L, et al. PD-L1 Protein Expression on Both Tumor Cells and Macrophages are Associated with Response to Neoadjuvant Durvalumab with Chemotherapy in Triple-negative Breast Cancer. Clin Cancer Res. 2020;26(20):5456-61.

35. Boman C, Zerdes I, Mårtensson K, Bergh J, Foukakis T, Valachis A, et al. Discordance of PD-L1 status between primary and metastatic breast cancer: A systematic review and meta-analysis. Cancer Treat Rev. 2021;99:102257.

36. Hsieh CH, Jian CZ, Lin LI, Low GS, Ou PY, Hsu C, et al. Potential Role of CXCL13/CXCR5 Signaling in Immune Checkpoint Inhibitor Treatment in Cancer. Cancers (Basel). 2022;14(2).

37. Odagiu L, May J, Boulet S, Baldwin TA, Labrecque N. Role of the Orphan Nuclear Receptor NR4A Family in T-Cell Biology. Front Endocrinol (Lausanne). 2020;11:624122.

38. Lee DH, Jaggi U, Ghiasi H. CCR2+ migratory macrophages with M1 status are the early-responders in the cornea of HSV-1 infected mice. PLoS One. 2019;14(4):e0215727.

39. Lv Q, Zhang Y, Gao W, Wang J, Hu Y, Yang H, et al. CSF1R inhibition reprograms tumor-associated macrophages to potentiate anti-PD-1 therapy efficacy against colorectal cancer. Pharmacol Res. 2024;202:107126.

40. Kuonen F, Laurent J, Secondini C, Lorusso G, Stehle JC, Rausch T, et al. Inhibition of the Kit ligand/c-Kit axis attenuates metastasis in a mouse model mimicking local breast cancer relapse after radiotherapy. Clin Cancer Res. 2012;18(16):4365-74.

41. D'Alterio C, Buoncervello M, Ieranò C, Napolitano M, Portella L, Rea G, et al. Targeting CXCR4 potentiates anti-PD-1 efficacy modifying the tumor microenvironment and inhibiting neoplastic PD-1. J Exp Clin Cancer Res. 2019;38(1):432.

42. Schreiber TH, Wolf D, Bodero M, Gonzalez L, Podack ER. T cell costimulation by TNFR superfamily (TNFRSF)4 and TNFRSF25 in the context of vaccination. J Immunol. 2012;189(7):3311-8.

43. Qi Y, Zhang W, Jiang R, Xu O, Kong X, Zhang L, et al. Efficacy and safety of PD-1 and PD-L1 inhibitors combined with chemotherapy in randomized clinical trials among triple-negative breast cancer. Front Pharmacol. 13. Switzerland: Copyright © 2022 Qi, Zhang, Jiang, Xu, Kong, Zhang, Fang, Wang and Wang.; 2022. p. 960323.

44. Hammerl D, Martens JWM, Timmermans M, Smid M, Trapman-Jansen AM, Foekens R, et al. Spatial immunophenotypes predict response to anti-PD1 treatment and capture distinct paths of T cell evasion in triple negative breast cancer. Nat Commun. 2021;12(1):5668.

45. Terranova-Barberio M, Pawlowska N, Dhawan M, Moasser M, Chien AJ, Melisko ME, et al. Exhausted T cell signature predicts immunotherapy response in ER-positive breast cancer. Nature communications. 2020;11(1):3584.

46. Khan O, Giles JR, McDonald S, Manne S, Ngiow SF, Patel KP, et al. TOX transcriptionally and epigenetically programs CD8(+) T cell exhaustion. Nature. 2019;571(7764):211-8.

47. Zhu YD, Lu MY. Increased expression of TNFRSF14 indicates good prognosis and inhibits bladder cancer proliferation by promoting apoptosis. Mol Med Rep. 2018;18(3):3403-10.

48. Szekely B, Bossuyt V, Li X, Wali VB, Patwardhan GA, Frederick C, et al. Immunological differences between primary and metastatic breast cancer. Ann Oncol. 2018;29(11):2232-9.

49. Zhu L, Narloch JL, Onkar S, Joy M, Broadwater G, Luedke C, et al. Metastatic breast cancers have reduced immune cell recruitment but harbor increased macrophages relative to their matched primary tumors. J Immunother Cancer. 2019;7(1):265.

50. Sharma SK, Chintala NK, Vadrevu SK, Patel J, Karbowniczek M, Markiewski MM. Pulmonary alveolar macrophages contribute to the premetastatic niche by suppressing antitumor T cell responses in the lungs. J Immunol. 2015;194(11):5529-38.

51. Zhu Y, Knolhoff BL, Meyer MA, Nywening TM, West BL, Luo J, et al. CSF1/CSF1R blockade reprograms tumor-infiltrating macrophages and improves response to T-cell checkpoint immunotherapy in pancreatic cancer models. Cancer Res. 2014;74(18):5057-69.

52. Lin L, Chen S, Wang H, Gao B, Kallakury B, Bhuvaneshwar K, et al. SPTBN1 inhibits inflammatory responses and hepatocarcinogenesis via the stabilization of SOCS1 and downregulation of p65 in hepatocellular carcinoma. Theranostics. 2021;11(9):4232-50.

53. Neubert NJ, Schmittnaegel M, Bordry N, Nassiri S, Wald N, Martignier C, et al. T cell-induced CSF1 promotes melanoma resistance to PD1 blockade. Sci Transl Med. 2018;10(436).

54. Cai H, Zhang Y, Wang J, Gu J. Defects in Macrophage Reprogramming in Cancer Therapy: The Negative Impact of PD-L1/PD-1. Front Immunol. 2021;12:690869.

55. Wang L, Guo W, Guo Z, Yu J, Tan J, Simons DL, et al. PD-L1-expressing tumor-associated macrophages are immunostimulatory and associate with good clinical outcome in human breast cancer. Cell Rep Med. 2024;5(2):101420.

56. Saung MT, Muth S, Ding D, Thomas DL, 2nd, Blair AB, Tsujikawa T, et al. Targeting myeloid-inflamed tumor with anti-CSF-1R antibody expands CD137+ effector T-cells in the murine model of pancreatic cancer. J Immunother Cancer. 2018;6(1):118.

57. Zong Z, Zou J, Mao R, Ma C, Li N, Wang J, et al. M1 Macrophages Induce PD-L1 Expression in Hepatocellular Carcinoma Cells Through IL-1β Signaling. Front Immunol. 2019;10:1643.

58. Gombos A, Goncalves A, Curigliano G, Bartsch R, Kyte JA, Ignatiadis M, et al. How I treat endocrine-dependent metastatic breast cancer. ESMO Open. 2023;8(2):100882.

59. Herzog SK, Fuqua SAW. ESR1 mutations and therapeutic resistance in metastatic breast cancer: progress and remaining challenges. Br J Cancer. 2022;126(2):174-86.

60. Chakraborty B, Byemerwa J, Krebs T, Lim F, Chang CY, McDonnell DP. Estrogen Receptor Signaling in the Immune System. Endocr Rev. 2023;44(1):117-41.

CHAPTER 5:

Conclusions and Future Directions

Conclusions:

In Chapter 2, we explored how obesity interacts with other breast cancer risk factors such as breast density to alter the non-tumor bearing mammary gland and tumorigenesis in the context of collagen deposition and immune recruitment. Using a HFD-induced model of obesity and mice that express a mutation leading to accumulation of collagen, we found obesity increases collagen around ducts compared to their LFD-fed counterparts. Increased collagen around ducts could increase overall breast cancer risk by increasing the invasiveness of epithelium (1). We confirmed previous reports of increased macrophage-driven inflammation within obese mammary glands (2). This was measured by increased F4/80+ cells surrounding mammary ducts and increased macrophages forming CLS around adipocytes. CD8+ T cell recruitment within non-tumor-bearing glands was also reduced in a diet-dependent manner.

To model how these risk factors affected breast cancer progression, we utilized the MMTV-PyMT model of spontaneous mammary tumor growth. Overall, we did not see an effect on progression due to risk factors on this model at 9 weeks nor did we see differences in tumor growth at 15 weeks. However, metastasis to the lungs was significantly enhanced at 15 weeks in mice with both risk factors compared to LFD/WT and HFD/WT mice. Early in tumor formation, we did not observe differences in macrophages. However, as tumors formed, there were significant increases in F4/80+ macrophages around tumors of mice with either risk factor.

Overall, Chapter 2 shows that **(1) a combination of breast density and obesity together can enhance macrophage inflammation and collagen deposition that may increase breast cancer risk beyond one risk factor alone. (2) During the progression of breast cancer, both risk factors together seem to promote metastasis to the lung, which may translate to an overall poorer survival outcome in patients with both conditions at the time of breast cancer development.**

Obesity also contributes to more metastasis in breast cancer patients, particularly to the lungs. In Chapter 3, we explored the phenotype of CD8+ T cells before and after ERα+ breast cancer metastasis to the lungs. In non-tumor bearing mice, we discovered that although CD8+ T cell numbers are not different between LFD or HFD fed mice in the lung, CD8+ T cells in obese mice had higher expression of PD-1 and had impaired responses to *in vitro* stimulation. CD8+ T cells from HFD-fed mice did not produce significantly higher levels of TNF-α in response to stimulation, whereas CD8+ LFD-fed mice robustly responded to stimulation and produced significant amounts of TNF-α. RNA analysis from NanoString nCounter Immune Exhaustion Panel revealed that T cells in non-tumor bearing mice in the lungs had increased T cell receptor signaling (TCR) and upregulation of some genes of T cell immune checkpoints such as *Tigit*. Overall, the dysfunctional response to stimulation coupled with increased immune checkpoint expression may point to obesity promoting T cell exhaustion in CD8+ T cells prior to tumor burden and metastasis. This could create a pre-metastatic niche that is more conductive for metastasis.

Mice orthotopically injected with ERα+ mammary tumor cells showed differential immune responses in the lungs of HFD-fed mice compared to LFD-fed mice. Total

immune infiltration measured by an increase in total CD45+ cells was higher in HFD-fed mice after metastasis. Similar to non-tumor bearing mice, lungs from HFD-fed mice with metastasis had an increase of PD1+ CD8+ T cells. Lungs with metastases from HFD-fed mice showed a significant increase in Tregs which may play a role in immunosuppression (3). Expression analysis of CD45+ immune cells isolated from the metastatic lungs of HFD-fed mice revealed increases in T cell receptor signaling and cytotoxicity but downregulation of IFN signaling and TNF signaling. These results indicated, that despite increased T cell receptor activation, there may be an impairment of cytokine production by CD8+ T cells. To test this, we repeated the stimulation of CD8+ T cells isolated from lungs with TC2 metastasis. Surprisingly, CD8+ T cells from HFD-fed mice responded to stimulation to produce high levels of TNF-α. This suggests despite PD-1 expression, CD8+ T cells in metastasis might retain some function in obesity. Since genes associated with T cell exhaustion were not upregulated in our NanoString analysis, we propose that in HFD-fed mice, after metastasis CD8+ T cells may have a different exhausted-like phenotype.

Pathways such as IFN signaling, TNF signaling, and cytotoxicity are not all T cell specific, and it is possible that other cell types may be involved since we analyzed the whole CD45+ population. Therefore, decreased cytokine signaling could be due to other cell types. We also observed an upregulation of genes associated with natural killer (NK) cell exhaustion and increased B cell receptor (BCR signaling). Thus, NK cells and B cells could play a role in immune cell dysfunction in lung metastasis in HFD-fed mice. Further studies are needed to explore how NK cell and B cell function could contribute to worse metastatic disease in HFD-fed mice. Chapter 3 highlights that **(1) Obesity**

impairs CD8+ T cell function to an exhausted-like state in the lungs of non-tumor bearing mice. (2) After metastasis, CD8+ T cells in the lungs of obese mice express PD-1, but they retain function after *in vitro* stimulation, which indicates that they may have a different T cell phenotype following metastasis. (3) NK and B cells may contribute to metastatic progression in HFD-fed mice.

In Chapter 4, we investigated how anti-PD-1 and anti-CSF-1R antibodies affect immune responses in TC2 ERα+ metastasis in obese and lean mice. In LFD-fed mice treated with anti-PD-1 antibodies alone reduced lung metastasis but not HFD-fed mice. To further investigate how immune cells change within metastasis to the lung, we sorted CD45+ from TC2 tumor bearing mice treated with IgG or anti-PD-1 antibodies. Analysis from the NanoString immune exhaustion panel revealed that anti-PD-1 therapy increased genes associated with cytotoxicity but only in LFD-fed mice. In HFD-fed mice, immune checkpoints such as *Lag-3* and *Tigit* were upregulated, indicating exhaustion in response to anti-PD-1 antibodies in obese mice. Coinciding with this data, only LFD-fed mice had a reduction in lung metastasis. Although HFD-fed mice were the only group that saw increases in CD8+ T cells after anti-PD-1 antibody treatment, these T cells were exhausted in HFD-fed mice. HFD-fed mice also showed a trending increase in PD-L1+ myeloid cells. Previous studies have shown an increase of immunosuppressive myeloid cells within lung metastasis of HFD-fed mice (4, 5). To see if macrophages could be playing this immunosuppressive role and inhibiting responses to anti-PD-1 inhibitors, we co-cultured macrophages isolated from ERα+ metastasis from HFD or LFD-fed mice with control splenic CD8+ T cells. Macrophages from HFD-fed mice

reduced TNF-α expression in unstimulated CD8+ T cells. Thus, these macrophages could be playing an inhibitory role.

To deplete macrophages, we used anti-CSF-1R antibodies. In mice with intact tumors, CSF-1R treatment did not significantly reduce tumor growth in either obese or lean mice. However, we hypothesized it could affect the progression of metastatic disease in the lungs. NanoString analysis with the Myeloid Innate Immunity Panel revealed LFD-fed mice had increased lymphocyte activation in response to anti-CSF-1R antibody treatment. Chemokines related to monocyte recruitment and immune evasion were downregulated in both LFD and HFD-fed mice but different chemokines were altered in mice from the different diet groups. HFD-fed mice had a reduction in cytokines involved with immunosuppression. Thus, further investigation was warranted to determine whether HFD or LFD-fed mice would have better responses to anti-CSF-1R antibody treatment alone. We analyzed immune cells via flow cytometry between anti-CSF-1R or IgG antibody treated groups. CSF-1R inhibition increased CD45+ and CD11b+ cells in HFD-fed mice only and reduced PD-L1+ myeloid cells. Therefore, in obesity, CSF-1R treatment improves inflammatory responses more than in LFD-fed mice. To match this change in immune cell response, HFD-fed anti-CSF-1R treated mice had reduced metastasis, but this was not significant compared to HFD-fed IgG controls. However, anti-CSF-1R treatment increased PD-1+ CD8+ T cells and had increased levels of PD-L1+ metastasis. Therefore, HFD-fed mice might benefit more from a dual anti-CSF-1R, anti-PD-1 combination therapy than LFD-fed mice.

To test if HFD-fed mice would benefit from dual macrophage depletion and PD-1/PD-L1 blockade, we treated mice with resected tumors with a loading does of anti-

CSF-1R to deplete macrophages before anti-PD-1 treatment. Mice then received anti-CSF-1R and anti-PD-1 antibodies together. HFD-fed mice, as hypothesized, had the best responses to dual immunotherapy. HFD-fed mice saw an increase in total CD45+ immune cells in response to dual therapy, which was not seen in LFD-fed mice. HFD-fed mice also had reduced metastasis in response to dual therapy compared to LFD-fed mice on dual immunotherapy. Overall, obesity had more robust responses to dual immunotherapy than LFD-fed mice by increasing immune recruitment. **In Chapter 4, we conclude (1) Under conditions of obesity, responses to anti-PD-1 antibodies are limited. (2) Obese mice had more robust responses to anti-CSF-1R in the lungs which was due in part due to increased inflammation and reduction immunosuppressive macrophages and PD-L1+ myeloid cells. (3) Obese mice also had more robust responses to a dual combination of anti-CSF-1R and anti-PD-1 antibodies within lung metastasis.**

This body of work still leaves many unanswered questions regarding obesity's role in breast cancer risk, progression to metastasis, and its effects on immunotherapy responses. Below is a summary of further experiments that would uncover answers to lingering questions. In addition, this thesis points to new avenues of investigation for future work understanding obesity-associated breast cancer for the benefit of future patients.

Future Directions:

Investigating the effects of obesity and breast density on breast cancer risk and progression

To investigate the relationship between obesity and breast density to impact breast cancer risk, we should further quantify collagen deposition in mammary glands of LFD and HFD-fed WT and Het mice in the surrounding stroma and adipose tissue. We were surprised that we did not observe significant differences in collagen surrounding the mammary ducts of LFD-fed Het mice at the early or late time point. The significant increases in collagen surrounding mammary ducts in HFD-fed mice points to a possible difference in pattern in collagen deposition between obesity and this transgenic model, which could be studied using different imaging modalities such as second harmonic generation microscopy to identify changes to the organization of the collagen. These differences could point to new avenues of study on collagen deposition patterns in the non-tumor bearing mammary gland and its effects on breast cancer risk.

We also did not look at intrinsic differences in epithelial cells within the mammary gland of PyMT- mice. Markers like Ki67, which can be measured via immunohistochemistry, could identify potential differences proliferation in epithelial cells among the groups which have been shown to increase breast cancer risk in premenopausal women (6, 7). Further, quantification of estrogen receptor (ER) could identify potential risk of ERα+ breast cancer, however, the data linking ER expression to breast cancer risk is inconsistent (7). Cells that express both Ki67 and ER correlated with increasing age and were present in high-risk DCIS lesions, therefore they may be involved in the early stages of developing breast cancer (8). Identifying these cells could further give insight to how these risk factors together could contribute risk. ER expression is increased in epithelial cells under obese conditions in non-tumor bearing mammary glands (9). In contrast, breast density is associated with stromal expression

of ER rather than increased epithelial expression of ER (10, 11). Both breast density and obesity are associated with the development of ERα+ breast cancer (12, 13). Thus, both risk factors together could transform epithelium to a luminal Ki67/ER+ state and ERα+ stroma to increase the risk of ERα+ breast cancer.

While we did not perform any assays to identify functional changes in immune cells like macrophages or CD8+ T cells in PyMT- and PyMT+ mammary glands. A cytokine array within PyMT- and PyMT+ glands could give an insight to what cytokines are being produced by both myeloid and adaptive immune cells between glands under the influence of different risk factors. Further, flow cytometry would aid in identifying other immune cells that change due to breast density and obesity. This approach would provide an opportunity to look at makers associated with macrophage polarization such as MHCII and CD80/CD86 to identify M1 macrophages and CD163 and CD206 to designate M2 macrophages. CCR7 has also been suggested as an M1 marker (14). Although macrophages are increased in both dense mammary glands and obesity, they may have different functions among the groups. In non-tumor bearing mammary glands, we also saw lower CD8+ T cell recruitment in HFD-fed mice but similar levels of CD8+ T cells between LFD-fed groups. Other studies have shown that breast density increased PD-1 expression within the mammary gland (15). Although CD8+ T cells were not different between LFD/WT and LFD/Het groups, there may be differences in function. Exploring CD8+ T cell dysfunction within dense mammary glands may identify how collagen alters CD8+ T cell immune surveillance of pre-neoplastic cells and point to mechanisms that drives breast cancer in dense breast tissue.

We used the MMTV-PyMT+ model to investigate how breast density and obesity interacted to promote tumorigenesis. We did not see any obvious differences with the MMTV-PyMT model and tumor progression in obesity at 9 or 15 weeks of age. We hypothesized that risk factors would affect early lesions and accelerate tumorigenesis in a significant manner by 15 weeks. However, due to the nature of this model and its fast progression to adenocarcinoma, future studies should look at how these risk factors affect MMTV-PyMT at later timepoints, such as 20-30 weeks. At this timepoint, obesity as well as breast density will be well established and may be more likely to affect tumor growth. At 9 weeks, although HFD-fed mice were significantly heavier, obesity levels were higher at 15 weeks. At 15 weeks, we started to see differences in immune cell recruitment around tumors and saw increases in metastasis. We observe peak increases in obesity induced inflammation in the mammary gland at a 16-weeks timepoint, and later timepoints may reveal more differences. However, with mice currently collected for this manuscript, an IHC stain of Ki67 could be used to identify if epithelium from LFD/Het, HFD/WT or HFD/Het tumors have early proliferative capacities. Lastly, due to the link of collagen and tumor invasiveness, we could look at extracellular matrix (ECM) deposition in PyMT+ tumors with these risk factors. Collagen may be enhanced in HFD/Het tumors which metastasized more to the lungs compared to WT obese mice (1).

There are other ways to model breast density and obesity associated mammary tumorigenesis in mice for further *in vivo* exploration. Orthotopically injecting mice with diet-induced obesity, transgenic Col1a1^{tmJae} mice , and Col1a1^{tmJae} mice fed a HFD with tumor cell lines gives opportunity to investigate different subtypes of breast cancer as

well as more flexibility with the latency of tumor growth. To further study these risk factors, MET-1 cells, which are derived from the MMTV-PyMT model and metastasize to the lungs, could be orthotopically injected to model TNBC (16). ERα+ breast cancers could also be studied by using cell lines like TC2 cells, but TC4 and TC11 variants could also be used to see if there are differences between different breast cancer subtypes. After 16 weeks fed either a LFD or HFD, Col1a1^{tmJae} (Het) and WT mice would be orthotopically injected with ERα- or ERα+ cell lines to see the effects of these risk factors on both subtypes.

We observed an increase in metastasis in HFD-fed Het mice compared to LFD-fed WT and Het mice. Although we quantified metastasis number, metastatic area may be larger in HFD-fed Het mice. We did not identify a mechanism for this increased level of metastasis in mice with both risk factors. Further exploration of differences in the extracellular matrix and immune cell recruitment in tumors could help explain these results. However, the changes in the metastatic microenvironment of the lungs could be explored in dual risk factor mice to better understand increased metastasis in these mice. Overall, the interactions of obesity and breast density together on breast cancer risk and metastasis to the lung should continue to be explored.

Defining CD8+ T cells phenotypes before and after breast cancer metastasis under obese and lean conditions

In Chapter 3, we did not fully define the phenotype of CD8+ T cells in the lungs before and after breast cancer metastasis. Our data supports the conclusion that before metastasis, CD8+ T cells from lungs of obese mice are exhausted at some level. While CD8+ T cells had more PD-1 expression in lungs of obese mice before metastasis,

genes associated with T cell exhaustion were not widely upregulated. Before metastasis, we identified an upregulation of gene expression of *Tigit*, which can be seen on exhausted or senescent cells (17, 18). Lower cytokine production and an upregulation of PD-1 after stimulation in HFD-fed mice also matches an exhausted phenotype. Since PD-1 is not associated with senescence, it is likely these T cells are exhausted (19). However, more recent reviews suggest PD-1 expression on senescent cells is controversial (20) In mice with metastasis, CD8+ T cells also expressed more PD-1 in HFD-fed mice. Surprisingly, CD8+ T cells in obese mice showed some retention of cytokine production after stimulation, specifically an ability to produce TNF-α, unlike before metastasis. These results suggested that the phenotype of CD8+ T cells differ after metastatic establishment in the lungs. We were surprised that CD8+ T cells exposed to metastasis produced more cytokines than prior to disease. It's unclear why CD8+ T cells are not effective in eliminating tumor cells in the lungs. Experiments are necessary to identify the mechanisms for these differences and to precisely classify CD8+ T cell populations through genetic, epigenetic, and analysis of identified surface markers for different types of exhaustion or dysfunction.

Recent research suggests that exhausted CD8+ T cells are heterogeneous. It is now understood there are two categories of exhaustion CD8+ T cells defined as progenitor exhausted and terminally exhausted. Progenitor exhausted T cells (Tpex) are stem-like and can be identified by intermediate levels of PD-1. They are express the transcription factor TCF1. Terminally exhausted T cells (Ttex) are differentiated and derived from Tpex (21). Ttex are identified as TCF1- and express high levels of PD-1 and other inhibitory receptors like TIM-3 (22). Ttex cells were found to express more

granzyme B than Tpex cells and had reduced proliferation capacity than Tpex after restimulation (22). Incorporating different exhaustion markers (TIM-3, LAG-3, TIGIT etc.) in our future flow panels, staining for other cytotoxic proteins like granzyme B, and incorporating a test for T cell proliferation, such as by labeling with BrdU, may further define these T cell phenotypes within the lungs of obese and lean mice. Tpex cells respond to anti-PD-1 inhibitors, leading to enhanced proliferation (21). In Chapter 4, we identified anti-PD1 treatment increased CD8+ T cells in obese metastasis but not in lean mice. It is worthwhile to identify if there is a change in CD8+ T populations after metastasis to increase Tpex. Identifying Tpex in the lungs after metastasis under conditions of obesity may provide a biomarker for treatment of advanced ERα+ disease with ICB.

Generally, senescent T cells are not thought to respond to stimulation or express PD-1. However, obesity increases PD-1+ senescent-like T cells in adipose tissue (23). As a future point of exploration, we did not confirm that senescent CD8+ T cells are not present in metastasis. It is possible senescent cells made up a portion of the PD-1- CD8+ population in the lungs or senescent-like PD-1+ cells could be present. β-galactosidase is a reliable marker for cellular senescence that could be identified by IF staining or flow cytometry. Coupling β-galactosidase with quantification of intracellular cytokines and proliferation markers using flow cytometry would solidify the identity of senescent CD8+ T cells.

How do other cells in the adaptive immune system play a role in breast cancer metastasis under the conditions of obesity?

In Chapter 3, we identified that NK cells may be exhausted in the lungs of HFD-fed mice with metastasis. A future direction would be to explore in-depth NK cell function within metastasis. We could quantify NK cells via IF staining to see if NK cells are reduced in the lungs of obese mice before and after ER+ metastasis. Markers like CD161 are found on a majority of NK cells and are associated with activated NK cells which have higher proliferative capacities (24). It is possible that there are less CD161+ NK cells in the lungs of obese mice, particularly with metastasis.

NK cells may be important in the context of understanding why obese patients have better responses to PD-1/PD-L1 inhibitors (25). NK cells also express PD-1, and this expression should be explored in metastasis in the context of obesity (25, 26). It has been shown NK cells can inhibit ICB responses in melanoma lung metastasis (27). It is a fascinating avenue to investigate NK cell phenotypes, like exhaustion, within breast cancer metastasis under obese conditions and how these phenotypes relate to immunotherapy responses.

It is likely other compartments of the immune system are impaired in metastatic disease in obesity. We also saw in chapter 3 an increase in B cell receptor (BCR) signaling. B cells can also have an exhausted phenotype and may contribute to metastatic growth in obese mice (28). B cells can also express PD-1, and PD-1+ B cells can contribute to T cell dysfunction (29). Exploring B cell numbers with markers like CD19 and CD20 could identify B cells within metastasis to see if they are increased or reduced under obese conditions. It is clear that CD8+ T cells are not the only

contributing factor to immune evasion of metastasis and response to PD-1/PDL-1 inhibitors and understanding the function of other cell types could help to predict ICB therapy responses.

Explore macrophage populations in obese lungs before and after metastasis

In Chapter 4, we identified that CSF-1R+ macrophages impacted the metastatic microenvironment differently between obese and lean mice. Although blocking CSF-1/CSF-1R is generally thought to decrease M2 macrophages, the phenotype of CSF-1R+ macrophages has not been explored under conditions of obesity (30). However, CSF-1R treatment reduced PD-L1+ myeloid cells in the lungs of obese mice. PD-L1+ macrophages are classically thought to be immunosuppressive, there may be differences between PD-L1-/low macrophages and PD-L1+/high and their ability to activate T cells (31). Our results, showing depletion of macrophages and subsequent increase in total immune cell recruitment after anti- CSF-1R treatment may suggest PD-L1+ macrophages were immunosuppressive in HFD mice, as we suggested in Chapter 4. However, the possibility that M1-macrophages may also be playing a role in obese metastasis should further be explored with markers mentioned above.

How does adaptive immune cell dysfunction play a role in mammary tumors?

The focus of this dissertation was mostly on the metastatic microenvironment rather than the tumor microenvironment under the influence of obesity. In Chapter 2, we observed that obesity increased macrophages and reduced intertumoral CD8+ T cell infiltration. Supporting studies with EO771 cells saw reduce CD8+ T cells in tumors of obese mice (32). Others have shown that CD8+ T cells express less granzyme B

(GzmB) in mammary tumors of obese mice which may suggest T cell dysfunction (33). Further studies could explore how obesity alters CD8+ T cells in the tumor microenvironment of ER+ tumors. Increased macrophages due to obesity have not been seen in all models of breast cancer, and we have not observed increased macrophages in TC2 tumors (34). Although the total number macrophages may not be different in certain breast cancer subtypes or stages, polarization may be different (34). Obesity has been shown to decrease the ratio of M1/M2 polarized macrophages in tumors (32). Reducing M1/M2 ratios are thought to be tumor promoting, but it is unclear under obese conditions how this could affect immunotherapy responses to ICB. Further studies are needed to understand the tumor microenvironment of different subtypes of breast cancer under obese conditions. Further, how this effects responses to anti-PD-1 and anti-CSF-1R treatment should be explored as we saw different responses in the primary tumor compared to metastatic environments like the lungs.

In obese conditions, do other therapy combinations improve responses to anti-PD-1 therapies?

There are plenty of opportunities to pair anti-PD-1 or anti-PD-L1 inhibitors with other therapies to improve responses to lung metastasis in lean and obese patients with breast cancer. In this work, we mostly focused on ERα+ tumor models as little is known about ICB response in ERα+ breast cancer. A limitation to Chapter 4, is that most patients receive standard of care or a combination of therapies before receiving experimental immunotherapy combinations. The standard of care for advanced metastatic ERα+ breast cancer is endocrine therapy, usually with multiple different types including tamoxifen, aromatase inhibitors, and fulvestrant coupled with cyclin-dependent

kinases (CDK) 4/6 inhibitors after surgery (35, 36). Palliative chemotherapy is offered if endocrine resistance occurs (35). Standard of care endocrine therapies could alter the efficacy of ICB. In a lung cancer model, anti-estrogen fulvestrant and a pan-HER inhibitor dacomitinib reduced IFN-γ and TNF-α production by CD8+ T cells and increased PD-1 expression. Combining fulvetrant, dacomitinib, and anti-PD-1 was more efficacious than fulvestrant and dacomitinib alone (37). Immune cells express ERα and ERβ and ER/ER2 signaling play a pivotal role in the differentiation of immune cells (38). ER signaling by the immune system has been linked to more autoimmune disease in women (39). Further, anti-PD-1 inhibitors have been linked to enhanced efficacy in men (40). Despite these trends, women with ERα+ breast cancer that have blocked ER/E2 signaling may benefit from PD-1 inhibitors. The effect of ER is profound on the immune system, this opens the door for fulvestrant use in ER subtypes of breast cancer in combination with anti-PD-1/PD-L1 inhibitors. Preclinical models have already begun to explore fulvestrant use in combination with radiation and anti-PD-L1 in ERα+ breast cancer, showing decreased tumor volumes compared to radiation therapy and anti-PD-L1 alone (41). How obesity effects this combination of therapies is currently unknown. Overall, the complex biology of estrogen signaling and immune checkpoint signaling under the influence of obesity should further be explored.

References:

1. Provenzano PP, Inman DR, Eliceiri KW, Knittel JG, Yan L, Rueden CT, et al. Collagen density promotes mammary tumor initiation and progression. BMC Med. 2008;6:11.

2. Chamberlin T, Thompson V, Hillers-Ziemer LE, Walton BN, Arendt LM. Obesity reduces mammary epithelial cell TGFβ1 activity through macrophage-mediated extracellular matrix remodeling. Faseb j. 2020.

3. Chen ML, Pittet MJ, Gorelik L, Flavell RA, Weissleder R, von Boehmer H, et al. Regulatory T cells suppress tumor-specific CD8 T cell cytotoxicity through TGF-beta signals in vivo. Proc Natl Acad Sci U S A. 2005;102(2):419-24.

4. McDowell SAC, Milette S, Doré S, Yu MW, Sorin M, Wilson L, et al. Obesity alters monocyte developmental trajectories to enhance metastasis. J Exp Med. 2023;220(8).

5. Hillers-Ziemer LE, Williams AE, Janquart A, Grogan C, Thompson V, Sanchez A, et al. Obesity-Activated Lung Stromal Cells Promote Myeloid Lineage Cell Accumulation and Breast Cancer Metastasis. Cancers (Basel). 2021;13(5).

6. Huh SJ, Oh H, Peterson MA, Almendro V, Hu R, Bowden M, et al. The Proliferative Activity of Mammary Epithelial Cells in Normal Tissue Predicts Breast Cancer Risk in Premenopausal Women. Cancer Res. 2016;76(7):1926-34.

7. Oh H, Eliassen AH, Wang M, Smith-Warner SA, Beck AH, Schnitt SJ, et al. Expression of estrogen receptor, progesterone receptor, and Ki67 in normal breast tissue in relation to subsequent risk of breast cancer. NPJ Breast Cancer. 2016;2:16032-.

8. Shoker BS, Jarvis C, Clarke RB, Anderson E, Hewlett J, Davies MP, et al. Estrogen receptor-positive proliferating cells in the normal and precancerous breast. Am J Pathol. 1999;155(6):1811-5.

9. Chamberlin T, D'Amato JV, Arendt LM. Obesity reversibly depletes the basal cell population and enhances mammary epithelial cell estrogen receptor alpha expression and progenitor activity. Breast Cancer Res. 2017;19(1):128.

10. Gabrielson M, Chiesa F, Paulsson J, Strell C, Behmer C, Rönnow K, et al. Amount of stroma is associated with mammographic density and stromal expression of oestrogen receptor in normal breast tissues. Breast Cancer Res Treat. 2016;158(2):253-61.

11. Ghosh K, Brandt KR, Reynolds C, Scott CG, Pankratz VS, Riehle DL, et al. Tissue composition of mammographically dense and non-dense breast tissue. Breast Cancer Res Treat. 2012;131(1):267-75.

12. Conroy SM, Pagano I, Kolonel LN, Maskarinec G. Mammographic density and hormone receptor expression in breast cancer: the Multiethnic Cohort Study. Cancer Epidemiol. 2011;35(5):448-52.

13. Menikdiwela KR, Kahathuduwa C, Bolner ML, Rahman RL, Moustaid-Moussa N. Association between Obesity, Race or Ethnicity, and Luminal Subtypes of Breast Cancer. Biomedicines. 2022;10(11).

14. Kwiecień I, Polubiec-Kownacka M, Dziedzic D, Wołosz D, Rzepecki P, Domagała-Kulawik J. CD163 and CCR7 as markers for macrophage polarization in lung cancer microenvironment. Cent Eur J Immunol. 2019;44(4):395-402.

15. Huo CW, Hill P, Chew G, Neeson PJ, Halse H, Williams ED, et al. High mammographic density in women is associated with protumor inflammation. Breast Cancer Research2018.

16. Christenson JL, Butterfield KT, Spoelstra NS, Norris JD, Josan JS, Pollock JA, et al. MMTV-PyMT and Derived Met-1 Mouse Mammary Tumor Cells as Models for Studying the Role of the Androgen Receptor in Triple-Negative Breast Cancer Progression. Horm Cancer. 2017;8(2):69-77.

17. Kong Y, Zhu L, Schell TD, Zhang J, Claxton DF, Ehmann WC, et al. T-Cell Immunoglobulin and ITIM Domain (TIGIT) Associates with CD8+ T-Cell Exhaustion and Poor Clinical Outcome in AML Patients. Clin Cancer Res. 2016;22(12):3057-66.

18. Song Y, Wang B, Song R, Hao Y, Wang D, Li Y, et al. T-cell Immunoglobulin and ITIM Domain Contributes to CD8(+) T-cell Immunosenescence. Aging Cell. 2018;17(2).

19. J C, H S, TH W, Z T, W Z. T cell anergy, exhaustion, senescence, and stemness in the tumor microenvironment. Current opinion in immunology. 2013;25(2).

20. Kasamatsu T. Implications of Senescent T Cells for Cancer Immunotherapy. Cancers (Basel). 2023;15(24).

21. Blank CU, Haining WN, Held W, Hogan PG, Kallies A, Lugli E, et al. Defining 'T cell exhaustion'. Nat Rev Immunol. 2019;19(11):665-74.

22. Miller BC, Sen DR, Al Abosy R, Bi K, Virkud YV, LaFleur MW, et al. Subsets of exhausted CD8(+) T cells differentially mediate tumor control and respond to checkpoint blockade. Nat Immunol. 2019;20(3):326-36.

23. Shirakawa K, Yan X, Shinmura K, Endo J, Kataoka M, Katsumata Y, et al. Obesity accelerates T cell senescence in murine visceral adipose tissue. J Clin Invest. 2016;126(12):4626-39.

24. Kurioka A, Cosgrove C, Simoni Y, van Wilgenburg B, Geremia A, Björkander S, et al. CD161 Defines a Functionally Distinct Subset of Pro-Inflammatory Natural Killer Cells. Front Immunol. 2018;9:486.

25. Quatrini L, Mariotti FR, Munari E, Tumino N, Vacca P, Moretta L. The Immune Checkpoint PD-1 in Natural Killer Cells: Expression, Function and Targeting in Tumour Immunotherapy. Cancers (Basel). 2020;12(11).

26. Sivori S, Pende D, Quatrini L, Pietra G, Della Chiesa M, Vacca P, et al. NK cells and ILCs in tumor immunotherapy. Mol Aspects Med. 2021;80:100870.

27. Nakamura T, Sato T, Endo R, Sasaki S, Takahashi N, Sato Y, et al. STING agonist loaded lipid nanoparticles overcome anti-PD-1 resistance in melanoma lung metastasis via NK cell activation. J Immunother Cancer. 2021;9(7).

28. Roe K. NK-cell exhaustion, B-cell exhaustion and T-cell exhaustion-the differences and similarities. Immunology. 2022;166(2):155-68.

29. Wang X, Wang G, Wang Z, Liu B, Han N, Li J, et al. PD-1-expressing B cells suppress CD4(+) and CD8(+) T cells via PD-1/PD-L1-dependent pathway. Mol Immunol. 2019;109:20-6.

30. Wen J, Wang S, Guo R, Liu D. CSF1R inhibitors are emerging immunotherapeutic drugs for cancer treatment. Eur J Med Chem. 2023;245(Pt 1):114884.

31. Wang L, Guo W, Guo Z, Yu J, Tan J, Simons DL, et al. PD-L1-expressing tumor-associated macrophages are immunostimulatory and associate with good clinical outcome in human breast cancer. Cell Rep Med. 2024;5(2):101420.

32. Núñez-Ruiz A, Sánchez-Brena F, López-Pacheco C, Acevedo-Domínguez NA, Soldevila G. Obesity modulates the immune macroenvironment associated with breast cancer development. PLoS One. 2022;17(4):e0266827.

33. Zhang C, Yue C, Herrmann A, Song J, Egelston C, Wang T, et al. STAT3 Activation-Induced Fatty Acid Oxidation in CD8(+) T Effector Cells Is Critical for Obesity-Promoted Breast Tumor Growth. Cell Metab. 2020;31(1):148-61.e5.

34. Kuziel G, Moore BN, Haugstad GP, Xiong Y, Williams AE, Arendt LM. Alterations in the mammary gland and tumor microenvironment of formerly obese mice. BMC Cancer. 2023;23(1):1183.

35. Gombos A, Goncalves A, Curigliano G, Bartsch R, Kyte JA, Ignatiadis M, et al. How I treat endocrine-dependent metastatic breast cancer. ESMO Open. 2023;8(2):100882.

36. Herzog SK, Fuqua SAW. ESR1 mutations and therapeutic resistance in metastatic breast cancer: progress and remaining challenges. Br J Cancer. 2022;126(2):174-86.

37. Almotlak AA, Farooqui M, Soloff AC, Siegfried JM, Stabile LP. Targeting the ERβ/HER Oncogenic Network in KRAS Mutant Lung Cancer Modulates the Tumor

Microenvironment and Is Synergistic with Sequential Immunotherapy. Int J Mol Sci. 2021;23(1).

38. Chakraborty B, Byemerwa J, Krebs T, Lim F, Chang CY, McDonnell DP. Estrogen Receptor Signaling in the Immune System. Endocr Rev. 2023;44(1):117-41.

39. Moulton VR. Sex Hormones in Acquired Immunity and Autoimmune Disease. Front Immunol. 2018;9:2279.

40. Hu W, Qian X, Wang S, Gao L, Xu J, Yan J. Sex - a potential factor affecting immune checkpoint inhibitor therapy for cancers. Front Immunol. 2022;13:1024112.

41. O'Leary KA, Bates AM, Jin WJ, Burkel BM, Sriramaneni RN, Emma SE, et al. Estrogen receptor blockade and radiation therapy cooperate to enhance the response of immunologically cold ER+ breast cancer to immunotherapy. Breast Cancer Res. 2023;25(1):68.

CHAPTER 6

When your immune system helps cancer grow: A story of obesity and breast cancer

Communicating Science to a broader audience as part of the Wisconsin Initiative for Science Literacy Program

To the reader:

I decided to conclude my Ph.D. dissertation with a chapter dedicated to you, a non-expert in the field of obesity-associated breast cancer, so my work can reach a broader audience. This chapter is brought to you thanks to the Wisconsin Initiative for Science Literacy (WISL) at UW-Madison. This chapter gives you a non-technical explanation of my thesis entitled “Obesity enhances breast cancer risk, metastasis, and response to Immunotherapy.”

Science communication is an important part of being an effective scientist. Our work cannot benefit you if you are not able to access the information. In recent years, with the widespread use of the internet and multiple media sources, it is very easy for scientific information to be misrepresented, unbeknown to the person enjoying that content. As scientists, we often focus on the gritty details of what questions we are trying to answer. Most of our day-to-day communication about our science is with other scientists that have similar expertise to our own. We sometimes forget how to communicate with non-scientists. It is an art to communicate research, specifically biomedical research in my case, to a non-expert. Science is its own language, and it takes years to learn. However, it doesn’t have to be inaccessible to you.

During my Ph.D., the COVID-19 pandemic highlighted a failure of scientific communication to the public by scientists. This in turn resulted in deaths that were likely preventable. With improved scientific education and communication, the public will be able to know how to protect themselves from the latest public health threat, as well as help communicate to others how to do the same. I know everyone cannot fall in love with science as much as me, but I hope everyone can find a trusted friend in science,

and is able to understand, enjoy, and benefit from when she reveals her exciting new secrets.

Introduction:

Many families have been affected by breast cancer. You may be familiar with the pink folded ribbon, a recognizable symbol for breast cancer awareness, but you may not know what health factors could increase your chances for developing this disease. Two of those risk factors, which were the focus of my dissertation, are breast density and obesity. Some women that have high breast density may become obese in their lifetime. It is unknown how these risk factors together might affect breast cancer risk. Not only do higher breast density and obesity affect the likelihood of developing breast cancer, but they also can affect how breast cancer grows and spreads.

Cancer is an overgrowth of the body's own cells until they form a **tumor,** or mass. Breast cancer is an overgrowth of breast cells, or **epithelium**. In humans, obesity has been shown to increase both breast cancer tumor size and the cancer's ability to spread, or **metastasize**, to the lungs. Cancer metastasis is often fatal for cancer patients. It is currently unknown why obese patients have larger tumors at diagnosis, and more metastasis to the lung. Women with dense breasts also have worse overall outcomes when they develop breast cancer. The first aim of my work was to test if breast density and obesity together would accelerate risk and tumor progression more than one risk factor alone. Second, I focused on obesity only to understand why these patients may have more metastasis in the lungs. Thirdly, I investigated why obese patients have better responses to some types of cancer therapy.

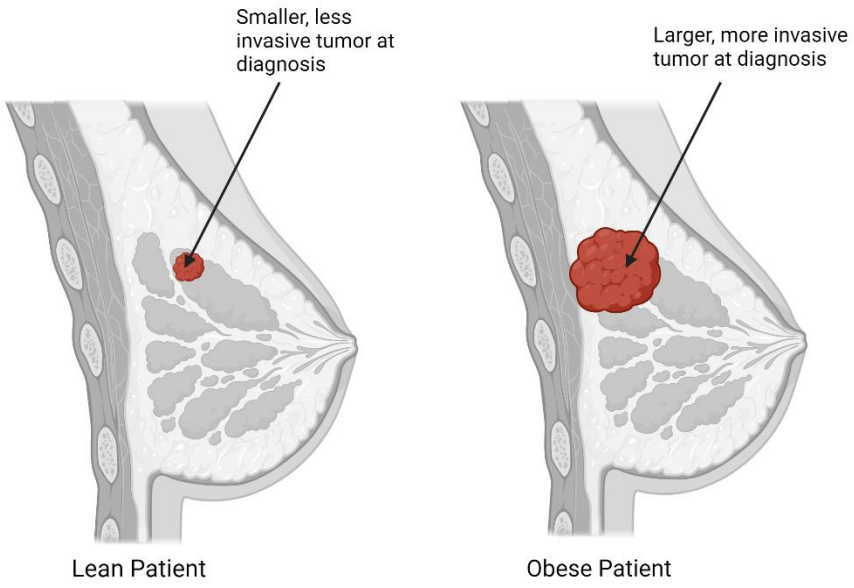

Figure 6-1 Obese patients frequently have larger, more invasive breast tumors at the time of diagnosis: Shows an example of a tumor at the time of diagnosis in lean women and a tumor at diagnosis in an obese patient. Obese women at the time of diagnosis frequently have larger tumors that are more invasive. Invasive tumors have spread farther into the surrounding breast and eventually into the chest.

What is breast density?

Breast density is an increase in glandular tissue and structural support fibers, like collagen, in the gland. **Glandular tissue** includes the epithelium, ducts and lobes of the mammary gland. The rest of the mammary gland mostly consists of fat. The mammary gland has many fibers that provide structural support to the gland, including **collagen.** Collagen is one of the main structural support fibers in the mammary gland. It is not completely understood how increased collagen contributes to breast cancer risk. In tumors, collagen can structurally help tumors grow. Breast density is thought to make it more difficult for doctors to see early breast cancer on a mammogram. Fat is black on a mammogram, while glandular tissue, collagen, and breast cancer are white on this

scan. Mammary density blocks the visualization of small breast tumors on scans because it shows up as the same color. Although high breast density may contribute to breast cancer being missed on scans, evidence also suggests that increased glandular tissue, collagen and other fibers may change the breast environment to promote cancer.

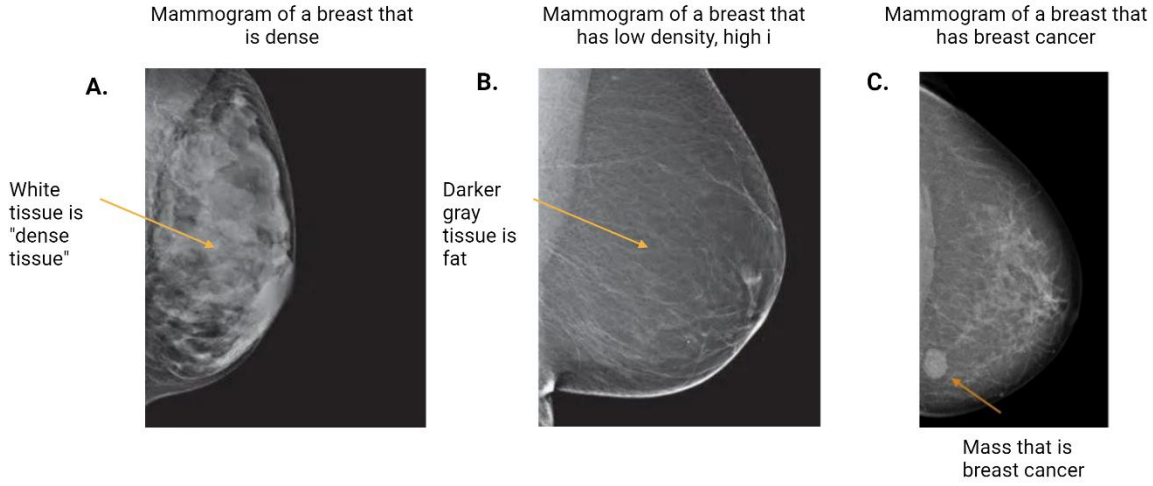

Figure 6-2: Breast density on a mammogram can make it challenging to identify early breast cancer lesions. Breast density is thought to consist of increased glandular tissue taking up a majority of the area of the breast. Breast density also consists of increased structural support fibers like collagen. Collagen and glandular tissue appear white on a mammogram, while fat appears dark gray. **(A)** Shows a mammogram of a dense breast. **(B)** Shows a mammogram of a low dense/fatty breast and **(C)** Shows a mammogram of a breast with a large breast cancer mass. A low-density breast consists mostly of fat. The breast appears mostly dark gray with a few white areas appearing, representing collagen and glandular tissue. Early and small breast tumors will be easier to see in breasts with low density. The last mammogram shows a breast with a large tumor in the lower left corner (C). The tumor shows up on the mammogram as white, similar to dense issue. The tumor is present in a breast with some density. Hopefully you can appreciate if this tumor was smaller and within a more dense breast like in (A), the tumor would be difficult to identify. Images are from the American Cancer Society https://www.cancer.org/cancer/types/breast-cancer/screening-tests-and-early-detection/mammograms/breast-density-and-your-mammogram-report.html and *Nature* *https://www.nature.com/articles/s41598-020-77053-7*

Obesity

Obesity is defined as having a body mass **index (BMI) of ≥30 kg/m^2.** BMI is calculated by taking a person's weight divided by the square of a person's height in meters. It is not always an accurate measurement to determine if someone is obese. However, it is still used in humans today to determine a person's level of obesity. More accurately, obesity is defined as an excess of adipose tissue in the body, often caused by an excess caloric intake. Obesity affects the mammary tissue by increasing the size and amount of fat cells in the gland. These fat cells are called **adipocytes**. These adipocytes are large cells that store fat in the body. As a person becomes more obese these cells expand and become stressed. They will eventually die from this stress. Macrophages, a cell that is part of our **immune system,** helps "**clean up**" cells when they die.

The immune system is made up of many types of cells, including macrophages, that protect our bodies from bacteria, viruses and fungi. Immune cells can also protect our bodies from cancer. In fact, they play an important role in preventing and fighting cancer. However, sometimes immune cells can promote the development of cancer. Fat cells that die cannot remain where they are, they need to make room for new cells. Multiple macrophages will surround a dying adipocyte and start to "eat" the adipocyte. We can visualize macrophages doing this under a microscope. We call these structures of macrophages and adipocytes **crown like structures (CLS)**. However, a lot of CLS in a mammary gland is **not** considered normal. In lean people, we can see very few CLS because adipocytes are a healthy size. These CLS can be present before cancer develops, and also after. In general, CLS are thought to possibly increase breast cancer

risk because they are signs of **inflammation.** However, a direct link between CLS and breast cancer risk has not been identified.

Inflammation is an increase in immune cells and **cytokines** that activate or turn off immune cells. Cytokines are substances that are produced by immune cells, to communicate to other immune cells to help fight infections and cancer. Sometimes immune cells will be activated and produce inflammation cytokines when it is unnecessary. Chronic inflammation increases the risk for cancer. We do not want our immune system to be overly active all the time, instead we only want the immune system active when we have an illness, are responding to vaccines, or other immune therapy.

In obesity, inflammation often is high, even if a person does not have an infection or cancer. Macrophages are one of these cells that cause inflammation, and although they are cleaning up dying fat cells, they can produce proteins that promote the growth of epithelium. Macrophages are around **mammary ducts,** in addition to forming CLS (crown like structures). Mammary ducts are part of the glandular tissue in the breast and help transport milk during lactation. In obesity, there is more macrophage-driven inflammation in the mammary gland. Inflammation is a hallmark of cancer, and these macrophages could increase risk. However, a direct link between inflammation in the mammary gland and breast cancer has not been identified. This is a current area of research, as other labs try to identify how macrophages contribute to breast cancer risk.

Inflammation also results in cells in the breast producing extra collagen or structural support fibers. Too much collagen could increase breast cancer risk, and can later help early cancer cells spread to other parts of the gland, and eventually other

organs. Like high breast density, obesity causes an increase in collagen production in the breast. Specifically, we have seen increased collagen around mammary ducts. Mammary ducts are lined with epithelium, and these are the cells that will eventually turn into cancer if they are damaged. As part of my research, I quantify macrophages and collagen to try to measure inflammation and breast density.

Breast density can also increase macrophages and breast inflammation. It is unknown if both obesity and breast density together may further breast cancer risk or further increase both collagen deposition and inflammation.

Obesity effects on tumors in the breast

Think of the tumor as an ecosystem. When talking about the cells, cytokines, and structural support fibers, like collagen, we often call this the **tumor microenvironment (TME).** Multiple cell types are found within the tumor. Remember, a tumor is an overgrowth of our own cells because cells have lost their ability to control their growth. A breast cancer tumor is made of mostly abnormal breast epithelium. However, immune cells are incorporated into the tumor as well, cells like macrophages. Breast tumors are also surrounded by adipocytes or fat cells. These fat cells can affect how the tumor grows, and they function differently in obesity. Macrophages have been shown, in some studies, to be increased around and within breast tumors. Macrophages are thought to contribute to tumor growth. In fact, more macrophages within mammary tumors can be associated with worse outcomes for patients.

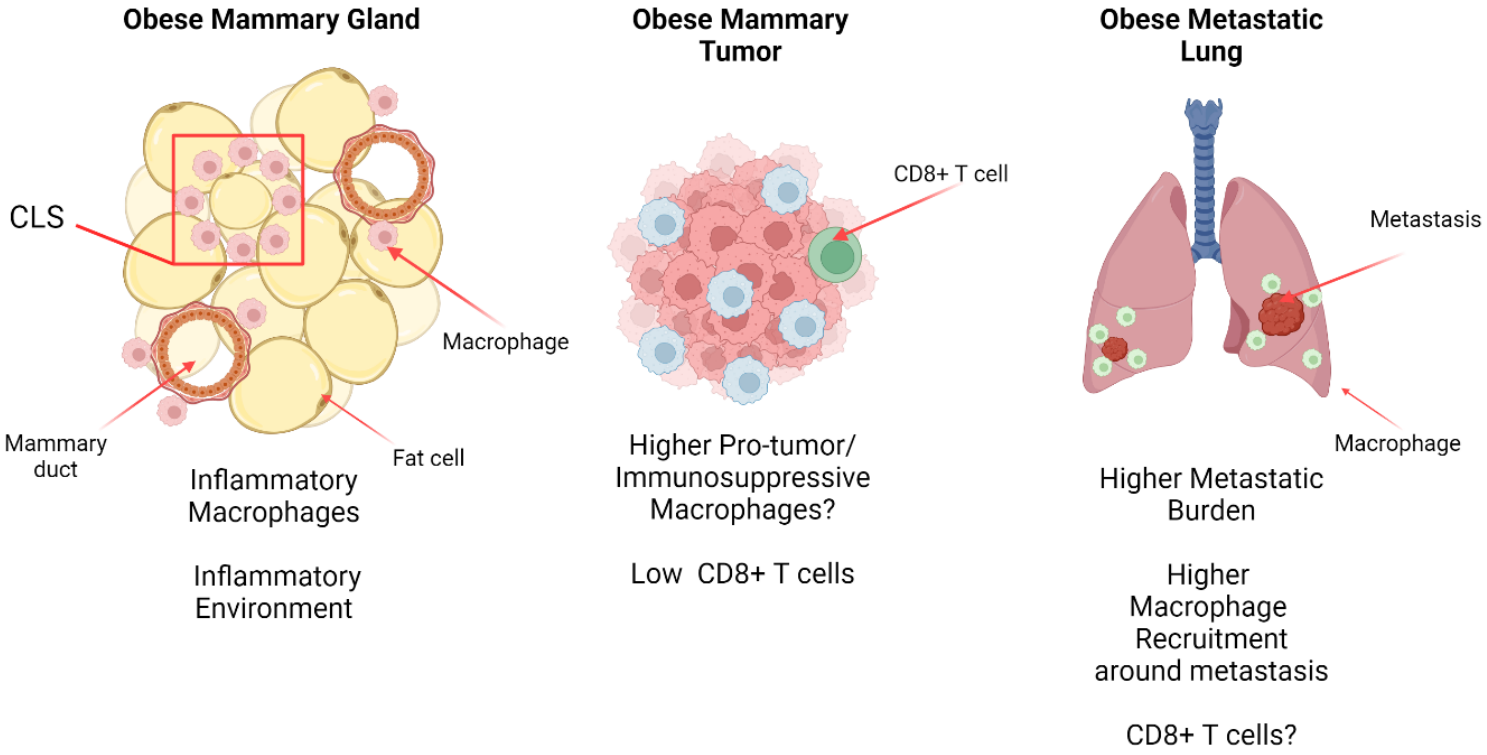

Figure 6-3: Obesity changes the immune system in the mammary gland, mammary tumor, and in the lung. (A) Obesity increases inflammation in the mammary gland before cancer occurs. This inflammation can increase breast cancer risk. Inflammation in the mammary gland is mostly driven by macrophages that have been recruited to the gland to "clean up" or "eat" dying or dead fat cells. Macrophages will also be present around ducts and are increased in obesity. **(B)** Macrophages in tumors are sometimes thought to be immunosuppressive or "pro-tumor." They can suppress other cells like CD8+ T cells from recruiting into the tumor. Obese mammary tumors have been shown to have less CD8+ T cells in mice. Therefore, these cells cannot kill tumor cells and shrink tumors. **(C)** Breast cancer can spread to the lung. These masses or small tumors are called metastasis. My lab has shown there are increased macrophages physically around metastasis in obese mice. However, it is unknown if, in the lung, these macrophages are pro- or anti-tumor and if they suppress CD8+ T cells like we see in tumors.

The tumor microenvironment, or TME, is complicated. Sometimes increased levels of certain types of cells are beneficial to killing tumor cells and thereby shrinking tumors, however, sometimes immune cells can suppress other parts of the immune system from killing cancer cells. In normal tissue, we generally do not want many

immune cells, like macrophages, because of the associated inflammation. Macrophages can either promote tumor growth or support tumor killing. Although we don't fully understand the phenomenon, there are more macrophages within tumors in patients with worse outcomes (tumors that grow fast), and we believe these macrophages promote tumor growth by suppressing other cells. Therefore, in obesity, macrophages could be causing other cells to be excluded or "turned off" in tumors.

In fact, in our mouse experiments in my lab, we have shown that **CD8+ T cells** can be excluded from tumors in obese mice. CD8+ T cells are a cell that can directly kill tumors with "toxic" proteins. Macrophages in obesity may be playing a role in suppressing important cells like CD8+ T cells from entering the tumor. In tumors from lean mice and people, this occurrence has been well studied, however, it is uncertain if this also occurs in metastasis.

Remember, metastasis is the spread of breast tumor cells to other organs, like the **lungs**. The lungs are a common site for metastasis to grow. Obese patients are known to have more metastasis and have a higher risk for metastatic spread. Why obese patients have more metastasis is **unknown**.

Many studies have looked at how macrophages change the mammary gland to possibly increase breast cancer risk and affect its growth and spread. However, it is unknown how macrophages could be aiding growth of breast cancer in the lungs under obese conditions. In previous work in Dr. Lisa Arendt's Lab, we saw an increase in macrophages surrounding metastasis in obese mice, with macrophages in direct physical contact with metastasis. This contact may create a barrier for CD8+ T cells, preventing them from reaching and killing the tumor cells. In addition, macrophages may

produce signals that impede CD8+ T cell recruitment or **exhaust** CD8+ T cells by sending too many activating signals. We thought that these macrophages may be increasing metastasis growth by impairing CD8+ T cells ability to kill breast cancer cells in the lung. However, it is currently unknown if this is true, especially when patients are also obese.

CD8+ T cells

CD8+ T cells are lymphocyte immune cells that directly attack cancer cells . They kill cancer cells by identifying them with a **receptor called the T-cell receptor (TCR), a protein on the cell's surface that identifies other proteins**. CD8+ T cells can only kill cells they are designed to recognize. For example, a CD8+ T cell that is programmed to kill a breast cancer cell will not kill a liver cell.

All of our cells express proteins known as **antigens** that are specific to their cell type. Antigens act like “tags” that signal to other cells, like cells in the immune system, what they are. Antigens can tell immune cells “I am not normal; I am a cancer cell” or “I am a cell infected with a virus.” Macrophages can pick up these antigens from dead cancer cells and **present** them to CD8+ T cells, activating those T cells to kill surrounding live cancer cells.

When T cells are activated, they begin to produce their own cytokines and cancer killing proteins. Remember that cytokines are how immune cells communicate to help fight infections and cancer. CD8+ T cells with low cytokine production may be **exhausted.** CD8+ T cells become “tired” or **exhausted** from killing tumor cells. The second aim of my thesis was to identify if CD8+ T cells are exhausted in obese lungs

before or after metastasis, which may explain why obese patients have more metastatic burden.

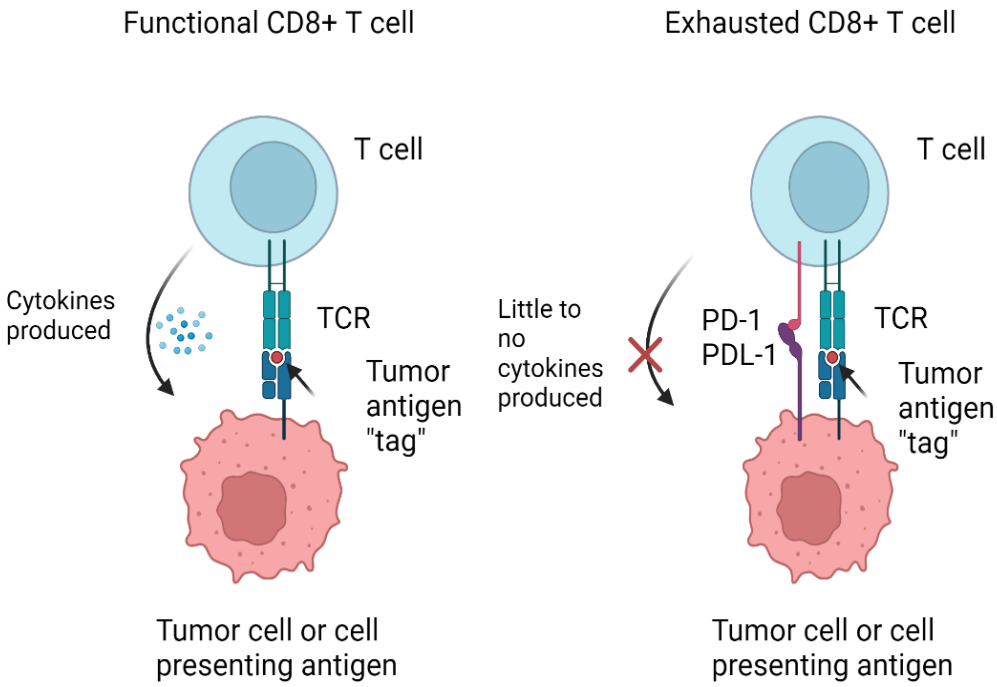

Figure 6-4: T cells can become exhausted when killing tumor cells. When CD8+ T cells interact with tumor antigens or “tags” with their T cell receptor (T cell uses this to recognize the tumor), they produce cytokines (anti-cancer proteins) to kill cancer cells. However, when exhausted CD8+ T cells interact with tumor antigens, they cannot produce cytokines, and tumor cells survive. This is because these CD8+ T cells express PD-1 and it binds to a PD-L1 positive cell (tumor cell or cell presenting antigen).

When CD8+ T cells are activated, they raise a “flag” or **receptor** on their surface known as programmed cell death-1, or **PD-1,** after they start killing cancer cells. When they receive an activation signal by tumor cells or cells like macrophages, they produce more PD-1. When PD-1 binds to its “partner” **PD-L1, it acts like pressing the “off” button, causing** CD8+ T cells to become exhausted and dampening their ability to kill

cancer cells. This can eventually cause CD8+ T cells to die (Figure 6-4). Oncologists can block this interaction so CD8+ T cells can stay “on” and continue to clear cancer cells.

How we can reduce tumor promoting macrophages and keep CD8+ T cells “on”

Doctors that treat cancer, known as **oncologists**, use drugs and other agents to improve the immune system’s ability to fight cancer, a strategy called **immunotherapy**. Popular immunotherapies target cancer-promoting macrophages and exhausted CD8+ T cells. Depleting macrophages from breast tumors has been shown to reduce tumor size. We can deplete macrophages using **colony stimulating factor-1 receptor (CSF-1R)** blocking agents to inhibit macrophage recruitment to tumors and metastasis. Decreasing macrophages can also increase CD8+ T cells in the tumor, improving the body’s immune response, and shrinking tumors, in part because CD8+ T cells are able to come in contact with the tumor cells. However, these newly recruited CD8+ T cells can still become exhausted and express PD-1. This is why a combined anti-CSF-1R and anti-PD-1 approach is promising for the removal of breast cancer metastasis.

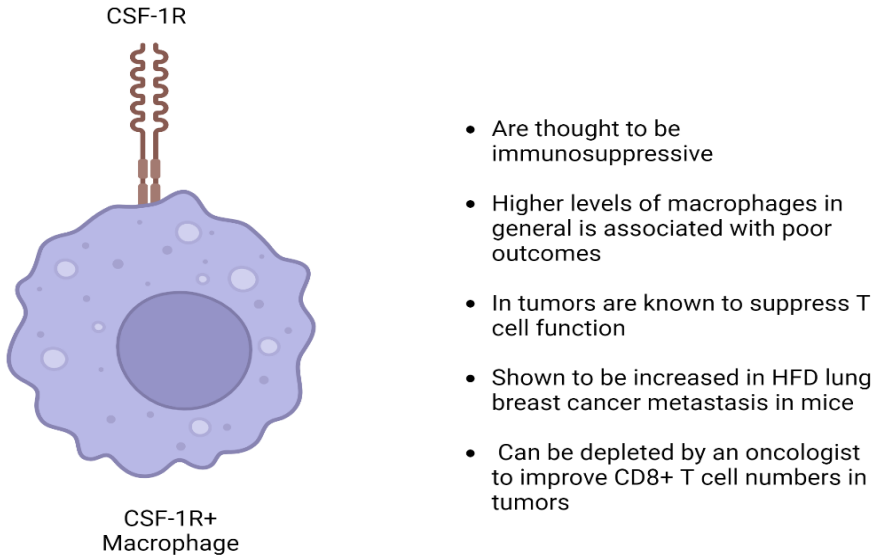

Figure 6-5: Macrophages express colony stimulating factor-1 receptor (CSF-1R). Macrophages express CSF-1R that can affect their recruitment and development in tumors. Blocking this receptor with anti-CSF-1R, removes macrophages from the tumor, overall improving CD8+ T cell numbers and activity.

When it works, blocking PD-1/PD-L1 causes tumors to shrink and metastasis to be cleared. However, it does not always work for some patients. One reason for this is that CD8+ T cells sometimes cannot get into the tumor to fight it. The therapeutic combination of depleting macrophages and blocking PD-1 results in reduced tumor sizes compared to one therapy alone in many cancers.

To summarize, breast tumors with high macrophages and low CD8+ T cells have an overall poorer prognosis (Figure 6-6A). When macrophages are reduced in the tumor, CD8+ T cells are increased to the tumor (Figure 6-6B). These CD8+ T cells begin to shrink the tumor, but CD8+ T cells become exhausted or “tired” and increase their

expression of PD-1 (Figure 6-6C). An oncologist can block PD-1 to keep the newly recruited CD8+ T cells turned “on,” shrinking tumors or metastasis further (Figure 6-6D).

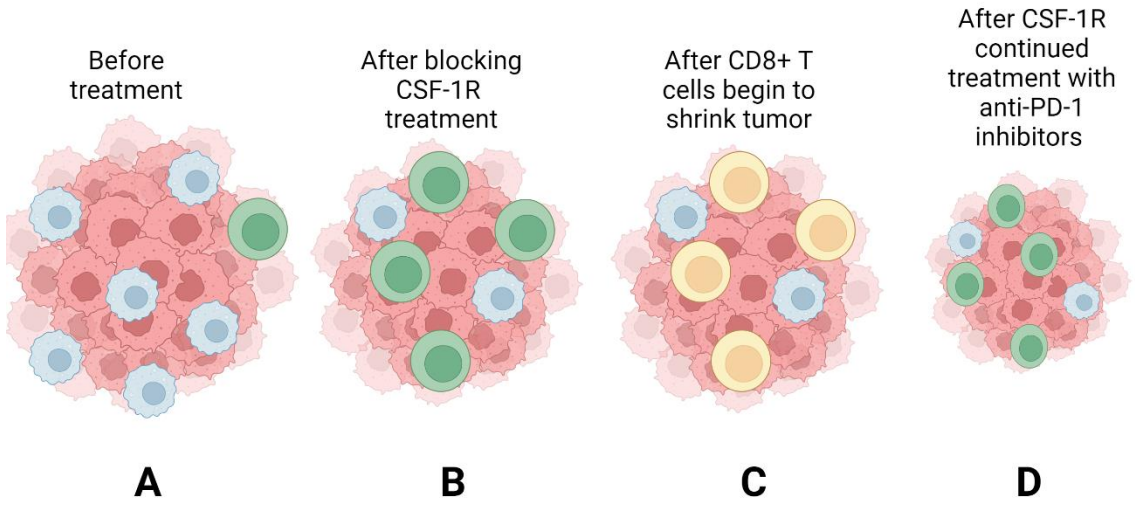

Figure 6-6: How anti-CSF-1R and anti-PD1 may shrink breast tumors (A) Shows a tumor prior to treatment. Macrophages, in blue, are high, and suppress CD8+ T cells (green). (B) When macrophages are depleted with anti-CSF-1R, CD8+ T cells increase in the tumor. These CD8+ T cells are active and functional and produce cytokines (anti-tumor proteins) to aid in the anti-tumor immune response. (C) As CD8+ T cells kill tumor cells and recognize more and more tumor antigen “tags” they become tired or exhausted. Exhausted T cells (yellow) will express PD-1 and lose their ability to kill cancer cells. (D) After blocking PD-1 and continuing to keep macrophages low with anti-CSF-1R, CD8+ T cells are able to be turned back “on” and become activated. These CD8+ T cells are able to continue to kill cancer cells and overall shrink the tumor.

Surprisingly, obese patients have longer overall survival on therapies targeting PD-1/PD-L1 binding on CD8+ T cells compared to lean patients. This is shocking because in obese mouse models, and as shown in some human studies, CD8+ T cells are low in the tumor. However, the mechanism behind this better response in patients with obesity is unknown. With obesity increasing macrophages around metastasis in the lung, and clinical evidence that obese patients respond better to PD-1/PD-L1 targeted

therapy, I believe that obese patients with metastasis might respond better to a combination approach targeting macrophages and exhausted CD8+ T cells.

To test these questions, I used mice to model how obese and lean patients with metastasis may respond to these therapies. The last aim of my thesis was to investigate if obese mice will have reduced metastasis to the lung on a dual macrophage, CD8+ T cell targeted therapeutic approach, or if targeting macrophages or CD8+ T cells alone will be more efficacious. Lastly, if responses are different than in lean mice, why?

How we study breast cancer risk and progression in the lab:

Mice are an important tool used in biomedical research to study diseases like cancer and can help us answer questions about cancer progression. There is a lot we do not know about the body, so using an animal model helps us mimic as closely as possible what might happen in you or me. Many factors affecting cancer growth involve the whole body, or "system." We call these factors **systemic** effects. One systemic factor is our immune system. Immune cells are in our tissues, blood and lymph system, surveying and killing pathogens, including cancer cells. Cancer metastasis involves cancer cells surviving leaving the primary tumor (in the mammary gland, in this case), traveling in circulation in the body, and entering secondary organs, like the lungs. Mouse models allow us to mimic this process as closely as possible to what would happen in a cancer patient.

In my thesis work, I used different diets to induce obesity. Lean mice received a low-fat diet, and obese mice received a high-fat diet. I utilized a mouse model where mice are born with abnormal mammary epithelium that is genetically altered to form

multiple mammary tumors. These mice will begin to form tumors from birth. These models are useful for us to study the early stages of breast cancer (Figure 6-7). I used these genetically altered mice to study early and late tumor formation under conditions of obesity and breast density. Later, to study later stage metastatic breast cancer, I inject tumor cells into the mammary gland so I can remove the tumors surgically (Figure 6-8). This is to mimic when tumors are removed in breast cancer patients before their metastasis is treated.

Mammary glands are composed of many ducts that are lined with a single layer of epithelial cells. When you look at mammary glands under a microscope, you are looking down the center of the mammary duct, like looking down an innertube. The center of the duct is referred to as the **lumen**, a hollow space that allows milk to flow out of the mammary gland during lactation. As these cells begin to divide, they form additional layers, filling the lumen of the duct. In the normal mammary gland, these cells do not fill the lumen, and this space is empty until a woman would begin to lactate after giving birth. In cancer, epithelial cells continue to divide, the entire lumen will be filled, and the lumen is no longer visible. Eventually the structure of the duct cannot withstand the rapidly dividing cells. The now cancerous epithelium breaks the outer structure of the duct and continues to divide and fill up the surrounding gland (Figure 6-7). Eventually these mice will form multiple tumors that metastasize to the lung. This is how tumors progress in genetically engineered mice. These genetically engineered mice can also be fed a HFD (high-fat-diet) to induce obesity. Thus, we can observe how these early tumor stages are affected by obesity.

As I previously mentioned, breast density can include a buildup of “structural support fibers,” known as collagen. To model breast density we used mice that lack the ability to break down collagen in the mammary gland. In normal mice, and in you and I, collagen is broken down and rebuilt as tissue adapts to changes. However, the bodies of these mice can’t break collagen apart into pieces; instead, the collagen forms a dense network in the mammary gland. We can cross collagen-dense with mice that form mammary tumors to model breast cancer under high density conditions. These mice can also be fed a HFD so we can model obesity and breast density together.

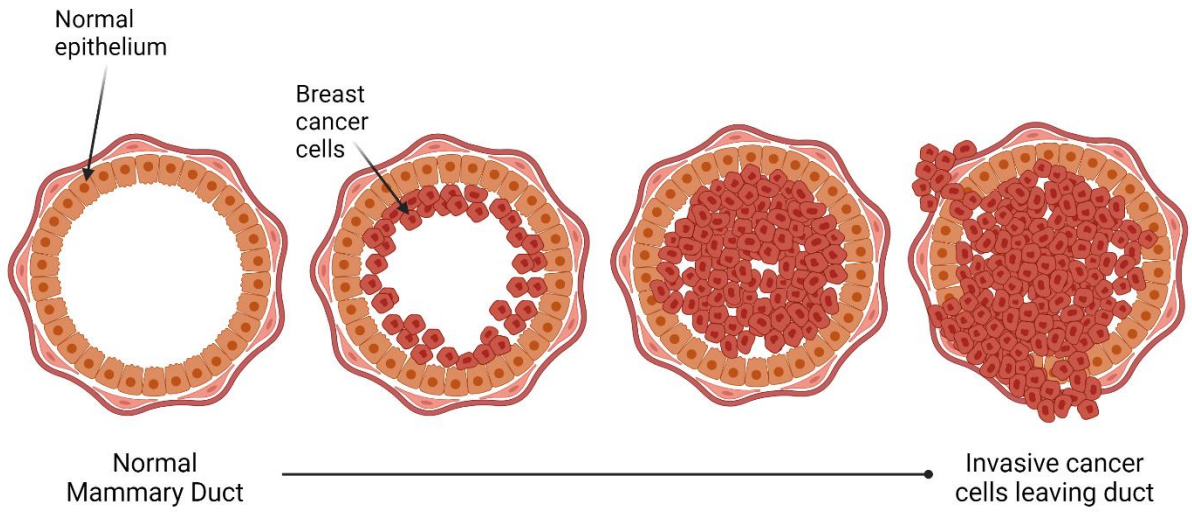

Figure 6-7: The progression of breast cancer. Normal epithelium lines the mammary duct. Cancer cells begin to fill the lumen of the duct until they invade into the surrounding mammary gland.

After mice become obese, I can induce a mammary tumor by injecting mammary tumor cells directly into the mammary gland on each flank of the mouse. Two tumors will then grow and form noticeable lumps under the skin on each side of the mouse. Once one tumor reaches 0.5 cm in size, tumors can be surgically removed from the mice. I removed the tumors in our mice to mimic when there is a resection (removal) of breast cancer in women. Although women have their breast tumors removed, cancer

cells still might be present throughout other parts of the body. The cells may grow and form metastasis. We used this model over a genetically engineered tumor model because it allows us to remove tumors from mice (Figure 6-8). Women often have their tumors removed prior to some types of therapy so it is important to try to model this in our mice.

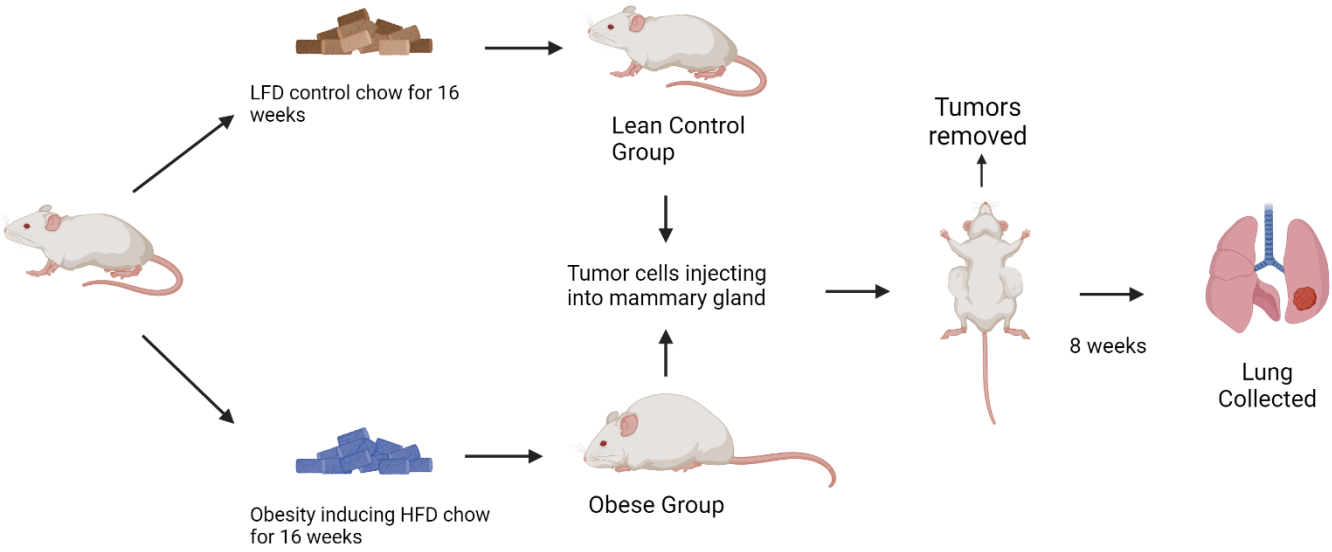

Figure 6-8: Methods for inducing breast cancer metastasis in obese mice. Female mice were fed a low-fat diet or high-fat diet for 16 weeks. Once mice fed a high-fat diet were obese, tumor cells (mammary cancer cells) were injected into the mouse's mammary glands. These cells were then left to grow in lean and obese mice. At a certain size, I removed the tumors surgically from the mice to mimic when women have their tumors removed. I then waited another 8 weeks for metastasis to grow in the lung before I analyzed the metastasis and immune cells in each group. This is a great way to model obesity-induced breast cancer in mice.

The main results of my PhD

Obesity and breast density on breast cancer risk and progression

My work revealed that in mice without mammary tumors, breast density and obesity increased macrophage-driven inflammation. Mice with high breast density and obesity had more CLS (crown like structures, or macrophages around dying adipocytes), indicating more adipocyte death and total inflammation within the gland. I also saw increased collagen around ducts in these mice compared to control mice. CD8+ T cells were reduced in the mammary gland of obese mice, but not in lean mice. This indicates obesity specifically decreases CD8+ T cells, potentially causing the immune system to miss the development of early mammary tumor stages.

Evaluating tumor-bearing mice, I did not see differences in tumor progression in the mammary glands of mice with high density breasts, obesity, or both risk factors combined. However, there were more macrophages around tumors in mammary dense mice, obese mice, and mice with both risk factors combined. CD8+ T cells were only reduced in tumors of obese mice, with or without increased breast density. Lean mice with dense mammary glands did not have less CD8+ T cells, like what I saw in mice

without cancer. Low CD8+ T cells in tumors and higher macrophages around the edges may increase cancer metastasis (Figure 6-9).

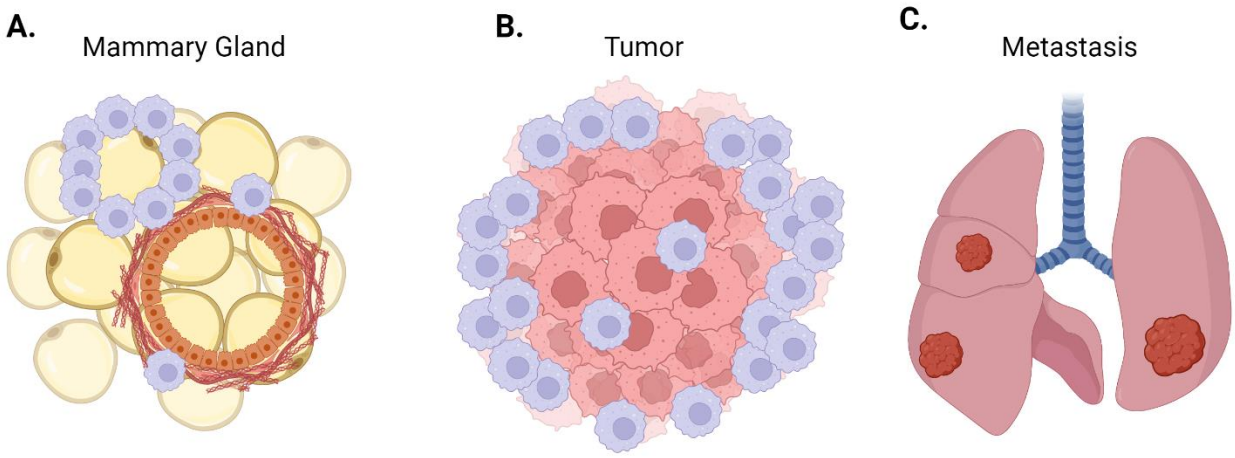

Figure 6-9: Results showed obesity and breast density together may increase breast cancer risk and metastasis to the lung. (A) In the normal mammary gland, obesity and breast density together increased crown-like structures (CLS), or macrophages around dying adipocytes, compared to one risk factor alone in young mice. Collagen was also increased around ducts of mice with both risk factors. This may correlate with a higher risk for breast cancer development. (B) Although we didn't find any differences with tumor size. Tumors from mice with both risk factors have more macrophages surrounding the tumor edge. This may lead to more invasive tumors and worse prognosis. (C) In the lung, mice with both risk factors had more metastasis compared to mice with one or no risk factors. Therefore, women with breast density and obesity may be at higher risk for metastatic spread to the lung.

Lastly, measuring metastasis to the lung, mice with both risk factors had increased levels of metastasis in the lungs (Figure 6-9C). However, mice with just high mammary density or obesity alone did not have increased metastasis compared to our control mice. I found this surprising, as it shows that a combination of higher breast density and obesity could really promote cancer spread to the lungs. Overall, I concluded that **(1) a combination of breast density and obesity together may increase breast cancer risk beyond one risk factor alone. (2) During the**

progression of breast cancer, both risk factors together seem to promote metastasis to the lung, which may translate to an overall poorer survival outcome in patients with both conditions at the time of breast cancer development.

I discovered CD8+ T cells are more exhausted under obese conditions before metastasis

In my second project, I looked at how CD8+ T cells functioned in the lungs of obese and lean mice before and after metastasis. In non-tumor bearing mice, obesity increased PD-1+ (programmed cell death-1, a marker for exhaustion) in CD8+ T cells within the lungs. This indicated to me that they may be exhausted. Obesity also increased TCR (T cell receptor, what T cells used to recognize tumor cells) signaling within the lungs, which may indicate an over- activation of T cells, even before cancer is present. T cells also produced less cytokines in the lungs of obese mice. This data indicates that obesity exhausts T cells prior to tumor development in the lungs, which may render CD8+ T cells unable to kill cancer cells that make it to the lung early on .

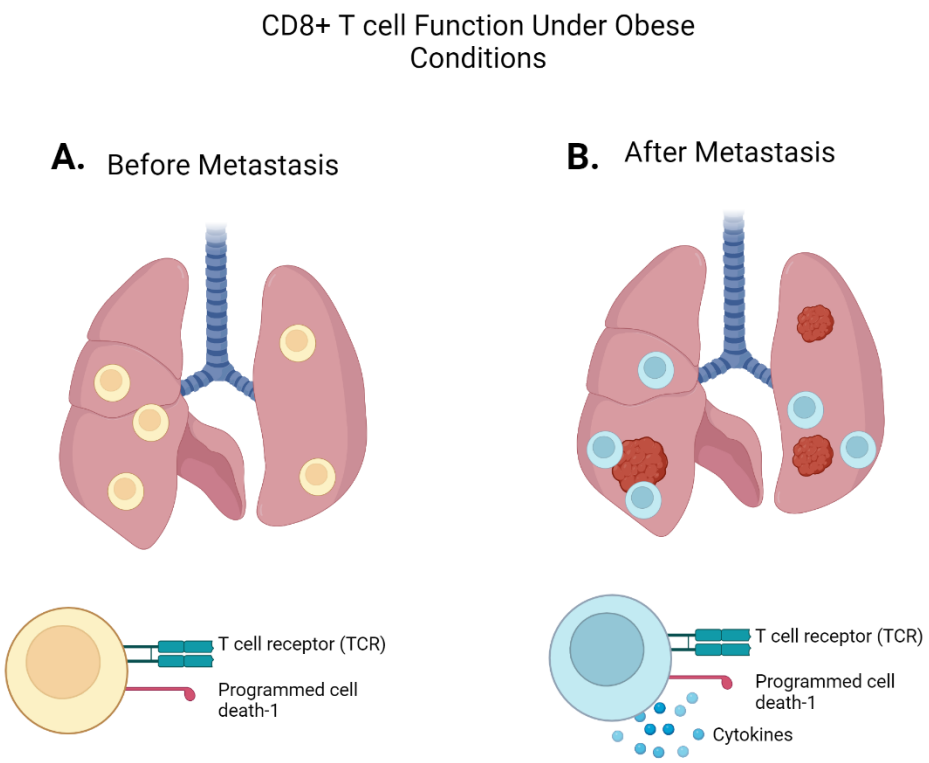

Figure 6-10: Obesity alters CD8+ T cell function in the lung. (A) Before metastasis, CD8+ T cells were more exhausted, failed to produce cytokines, and expressed PD-1 in obese mice compared to lean mice. This overall means these CD8+ T cells from obese lungs may be dysfunctional and therefore unable to clear early metastasis. (B) Obese mice had more metastasis than lean mice and also had more CD8+ T cells that expressed PD-1. However, in metastasis, obese CD8+ T cells were able to produce cytokines, which indicates that after metastasis CD8+ T cells are able to retain some function and may respond to anti-PD-1 inhibitors.

I showed that CD8+ T cells in obese mice with breast cancer metastasis express exhaustion markers like PD-1 but still can retain function

CD8+ T cells' exhaustion prior to tumor development allows cancer cells to evade the immune response in obese mice. Obese mice had more metastasis to the lung than lean mice, consistent with clinical data in humans and similar mouse studies. Contrary to my prediction, I found that CD8+ T cells were **not** decreased in obese mice lung

metastasis, though I did observe that PD-1 expression was higher, indicating possible exhaustion (Figure 6-10). However, CD8+ T cells from obese mice could still produce cytokines (the protein CD8+ T cells produce when activated, which helps kill cancer cells). Overall, this may suggest that in cases of lung metastasis, CD8+ T cells under conditions of obesity are able to retain some function. I concluded that **(1) Obesity impairs CD8+ T cell function to an exhausted-like state in the lungs of non-tumor bearing mice. (2) After metastasis, CD8+ T cells in the lungs of obese mice express PD-1, but they retain function.**

Out with the bad macrophages and in with the activated CD8+ T cells

I set out to test whether anti-PD-1 (a drug that blocks PD-1 from binding to PD-L1, keeping T cells “on”), anti-CSF-1R (a drug that blocks colony stimulating factor 1 receptor) depletion of macrophages, or a combination of both therapies would be better at removing breast cancer metastasis. I found that anti-PD-1 reduced metastasis in lean mice but not in obese mice. However, anti-PD-1 treatment in obese mice increased CD8+ T cells in the lungs. If CD8+ T cells are increased, I assumed that there would be more cells to clear metastasis from the lungs. Despite this increase, I suspected the CD8+ T cells were more exhausted. Indeed, other exhaustion markers were higher in these cells. What could be making them **exhausted** or **“turned off**?**”** I predicted it may be PD-L1+ (PD-L1 positive) macrophages! I saw that a population of cells, which includes macrophages, had higher PD-L1 expression! Therefore, macrophages may be decreasing anti-PD-1 response in obese mice

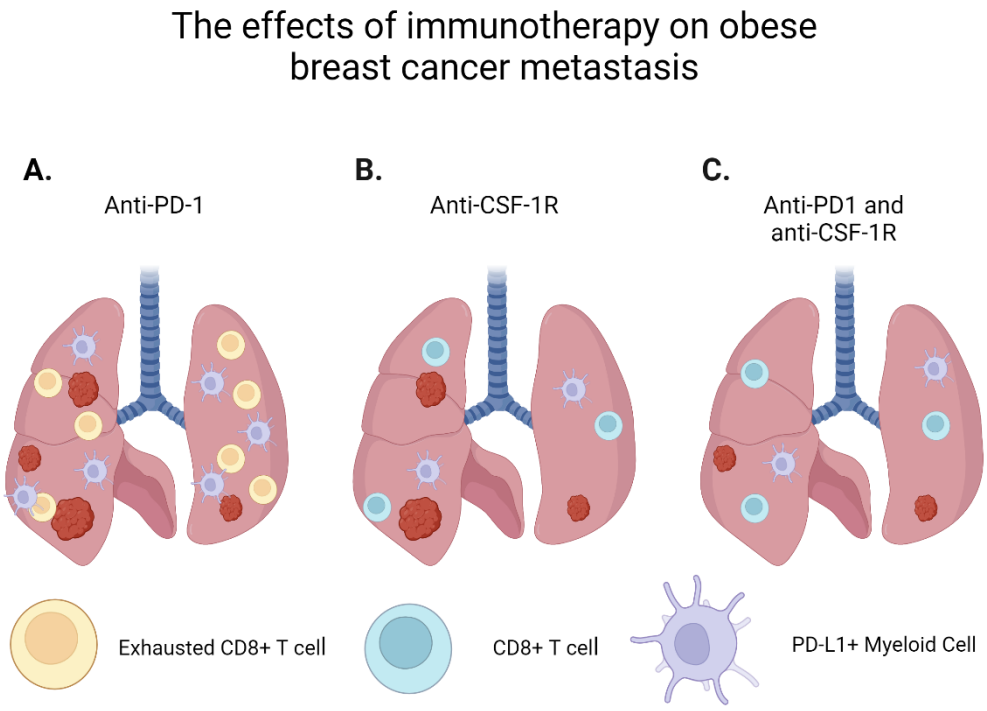

Figure 6-11: Obese mice responded better to immunotherapy. (A) Anti-PD-1 alone did not reduce metastasis in obese mice. It did increase the number of CD8+ T cells in obese lungs, but these CD8+ T cells were exhausted. In lean mice, CD8+ T cells were activated and were not increased. PD-L1+ Myeloid cells were also increased in obese lungs in response to anti-PD-1. Myeloid cells include macrophages! This might be why obese mice had a resistance to anti-PD-1 alone. (B) Macrophage depletion via anti-CSF-1R reduced PD-L1+ myeloid cells (probably macrophages) and reduced metastasis in obese mice. In lean mice, anti-CSF-1R did not reduce metastasis, suggesting macrophages are more tumor-promoting in obese metastasis. (C) Dual anti-PD-1 plus anti-CSF-1R was more efficient in obese mice, reducing metastasis and activating the immune system. Overall, macrophage depletion and dual therapy reduced metastasis more in obese mice compared to lean mice. This suggests that obese patients may benefit more from these therapies.

I found that anti-CSF-1R treatment increased activation of a population of cells, which includes CD8+ T cells, in lean mice. Therefore, depleting macrophages may improve T cell responses to cancer in lean mice. However, only in obese mice did depleting macrophages reduce metastasis. I also showed that only in obese mice did total immune cells increase. This was not seen in lean mice. It is possible that is why in lean mice, metastasis was not reduced.

PD-L1+ immune cells were reduced with anti-CSF-1R treatment only in obese mice, suggesting a reduction in cells that could exhaust CD8+ T cells. This also shows that macrophages are contributing to the PD-L1 expression in the lung. I also showed anti-CSF-1R treatment in obese mice increased PD-1 expression on CD8+ T cells (T cells could become exhausted!). This data suggested to me that combining anti-CSF-1R treatment with anti-PD-1 inhibitors could improve responses in obese mice. In fact, it did! I showed that a combination of anti-CSF-1R and anti-PD-1 reduced metastasis more in obese mice compared to lean (Figure 6-11). In this chapter we conclude **(1) Under conditions of obesity, responses to anti-PD-1 antibodies are limited. (2) Obese mice had more robust responses to anti-CSF-1R in the lungs, which was due in part to increased immune cells and decreased PD-L1+ macrophages (3) Obese mice also had more robust responses to a dual combination of anti-CSF-1R and anti-PD-1 antibodies within lung metastasis.**

Why this research matters:

My work showed that women with both high breast density and obesity may have a higher risk for breast cancer and could have worse overall survival. Identifying women with both risk factors may help diagnose women sooner and identify breast cancer patients that are at higher risk for metastasis. Additionally, investigating CD8+ T cells in the lung could identify new therapeutic targets for future patients. Lastly, exploring different patient demographics that have better responses to therapies already developed, like obese patients, helps us personalize cancer care, identify markers for therapy response, and save lives.